C.P. No. 818

C.P. No. 818

MINISTRY OF AVIATION

AERONAUTICAL RESEARCH COUNCIL

CURRENT PAPERS

Supersonic Wind Tunnel Tests on a 1/12th Scale Model of the Bristol Type 188 Research Aircraft

Part I: M = 1·4 to 2·0

by

C. R. Taylor and T. A. Cook

Part II: M = 2·0 to 2·7

by

T. A. Cook

LONDON: HER MAJESTY'S STATIONERY OFFICE

1965

PRICE £1 5s 0d NET

U.D.C. No. 533.652.1 : 533.6.011.5 : 533.6.013.12 :
533.6.013.412/413 : 533.694.23 : 533.695.3

C.P. No.818

September 1961

SUPERSONIC WIND TUNNEL TESTS ON A 1/12TH SCALE MODEL OF THE BRISTOL TYPE 188 RESEARCH AIRCRAFT, PART I; M = 1.4 TO 2.0

by

C. R. Taylor
and
T. A. Cook

SUMMARY

Six component force tests at Mach numbers 1.4, 1.6, 1.8 and 2.0 have been made on a 1/12th scale model of the Bristol Type 188 in the 8 ft tunnel at Bedford. The results are analysed to give drag, longitudinal and lateral stability data, and to show the effects of control movements, dive brakes, and nacelle spillage.

Some comparisons are made with the results of earlier tests on a 1/36th scale model.

LIST OF CONTENTS

LIST OF TABLES

LIST OF ILLUSTRATIONS

LIST OF ILLUSTRATIONS (CONTD.)

LIST OF ILLUSTRATIONS (CONTD.)

1 INTRODUCTION

The Bristol Type 188 is a twin-engined research aircraft of all-steel construction, designed, to Specification E.R.134, to fly at speeds up to Mach 2.5 and altitudes up to 60,000 feet, though it will initially be limited to Mach 2. A survey of constructional details and development is made in Ref.1.

The tests reported here were made on a 1/12th scale model of the aircraft in the 8 ft × 8 ft high speed wind tunnel at the Royal Aircraft Establishment, Bedford. This model has also been tested at transonic speeds in the 9 ft × 8 ft wind tunnel of the Aircraft Research Association Ltd[2]. Low speed tests on a 1/10th scale model are reported in Ref.3

Five component (i.e. normal force, pitching moment, side force, yawing moment, and rolling moment) tests at transonic and supersonic speeds up to Mach 2 have previously been made on a 1/36th scale model in the 3 ft × 3 ft tunnel at R.A.E. Bedford[4]. This model had a distorted rear fuselage to allow a single sting support system to be used. Tests on a larger model, supported on a twin-sting system, and having a representative fuselage, were required to provide more lateral stability data, to measure drag forces, and to make more accurate measurements of the effectiveness of control surfaces. A test was made with modifications to the fuselage, simulating the 1/36th scale model, to obtain a comparison between the results from the 3 ft × 3 ft tunnel and those from the 8 ft × 8 ft tunnel. This demonstrated the effects of (a) the rear fuselage distortion on the 3 ft × 3 ft tunnel model, and (b) the twin-sting support system of the present model.

The tests described in this paper cover the Mach number range 1.4 to 2.0. Tests covering the range 2.0 to 2.7 are reported in Part 2.

2 DESCRIPTION OF THE MODEL AND BALANCE

The general arrangement of the model and its twin-sting support system is shown in Figs.1 and 2. The principal dimensions and other model data are listed in Table 1.

The model was made of steel with a high accuracy of finish. It was a true reproduction of the full-scale aircraft, except for small changes in the shape of the engine nacelles. A small distortion of the nacelle tailpipes was found to be necessary in order to accommodate the sting supports, and to permit the estimation of the internal drag due to flow through the ducts. The layout of a nacelle depicting this distortion is shown in Fig.3. It was thought that constrictions inside the ducts (which could not be avoided on the model) would limit the intake mass flows, and some minor changes in the intake geometry were made in order to allow the intakes to run critically at the intake design Mach number (viz. $M = 2.1$) with the smaller mass flows expected in the tunnel.

The tailplane pivoted about an axis 37.5% of the root chord forward of the trailing edge, the range of settings available was from $+4^\circ$ to -14° (relative to the nacelle centre lines) in 2° steps. The complete tailplane and fin assembly could be removed and replaced by a blanking piece which preserved the fuselage lines. Aileron and rudder settings could be varied over the ranges $-25^\circ \leq \xi \leq 0$ and $-5^\circ \leq \zeta \leq 2.5^\circ$ respectively, using interchangeable hinge plates.

The forward nacelle cowlings were interchangeable with cowlings having spill vents (Fig.4) representing the fully-open position proposed for the aircraft. In tests with the spill vents open, the flow through the rear ducts was restricted by fitting throttling blocks to the stings at the duct exits.

The arrangement of the air-brakes in the fully-open position is shown in Fig.5; their position on the fuselage is shown in Fig.1. Other details are included in Table 1.

To enable a comparison to be made between the results on this twin-sting model and those obtained on the 3 ft × 3 ft tunnel single-sting model with a distorted rear fuselage, an alternative rear fuselage representative of the distortion was used. For tests with this configuration, a dummy central sting (not in contact with the model) was fitted to the yoke of the twin-sting support. This configuration is shown in Fig.6.

The strain-gauge balance system consisted of two four-component (viz. normal force, side force, axial force, and pitching moment) balances, one in each nacelle (see Fig.3).* The eight apparent loads (i.e. loads uncorrected for balance interactions) obtained from a set of readings were reduced to the usual six components as follows. Normal force, pitching moment, side force, and axial force, on the model were obtained by adding corresponding loads on each balance. Yawing moment and rolling moment were obtained by assuming them to be proportional to the differences in axial force and normal force between the two balances. The constants of proportionality were evaluated in the course of calibration. The six components thus formed were corrected for first order and second order balance interactions, as determined from the calibration, using the method of Ref.5.

The model was designed by the Aircraft Research Association Ltd., and manufactured by Test Equipment (Models) Ltd.

3 DETAILS OF THE TESTS

The tests were made at Mach numbers 1.4, 1.6, 1.8 and 2.0. The Reynolds number, based on the standard mean chord, was constant at 2.5×10^6. The different configurations tested, and the ranges of incidence and sideslip angles covered, are listed in Tables 2 and 3 respectively.

All the results presented in the next section of this Report refer to stability axes with their origin at a point in the plane of the nacelle centre lines, 3.75 in. aft of the leading edge of the inboard wing (i.e. at $0.18\ \bar{c}$). Incidence was measured with respect to the nacelle centre lines.** The angles of incidence and sideslip are defined as in current aircraft practice, (i.e. the tangent definition of incidence and the sine definition of sideslip[6] are used). The incidence and sideslip angles were corrected for sting and balance deflections.

---

* As this type of balance is not commonly used attention is drawn to the fact that a closed mechanical loop was formed by the model, the stings and balances and the rear yoke, and that slipping under load at the joints of the loop resulted in some hysteresis in the indicated loads.

** The wing-nacelle angle is 2°.

To accord with the practice of Bristol Aircraft Ltd., the pitching moment coefficients quoted here are based on the standard mean chord, and the lateral stability derivatives are defined as follows:-

$$y_v = \frac{1}{2}\frac{\partial C_y}{\partial \beta}, \qquad n_v = \frac{\partial C_n}{\partial \beta}, \qquad \ell_v = \frac{\partial C_\ell}{\partial \beta},$$

(β being in radians).

Axial force results were corrected for base pressures at the balance units and for the internal drag of the nacelles[7]. Prior to the tunnel tests the nacelles were connected to a high-pressure air supply and complete pitot and static pressure surveys made for a range of mass flows. The nacelle mass flow and the momentum flux at the measuring station were thus calibrated against the readings of one fixed pitot and one fixed static tube in each half duct (see Fig.3). This calibration was used, together with the pitot and static measurements obtained in the wind tunnel tests, to calculate the internal drag.

The mass flow measurements showed that the ratio A_o/A_{EN} (where A_o is the cross sectional area of the stream tube which enters the duct and A_{EN} is the area contained by the cowl lip) varied linearly with Mach number from 0.60 at $M = 1.4$ to 0.86 at $M = 2.0$.

The deflections under load of the rudder and ailerons were calculated using measured hinge stiffnesses, and either measured[8] or estimated hinge moments. For the rudder, the deflection was less than 1% of the control setting and for the ailerons less than 2%. These deflections were ignored in calculating the control powers.

Estimates of the accuracy of the results showed that the probable errors in the force and moment coefficients are as follows:-

$$\begin{aligned}
C_L &: \pm 0.003 \;\; \pm 0.004\, C_L \\
C_Y &: \pm 0.002 \;\; \pm 0.002\, C_Y \\
C_D &: \pm 0.004 \;\; \pm 0.007\, C_D \\
C_m &: \pm 0.0005 \;\; \pm 0.003\, C_m \\
C_\ell &: \pm 0.0007 \;\; \pm 0.004\, C_\ell \\
C_n &: \pm 0.0007 \;\; \pm 0.007\, C_n
\end{aligned}$$

The first term in each expression for the error is due to balance hysteresis and other resolution errors. The second term is based on estimates of the accuracy of the balance calibration. An additional error in the absolute value of the drag coefficient may exist, due to inaccuracies in the calculation of the internal drag of the ducts. This error is estimated to be smaller than ±0.003.

The random errors in angles of incidence and sideslip are less than 0.01°; however, local deviations of the air flow may have been as large as 0.20°.

In order to fix the position of boundary layer transition, the following roughness bands were painted on the model, using a mixture of grade 100 carborundum (i.e. particles about 0.008" in size) in aluminium paint:-

Fuselage: $\frac{1}{2}$" band, commencing 1" from nose.

Wings: from $2\frac{1}{2}$% to $7\frac{1}{2}$% chord.

Aileron horns: $\frac{1}{2}$% band commencing $\frac{1}{4}$" from leading edge.

Fin: $\frac{1}{2}$" band commencing at leading edge.

Tailplane: $\frac{1}{2}$" band commencing $\frac{1}{4}$" from leading edge.

Nacelle cowls: $\frac{1}{2}$" band commencing $\frac{1}{4}$" from lip.

Nacelle centre bodies: $\frac{1}{2}$" band commencing $\frac{1}{4}$" from apex.

4 PRESENTATION AND DISCUSSION OF THE RESULTS

The results of the tests are presented graphically in the accompanying figures. Tables of results have been omitted in order to limit the size of this Report but the numerical data are stored at R.A.E., Bedford and are available on request.

4.1 Longitudinal stability

Plots of those results pertaining to longitudinal stability are presented in Figs.7 to 16. The curves of C_L against α (Figs.7 to 10) and C_m against C_L (Fig.11) require little comment. The variation of lift coefficient with incidence is linear up to $C_L \approx 0.5$; at higher lift coefficients there are gradual decreases in slope. There are small decreases in $(\partial C_L/\partial \alpha)_{\alpha=0}$ with increasing negative tail setting (Fig.12). Except between M = 1.4 and 1.6 there is little variation of $(\partial C_m/\partial C_L)_{C_L=0}$ with Mach number (Fig.13), but as is shown in Fig.14 there are significant decreases in static stability margin with increasing lift coefficient at all Mach numbers. These decreases in stability are due to losses in tail effectiveness.

The variation of tailplane power (i.e. $\partial C_m/\partial \eta$ at constant incidences) with incidence is shown in Fig.15, where the measured values are compared with theoretical estimates based on the charts of Ref. 9. Theoretical values do not take into account effects due to other components of the model and the discrepancies between the measured and the theoretical values are due, at least partially, to changes in dynamic pressure at the tailplane, caused by the shock system ahead of the tailplane.

The measured tailplane powers were used in conjunction with the measured variations in pitching moment with incidence to calculate the effective downwash at the tailplane. This is plotted in Fig.16. Schlieren photographs (Figs.17-20) illustrate the shock system on the model at each Mach number. These indicate the complex nature of the flow in the neighbourhood of the tailplane which may account for the observed non-linearities in downwash.

To assist discussion of the lateral stability in section 4.2 and to give some idea of the requirements of the full-scale aircraft, graphs of the trimmed flight incidence and tail setting for a rigid aircraft are presented in Figs.21 and 22 respectively. It has been assumed that the aircraft weight is 32,000 lb, and that the centre of gravity coincides with the model moment reference point.

4.2 Lateral stability

Typical plots of the variations of the lateral coefficients C_y, C_n and C_ℓ with angle of sideslip are presented in Figs.23 to 25, and the variations with incidence of the derivatives y_v, n_v and ℓ_v are shown in Figs.26 to 28.

An unusual feature of these results is the increase in directional stability for the 'complete aircraft' configurations at constant tail setting with increasing incidence up to approximately 6°; above 6° incidence n_v decreases, (Fig.27). Comparison of the 'complete aircraft' values of n_v with those for the 'fin and tail off' case shows that these variations of directional stability with incidence are due mainly to changes in the empennage effectiveness. At all incidences the empennage effectiveness decreases with increasing negative tail setting, with the result that there is a much more pronounced loss of n_v with increasing incidence for the trimmed configuration than for the constant tail setting cases, (Fig.29).

4.3 Drag

Drag polars for the three tailplane settings tested, viz. -4°, -10°, -14°, and for the tailplane and fin-off case are shown in Figs.30 to 33. Parabolae of the form $C_D = C_{D_0} + \frac{K}{\pi A}(C_L - C_{L_0})^2$, where A is the aspect ratio of the wing, have been fitted to these curves up to a lift coefficient of 0.5, (above this value the polars cease to be parabolic). The variations with Mach number of the resulting values of minimum drag coefficient, C_{D_0}, and of induced drag factor, K, are plotted in Figs.34 and 35 respectively. The lift coefficient at minimum drag, C_{L_0}, does not appear to vary with Mach number, and the values obtained by fitting the parabolae are as follows:-

η	-4°	-10°	-14°	Tailplane and fin off
C_{L_0}	0.015	0.003	0	0.023

4.4 Effect of the rudder

Rudder power (Figs.36 and 37) was determined from a comparison of results with nominal rudder settings of 0, and -5°, for a tailplane setting of -4°. The rolling moment derivative due to rudder $-\ell_\zeta$, was too small to be measured. The plotted values of $-n_\zeta$ and y_ζ refer to zero angle of sideslip; the variations with sideslip angle were found to be negligible.

Rudder deflections had no significant effect on stability derivatives, and a comparison of the results from an additional test with a rudder setting of -2.5° and a tailplane setting of -14° with those for a tailplane setting of -4° indicated that rudder power was not measurably affected by tail setting.

4.5 Effect of ailerons

Tests to determine the effects of aileron movement were made with aileron settings 0, -10°, and -20°,* at a tail setting of -4°. The measured values of aileron power at zero sideslip are shown in Figs.38 and 39. The rate of change of rolling moment with aileron angle was found to be independent of aileron setting, and sideslip angle, within the test range; (i.e. for $0 \leq \xi \leq 20^\circ$ and $-6^\circ \leq \beta \leq 6^\circ$).

Movement of the ailerons produces significant side forces and yawing moments, which vary with incidence. These are plotted in Figs.40 and 41 respectively. Also shown in Figs.40 and 41 are the aileron induced side forces and yawing moments measured by Sutton, Hutton and Squire[10] in tests in the 3 ft × 3 ft tunnel at R.A.E. Bedford. They used a model with Type 188 wings and nacelles mounted on an ogive cylinder body without a fin. The results quoted were obtained with an aileron setting of -10° at Mach numbers 1.42 and 1.82. A comparison of the results of the two sets of tests suggests that the side force and yawing moment at zero incidence are due mainly to an induced sidewash at the fin, while the major part of the variation with incidence is due to other causes, such as differential aileron drag and cross-flows on the wings. The rudder angles needed to correct the yawing moment induced by -20° aileron movement at Mach numbers 1.4 and 2.0 have been estimated and are plotted against incidence in Fig.42.

The tests also showed that, except at $M = 1.4$, large aileron angles resulted in appreciable losses in n_v, but only small losses in y_v (Figs.43 and 44). Other derivatives were found to be virtually unaffected by ailerons.

4.6 Effect of air-brakes

Results of the tests with fully-open air-brakes were compared with those for the clean aircraft configuration with a tailplane setting of -4°.

The effect of the air-brakes on minimum drag coefficient is shown in Fig.45 and the effect on induced drag factor in Fig.46. Unlike the clean aircraft case, values of lift coefficient at minimum drag were not the same for each Mach number. Values obtained are as follows:

M	1.4	1.6	1.8	2.0
C_{L_o}	0.015	0.020	0.025	0.030

With the air-brakes extended there were significant reductions in longitudinal stability (Fig.47), and lateral stability (Fig.48).

---

* $\xi = -10^\circ$ means port aileron 10° down starboard aileron 10° up.

4.7 Effect of spill vents

Tests were made with the nacelle spill-vents fully open and each nacelle exit mass flow reduced by about 50%. With the exception of drag, the results were compared with those for the clean aircraft (tailplane setting -4°). No significant effect of spill-vents was observed. Since the internal drag of the ducts with spill vents open could not be calculated, it was not possible to determine the change in drag due to opening the spill vents.

5 MODEL COMPARISON TESTS

In this section a comparison is made between results obtained on three configurations:-

(a) the clean configuration tested in the 8 ft × 8 ft tunnel, (i.e. twin-sting support and undistorted fuselage);

(b) the model tested in the 3 ft × 3 ft tunnel[4] (i.e. a 1/36th scale single sting model with a distorted rear fuselage);

(c) the 8 ft × 8 ft tunnel model fitted with a distorted rear fuselage and a dummy rear sting.

The object of this comparison is to examine the interference effects of (i) the twin-sting support system used in the present tests ((b) and (c)) and (ii) the enlarged rear fuselage of the 3 ft × 3 ft tunnel model ((a) and (c)). The tests on (b) in the 3 ft × 3 ft tunnel were made at a Reynolds number of 1.2×10^6, compared with 2.5×10^6 for (a) and (c) in the 8 ft × 8 ft tunnel. As the 3 ft × 3 ft tunnel tests did not include measurements of axial force, normal force coefficients instead of lift coefficients are used in this comparison.

Considering firstly the lateral stability, comparisons of the derivatives y_v and n_v for the three configurations are shown in Figs.49 and 50.* The $\eta = -4^\circ$ results show that the twin-sting support has little effect on the lateral derivatives, but the rear fuselage distortion increases both $-y_v$ and n_v considerably.

Since the twin-sting support has only a small effect on y_v and n_v the fin off values for configuration (c) will be close to those measured for configuration (b). Thus the fin-off comparison between (a) and (b) suggests that only a small part of the increased stability of configurations (b) and (c) is due to a side force on the enlarged rear fuselage, the major part being due to an increase in fin effectiveness.

The analysis of the effects of the changes in configuration on longitudinal stability is not so conclusive as that for lateral stability. This is due to the absence of results for configuration (c) with tail settings different from -4° and, in particular, to the absence of tail off results. A comparison of the available data, in the form of plots of pitching moment against normal force at constant Mach number, is shown in Fig.51. It can be seen that, for the tail and fin off cases, configuration (b) is slightly more stable than (a); and that, with the tail and fin on, there is very little difference between the three configurations for $\eta = -4^\circ$, whereas, for $\eta = -10^\circ$,

* Configuration (b) was not tested at M = 1.4. At M = 1.8 ($\eta = -4^\circ$) and M = 1.6, 1.8 and 2.0 (tailplane and fin off) lateral tests were made for $\alpha = 0$ only.

(b) is slightly less stable than (a). A more sensitive comparison between (a) and (b) is given by the plots of downwash at the tailplane position in Fig.52 and of tailplane power in Fig.53.

It is probable that the small differences between (a) and (b) tail off are due to the fuselage distortion and not the sting support. The differences in stability with the tail on are due to the change in tailplane power. It does not appear possible, from the evidence available, to decide whether the 10% greater tail effectiveness of the larger model is caused by the rear fuselage or the twin supports; however the results of the tests of Ref.2 at M = 1.3 suggest that the rear fusleage distortion does decrease the tail effectiveness by roughly this amount.

6 CONCLUSIONS

The tests over the Mach number range 1.4 to 2.0 have shown that, in general, with the moment reference point of the model at $0.18\,\bar{c}$:-

(1) Longitudinal stability decreases with increasing incidence for lift coefficients greater than 0.2 approximately.

(2) The directional stability of the trimmed model decreases with increasing incidence, for incidences above 3°.

(3) Both longitudinal and lateral stability are decreased by extension of the air-brakes.

(4) Aileron movement results in significant variations of yawing moment and side force with incidence, and, at the higher Mach numbers, large movements of the ailerons cause a decrease in directional stability.

(5) Nacelle spillage does not have any significant effect on stability.

LIST OF SYMBOLS

A	wing aspect ratio
b	wing span
$\bar{c}$	standard mean chord
S	gross wing area
q	free stream dynamic pressure
M	free stream Mach number
C_L	lift coefficient = lift force /qS
C_Y	side force coefficient = side force/qS
C_D	drag coefficient = drag force /qS

LIST OF SYMBOLS (CONTD.)

C_m	pitching moment coefficient = pitching moment/$q\,S\,\bar{c}$
C_ℓ	rolling moment coefficient = rolling moment/$q\,S\,b$
C_n	yawing moment coefficient = yawing moment/$q\,S\,b$
C_N	normal force coefficient = normal force/$q\,S$
α	angle of incidence of nacelle centre lines
β	angle of sideslip
η	tailplane angle, measured relative to nacelle centre lines
ζ	rudder angle
ξ	aileron angle
ε	downwash angle, measured relative to free stream
y_v	side force due to sideslip = $\frac{1}{2}\,\partial C_Y/\partial\beta$, β in radians
ℓ_v	rolling moment due to sideslip = $\partial C_\ell/\partial\beta$, " "
n_v	yawing moment due to sideslip = $\partial C_n/\partial\beta$, " "
y_ζ	side force due to rudder = $\partial C_Y/\partial\zeta$ ζ in radians
n_ζ	yawing moment due to rudder = $\partial C_n/\partial\zeta$ " "
ℓ_ξ	rolling moment due to aileron = $\partial C_\ell/\partial\xi$ ξ in radians
C_{D_o}	minimum drag coefficient
C_{L_o}	value of C_L for which $C_D = C_{D_o}$
K	induced drag factor = $\pi A\ \partial C_D/\partial(C_L - C_{L_o})^2$

LIST OF REFERENCES

No.	Author	Title, etc.
1	-	A short review of research and development for the Bristol Type 188 supersonic research aircraft. Bristol Aircraft Ltd. PR/188/DIV/580. June, 1959.

LIST OF REFERENCES (CONTD.)

No.	Author	Title, etc.
2	Landon, R. H.	Longitudinal and lateral stability tests and effects of controls on a 1/12th scale model of the Bristol Type 188. Unpublished Aircraft Research AssAssn. Report.
3	Leathers, J. W.	Low speed wind tunnel tests on a 1/10th scale model of a twin jet aircraft, Bristol Type 188. RAE Tech. Note No. Aero 2515. ARC 20047. July 1957.
4	Squire, L. C.	Wind tunnel tests up to M = 2.0 on a model of the supersonic research aircraft ER 134 (Bristol 188). RAE Report No. Aero 2633. ARC 22064. December, 1959.
5	Cook, T. A.	A note on the calibration of strain gauge balances for wind tunnel models. RAE Tech. Note No. Aero 2631, Dec., 1959.
6	Warren, C. H. E.	The definitions of the angles of incidence and of sideslip. ARC C.P.124, August, 1952.
7	-	Report of the Definitions Panel on the definitions of the thrust of a jet engine and of the internal drag of a ducted body. ARC C.P.190. May, 1954.
8	Mabey, D. G. Arlott, G. P.	Measurement of aileron hinge moment on a 1/15th scale half-model of the Bristol 188. Unpublished M.O.A. Report.
9	Stanbrook, A.	The lift-curve slope and aerodynamic centre position of wings at subsonic and supersonic speeds. RAE Tech. Note No. Aero 2328. ARC 17615, Nov., 1954.
10	Sutton, E. P. Hutton, P. G. Squire, L. C.	Wind tunnel tests at Mach numbers up to 1.8 on a model with 1/36 scale wings and nacelles of a twin engined supersonic aircraft, (Bristol 188). ARC C.P. 798, February, 1958.

TABLE 1

Principal details of the model

Scale:	1/12th	
Wing:-		
	Area S (gross):-	2.75 ft^2
	Span b	2.924 ft
	Aspect ratio A	3.108
	Standard mean chord $\bar{c}$	0.941 ft
	Aerodynamic mean chord $\bar{\bar{c}}$	1.025 ft
	Distance of leading edge of $\bar{\bar{c}}$ aft of leading edge of inboard wing	0.143 ft
	Dihedral	0
	Wing-body angle	2°
	Sweep back of leading edge:	
	Inboard of nacelles	0
	Outboard of nacelles	38°
	Aileron horn	65°
	Sweep forward of trailing edge	5°
	Section (excluding aileron horns): Biconvex, circular arc, with sharp leading edge; t/c = 4%; maximum thickness at 55% on inboard wing, and 51% outboard	
	Section (aileron horns): faired from above to 8% RAE 104 at tip.	
	Gap between wing and aileron horn	0.008 in.
Fuselage:-	Length	5.917 ft
Fin:-		
	Area	0.528 ft^2
	Sweepback of leading edge	64°
	Section: Modified RAE 104 with constant maximum thickness. 4% t/c at tip chord	

TABLE 1 (CONTD.)

Tailplane:-

Area		0.484 ft^2
Span		1.292 ft
Aspect ratio		3.4
Root chord		0.50 ft
Tip chord		0.25 ft
Section: $4\frac{1}{2}$% circular arc		
Height of tailplane pivot above nacelle datum lines		0.682 ft

Nacelles:-

Distance outboard of fuselage centre line		0.625 ft

Air-brakes:-

Forward brakes:	gross area	3.03 in^2
	open area	0.89 in^2
Aft brakes:	gross area	3.05 in^2
	open area	0.79 in^2

TABLE 2

List of configurations tested

			Test range*
1	Clean aircraft	tailplane - 4^o	A
2	" "	" -10^o	A
3	" "	" -14^o	B
4	" "	tailplane and fin off	A
5	Ailerons -10^o	tailplane - 4^o	C
6	" -20^o	" -4^o	C
7	Rudder -2.5^o	" -4^o	C
8	" -2.5^o	" -14^o	C
9	" -5.0^o	" -4^o	C
10	Air-brakes extended	" -4^o	C
11	Spill vents open	" -4^o	C
12	Distorted rear fuselage	" -4^o	A

* See Table 3

TABLE 3

Model attitude ranges

Incidence* (degrees)	Sideslip* (degrees)		
	Range A	Range B	Range C
-4	0,±2	0,±2	0
-2	0,±2	0,±2	0
0	0,±1,±2,±4,±6	0,±1,±2,±4,±6	0,±2,±4,±6
2	0,±2	0,±2	0
4	0,±1,±2,±4,±6	0,±1,±2,±4,±6	0,±2,±4,±6
6	0,±2	0,±2	0
8	0,±1,±2,±4,±6	0,±1,±2,±4,±6	0,±2,±4,±6
10	0,±2	0,±2	0
12	0,±2	0,±2	0
14	0	0	0
16		0,±2	
18		0	
20		0,±2	

* Nominal settings

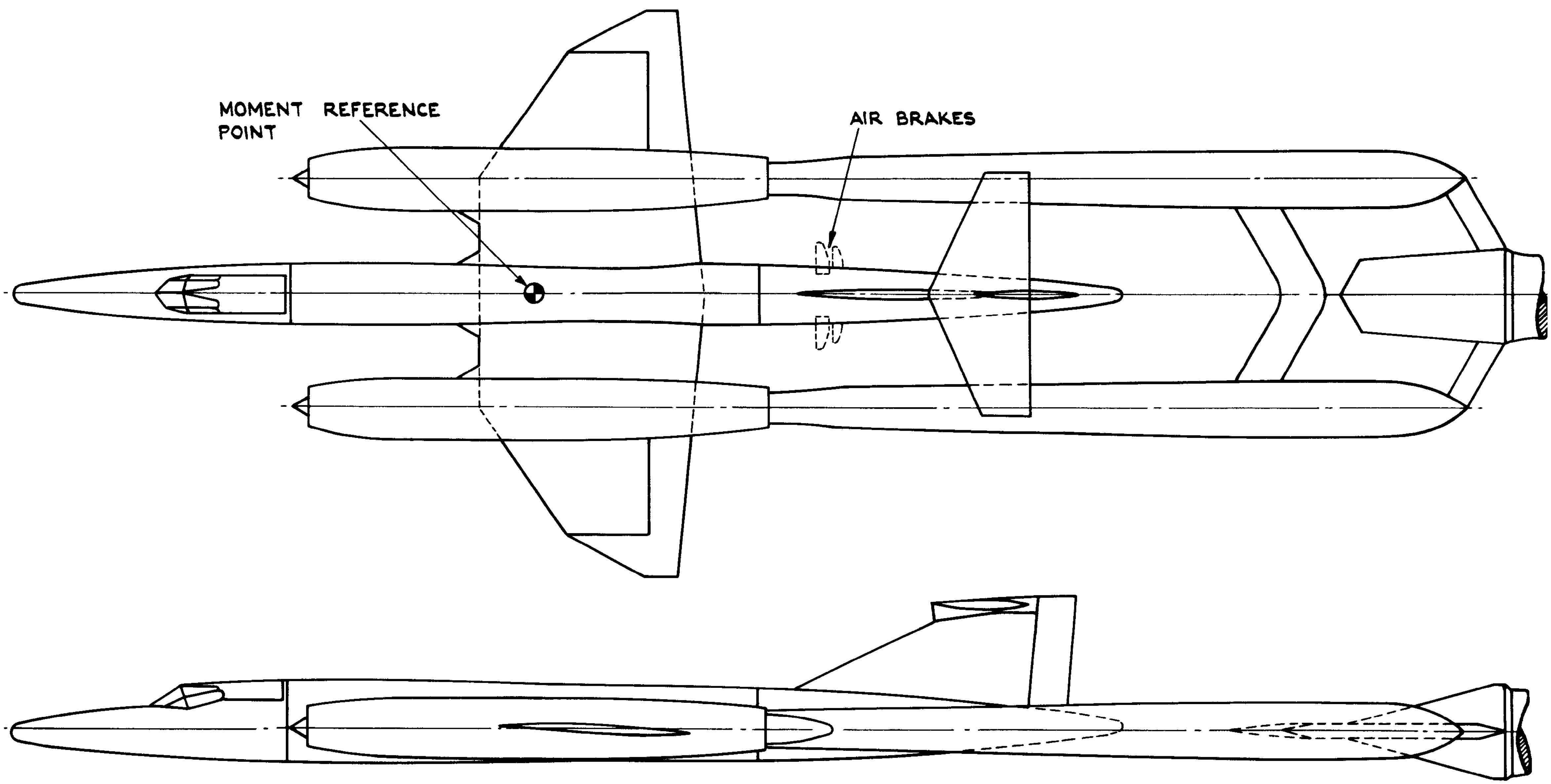

FIG. 1 GENERAL ARRANGEMENT OF MODEL AND SUPPORT SYSTEM.

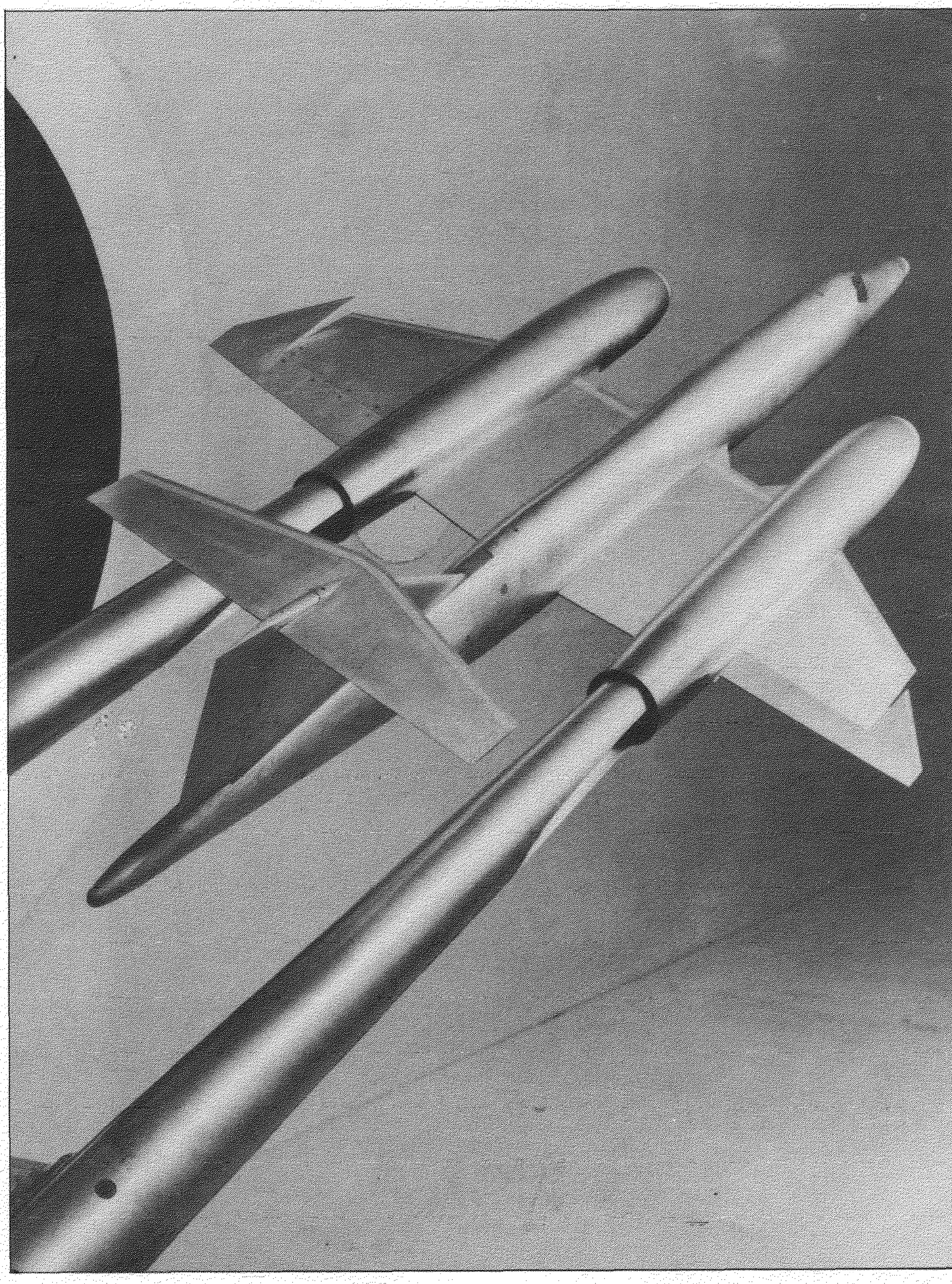

FIG.2. THE MODEL IN THE WIND TUNNEL

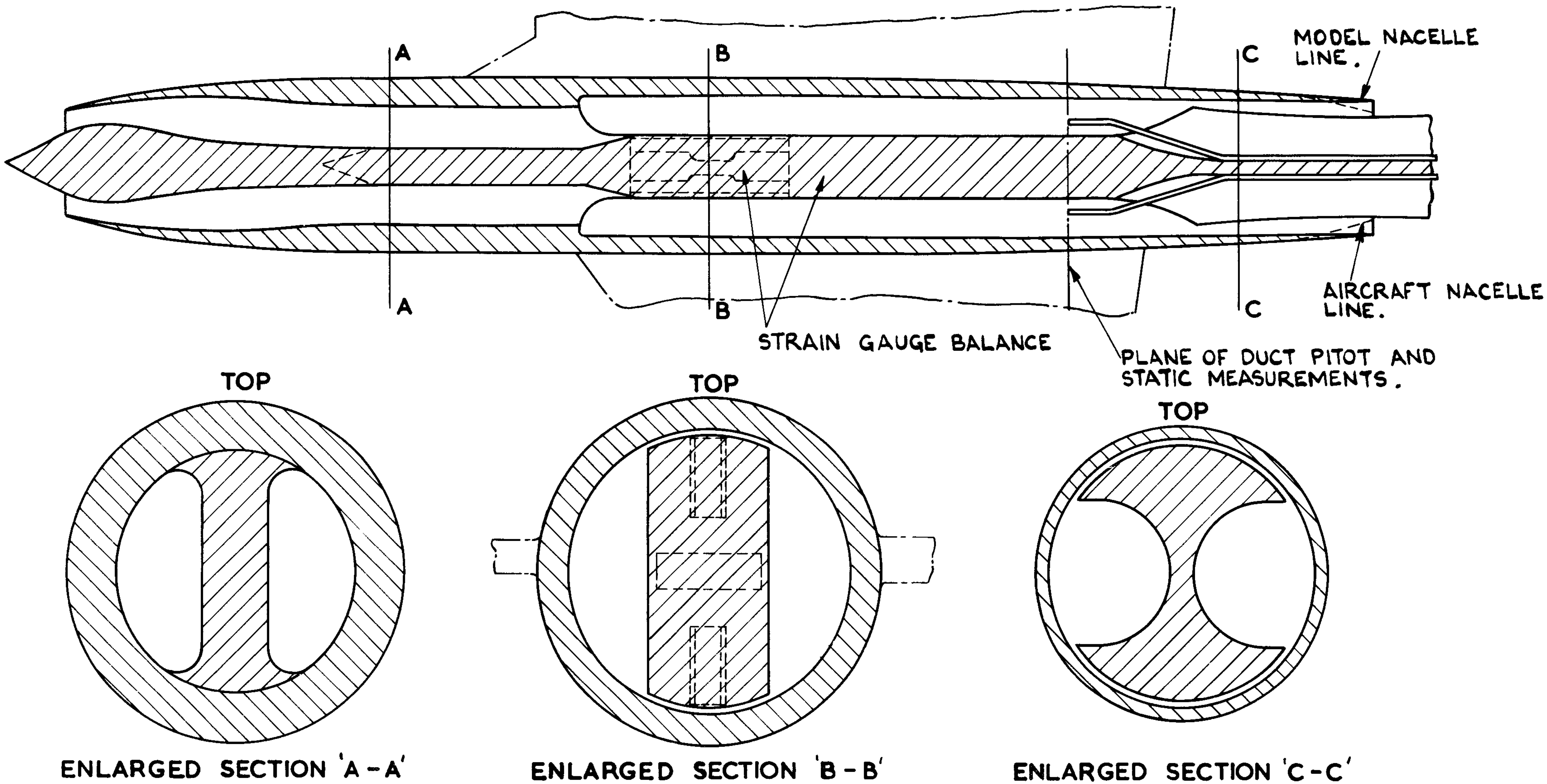

FIG. 3 GENERAL ARRANGEMENT OF NACELLE.

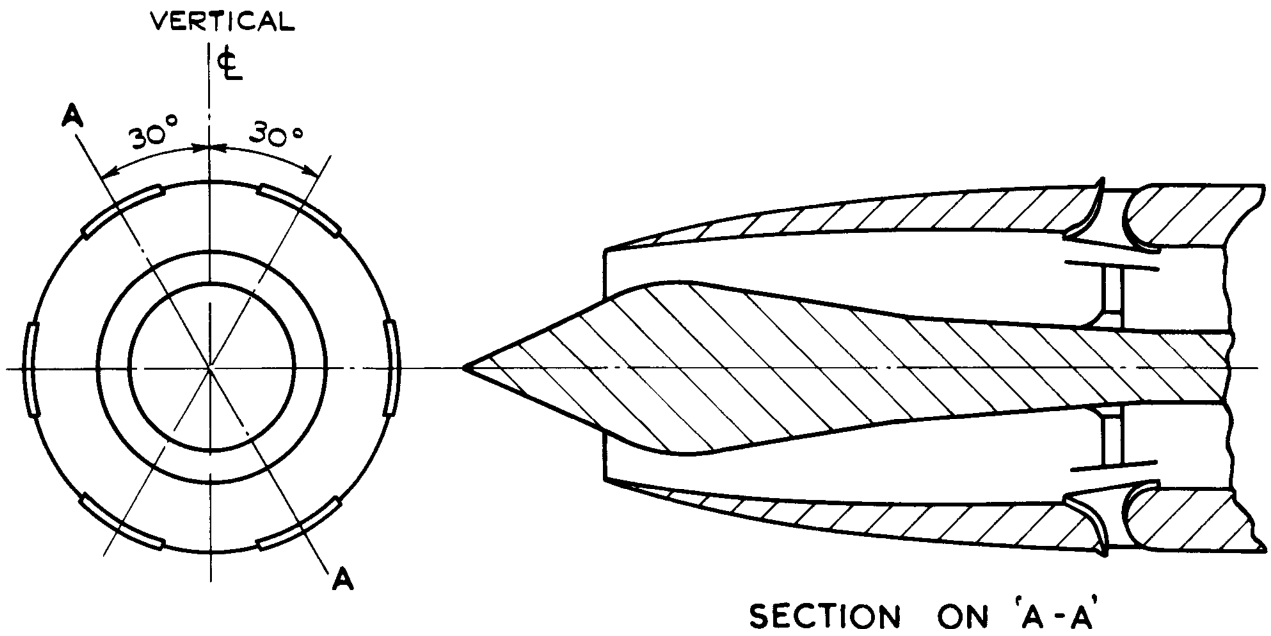

FIG. 4. SPILL VENT ARRANGEMENT.

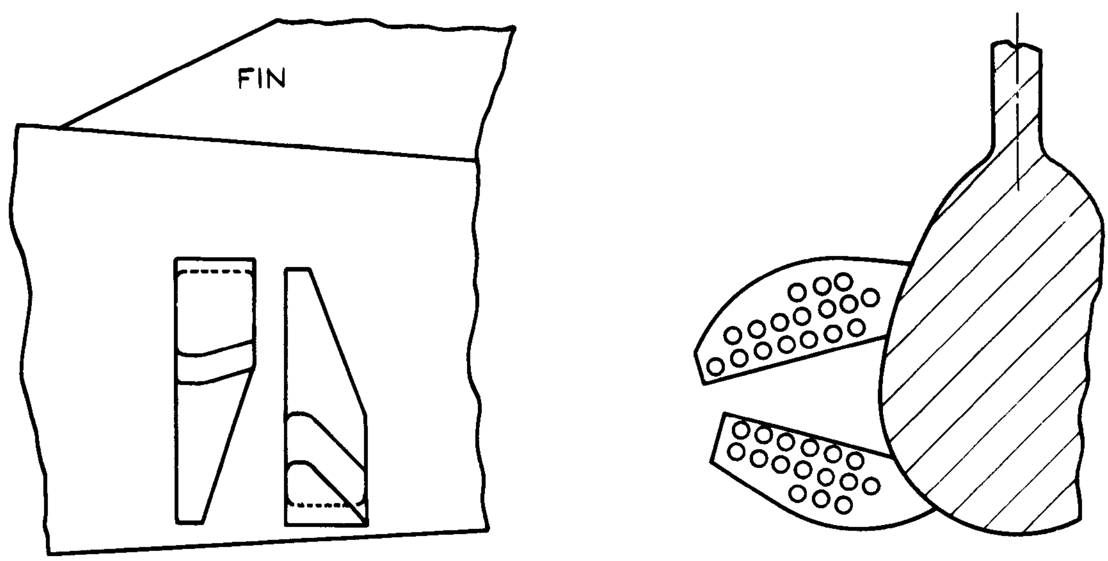

FIG. 5. AIR BRAKE ARRANGEMENT.
(FULLY OPEN POSITION)

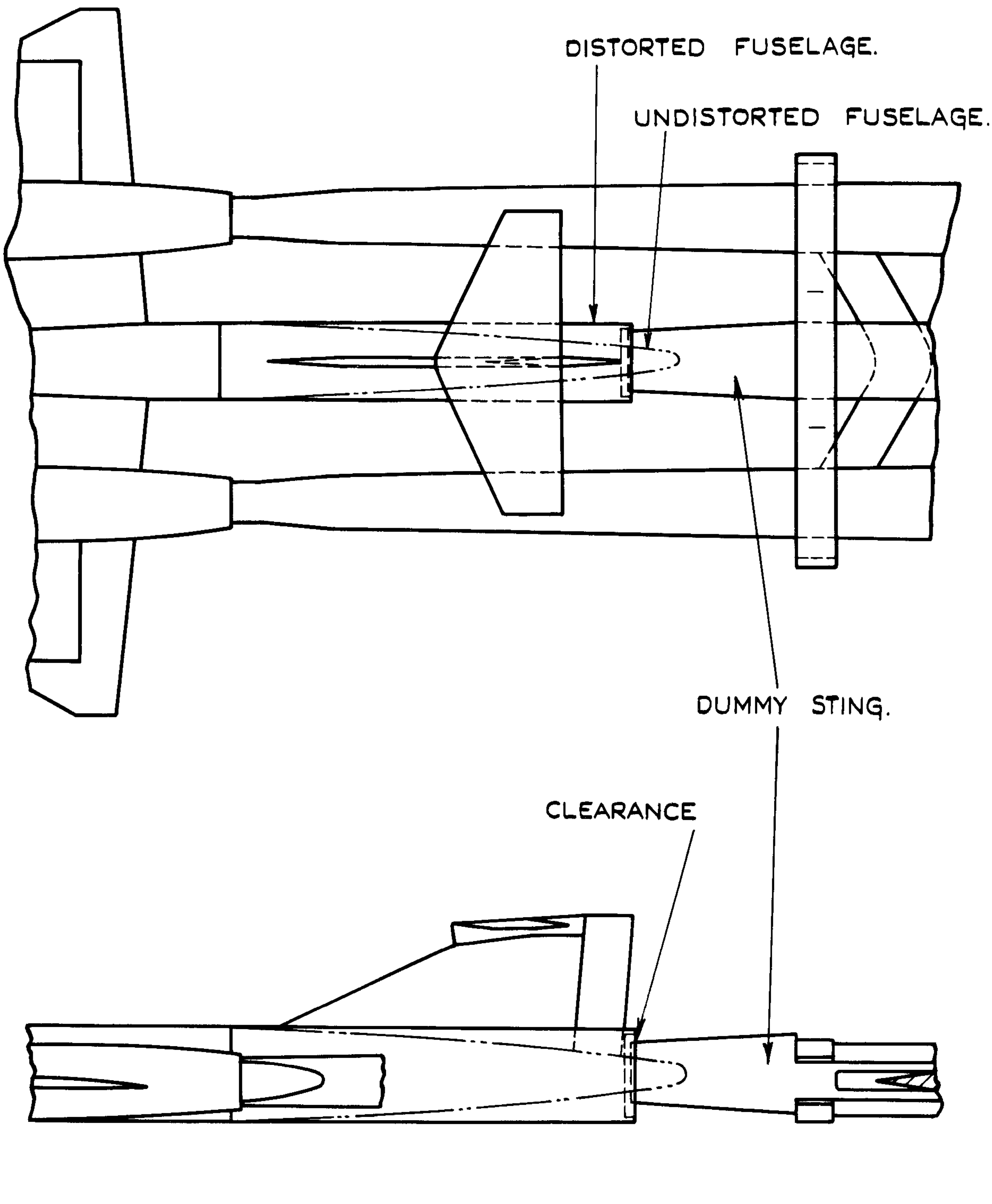

FIG. 6. ARRANGEMENT OF MODEL WITH DISTORTED REAR FUSELAGE AND DUMMY CENTRAL STING.

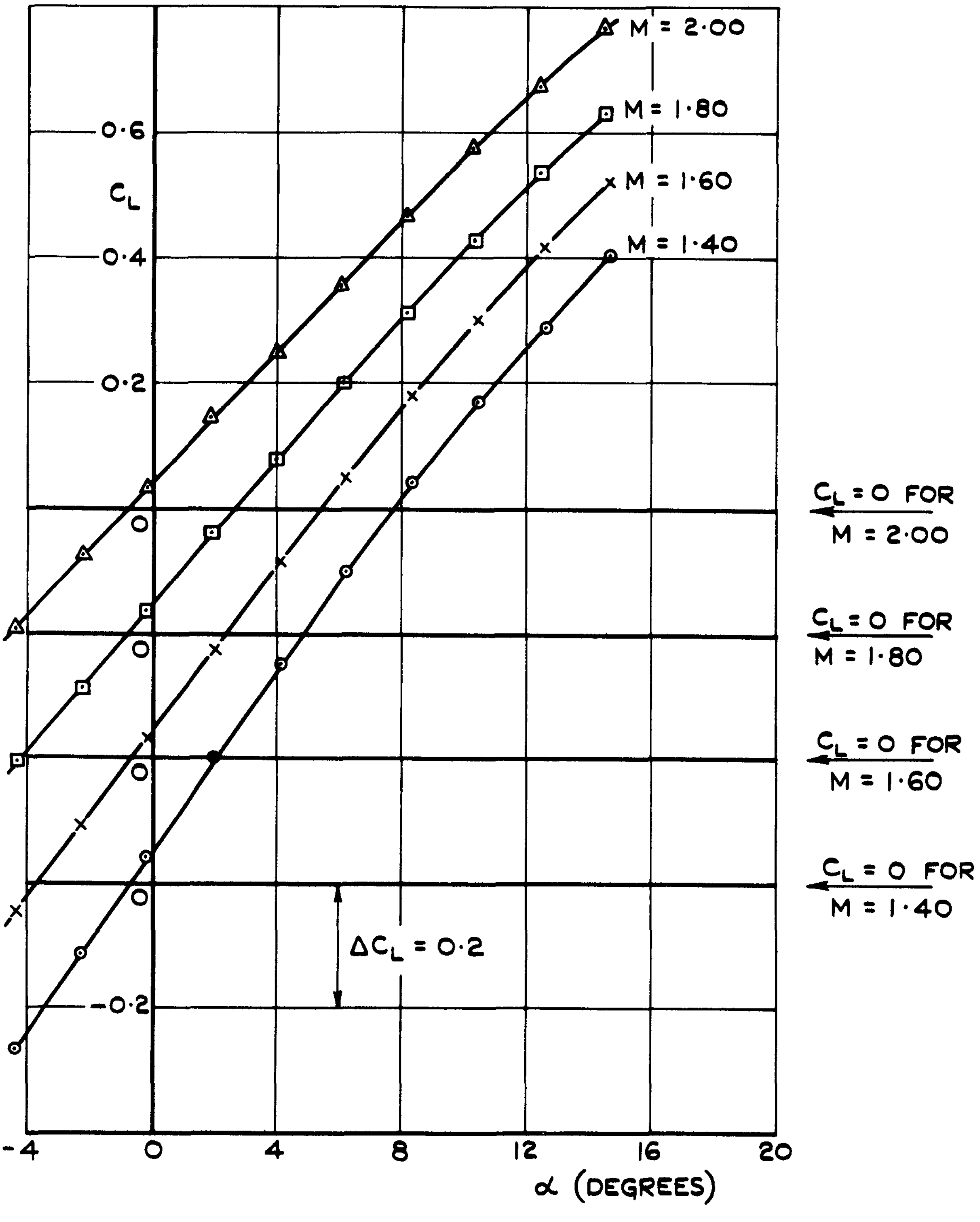

FIG. 7. VARIATION OF C_L WITH α AT CONSTANT MACH NUMBER: $\eta = -4°$.

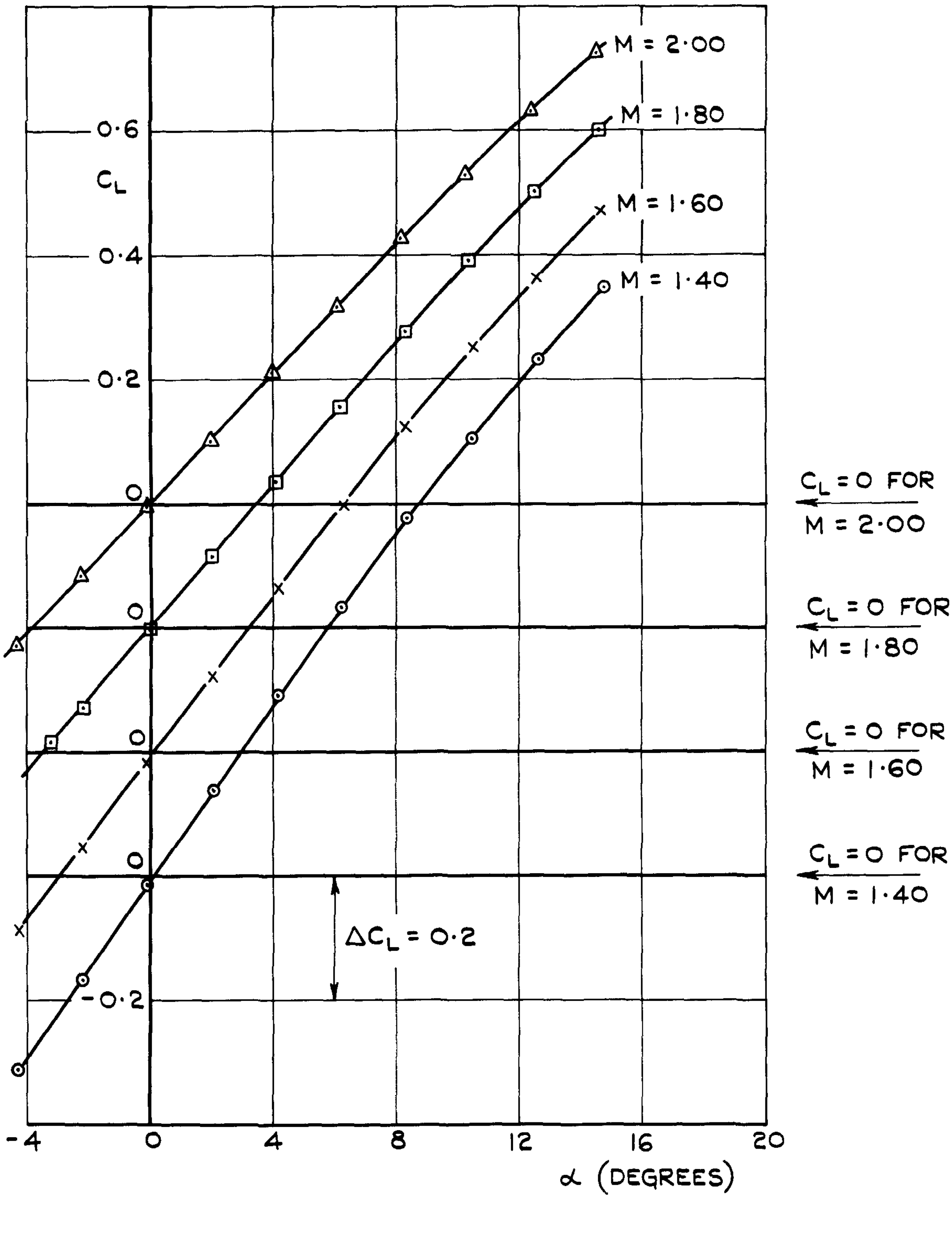

FIG. 8. VARIATION OF C_L WITH α AT CONSTANT MACH NUMBER: $\eta = -10°$.

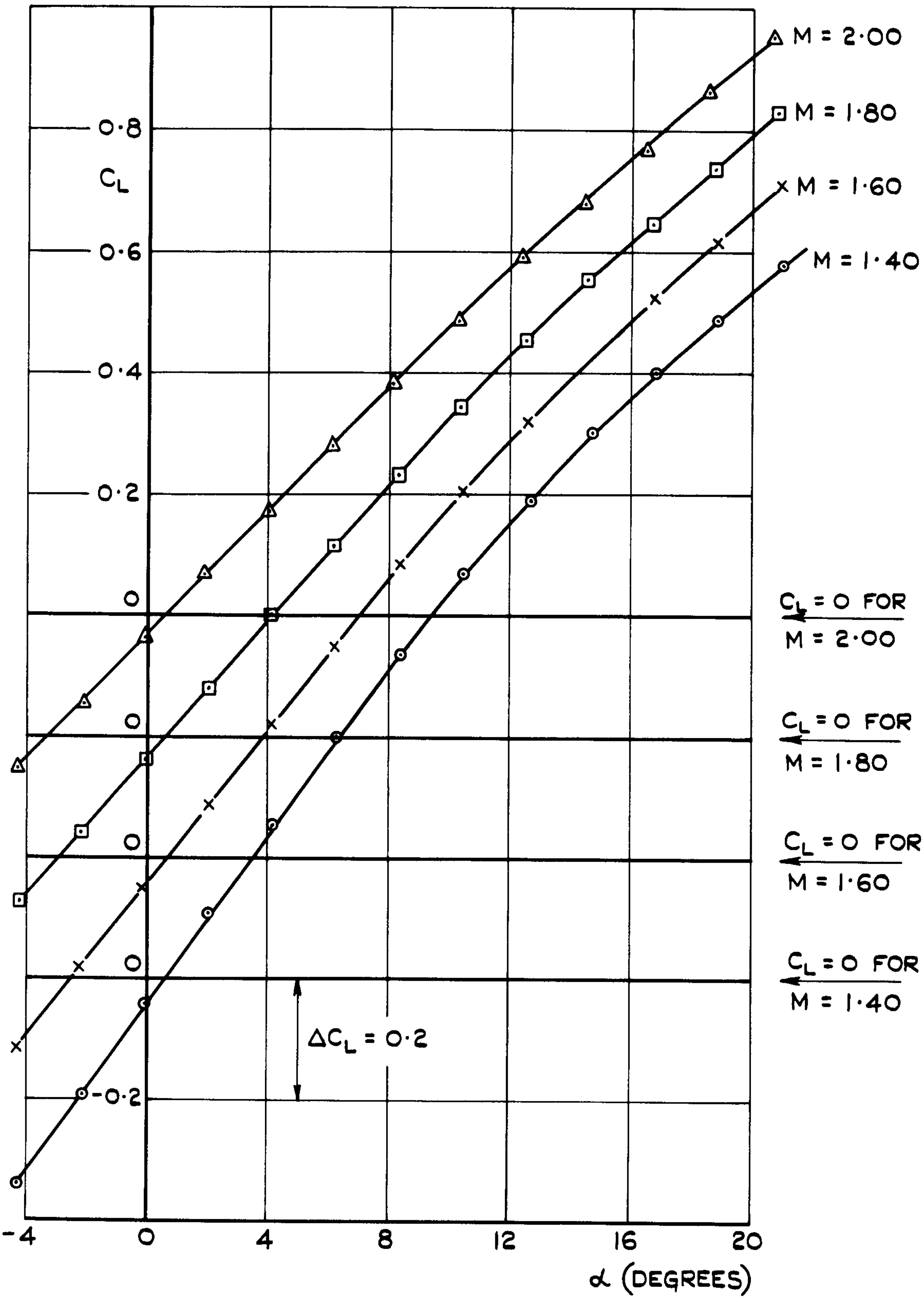

FIG. 9. VARIATION OF C_L WITH α AT CONSTANT MACH NUMBER : $\eta = -14°$

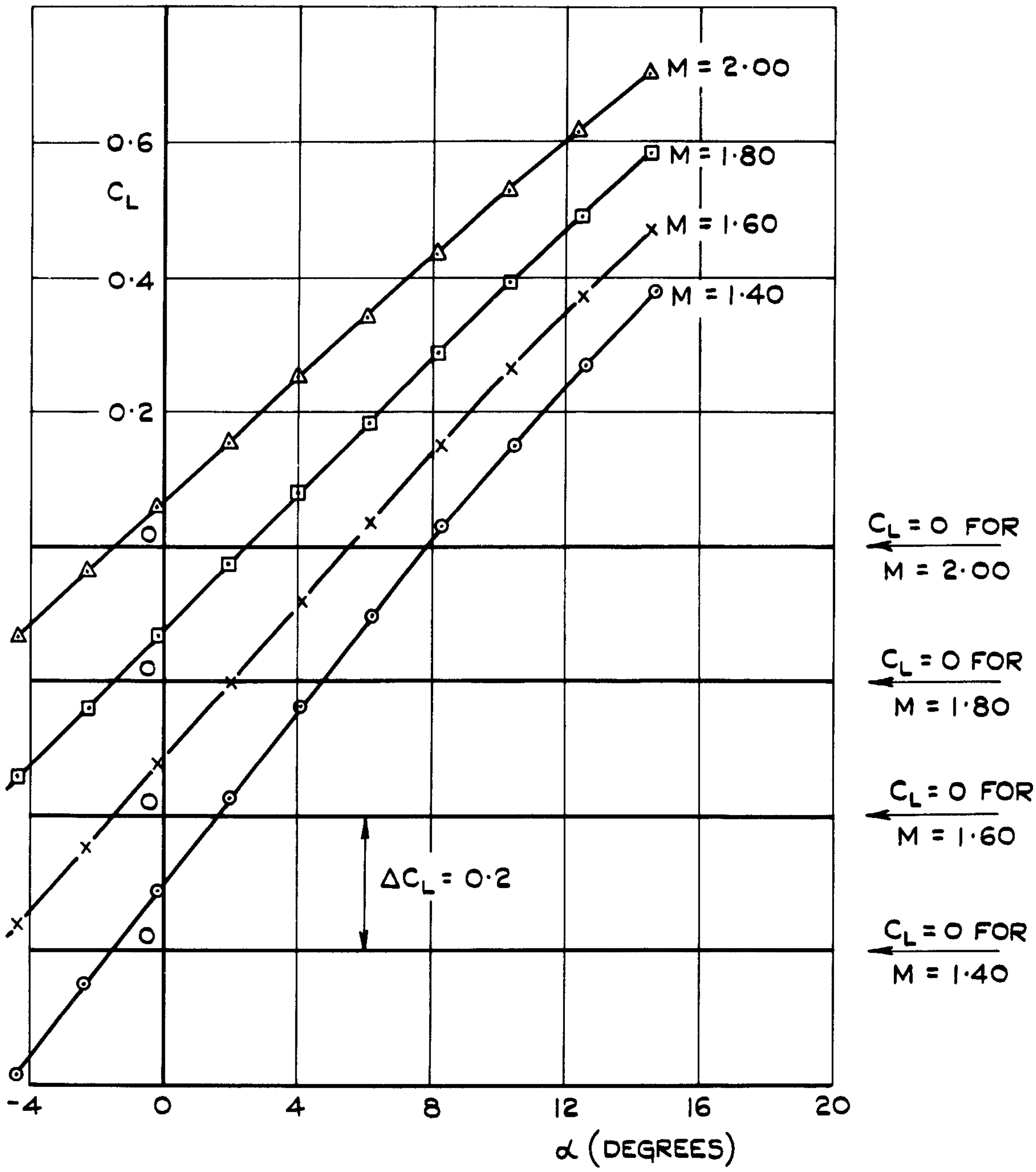

FIG. 10. VARIATION OF C_L WITH α AT CONSTANT MACH NUMBER : TAILPLANE AND FIN OFF.

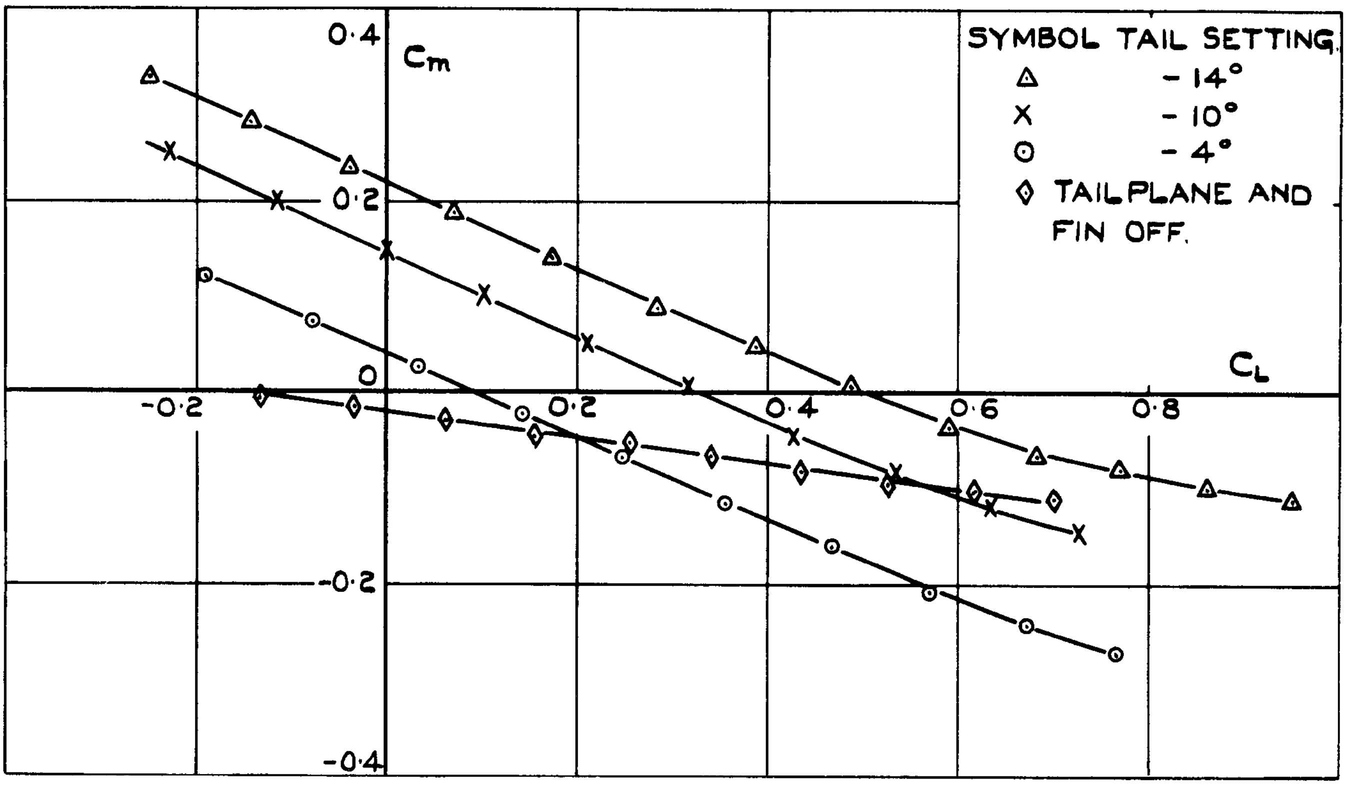

(a) M = 2·00.

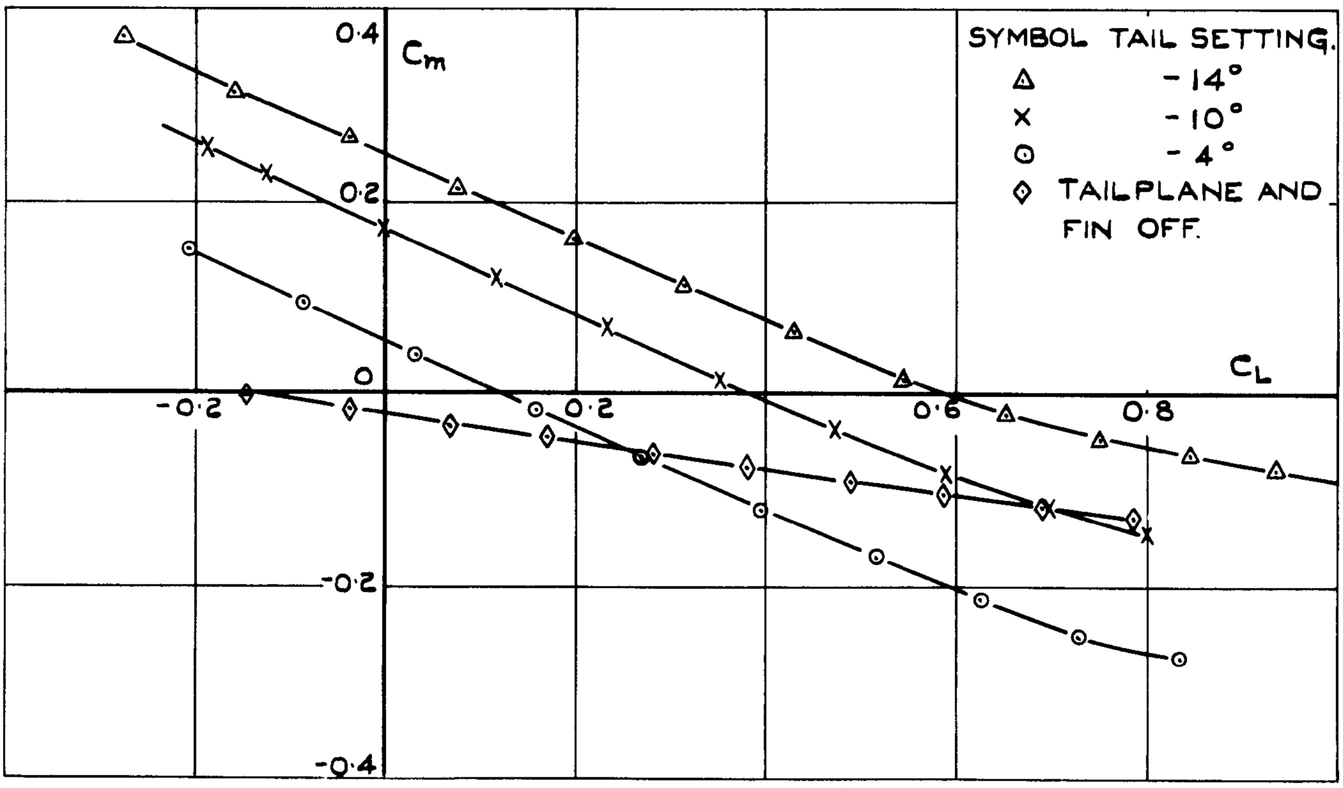

(b) M = 1·80.

FIG. 11. VARIATION OF C_m WITH C_L AT CONSTANT MACH NUMBER.

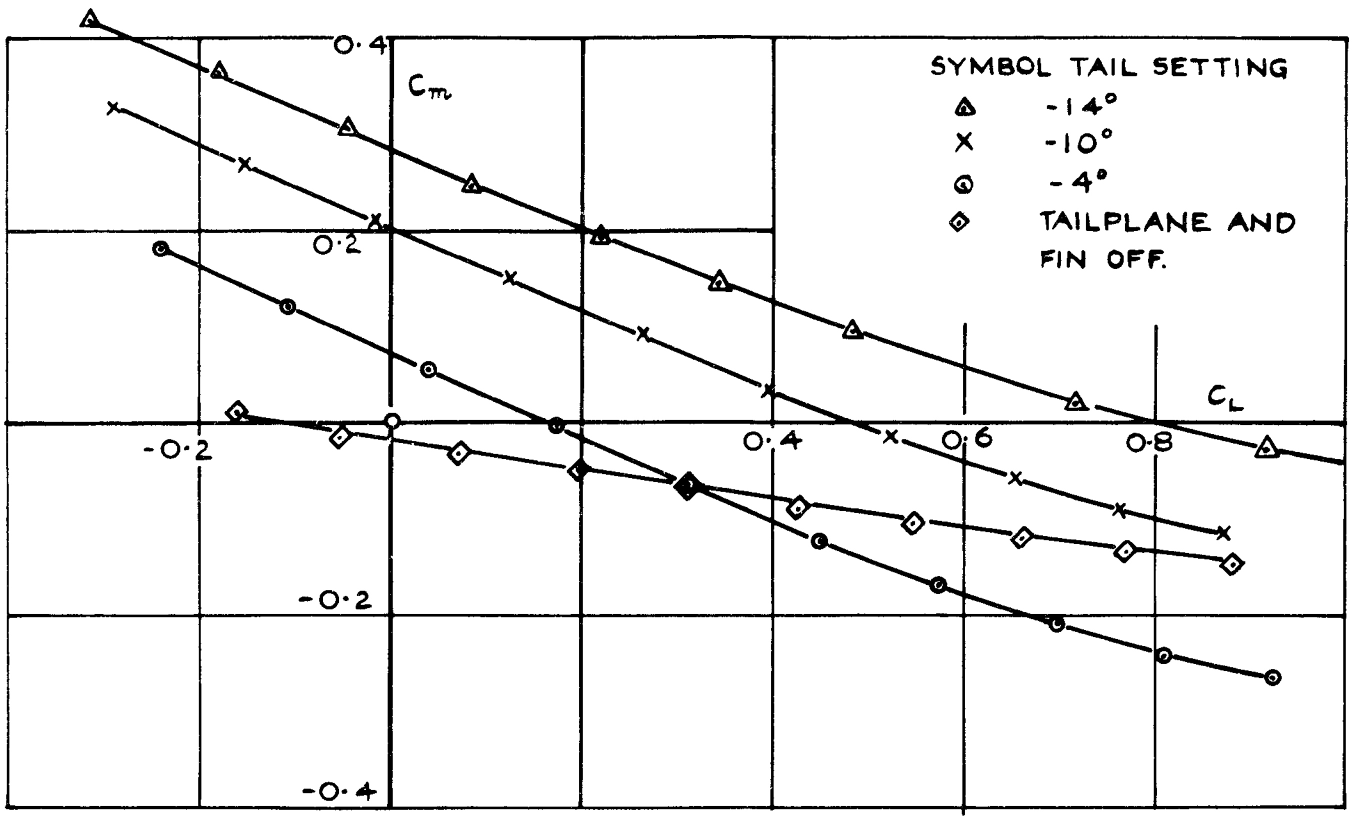

(c) M=1·60

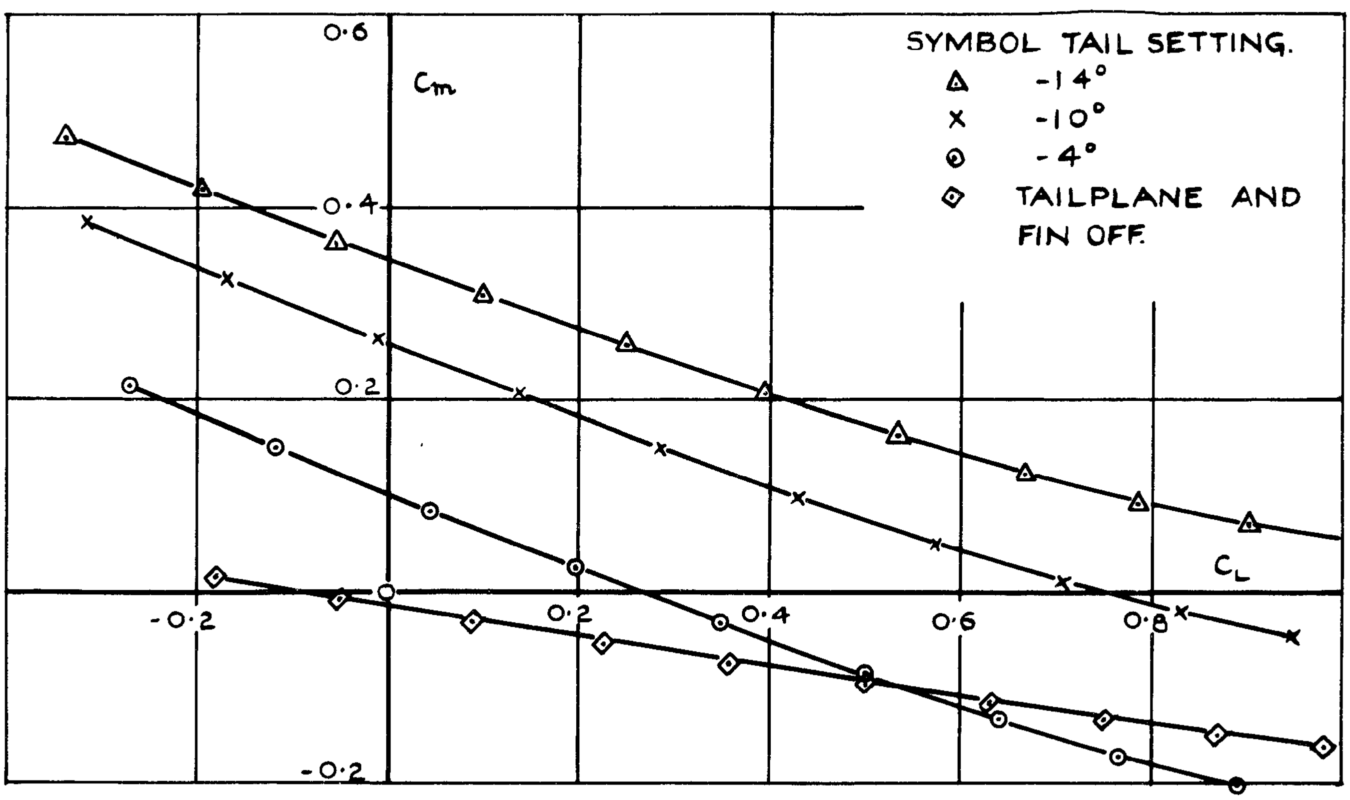

(d) M=1·40

FIG.11. (CONT.) VARIATION OF C_m WITH C_L AT CONSTANT MACH NUMBER.

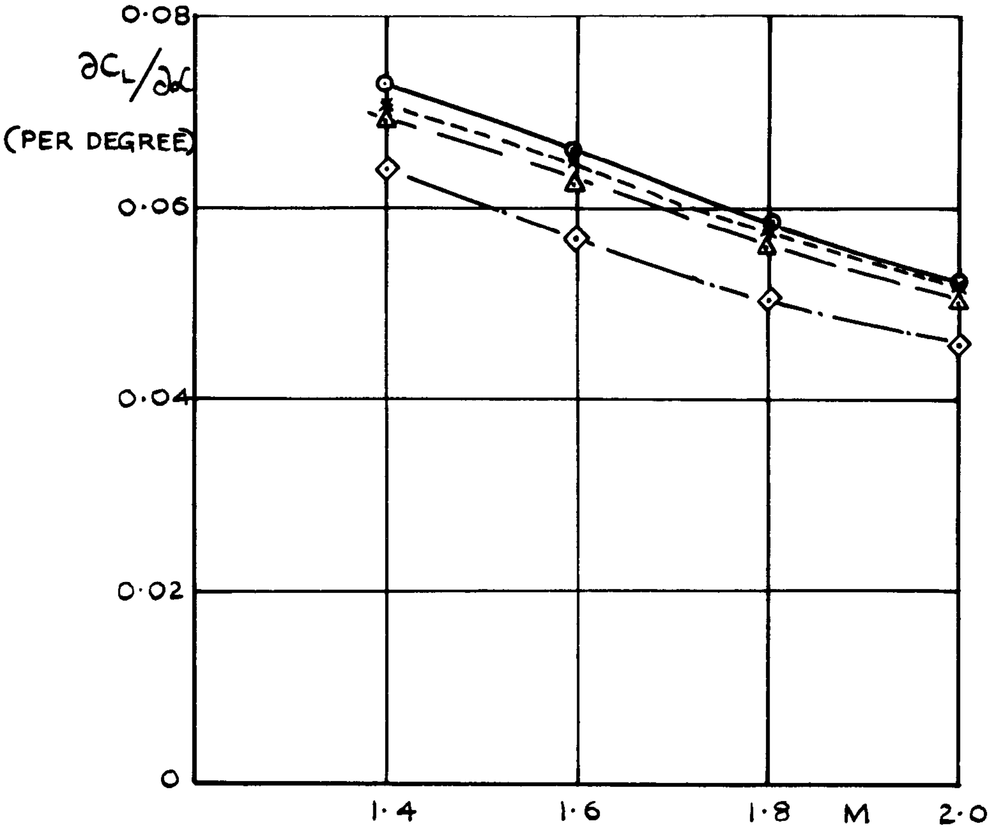

FIG. 12. VARIATION $\partial C_L/\partial \alpha$ AT ZERO INCIDENCE WITH MACH NUMBER.

KEY TO FIGS. 12 AND 13.

—⊙—	TAILPLANE	−4°
---×---	"	−10°
—△—	"	−14°
—◇—	TAIL AND FIN OFF	

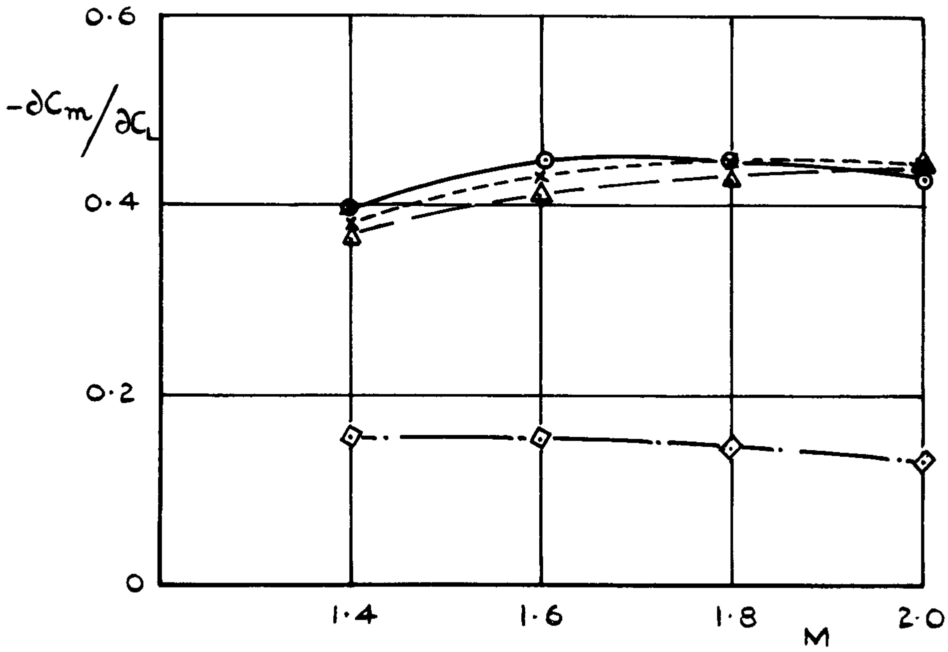

FIG. 13. VARIATION OF $-\partial C_m/\partial C_L$ AT ZERO LIFT WITH MACH NUMBER.

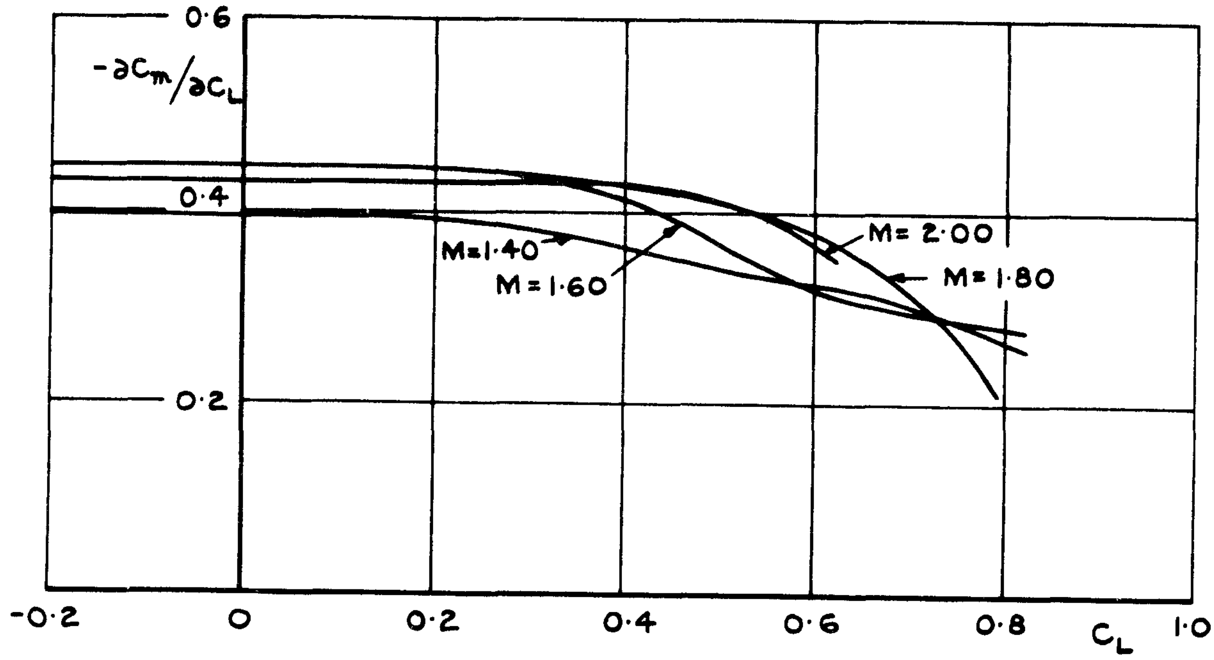

(a) TAILPLANE -4°.

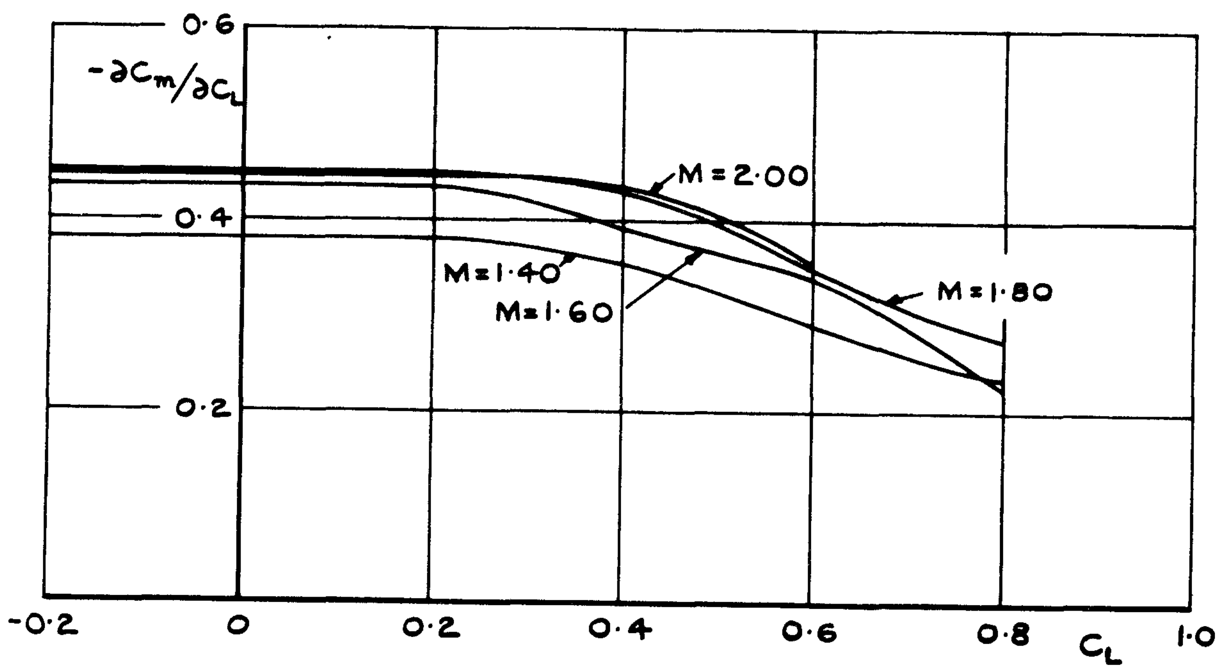

(b) TAILPLANE -10°.

FIG. 14. VARIATION OF $-\partial C_m/\partial C_L$ WITH C_L.

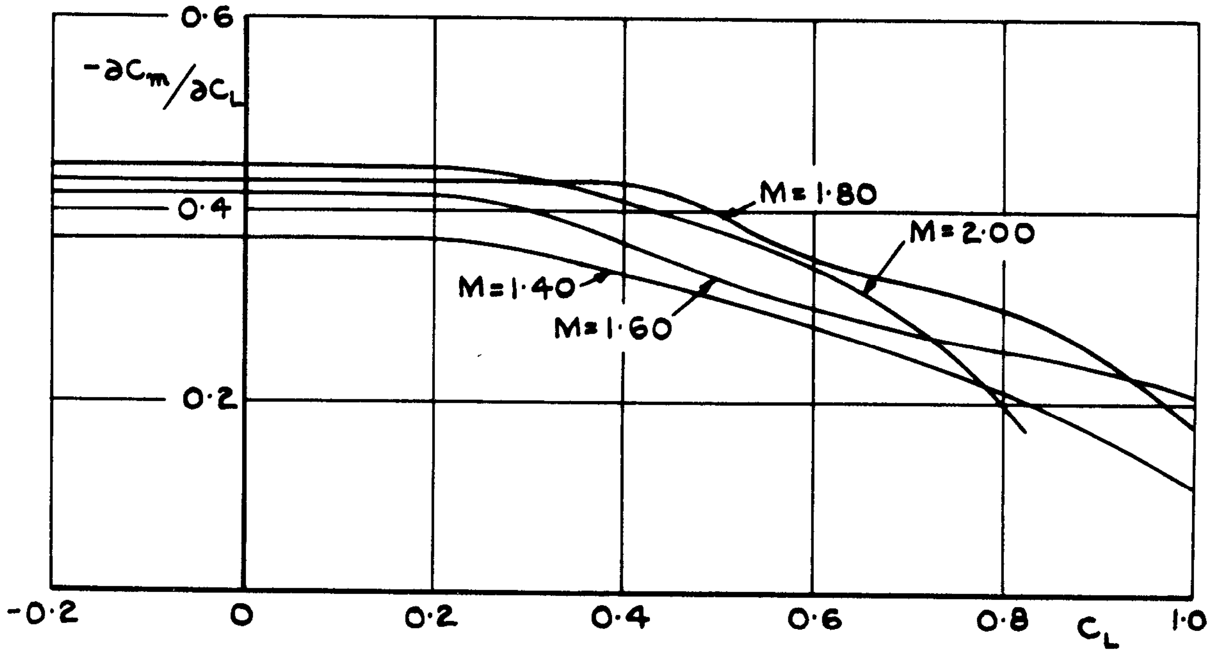

(c) TAILPLANE -14°.

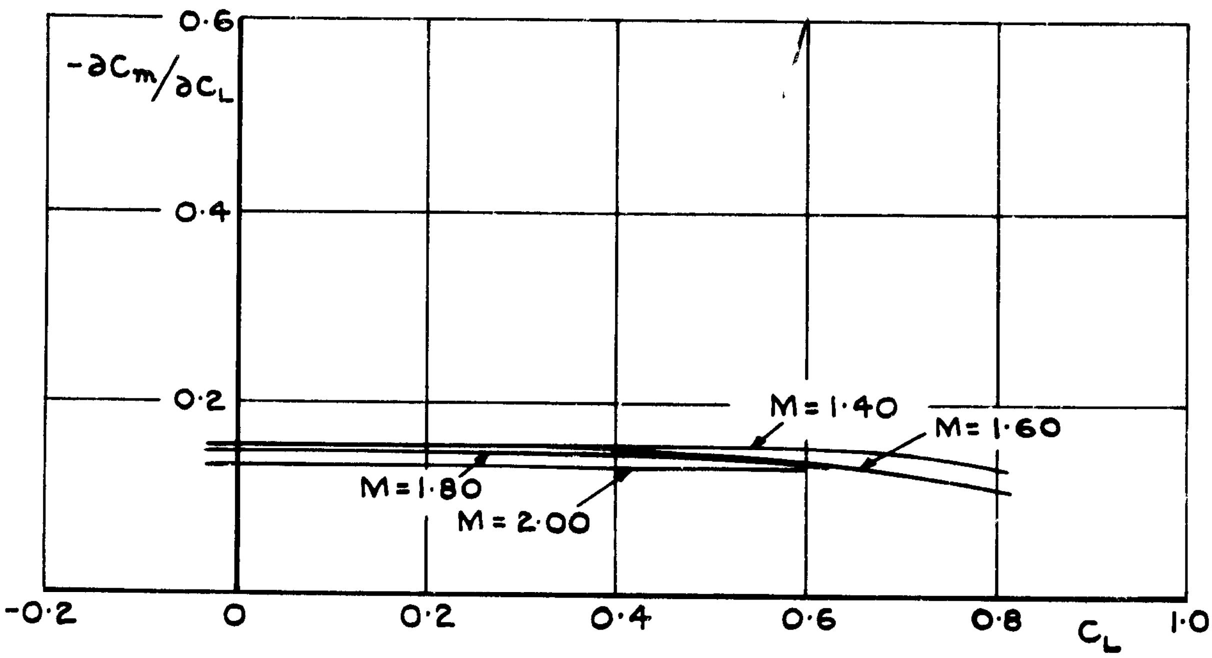

(d) TAIL AND FIN OFF.

FIG. 14 (CONT.). VARIATION OF $-\partial C_m/\partial C_L$ WITH C_L.

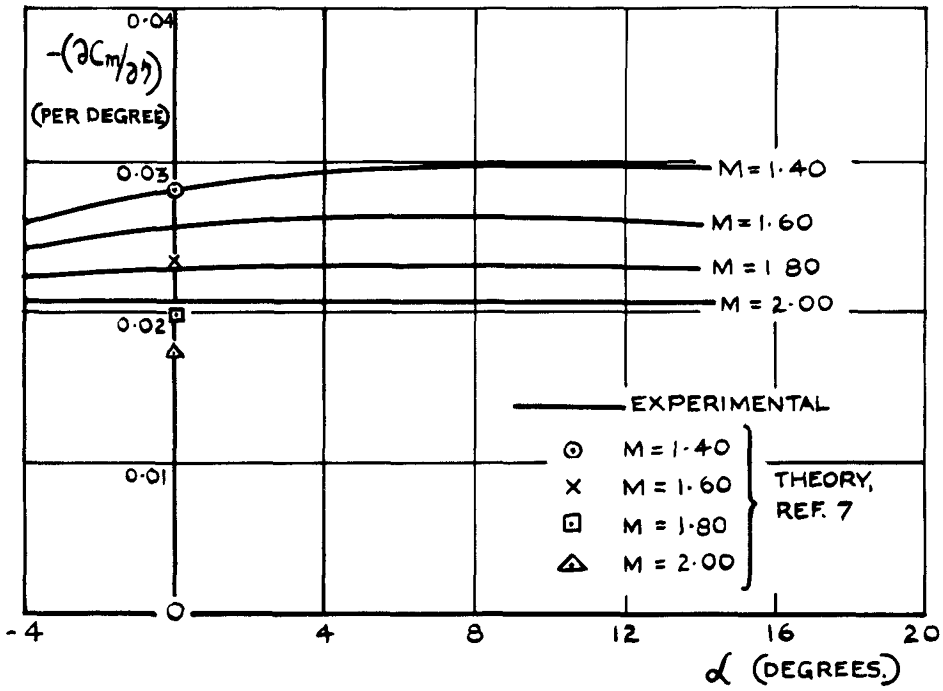

FIG. 15. VARIATION OF TAILPLANE POWER WITH MODEL INCIDENCE.

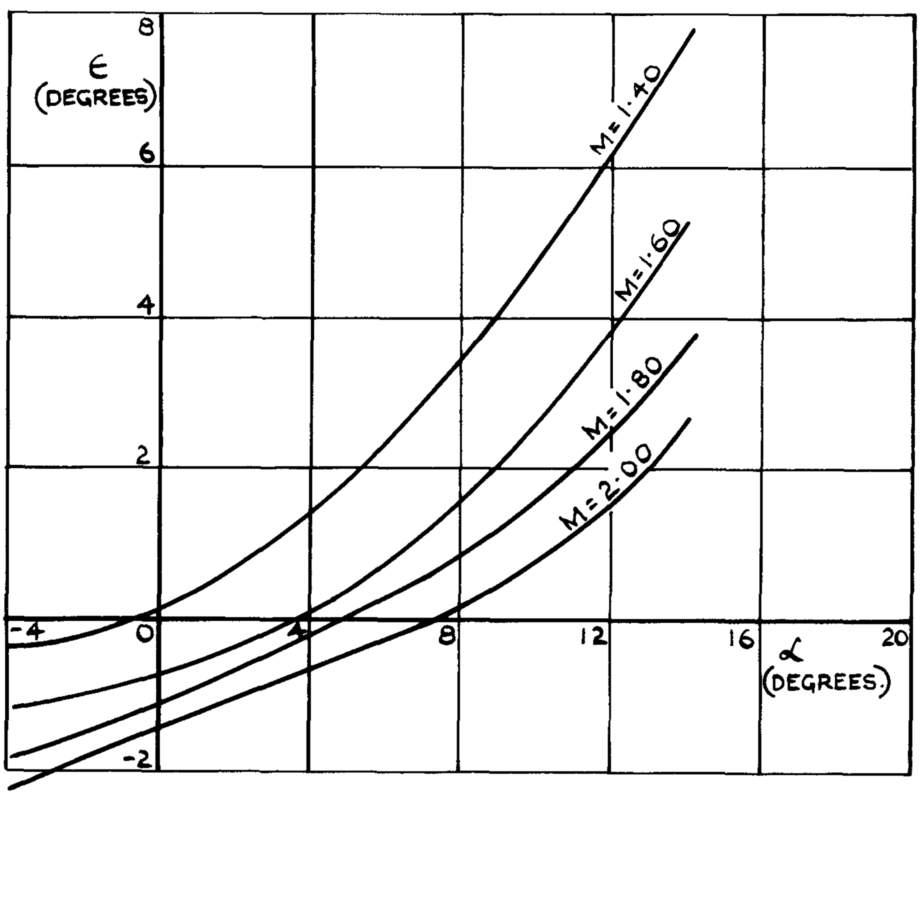

FIG. 16. VARIATION OF DOWNWASH AT POSITION OF TAILPLANE WITH MODEL INCIDENCE.

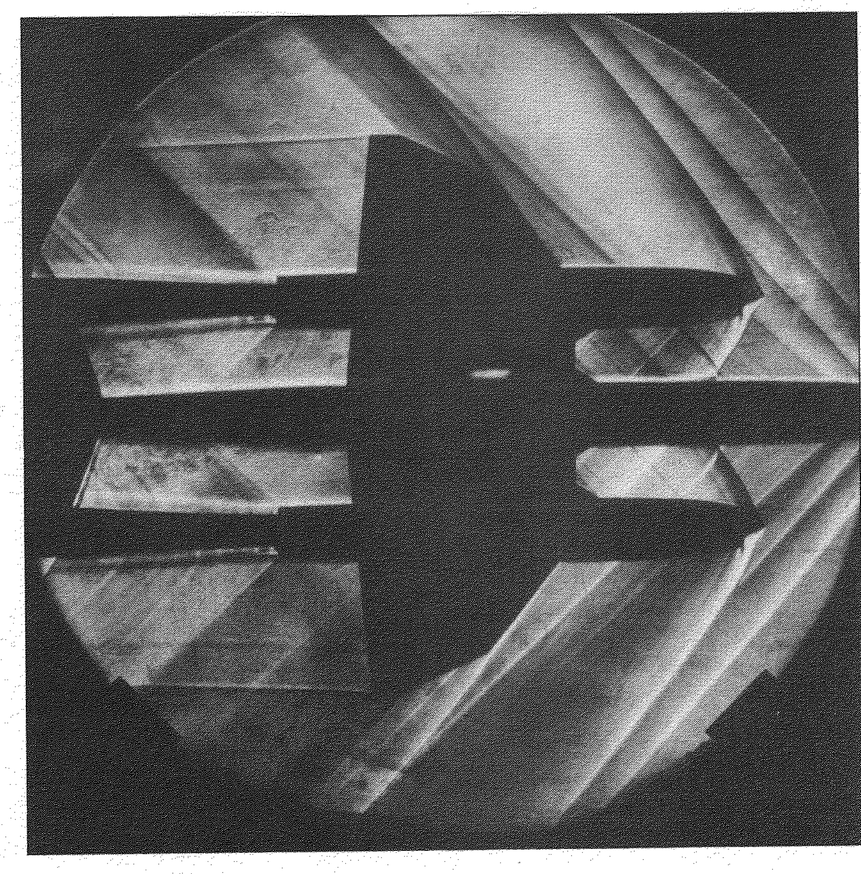

a. PLAN VIEW

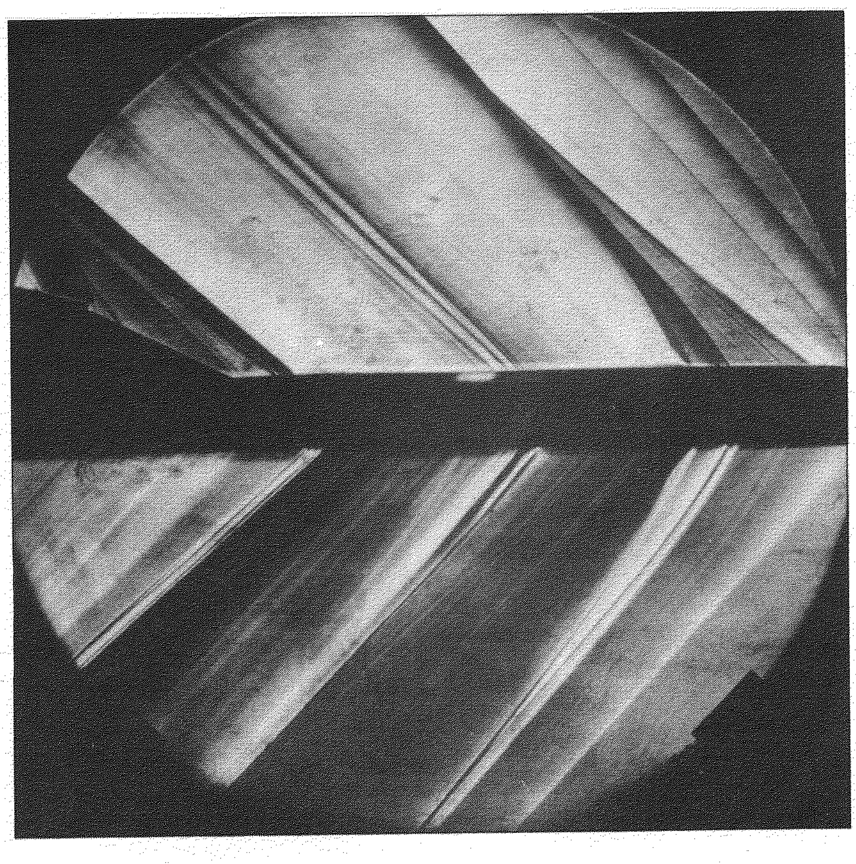

b. SIDE VIEW

FIG.17. SCHLIEREN PHOTOGRAPHS: $M = 1 \cdot 40$

$\alpha = \beta = 0$: Tailplane -10°

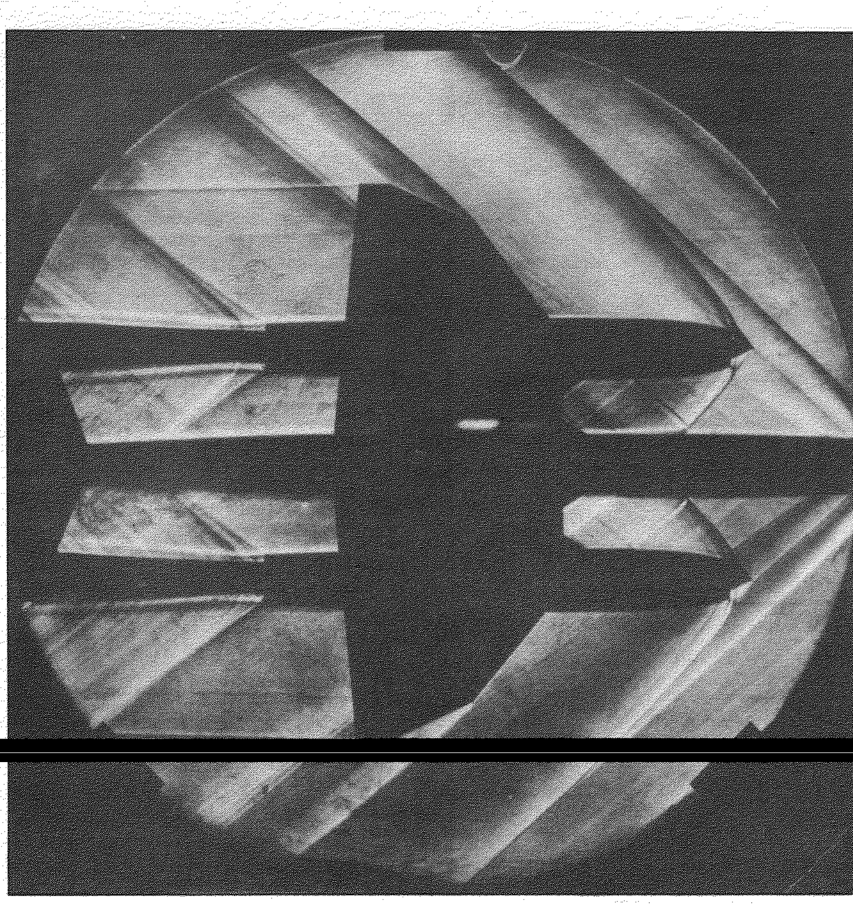

a. PLAN VIEW

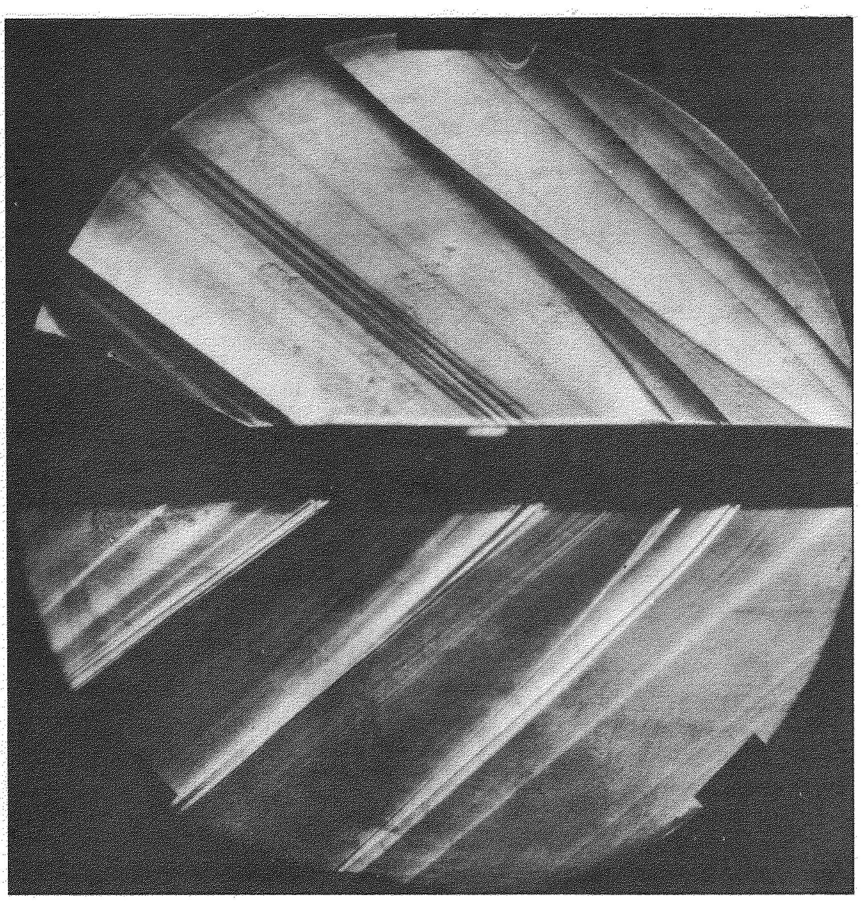

b. SIDE VIEW

FIG.18. SCHLIEREN PHOTOGRAPHS: $M = 1 \cdot 60$

$\alpha = \beta = 0$: Tailplane -10°

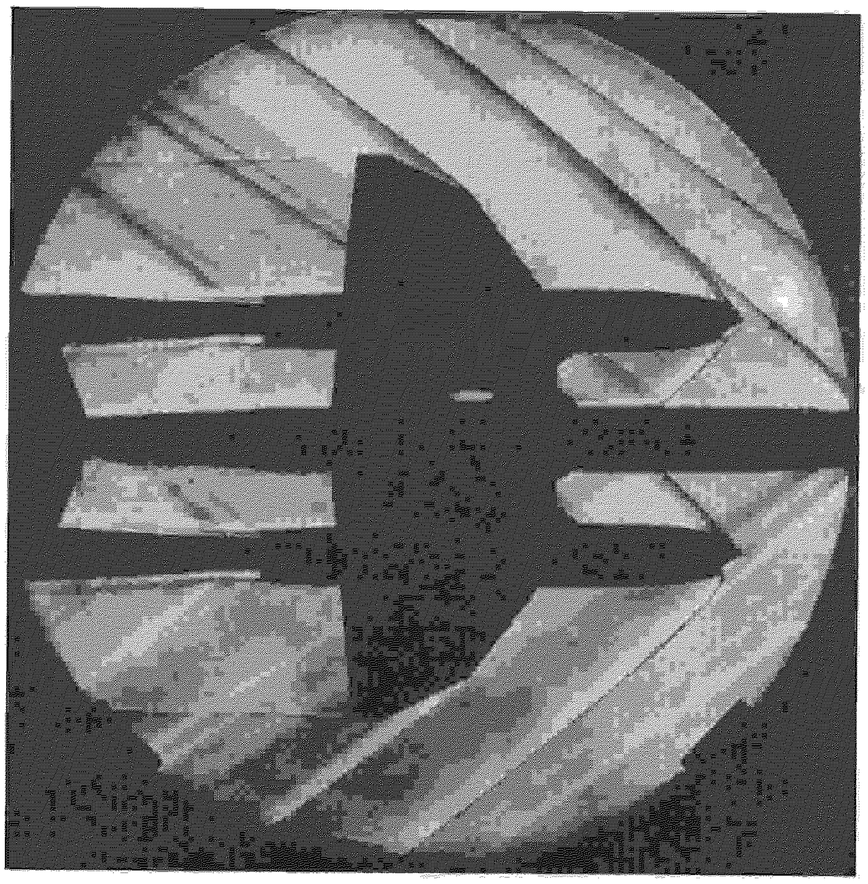

a. PLAN VIEW

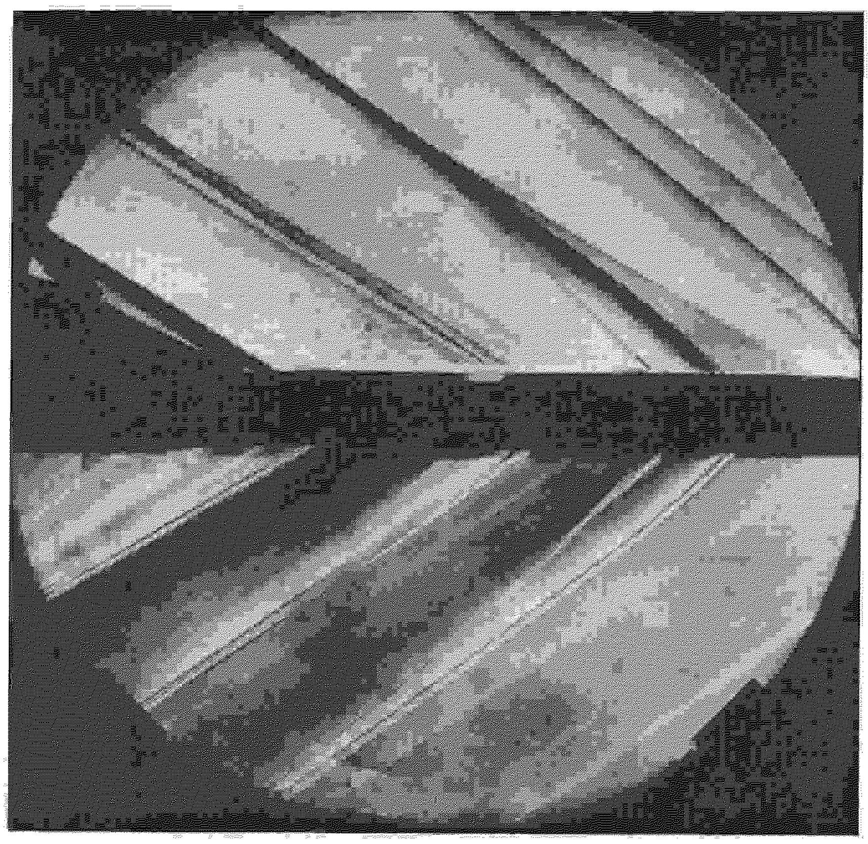

b. SIDE VIEW

FIG. 19. SCHLIEREN PHOTOGRAPHS: M = 1·80

$\alpha = \beta = 0$: Tailplane -10°

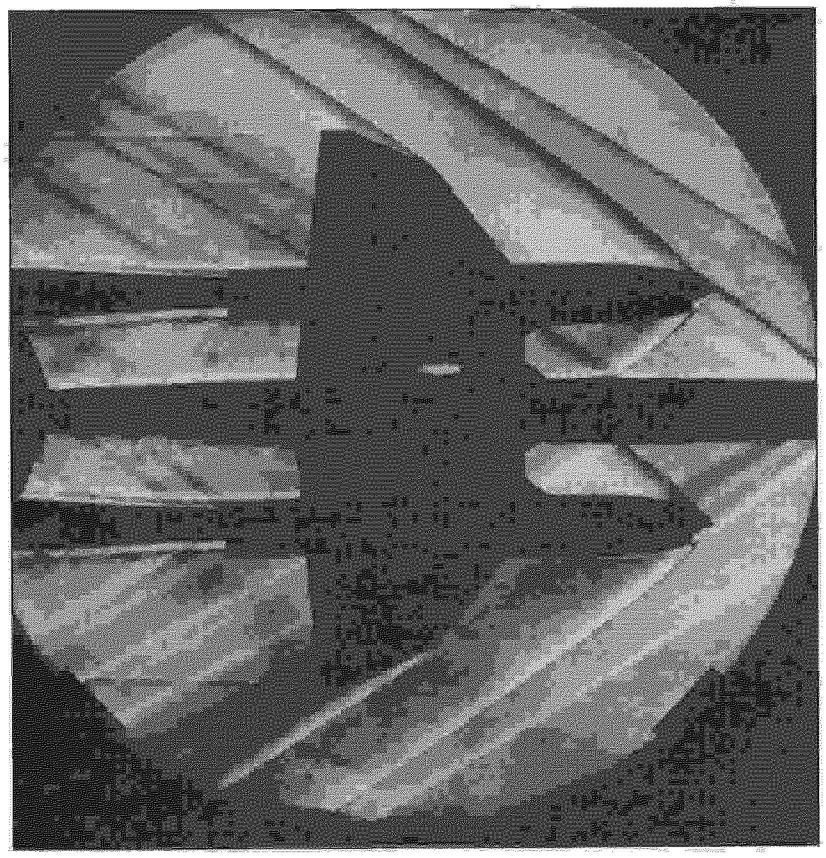

a. PLAN VIEW

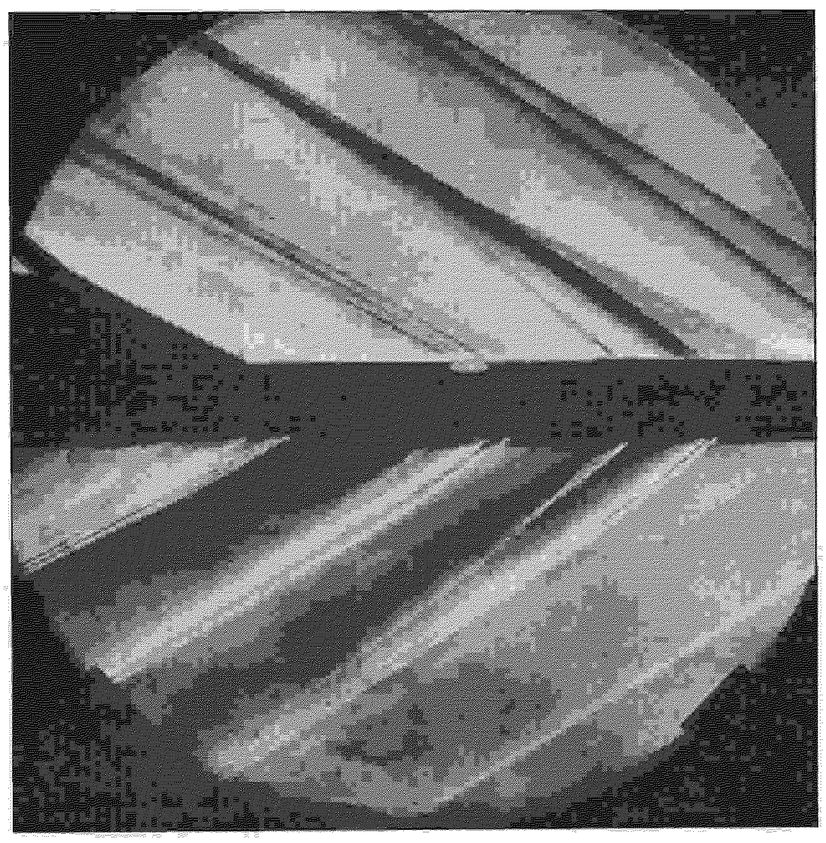

b. SIDE VIEW

FIG.20. SCHLIEREN PHOTOGRAPHS: M = 2·00

$\alpha = \beta = 0$: Tailplane -10°

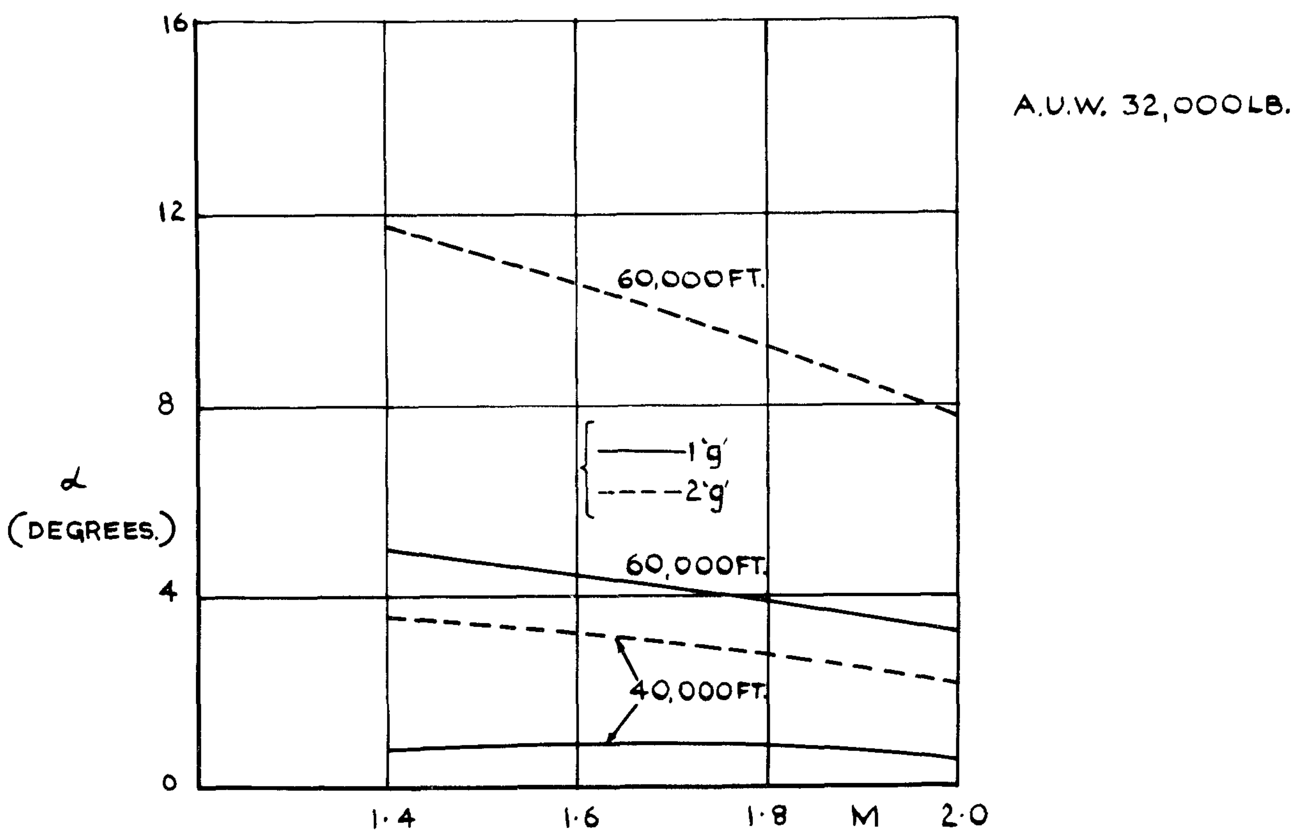

FIG. 21. ESTIMATED VARIATION OF FLIGHT INCIDENCE WITH MACH NUMBER FOR UNDISTORTED FULL-SCALE AIRCRAFT.

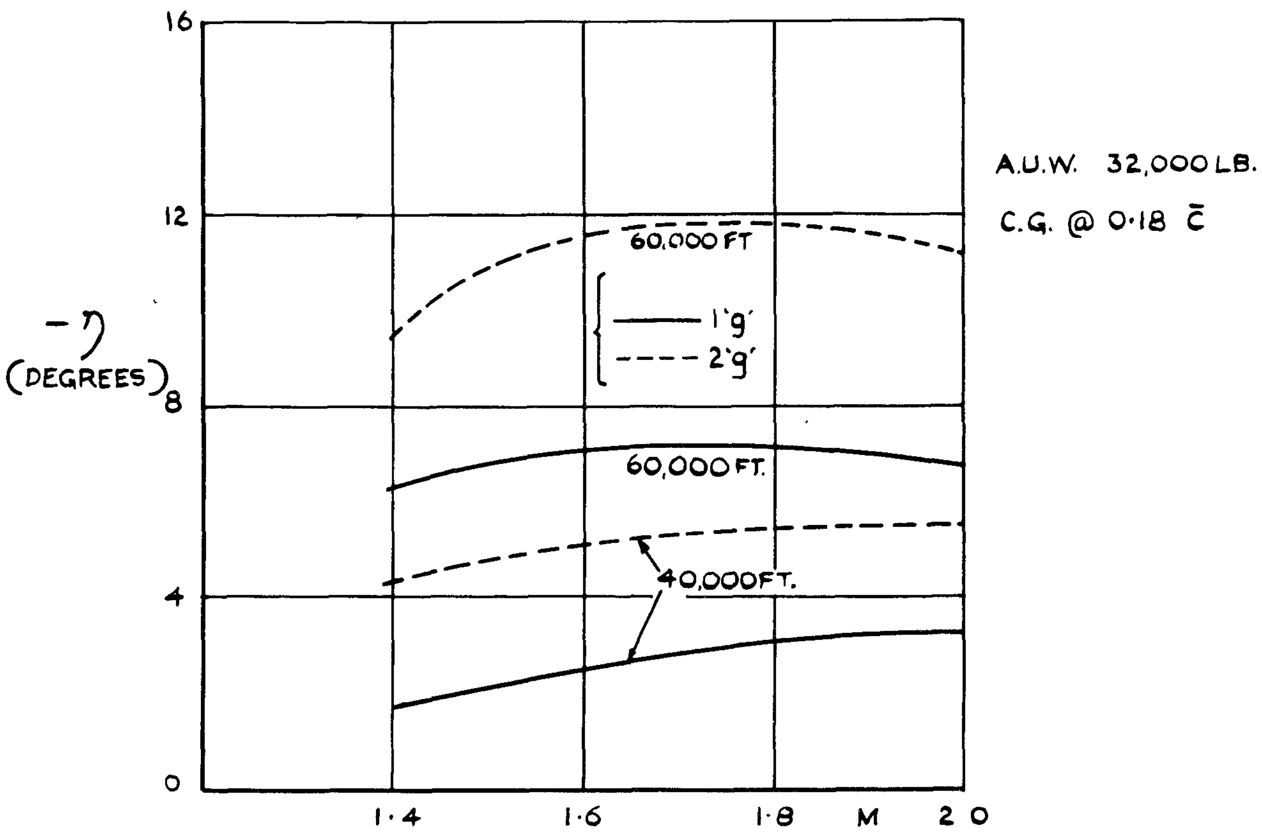

FIG. 22. ESTIMATED VARIATION OF TAILPLANE ANGLE TO TRIM WITH MACH NUMBER FOR UNDISTORTED FULL-SCALE AIRCRAFT.

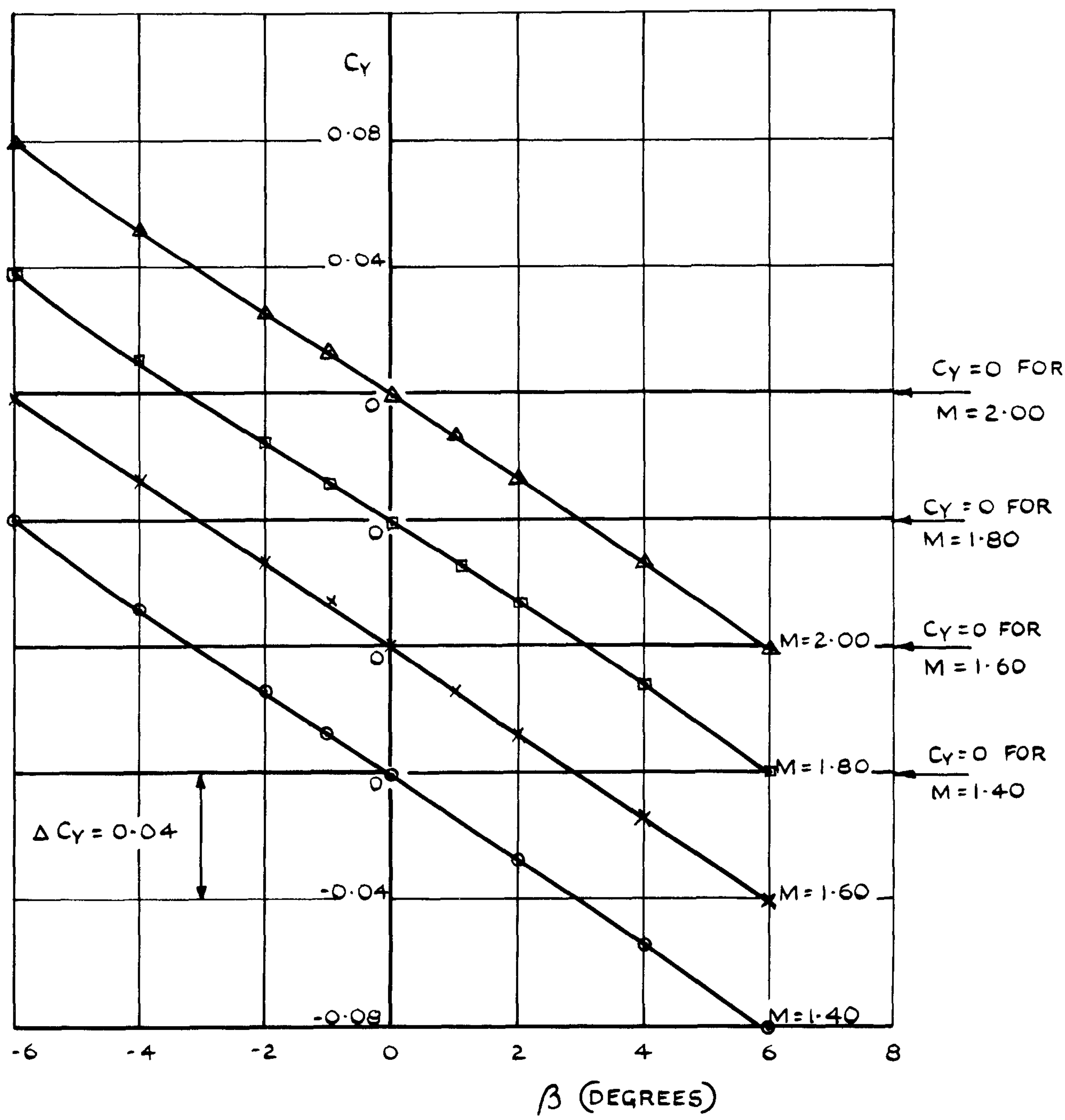

FIG. 23. VARIATION OF C_Y WITH β AT CONSTANT MACH NUMBER: $\zeta = -4°$; $\alpha = +4°$.

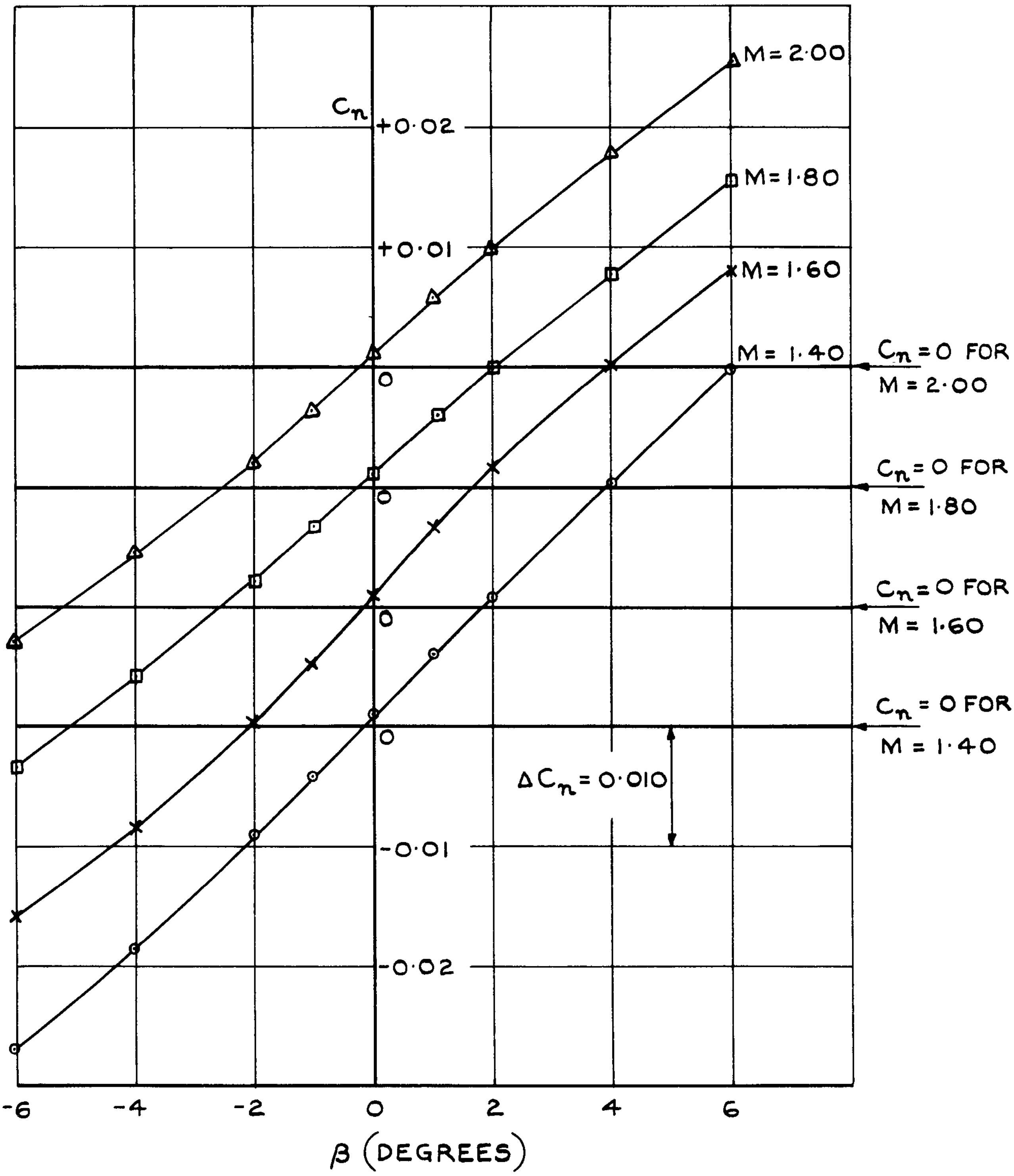

FIG.24. VARIATION OF C_n WITH β AT CONSTANT MACH NUMBER: $\eta = -4^\circ$; $\alpha = +4^\circ$.

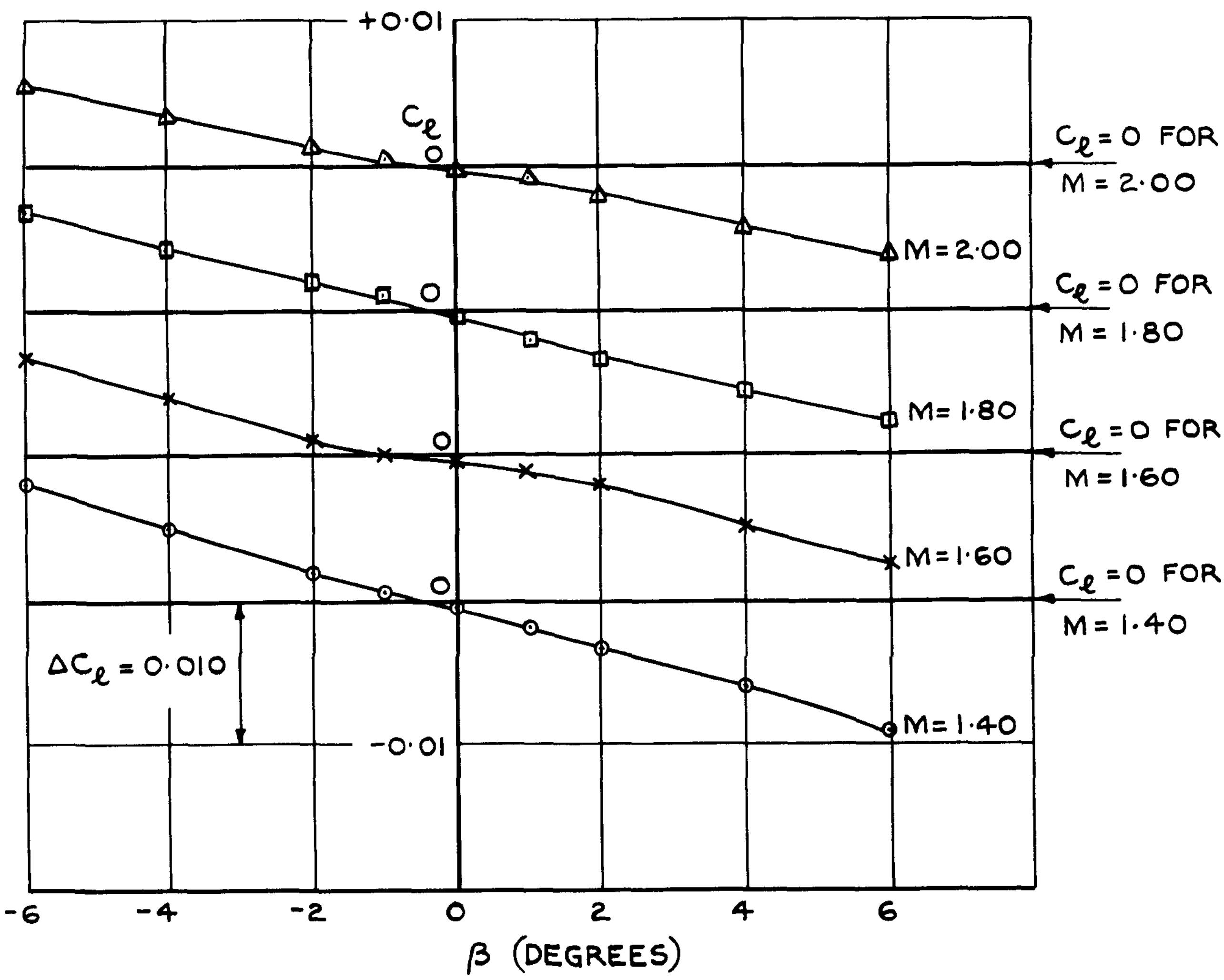

FIG. 25. VARIATION OF C_ℓ WITH β AT CONSTANT MACH NUMBER: $\eta = -4°$; $\alpha = +4°$.

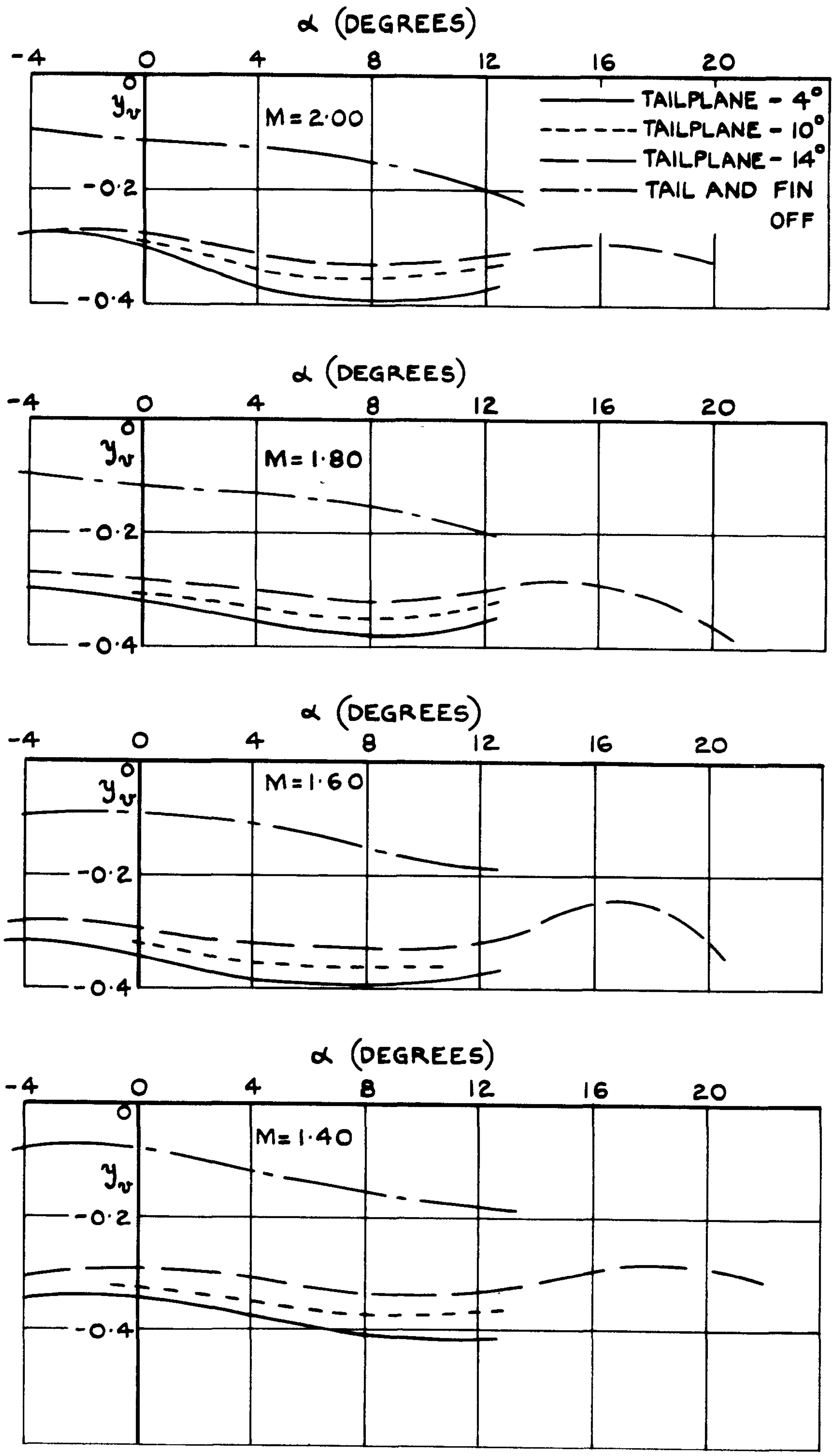

FIG. 26. VARIATION OF y_v WITH INCIDENCE.

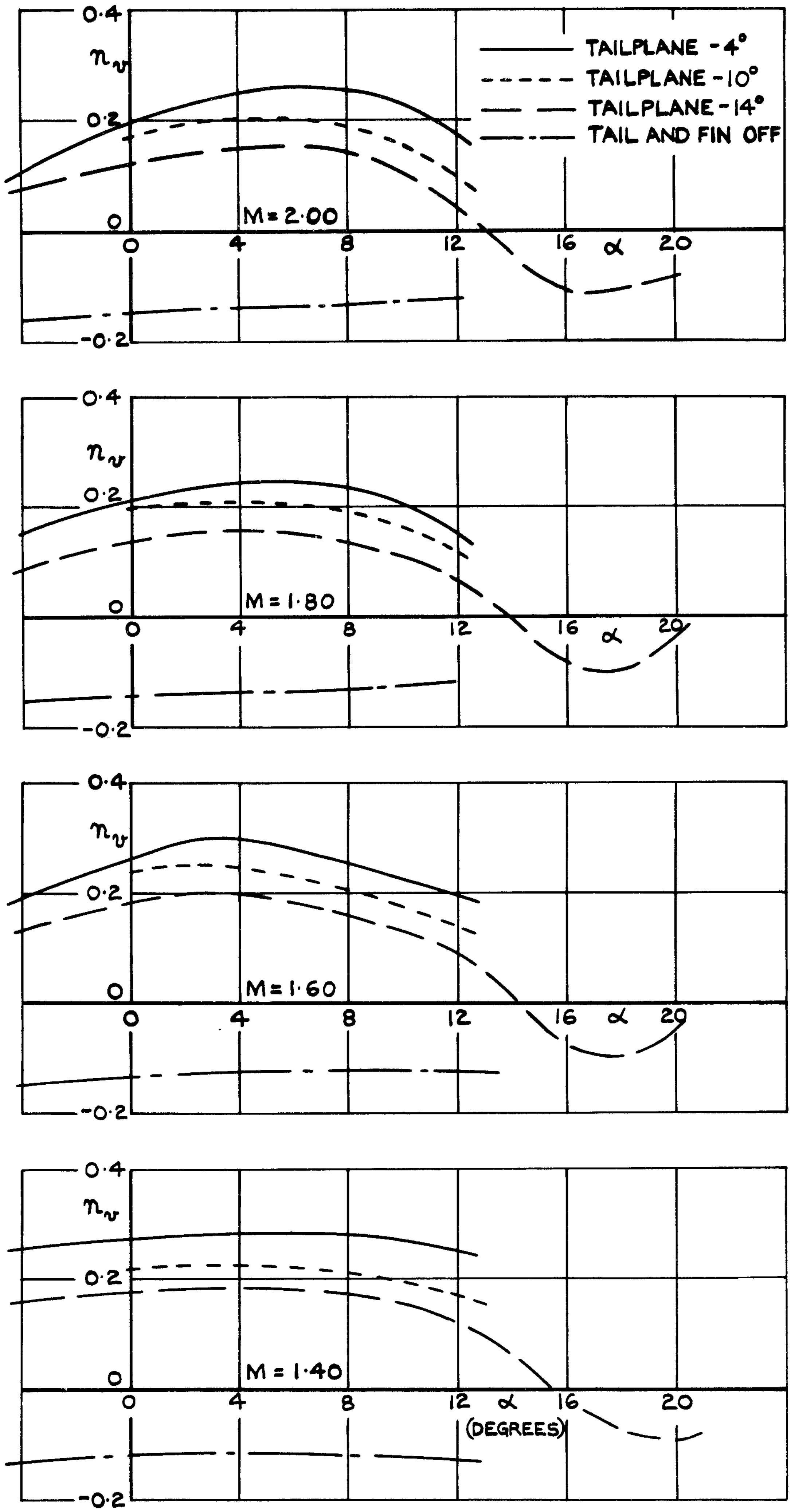

FIG. 27. VARIATION OF n_v WITH INCIDENCE.

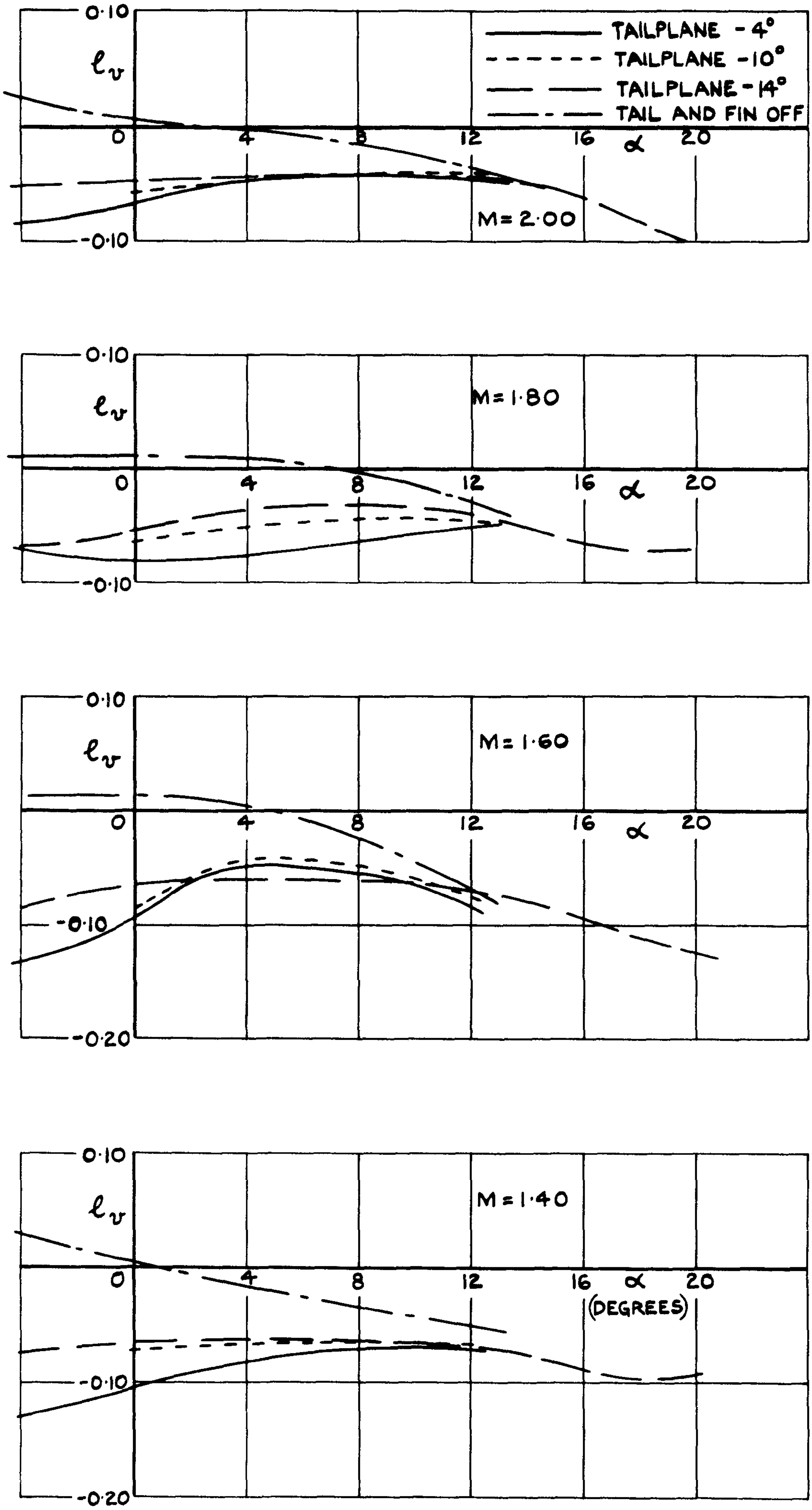

FIG. 28. VARIATION OF ℓ_v WITH INCIDENCE.

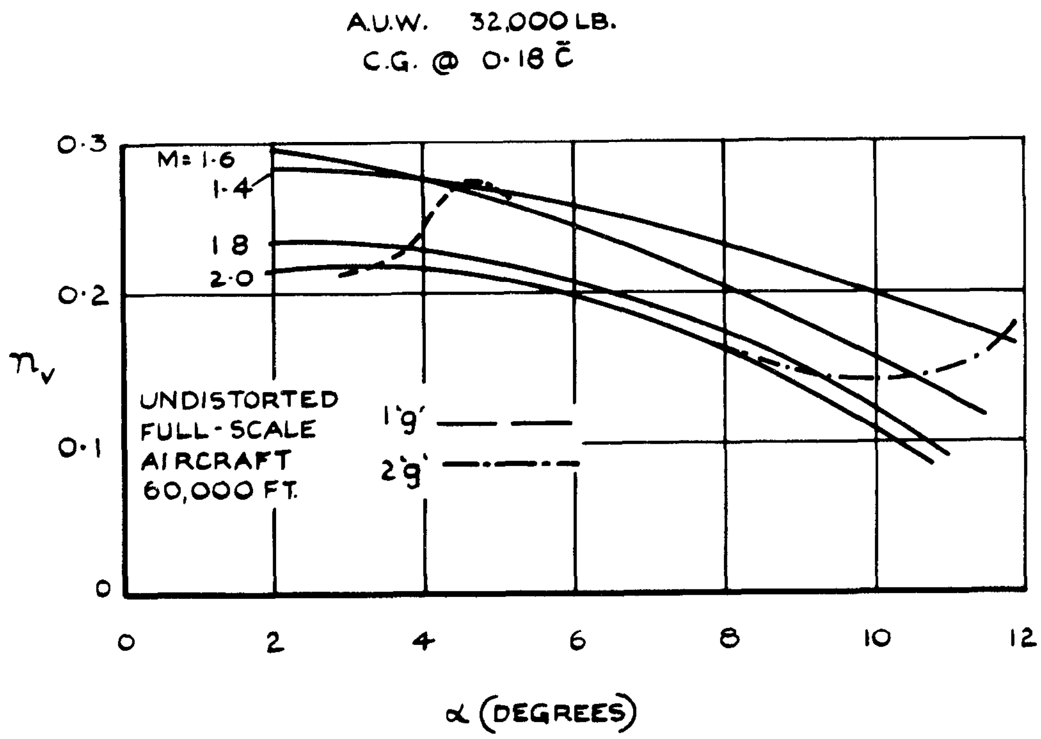

FIG. 29. VARIATION OF n_v WITH INCIDENCE FOR TRIMMED CONFIGURATION.

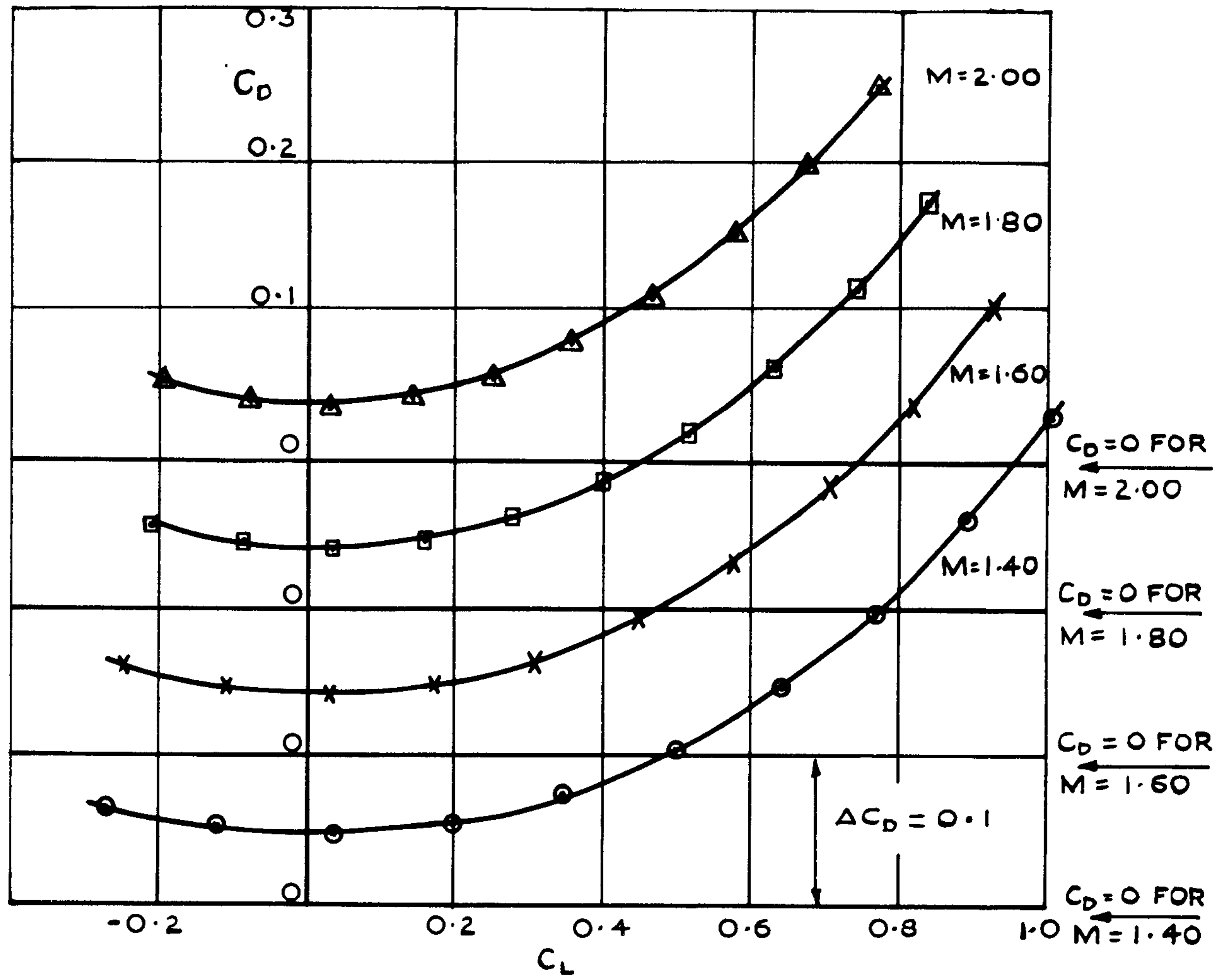

FIG. 30. VARIATION OF C_D WITH C_L AT CONSTANT MACH NUMBER: η=-4°.

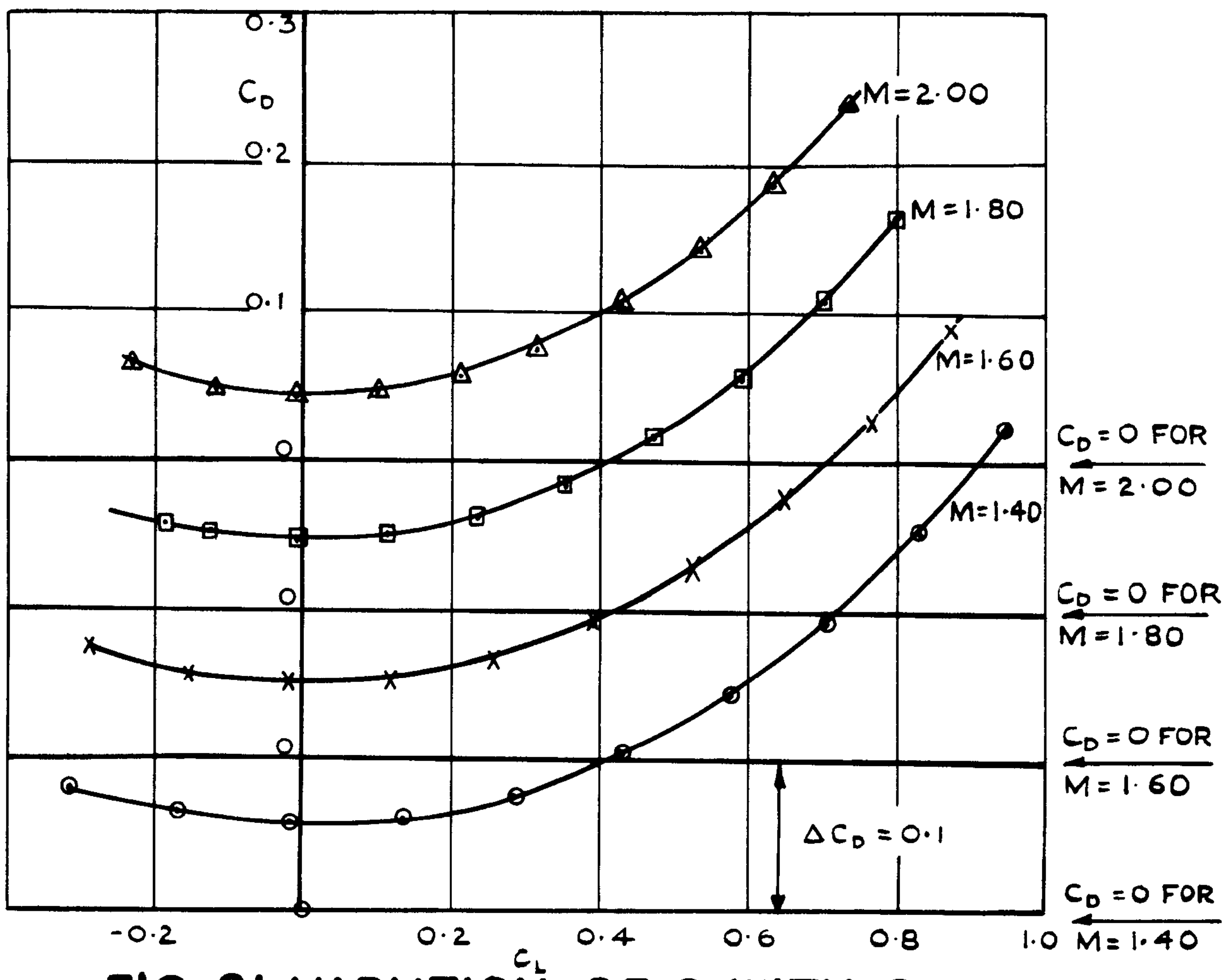

FIG. 31. VARIATION OF C_D WITH C_L AT CONSTANT MACH NUMBER: η = -10°.

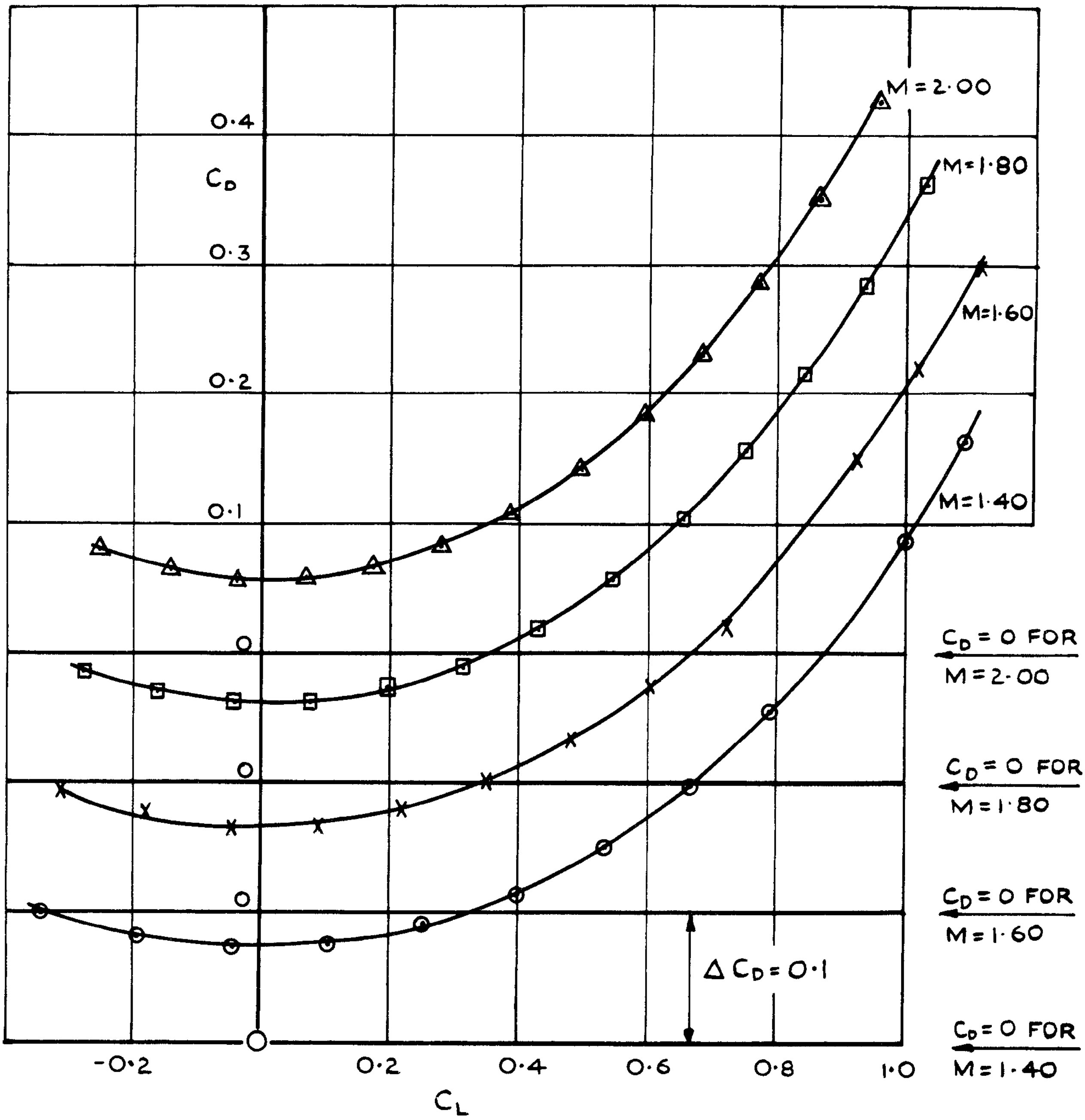

FIG. 32. VARIATION OF C_D WITH C_L AT CONSTANT MACH NUMBER: $\eta = -14^\circ$

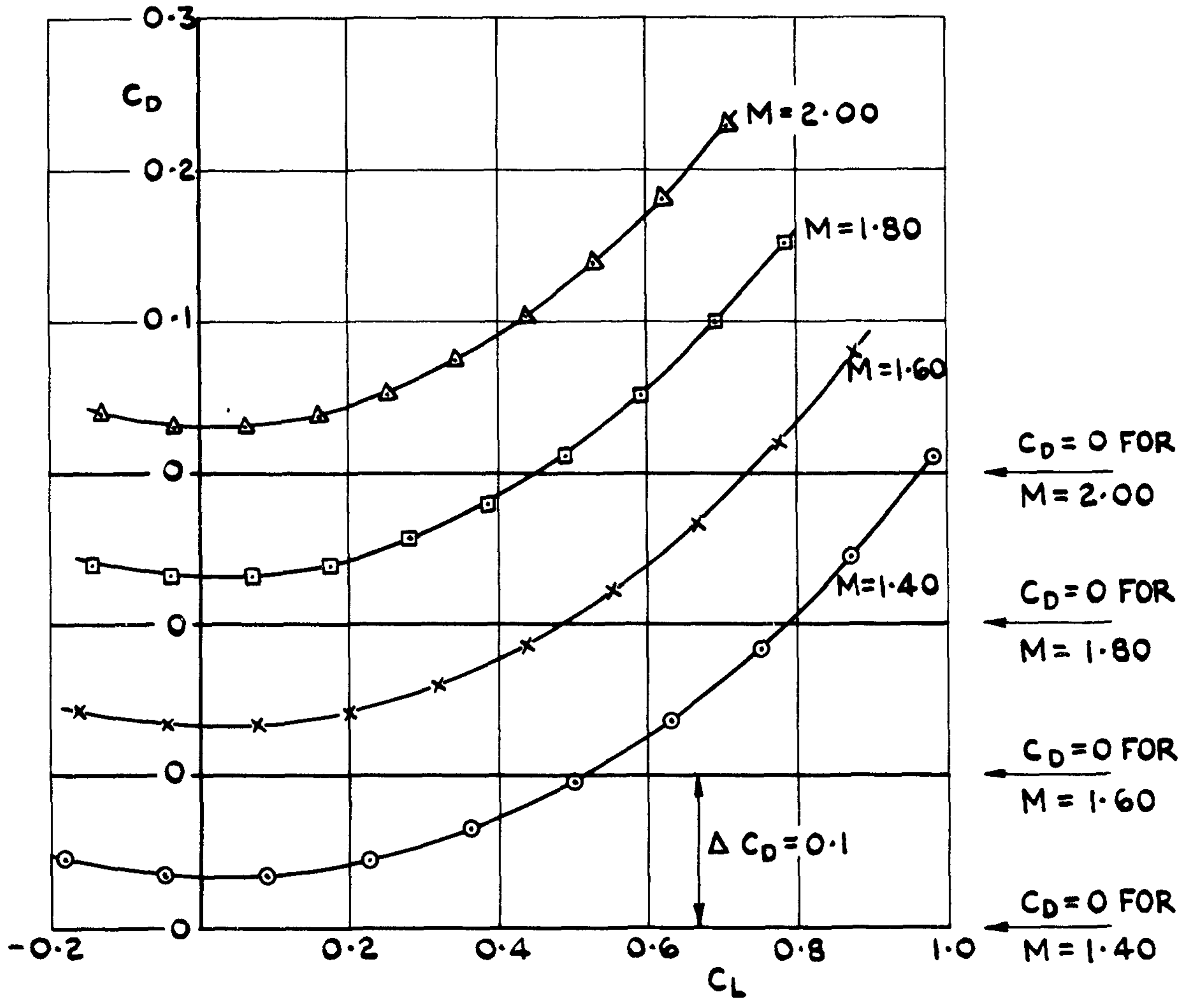

FIG. 33 VARIATION OF C_D WITH C_L AT CONSTANT MACH NUMBER : TAILPLANE AND FIN OFF.

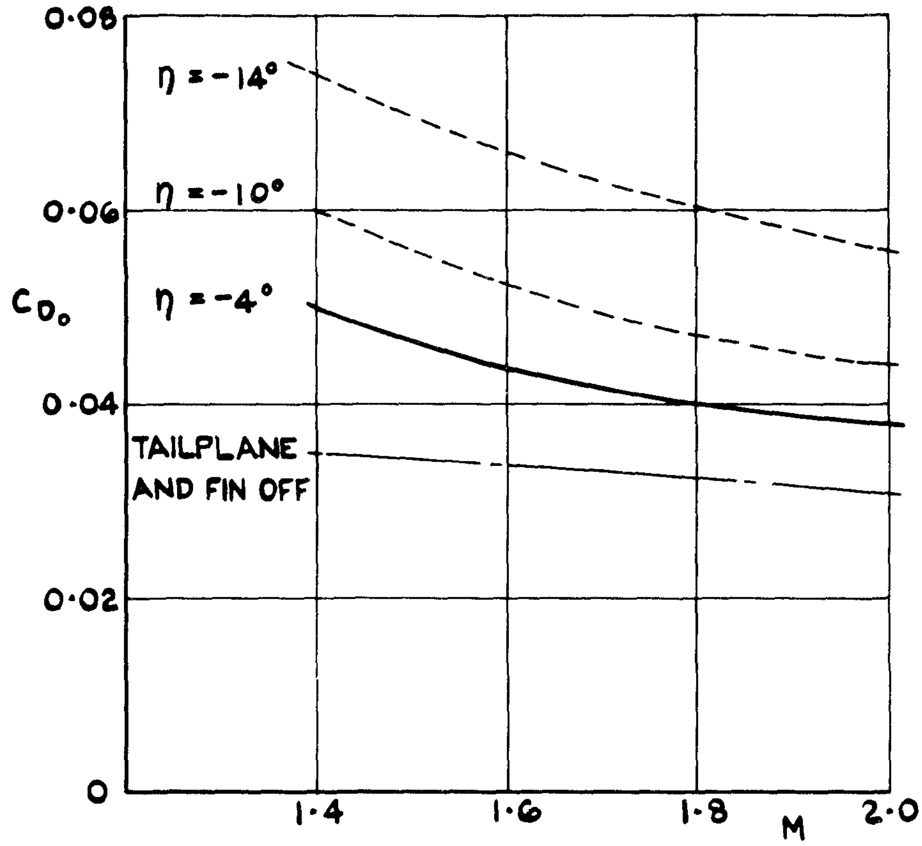

FIG. 34 VARIATION OF MINIMUM DRAG COEFFICIENT WITH MACH NUMBER.

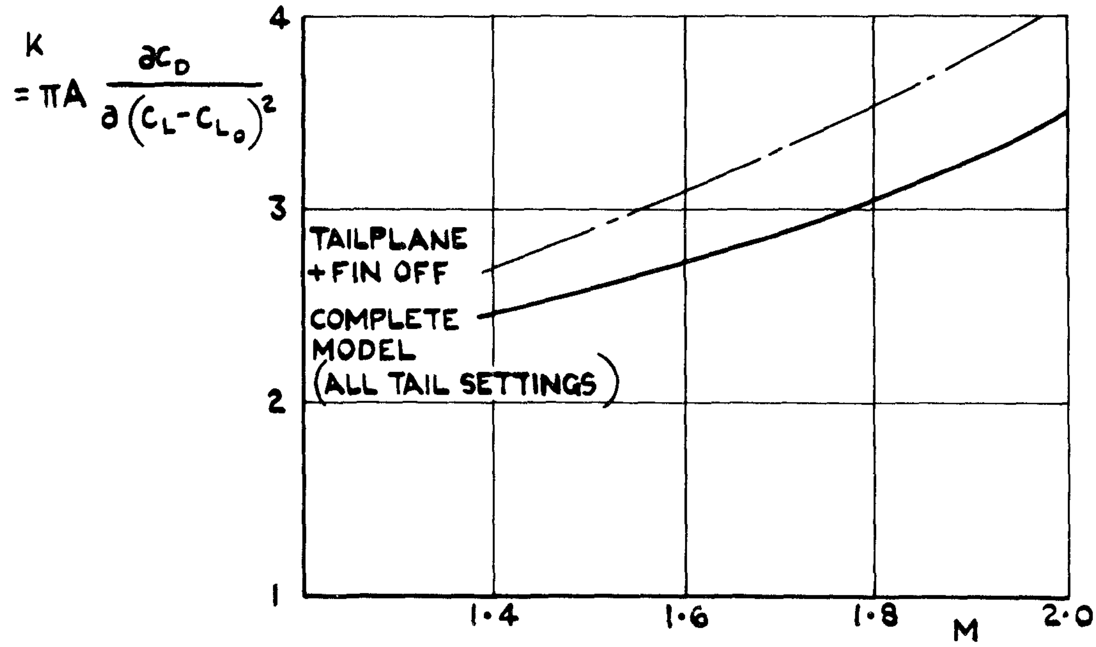

FIG. 35 VARIATION OF INDUCED DRAG FACTOR WITH MACH NUMBER.

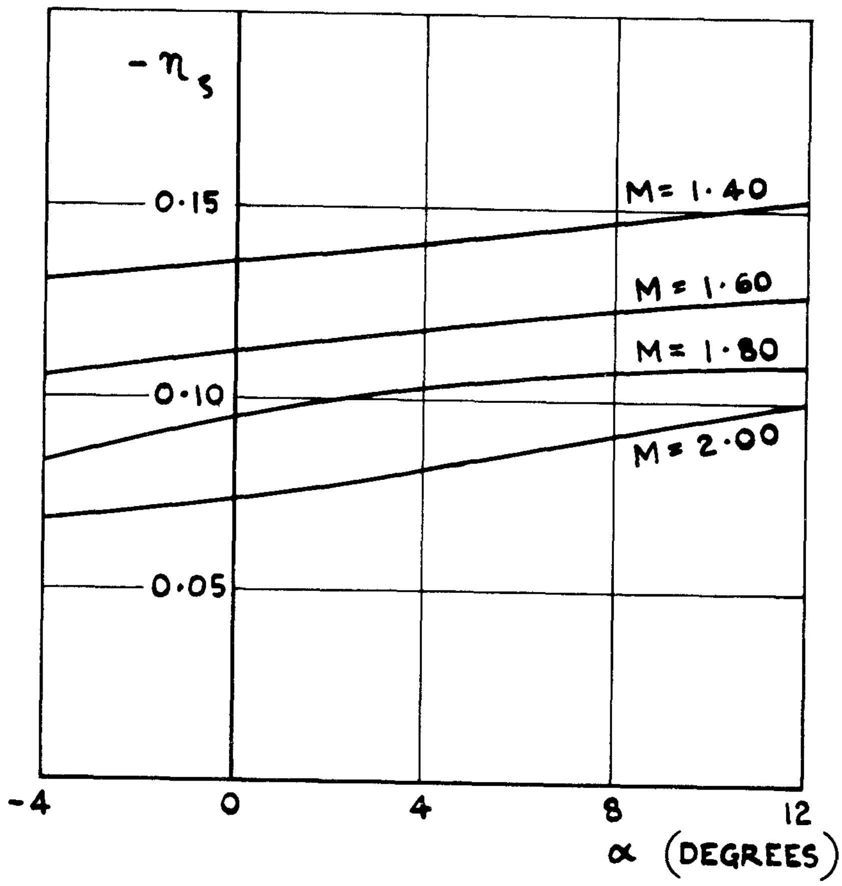

FIG. 36 VARIATION OF YAWING MOMENT DUE TO RUDDER WITH INCIDENCE.

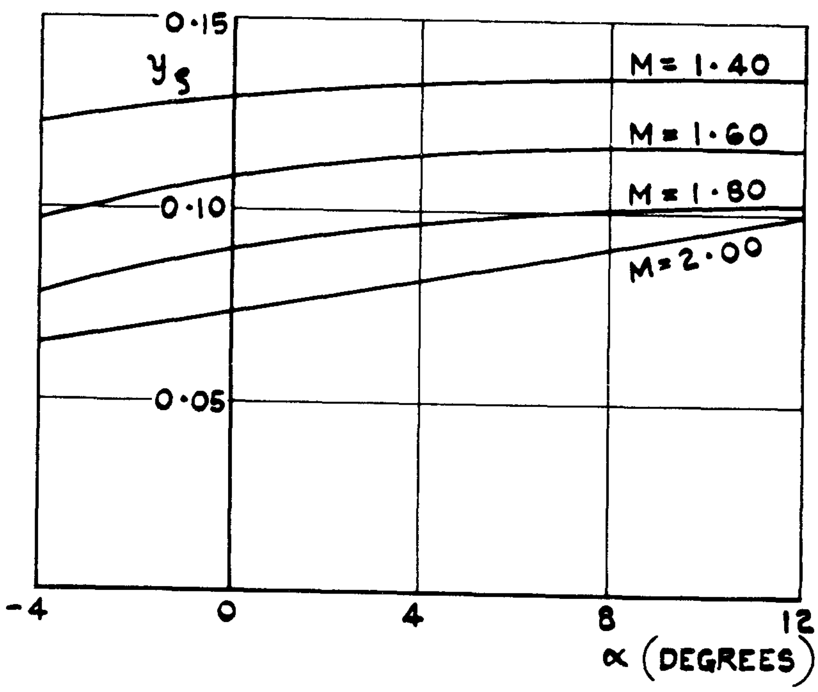

FIG. 37 VARIATION OF SIDE-FORCE DUE TO RUDDER WITH INCIDENCE.

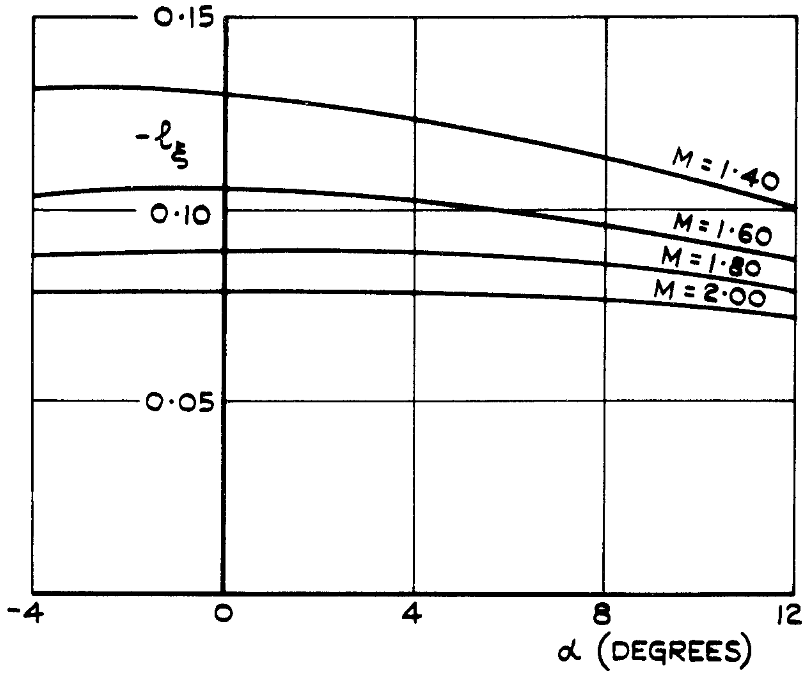

FIG. 38. VARIATION OF AILERON POWER WITH INCIDENCE.

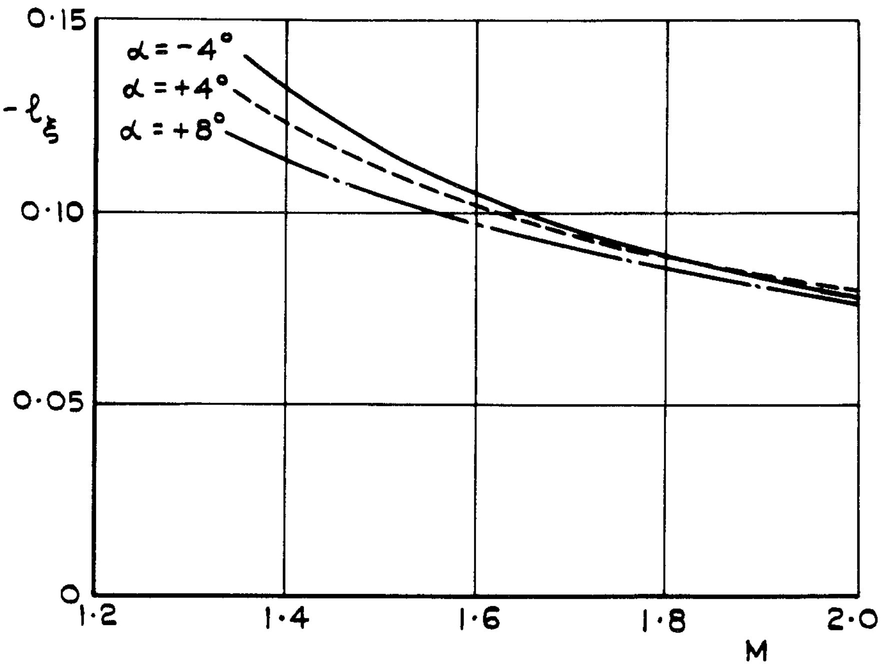

FIG. 39. VARIATION OF AILERON POWER WITH MACH NUMBER.

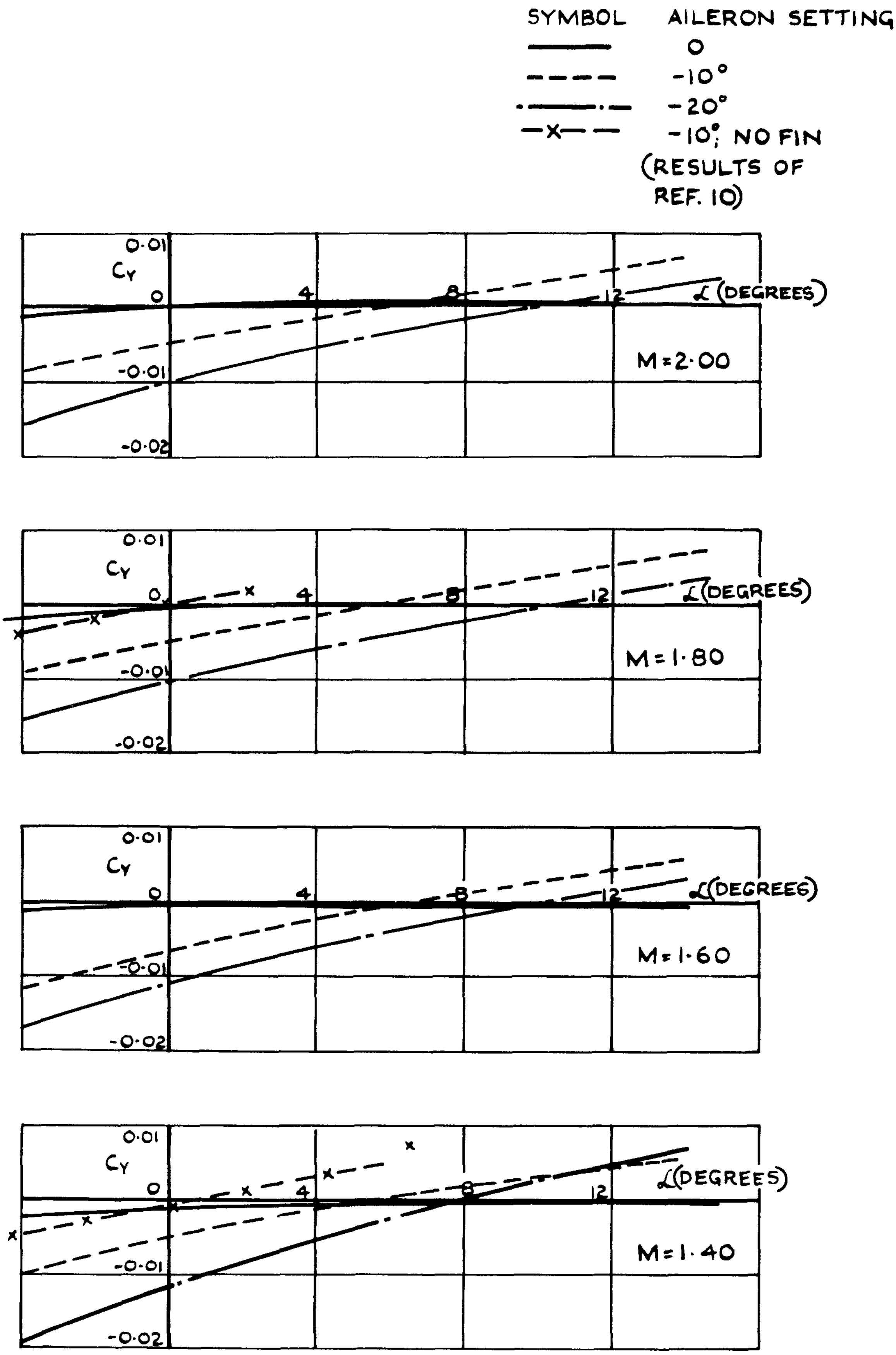

FIG. 40. VARIATION OF C_Y WITH α AT ZERO SIDESLIP FOR VARIOUS AILERON SETTINGS.

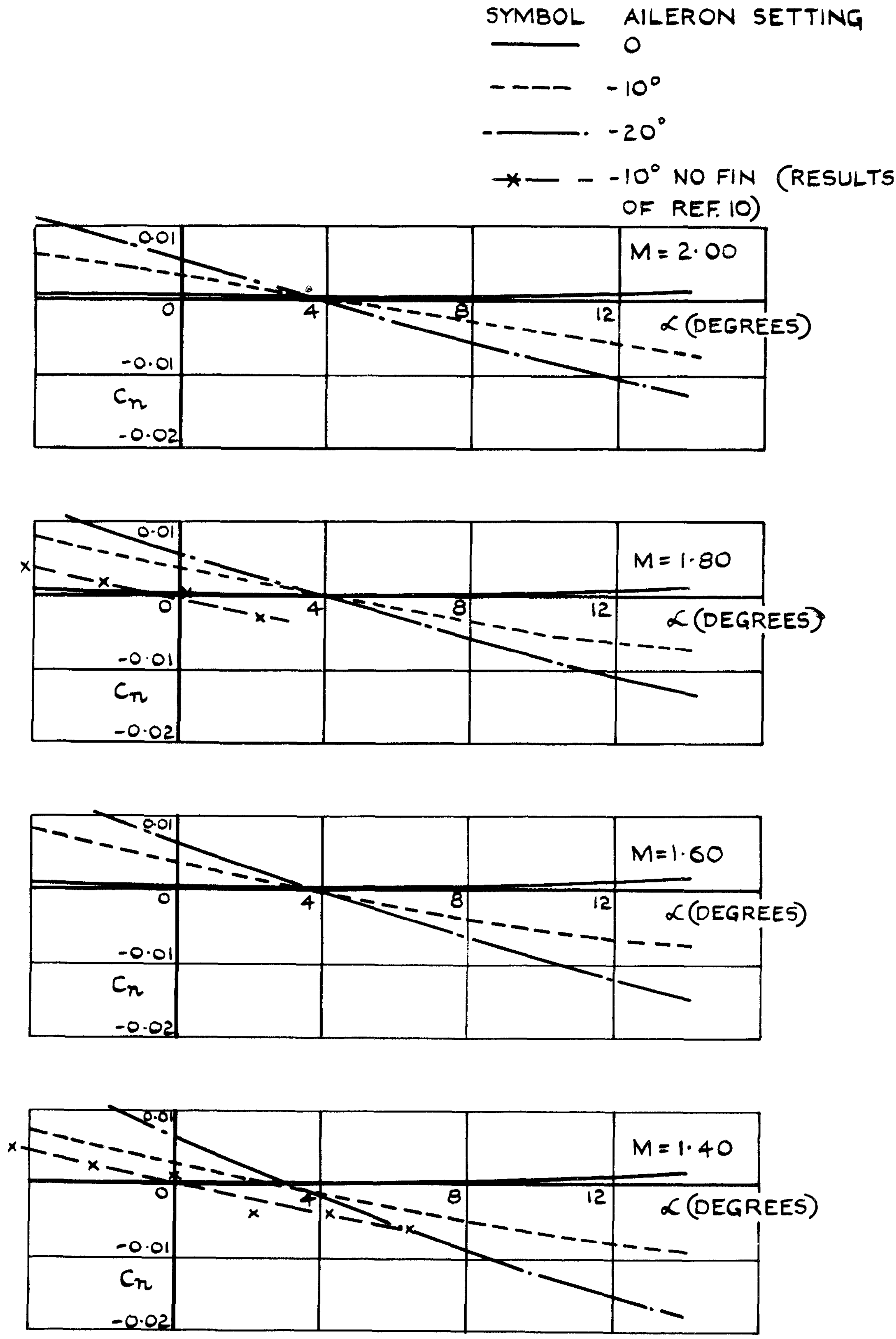

FIG. 41. VARIATION OF C_n WITH α AT ZERO SIDESLIP FOR VARIOUS AILERON SETTINGS.

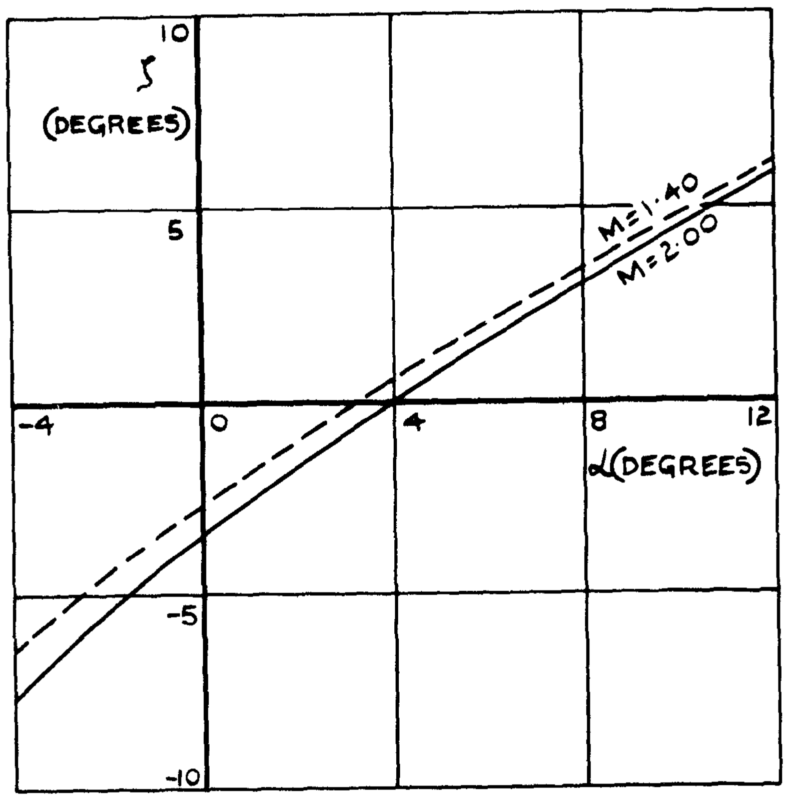

FIG. 42. RUDDER ANGLE TO CORRECT YAWING MOMENT INDUCED BY -20° AILERONS ($\beta = 0$)

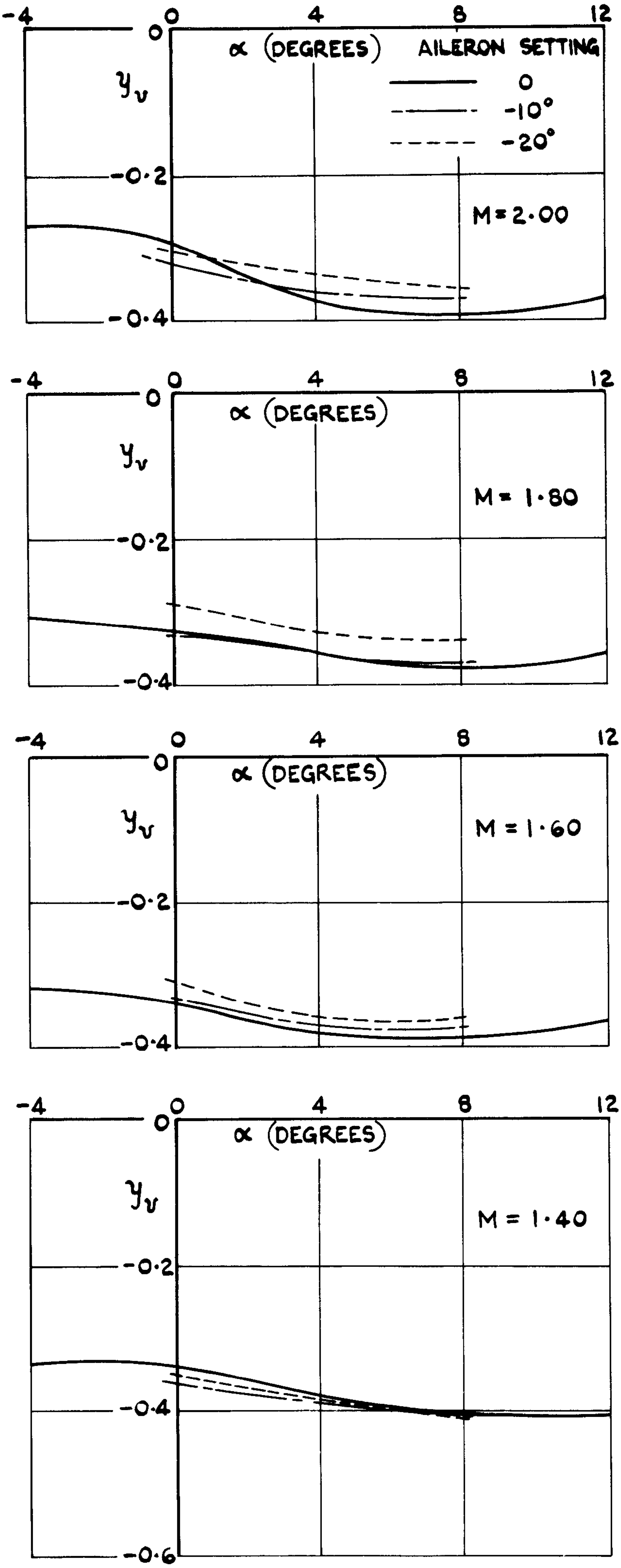

FIG.43 EFFECT OF AILERON SETTING ON VARIATION OF y_v WITH α : $\eta = -4°$.

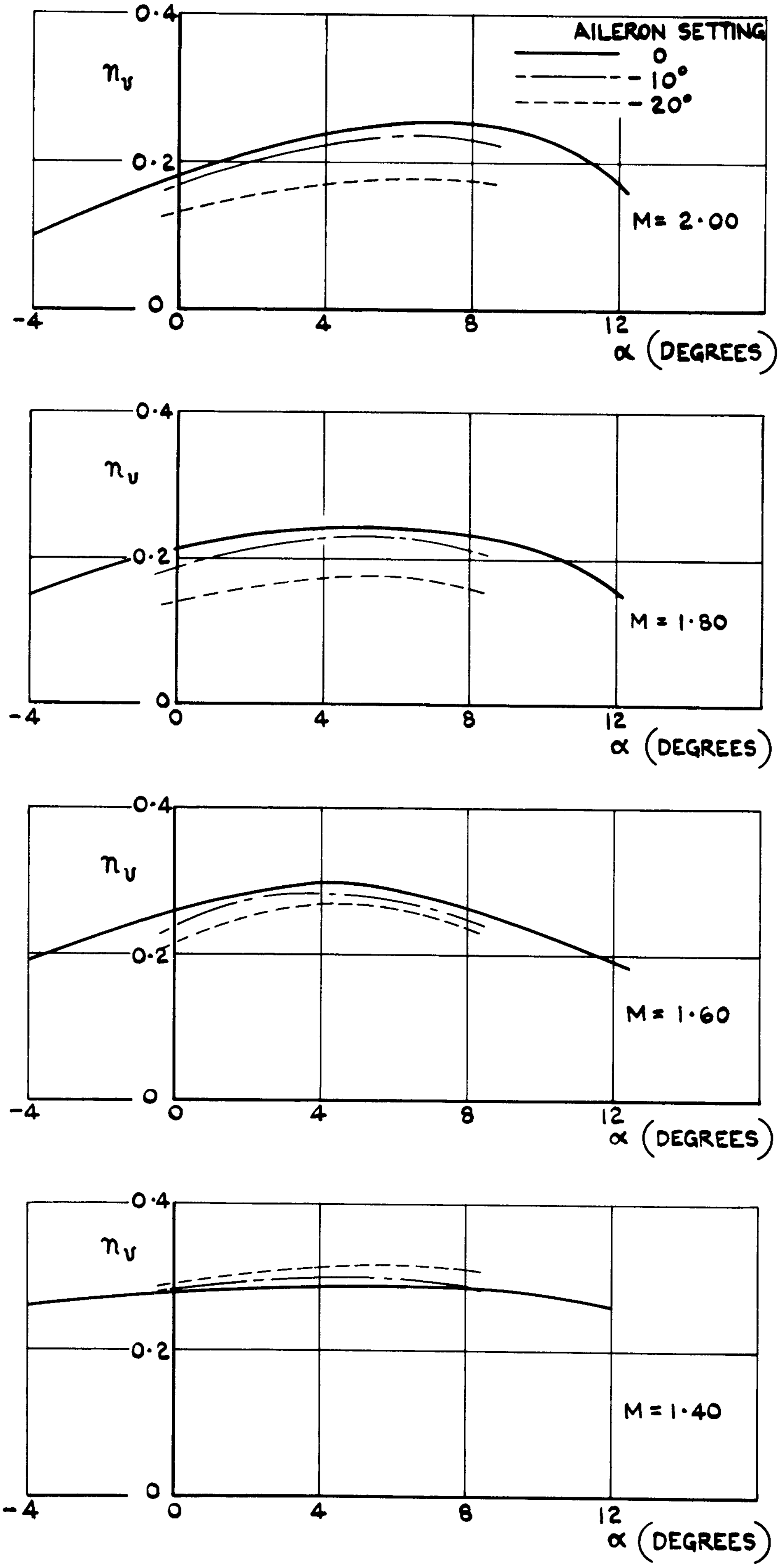

FIG. 44 EFFECT OF AILERON SETTING ON VARIATION OF n_v WITH α: $\eta = -4°$.

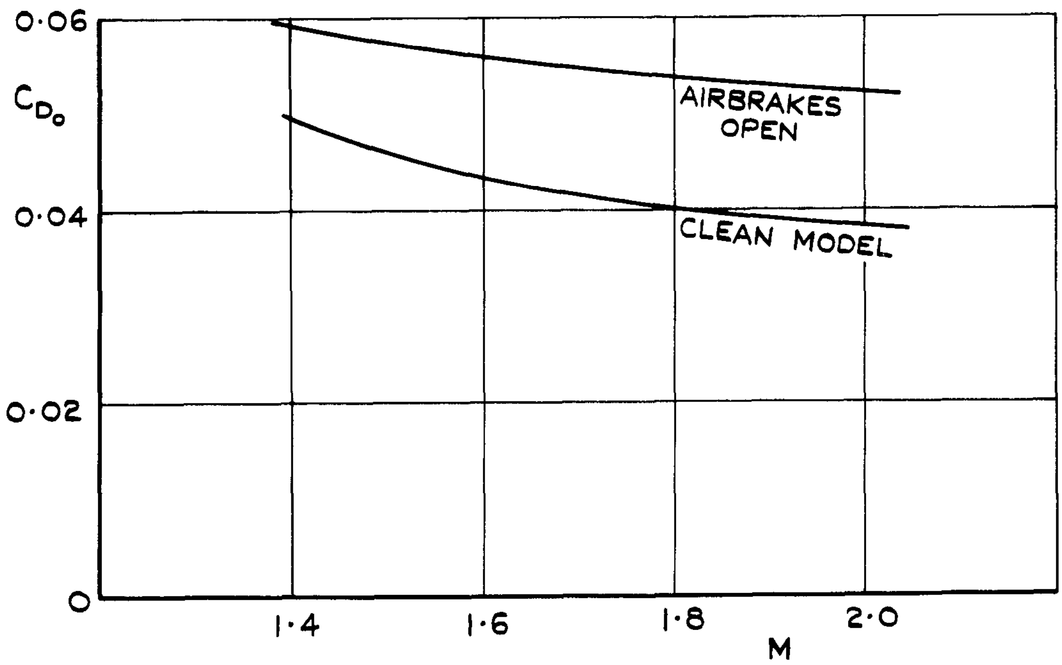

FIG. 45. EFFECT OF AIRBRAKES ON MINIMUM DRAG COEFFICIENT: $\eta = -4°$.

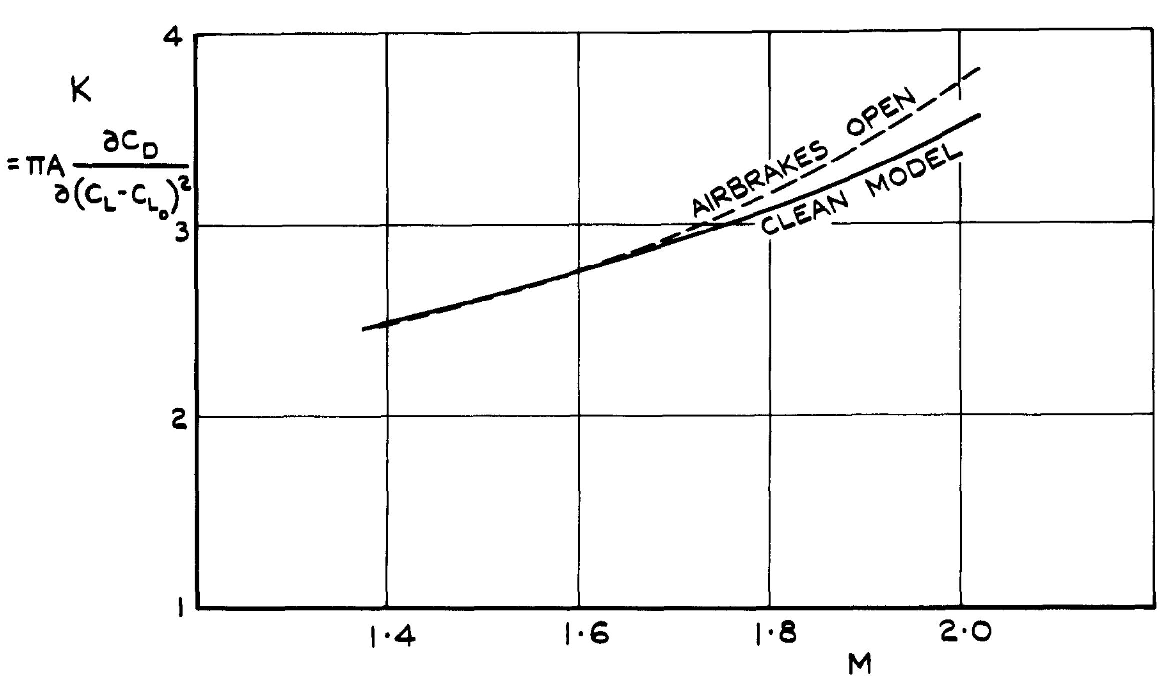

FIG. 46. EFFECT OF AIRBRAKES ON INDUCED DRAG FACTOR : $\eta = -4°$.

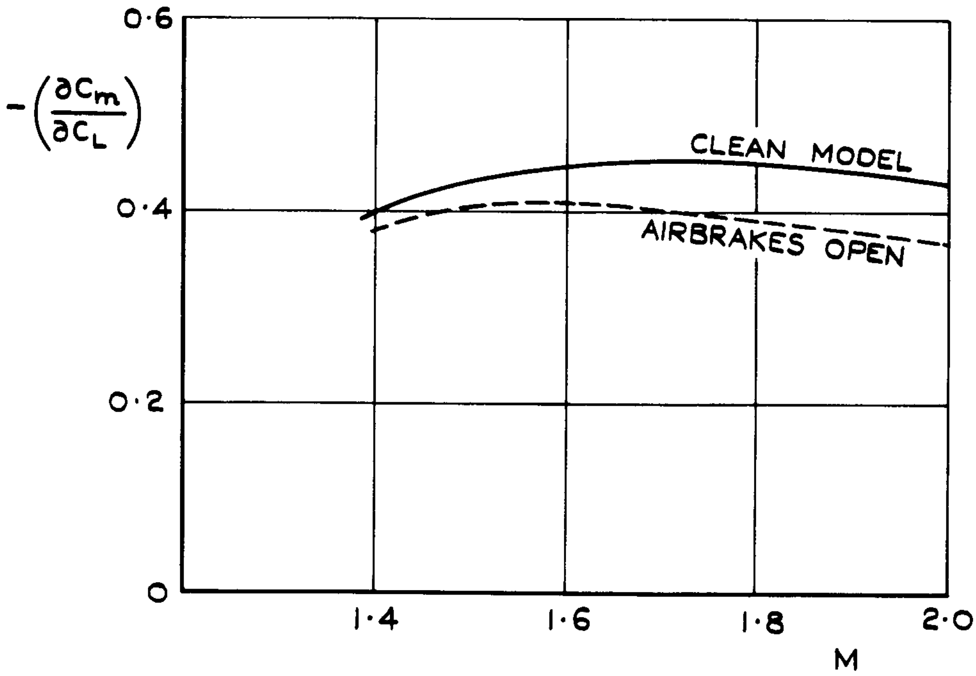

FIG. 47. EFFECT OF AIRBRAKES ON LONGITUDINAL STABILITY : $\eta = -4°$.

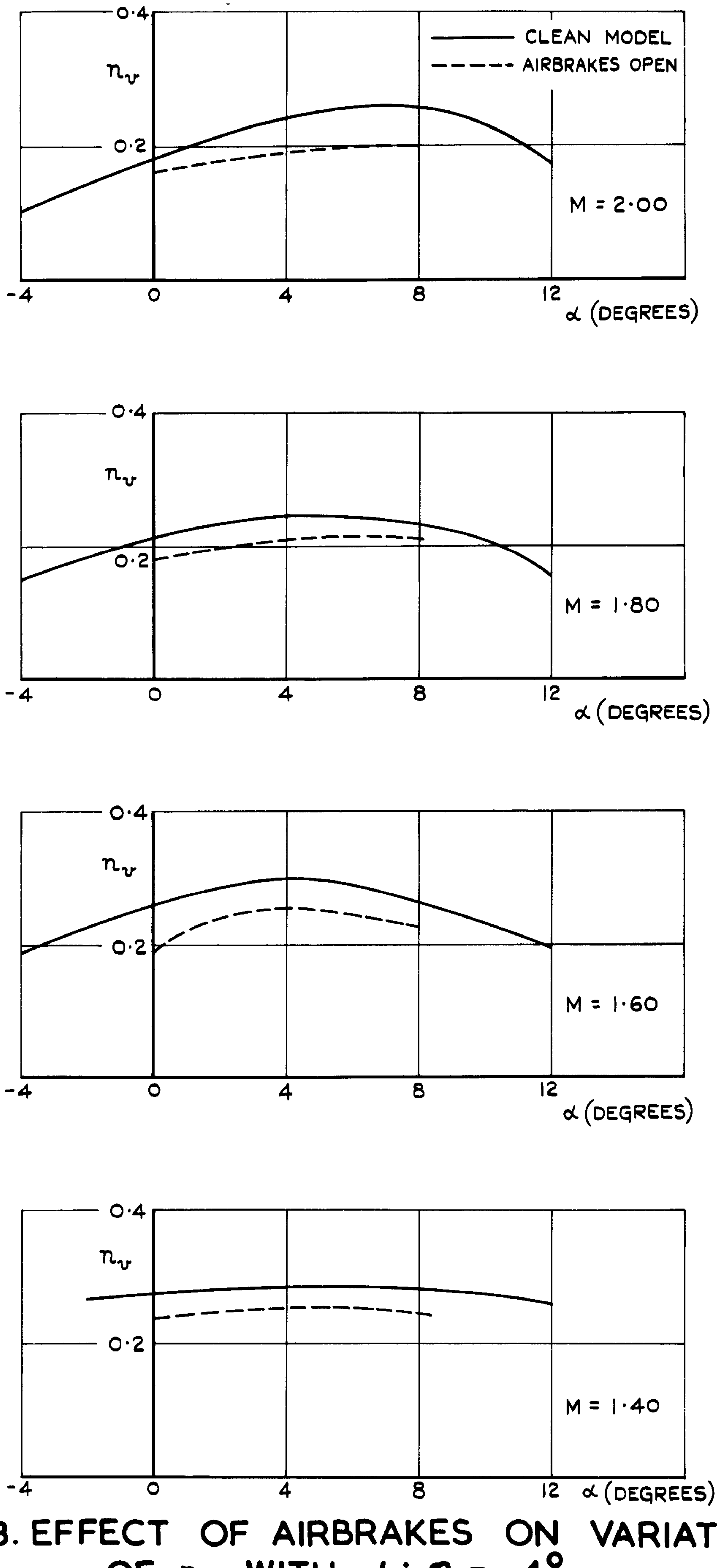

FIG. 48. EFFECT OF AIRBRAKES ON VARIATION OF n_v WITH α: $\eta = -4°$.

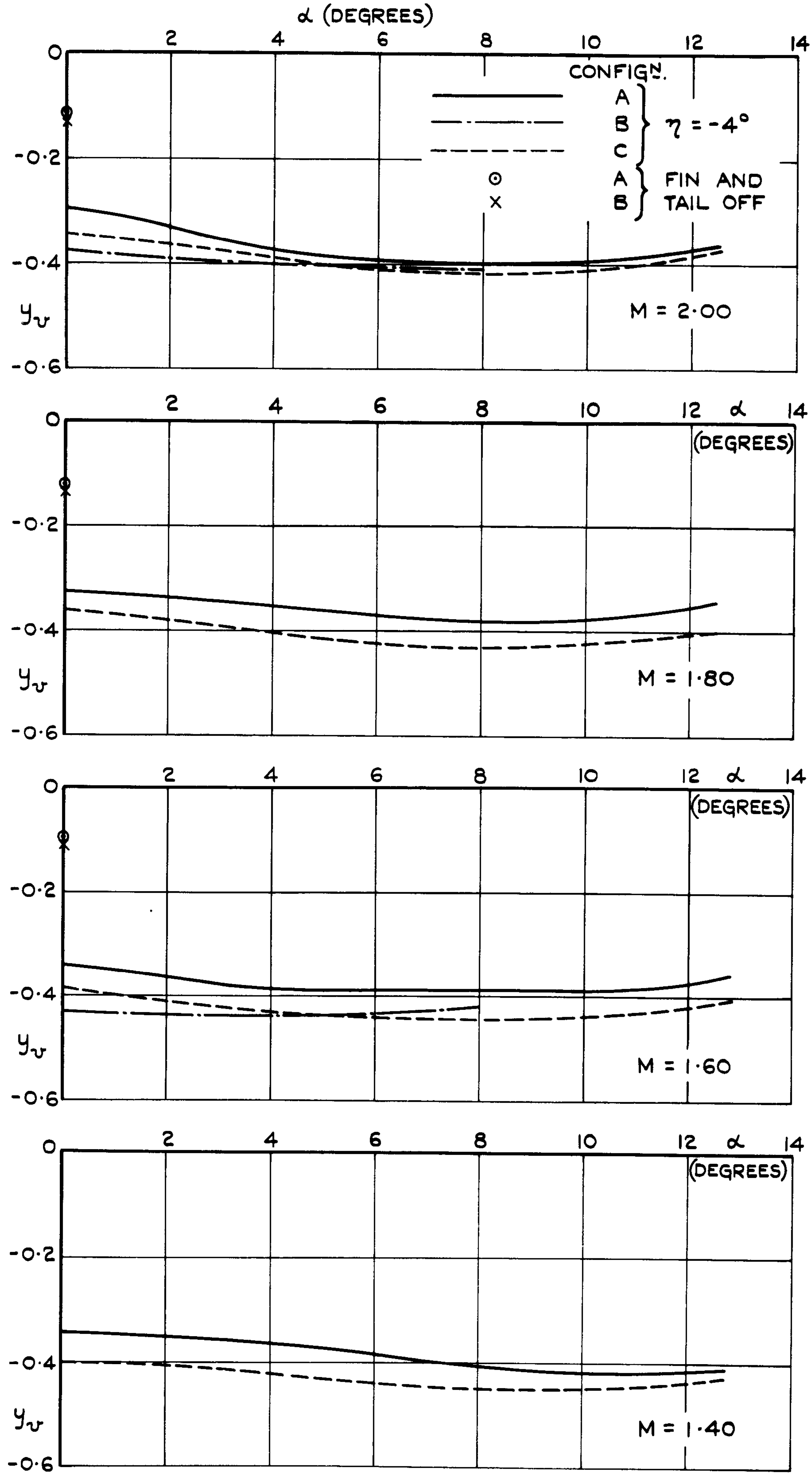

FIG. 49. VARIATION OF y_v WITH α: MODEL COMPARISON.

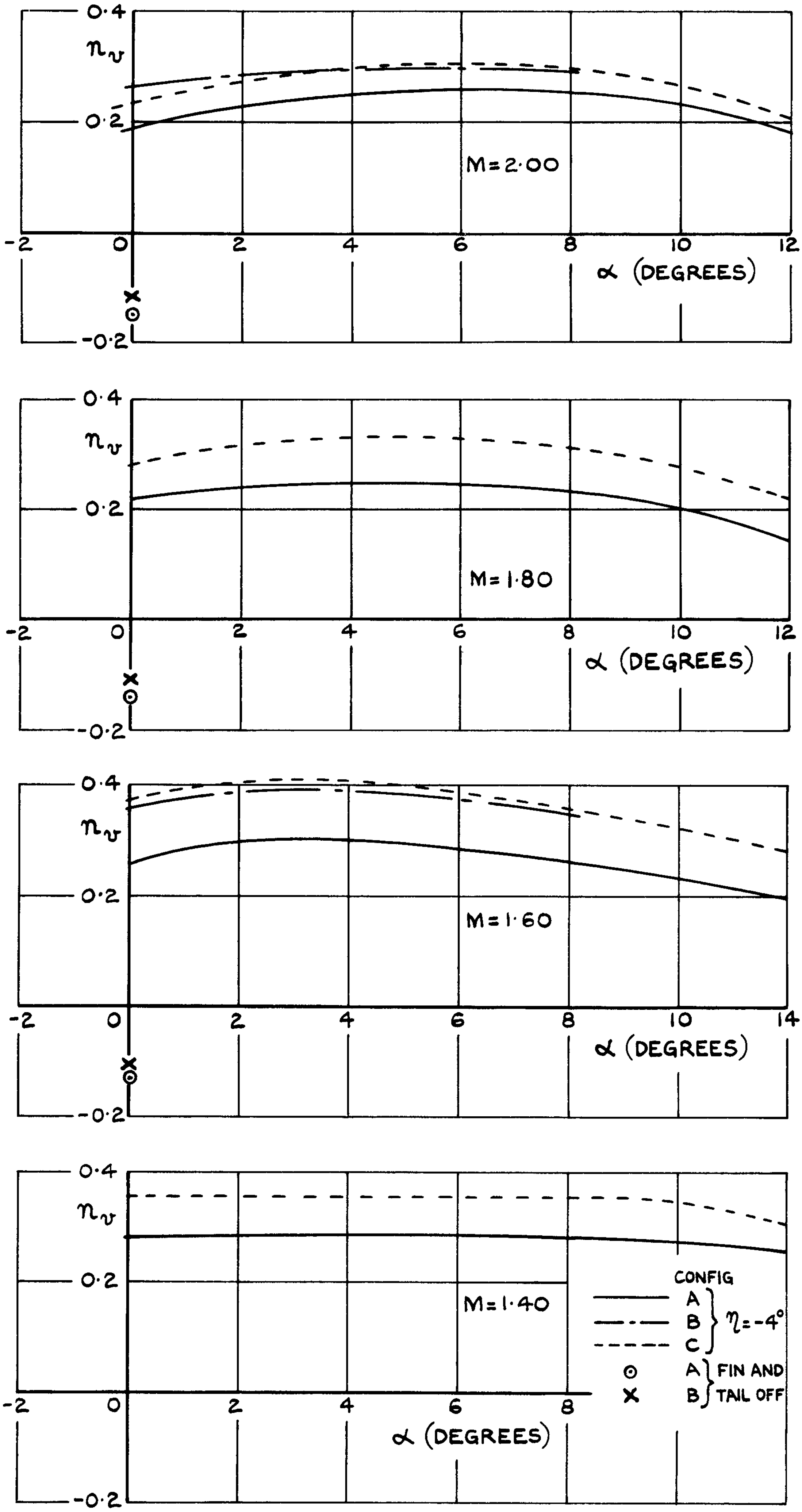

FIG. 50. VARIATION OF n_v WITH α: MODEL COMPARISON.

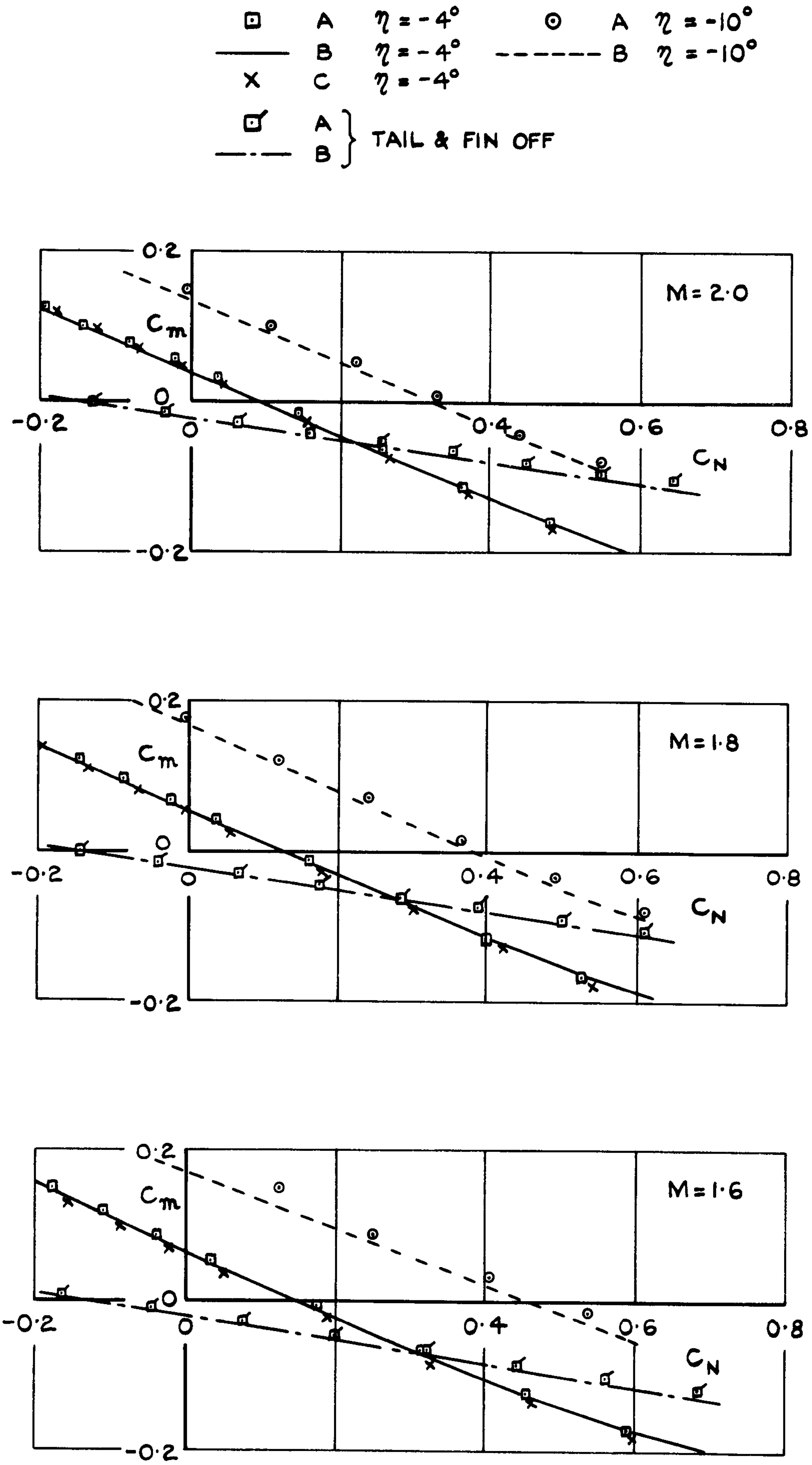

FIG. 51. VARIATION OF C_m WITH C_N AT CONSTANT MACH NUMBER: MODEL COMPARISON.

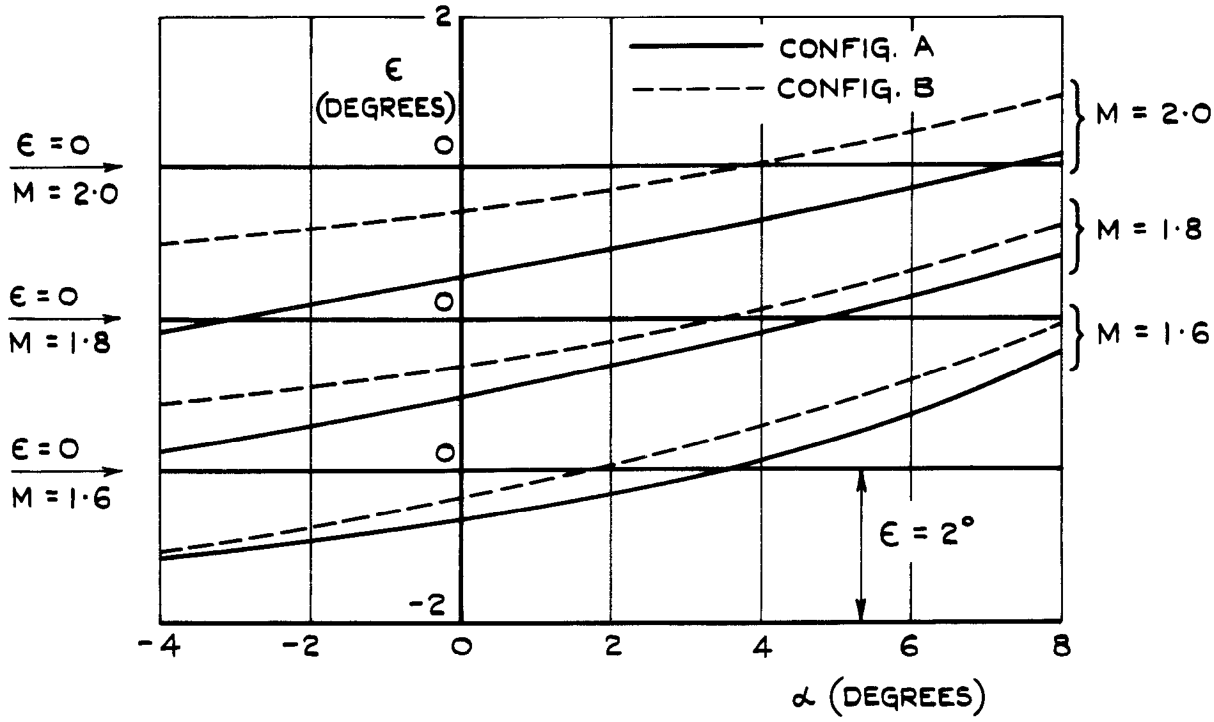

FIG. 52. VARIATION OF DOWNWASH AT POSITION OF TAILPLANE WITH INCIDENCE: MODEL COMPARISON.

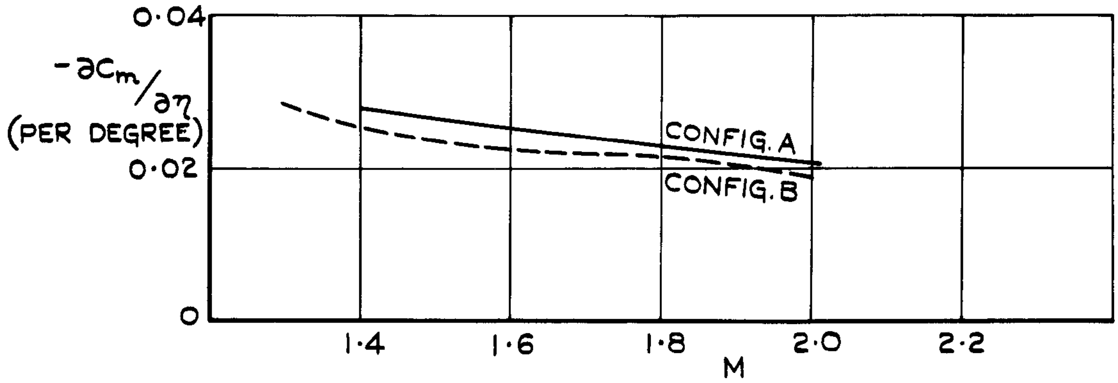

FIG. 53. VARIATION OF TAILPLANE POWER WITH MACH NUMBER: MODEL COMPARISON.

A.R.C. C.P. No.818
September, 1961

533.652.1: 533.6.013.412/413:
533.6.011.5: 533.694.23:
533.6.013.12: 533.695.3

SUPERSONIC WIND TUNNEL TESTS ON A 1/12TH SCALE MODEL OF THE BRISTOL TYPE 188 RESEARCH AIRCRAFT, PART I: M = 1.4 to 2.0. Taylor, C. R. and Cook, T. A.

Six component force tests at Mach numbers 1.4, 1.6, 1.8 and 2.0 have been made on a 1/12th scale model of the Bristol Type 188 in the 8 ft tunnel at Bedford. The results are analysed to give drag, longitudinal and lateral stability data, and to show the effects of control movements, dive brakes, and nacelle spillage.

Some comparisons are made with the results of earlier tests on a 1/36th scale model.

A.R.C. C.P. No.818
September, 1961

533.652.1: 533.6.013.412/413:
533.6.011.5: 533.694.23:
533.6.013.12: 533.695.3

SUPERSONIC WIND TUNNEL TESTS ON A 1/12TH SCALE MODEL OF THE BRISTOL TYPE 188 RESEARCH AIRCRAFT, PART I: M = 1.4 to 2.0. Taylor, C. R. and Cook, T. A.

Six component force tests at Mach numbers 1.4, 1.6, 1.8 and 2.0 have been made on a 1/12th scale model of the Bristol Type 188 in the 8 ft tunnel at Bedford. The results are analysed to give drag, longitudinal and lateral stability data, and to show the effects of control movements, dive brakes, and nacelle spillage.

Some comparisons are made with the results of earlier tests on a 1/36th scale model.

A.R.C. C.P. No.818
September, 1961

533.652.1: 533.6.013.412/413:
533.6.011.5: 533.694.23:
533.6.013.12: 533.695.3

SUPERSONIC WIND TUNNEL TESTS ON A 1/12TH SCALE MODEL OF THE BRISTOL TYPE 188 RESEARCH AIRCRAFT, PART I: M = 1.4 to 2.0. Taylor, C. R. and Cook, T. A.

Six component force tests at Mach numbers 1.4, 1.6, 1.8 and 2.0 have been made on a 1/12th scale model of the Bristol Type 188 in the 8 ft tunnel at Bedford. The results are analysed to give drag, longitudinal and lateral stability data, and to show the effects of control movements, dive brakes, and nacelle spillage.

Some comparisons are made with the results of earlier tests on a 1/36th scale model.

A.R.C. C.P. No.818
September, 1961

533.652.1: 533.6.013.412/413:
533.6.011.5: 533.694.23:
533.6.013.12: 533.695.3

SUPERSONIC WIND TUNNEL TESTS ON A 1/12TH SCALE MODEL OF THE BRISTOL TYPE 188 RESEARCH AIRCRAFT, PART I: M = 1.4 to 2.0. Taylor, C. R. and Cook, T. A.

Six component force tests at Mach numbers 1.4, 1.6, 1.8 and 2.0 have been made on a 1/12th scale model of the Bristol Type 188 in the 8 ft tunnel at Bedford. The results are analysed to give drag, longitudinal and lateral stability data, and to show the effects of control movements, dive brakes, and nacelle spillage.

Some comparisons are made with the results of earlier tests on a 1/36th scale model.

U.D.C. No. A.I(42)Bristol 188: 533.652.1:533.6.011.5:533.6.013.1:533.6.013.4

C.P. No.818
September, 1961

SUPERSONIC WIND TUNNEL TESTS ON A 1/12TH SCALE MODEL OF THE BRISTOL TYPE 188 RESEARCH AIRCRAFT
PART TWO: M = 2.0 TO 2.7

by

T. A. Cook, B.Sc.

SUMMARY

Six component force measurements have been made on a 1/12th scale model of the Bristol Type 188 in the 8 ft × 8 ft wind tunnel at R.A.E., Bedford, at Mach numbers of 2.00, 2.20, 2.40, and 2.70. The results of these measurements are presented graphically, with an analysis of the effects of tailplane movement, aileron and rudder controls, and airbrakes on longitudinal and lateral stability, and drag.

LIST OF CONTENTS

LIST OF TABLES

LIST OF ILLUSTRATIONS

LIST OF ILLUSTRATIONS (Contd.)

1 INTRODUCTION

This paper describes further tests in the 8 ft × 8 ft high speed wind tunnel at R.A.E., Bedford, on a 1/12th scale model of the Bristol Type 188. Part 1 of this paper[1] described tests and presented results for Mach numbers of 1.40, 1.60, 1.80 and 2.00. In the present series the tests are continued to Mach numbers of 2.20, 2.40 and 2.70. The tests were also repeated at a Mach number of 2.00 to provide continuity with the earlier tests: the results for this repeat case agreed with those of Part 1 within the limits of the experimental errors. In general the programme of tests was the same as that for the earlier tests, though some changes were made as a consequence of results obtained at the lower Mach numbers, (these changes are detailed in Section 3 below).

The principal references to other wind tunnel tests on models of the Bristol Type 188, already mentioned in Part 1, are included in the list of references appended to this report[2,3,4].

2 THE MODEL

The model has been fully described in Part 1[1]. The general arrangement is shown here in Fig.1 and a photograph of the model mounted in the wind tunnel in Fig.2. The principal dimensions of the model with other essential model details are listed in Table 1.

For the purpose of the present series of tests, the balance was completely recalibrated. Six-component force measurements were derived from the two four-component balances mounted in the nacelles[1] and were fully corrected for balance interactions.

3 DETAILS OF THE TESTS

The tests were made in the 8 ft × 8 ft high speed wind tunnel at R.A.E., Bedford, at Mach numbers of 2.00, 2.20, 2.40 and 2.70. The Reynolds number, based on standard mean chord, was maintained constant at 2.5×10^6, except at $M = 2.70$ where tunnel power limited the Reynolds number to 2.1×10^6.

The configurations of the model tested are listed in Table 2. This list is not identical to that of Part 1[1]. Tests with open spill vents were not continued since the spill vents were found to have negligible effects: likewise a test with a rudder setting of -2.5° and a tailplane setting of -14° was not made, since rudder power was found not to be significantly affected by tailplane setting. Some additions to the programme were also thought desirable. These included a test with the fin on and the tailplane removed, to investigate the contribution of the tailplane to the fin effectiveness. A test with the ailerons deflected and the tailplane and fin off was made to assist analysis of the side forces and yawing moments induced by aileron movement. Finally, a test with airbrakes open and a tailplane setting of -10° was included to examine possible effects of the airbrakes on tailplane power.

The results refer to stability axes with their origin (i.e. moment reference point) at 18% of the standard mean chord, in the plane of the nacelle centre lines. Incidences measured were those of the nacelle centre lines, (the wing-nacelle angle was $+2^\circ$). Angles of incidence and sideslip were computed using the tangent and sine definitions respectively and were corrected for balance and sting deflections. Pitching moment coefficients have been based on the wing standard mean chord: force measurements were corrected for the difference between free-stream static pressure and the pressure at the balance axial force units. Allowance was also made for the internal drag of the nacelle ducts.

The mass flow through each nacelle was calculated, using pitot and static pressure measurements near the exit, and expressed as the cross-sectional area (A_o) of a free-stream tube. This area, in terms of the area enclosed by the cowl lip of each nacelle, A_{E_N}, is plotted in Fig.3. Two cases are shown, for angles of incidence of zero and 14^o: the zero incidence case is compared with the calculated maximum intake mass-flow. The fact that the ratio A_o/A_{E_N} exceeds unity for the zero incidence case is due to errors in the determination of the effective mass flow area at each duct exit measuring station. Fig.3 shows that maximum mass flow at zero incidence is reached at a Mach number of about 2.40. (This conclusion can be roughly verified by comparison of the plan view schlieren photographs in Figs.14 to 17, from which it appears that the shock waves from the intake centre bodies lie just within the cowl lips at $M = 2.40$, though the presence of the shock waves from the canopy of the model introduces a complication.)

The position of boundary-layer transition on the wind-swept surfaces of the model was fixed using distributed roughness bands. These were formed by sprinkling grade 100 carborundum particles on to an araldite base: the approximate maximum projection height of the particles above the model surface was 0.008 in. The locations and widths of these bands are included in the model details of Table 1. The effectiveness of the roughness bands in fixing transition on the wings was verified at $M = 2.70$ and zero incidence and sideslip using the azobenzene technique.

Probable errors in the coefficients derived from the balance measurements were estimated to be as follows:-

C_L :	$\pm$ 0.003	$\pm$ 0.004	C_L
C_Y :	$\pm$ 0.002	$\pm$ 0.002	C_Y
C_D :	$\pm$ 0.007	$\pm$ 0.007	C_D
C_m :	$\pm$ 0.0005	$\pm$ 0.003	C_m
C_ℓ :	$\pm$ 0.0007	$\pm$ 0.004	C_ℓ
C_n :	$\pm$ 0.0007	$\pm$ 0.007	C_n

The first term in each error includes zero errors, resolution errors, balance hysteresis errors, and, in the case of drag, uncertainty in the correction for the internal drag of the engine nacelles. The second term in each error is based on balance calibration errors.

Angles of incidence and sideslip are accurate to $\pm 0.01^o$ in resolution, but tunnel flow deflections at the position of the model may have been as large as 0.2^o. Control plate deflections under load were less than 1% of the nominal setting for the rudder and 2% of the nominal setting for the ailerons.

4 PRESENTATION AND DISCUSSION OF THE RESULTS

Results of the tests are presented graphically in Figs.4 to 54. Included in the results are some estimates of flight conditions for the full-scale aircraft, based on the assumption that the aircraft does not suffer any aeroelastic distortions.

4.1 Lift and pitching moment

The model was tested with tailplane settings of -4°, -10° and -14°, relative to the nacelle centre-lines. Tests were also made with the tailplane and fin off, and, except at $M = 2.00$, with the tailplane off and the fin on. Differences in lift, pitching moment and drag between the latter two configurations were small and so only the results for the tailplane and fin off case have been plotted. The results for the tailplane off and fin on configuration have been used in the analysis to calculate downwash angles, (except at $M = 2.00$ where the tailplane and fin off results have had to be used).

Lift coefficients are plotted against incidence in Figs.4 to 7 and pitching moment coefficients against lift coefficient in Fig.8. Lift-curve slopes are shown in Fig.9 (mean values for the complete model have been plotted since the variation with tail setting was very small), and longitudinal stability slopes as functions of Mach number and lift coefficient are plotted in Figs.10 and 11 respectively. Tailplane power was calculated as the change in pitching moment, per degree, between tailplane setting of -4° and -14° and values are plotted against incidence in Fig.12.

Fig.11 shows a pronounced stability "peak" at $M = 2.70$ and a lift coefficient of about 0.4. This peak falls off as the tailplane angle becomes more negative, while, in the tailplane and fin off case (Fig.11(d)), there is a small but significant stability maximum under the same conditions. Since there is a small, corresponding increase in C_L for these configurations (Figs.4 to 7) this implies an increase in tailplane lift with a small contribution from the rear fuselage.

Downwash angles at the position of the tailplane have been estimated from the absolute values of the pitching moments produced by the tailplane and are plotted in Fig.13. Between model incidences of approximately 4° ($C_L \simeq 0.2$) and 12° ($C_L \simeq 0.5$), there are rapid variations in mean downwash angle at $M = 2.70$, which correspond to the stability changes. Smaller, similar effects are observed at $M = 2.40$ and $M = 2.20$.

The large variations in downwash are due to the change in position of the wing trailing edge shock wave relative to the tailplane of the model as incidence varies. From the schlieren photographs of Figs.17 and 18 and the explanatory diagram of Fig.19, it is evident that the wing trailing edge shock wave at $M = 2.70$ must lie either behind the tailplane or across it at low incidences, and move towards the leading edge of the tailplane as incidence increases. Thus, at low incidences, the tailplane is in the flow field of the upper surface of the wing with associated large flow angles, but, at higher incidences, it is in the wing wake with much smaller flow angles. Thus the fall in downwash angle, most pronounced at $M = 2.70$, is due to the movement of the tailplane out of the wing pressure field into the wing wake. This effect falls off rapidly with decreasing Mach number. It would appear that the wing trailing edge shock wave lies upstream of the tailplane at incidences greater than those corresponding to the minima of the downwash curves in Fig.13.

The slopes of plots of pitching moment due to the tailplane against tailplane setting, at $M_0 = 2.70$, were found to vary by up to 20% about the mean values over the range $-4^\circ \geq \eta \geq -14^\circ$ plotted in Fig.12. This variation is caused by the changes in downwash which can be expected over the region through which the tailplane sweeps when tailplane setting is varied at constant model incidence. This effect, together with that due to the change in model incidence (up to about 1.5^o) required to keep C_L constant, explains the large variations in the longitudinal stability of the model at zero lift for different tail settings at constant Mach number (Fig.10).

Figs.20 and 21 show trimmed lift curves and tailplane settings to trim respectively. Since the moment reference point of the model was chosen to coincide with the estimated centre of gravity of the full-scale aircraft, these curves apply to the aircraft as well as to the model. Estimates of the tailplane setting required and the aircraft incidence under a few flight conditions have been made, assuming an aircraft weight of 32,000 lb. These estimates are plotted in Figs.22 and 23 respectively.

4.2 Lateral coefficients

Typical plots of the lateral coefficients C_Y, C_n and C_ℓ against angle of sideslip are shown in Figs.24 to 26. The variations of the lateral derivatives n_v, y_v and ℓ_v, based on the changes in C_n, C_Y, C_ℓ between $\beta = +2^o$ and $\beta = -2^o$, are shown against incidence in Figs.27 to 30. In these figures the effects of varying tailplane setting and the contributions to the lateral derivatives of the fin and tailplane are compared.

Fig.27 shows an increase in n_v for the complete model up to an incidence in the region of 6^o to 8^o, except at $M = 2.70$. Since there is a decrease in n_v above about 2^o incidence for the tailplane off, fin on configuration, (i.e. a loss of fin effectiveness with the tailplane absent), it is apparent that the increase for the complete model is due to the influence of the tailplane on fin effectiveness. At zero incidence the contribution of the tailplane to fin effectiveness is very small or negative, but this contribution increases with increasing incidence. The tailplane effect is the result of two influences, viz the reflection plate effect of the tailplane on top of the fin, and the variation in dynamic pressure with incidence over part of the fin due to the tailplane lift. The latter effect is sensitive to downwash: both effects decrease with increasing Mach number since the region of the fin influenced by the tailplane decreases, (this would explain why n_v does not increase with incidence at $M = 2.70$). n_v is decreased by increasing negative tail setting, probably due mainly to the variation in dynamic pressure.

The loss of fin effectiveness in the absence of the tailplane above about 2^o incidence, and, with the exception of $M = 2.70$, with the tailplane present above about 8^o is probably due to the destabilising effect of vortices from the fuselage. (These vortices are visible in Figs.14 to 18.) The results for tailplane setting -14^o at $M = 2.40$ and 2.70 indicate, however, that this loss of fin effectiveness is only partial at these Mach numbers, in fact at $M = 2.70$ there is a further increase in n_v above about 12^o incidence. This latter effect is most probably a further consequence of the wing downwash field discussed in Section 4.1. (Comparing Figs.13 and 27, it will be noted that the downwash minimum at $\alpha = 12^o$ and $M = 2.70$ corresponds to the minimum of n_v for tailplane setting -14^o.)

The variation of n_v with incidence for the trimmed configuration is shown in Fig.28. As a result of the loss of n_v with increasing negative tail-setting, n_v shows no increase with incidence: in fact, there is a loss of n_v with increasing incidence over the whole range shown. Some full-scale flight estimates are included in this figure.

The variations of y_v and ℓ_v (Figs.29 and 30) show that, in both cases, there is a loss of fin effectiveness with the tailplane removed above about 2^o incidence. As in the case of n_v, this loss is alleviated by the presence of the tailplane. The results for ℓ_v show that, although the contribution of the fin and tailplane becomes zero at about 12^o incidence, the complete model remains stable in roll as a result of the increase with incidence in the roll stability of the rest of the model.

4.3 Drag

Variations of drag coefficient with lift coefficient for the model with various tail settings and with the tailplane and fin off are shown in Figs.31 to 34. These results have been analysed by assuming the curves to be of the form:

$$C_D = C_{D_o} + \frac{K}{\pi A}(C_L - C_{L_o})^2 ,$$

where C_{D_o} is the minimum drag coefficient, C_{L_o} is the value of the lift coefficient at which $C_D = C_{D_o}$, A is the aspect ratio of the wing, and K is a constant, the induced drag factor.

The applicability of this equation is illustrated in Fig.35 where C_D is plotted against $(C_L - C_{L_o})^2$ for one configuration. C_D was found to be a linear function of $(C_L - C_{L_o})^2$ up to a lift coefficient of approximately 0.5 for all Mach numbers.

C_{L_o} was found to vary little with Mach number for each configuration. The mean values of C_{L_o} are given in the following table:

Tailplane setting	-4^o	-10^o	-14^o	Tailplane and fin off
C_{L_o}	-0.004	-0.009	-0.011	+0.006

Values of C_{D_o} and K are plotted in Figs.36 and 37 respectively. Tailplane setting was found to have no significant effect on induced drag factor: consequently the mean values have been plotted in Fig.37.

It should be noted in connection with the drag results that the probable experimental errors were large, being $\geqslant 0.007$. Of this error $\pm$ 0.003 is ascribed to uncertainty in the correction for the internal drag of the ducts which is a constant error for the whole series of tests, and except for a small allowance for scatter, the rest of the error is uncertainty due to balance hysteresis. Neither of these two sources of error affect the induced drag factors measured, and, while both apply to C_{D_o}, only the hysteresis and scatter error, i.e. ±0.004, will apply to the differences between the C_{D_o} curves for different configurations. In Fig.36 results from Ref.1 are included and 'trend lines' have been drawn through the mean values from Ref.1 and the present tests at M = 2.00, and parallel to lines through the experimental points at Mach numbers above and below 2.00. This is thought to be the most suitable method of presenting the measured values of C_{D_o} but the difference at M = 2 between the two sets of tests illustrates the poor accuracy of absolute drag obtainable on this model.

4.4 Effect of the rudder

The model was tested with rudder settings of 0, -2.5° and -5°, at a fixed tailplane setting of -4°. Results for the configuration with a rudder setting of -5° were not obtained for M = 2.20.

Fig.38 shows the variation of yawing moment due to rudder for several angles of incidence of the model. This shows that rudder power varies with rudder setting for most angles of incidence: mean values of rudder power, i.e. the change in yawing moment per degree for a rudder movement of -5°, are plotted against incidence in Fig.39.

Side forces due to rudder movement were found to be small, corresponding in magnitude for the -5° rudder case to a change in sideslip angle of the model of approximately 0.5°.

4.5 Effect of the ailerons

The model was tested with aileron settings of 0, -10°, and -20° at a constant tailplane setting of -4°. Results for the case of aileron setting -10° were not obtained for M = 2.20. The model was also tested with an aileron setting of -20° and the tailplane and fin removed.

Fig.40 shows the variation of rolling moment due to aileron with aileron setting for angles of incidence of 0 and 12°. The variations shown are non-linear, but with no consistent trends. There is evidently very little variation of aileron power with model incidence: this is shown in Fig.41, where ℓ_ξ has been calculated from the changes in rolling moment produced by -20° aileron movement.

Associated with aileron movement are large variations of side force and yawing moment with incidence. These are plotted in Figs.42 and 43, where the side force and yawing moment changes induced by -20° ailerons are shown, with and without the tailplane and fin present. For the tailplane and fin off case, the variations of C_Y and C_n with incidence most likely have independent explanations. The side force can probably be ascribed to sidewash on the wing and nacelle surfaces induced by the pressure difference across the gaps between the aileron horns and the wings, while the yawing moment variations are due mainly to the differential drag of the two ailerons when the wing is at incidence. The latter explanation is supported by the fact that the induced yawing moments are zero at about -1° of incidence, which almost coincides with the attitude for zero wing incidence, viz -2° incidence, when the two ailerons should each have nearly the same drag.

The aileron-induced sidewashes produce an effect on the tailplane and fin which is approximately constant with incidence. This is surprising in view of the fact that the sidewash on the wing varies with incidence: it may be fortuitous in that, as incidence increases, the fin is moving out of the region influenced by the ailerons and that the reduction of side force expected for this reason cancels the increase due to the increase of sidewash with incidence. As Mach number increases, so the fin again moves out of the region of influence of the ailerons and the reduction in side force and yawing moment produced by the fin due to this cause is observed in the figures.

Aileron movement also results in significant changes in the lateral derivatives n_v, y_v and ℓ_v, (Figs.44 to 46). The variations of n_v with incidence (Fig.44) show a reversal of the effect of ailerons with increasing Mach number: at $M = 2.00$ aileron movement results in a loss of n_v but by $M = 2.70$ aileron movement causes an increase in n_v. y_v variations (Fig.45) are similar, but much smaller in magnitude than those of n_v. Generally, aileron movement causes loss of $-\ell_v$ (Fig.46), but this effect is irregular.

The effect of the ailerons on longitudinal stability is shown in Fig.47: stability is increased as a result of aileron movement.

4.6 Effect of the airbrakes

Tests were made with the airbrakes in the fully-open position and tailplane settings of -4° and -10°. The results are compared with those for the model with the airbrakes closed.

The effect of the airbrakes on drag is shown in Figs.48 and 49. The increment in minimum drag due to opening the airbrakes changed insignificantly with tailplane setting and so only the case for a tailplane setting of -4° is shown in Fig.48. The mean value of C_{L_o} over all Mach numbers for the configuration with open airbrakes and tailplane setting -4° was found to be $+0.001$.

The airbrakes were found to affect both longitudinal and lateral stability. The effects of the airbrakes on longitudinal stability are shown in Fig.50, from which it is seen that stability is reduced by opening the airbrakes at $M = 2.00$ but is increased at the higher Mach numbers. However the change in stability shows an irregular variation with Mach number and tailplane setting, which is no doubt a result of the complications added by the wake from the airbrakes to the already-complex flow around the fin and tailplane. Some Schlieren photographs of the model with open airbrakes are shown in Fig.51.

Tailplane powers, based on the differences in pitching moments between configurations with tailplane settings of -4° and -10°, are plotted in Fig.52. This shows some effect due to opening the airbrakes, but again the effect is irregular.

Opening the airbrakes generally results in small losses of $-y_v$ and n_v, (Figs.53 and 54 respectively). No significant effects of airbrakes on ℓ_v were observed.

5 CONCLUSIONS

Results of the tests for Mach numbers of 2.00, 2.20, 2.40 and 2.70 described in this report show the following main conclusions:-

1 Longitudinal stability changes appreciably with changes in Mach number, incidence and tailplane setting at the higher Mach numbers where the flow in the neighbourhood of the tailplane is strongly influenced by the position of the wing trailing edge shock pattern. Generally, longitudinal stability is increased by movement of the ailerons and by opening the airbrakes.

2 Yawing moment due to sideslip increases with incidence up to about 8° due to the influence of the tailplane but falls with increasing negative tail setting and with increasing incidence above 8°. For the trimmed configuration n_v decreases with incidence for all positive incidences. Aileron movement results in a loss of n_v at the lower test Mach numbers and an increase of n_v at the higher Mach numbers. Opening the airbrakes results in a small loss of n_v at all Mach numbers.

3 Rolling moment due to sideslip is decreased by increasing negative tail setting, but shows no regular variation with incidence, though the fin contribution decreases with increasing incidence. Generally, aileron movement results in a loss of $-\ell_v$.

4 Aileron movement produces large side force and yawing moment variations with incidence.

ACKNOWLEDGEMENT

The author is grateful to Mr. C. F. Millard for his work in preparing most of the figures for this report.

LIST OF SYMBOLS

A	Aspect ratio of nominal wing planform
b	Wing span
$\bar{c}$	Standard mean chord of wing
S	Gross area of nominal wing planform
q	Free-stream dynamic pressure
M	Free-stream Mach number
C_L	Lift coefficient = Lift force/qS
C_Y	Side force coefficient = Side force/qS
C_D	Drag coefficient = Drag force/qS
C_m	Pitching moment coefficient = Pitching moment/$qS\bar{c}$
C_ℓ	Rolling moment coefficient = Rolling moment/qSb
C_n	Yawing moment coefficient = Yawing moment/qSb

LIST OF SYMBOLS (Contd.)

α	Angle of incidence of nacelle centre lines
β	Angle of sideslip
η	Tailplane angle relative to nacelle centre lines
ζ	Rudder angle
ξ	Aileron angle
ε	Downwash angle relative to the free-stream direction
y_v	Side force due to sideslip $= \frac{1}{2}\,\partial C_Y/\partial\beta$, β in radians
n_v	Yawing moment due to sideslip $= \partial C_n/\partial\beta$, β in radians
ℓ_v	Rolling moment due to sideslip $= \partial C_\ell/\partial\beta$, β in radians
n_ζ	Yawing moment due to rudder $= \partial C_n/\partial\zeta$, ζ in radians
ℓ_ξ	Rolling moment due to aileron $= \partial C_\ell/\partial\xi$, ξ in radians
C_{D_o}	Minimum drag coefficient
C_{L_o}	Lift coefficient corresponding to $C_D = C_{D_o}$
K	Induced drag factor $= \pi A.\ \partial C_D/\partial(C_L - C_{L_o})^2$
A_o	Cross-sectional area of free-stream tube swallowed by either nacelle duct
A_{E_N}	Area enclosed by cowl lip of either nacelle

LIST OF REFERENCES

Ref.No.	Author(s)	Title, etc.
1	Taylor, C.R. Cook, T.A.	Supersonic wind tunnel tests on a 1/12th scale model of the Bristol Type 188 research aircraft, Part 1, M = 1.4 to 2.0. **Part 1 of this Current Paper.**
2	Leathers, J.W.	Low speed wind tunnel tests on a 1/10th scale model of a twin jet aircraft, Bristol 188. RAE Tech Note No. Aero 2515, ARC 20047 July 1957.

LIST OF REFERENCES (Contd)

Ref.No.	Author	Title, etc.
3	Squire, L.C.	Wind tunnel tests up to M = 2.0 on a model of the supersonic research aircraft ER134 (Bristol 188). RAE Report No. Aero 2633, ARC 22,064 December 1959.
4	Landon, R.H.	Longitudinal and lateral stability tests and effects of controls on a 1/12th scale model of the Bristol Type 188. Unpublished Aircraft Research Assocn. Report.

TABLE 1

Principal details of the model

Scale: 1/12th

Wing:

Area S (gross) :-	2.75 ft^2
Span b:-	2.924 ft
Aspect ratio A:-	3.108
Standard mean chord $\bar{c}$:-	0.941 ft
Aerodynamic mean chord $\bar{\bar{c}}$:-	1.025 ft
Distance of leading edge of $\bar{c}$ aft of leading edge of inboard wing:-	0.143 ft
Dihedral:-	0
Wing-body (and wing-nacelle) angle	2^{o}
Sweep back of leading edge:-	
Inboard of nacelles:-	0
Outboard of nacelles:-	38^{o}
Aileron horn:-	65^{o}
Sweep forward of trailing edge:-	5^{o}
Section (excluding aileron horns):- Biconvex, circular arc, with sharp leading edge, t/c = 4%; maximum thickness at 55% on inboard wing, and 51% outboard.	
Section (aileron horns):- faired from above to 8% RAE 104 at tip	
Gap between wing and aileron horn:-	0.008 in.

Fuselage:

Length:-	5.917 ft

Fin:

Area:-	0.528 ft^2
Sweep back of leading edge:-	64^{o}
Section:- Modified RAE 104 with constant maximum thickness. 4% t/c at tip chord	

Tailplane:

Area:-	0.484 ft^2
Span:-	1.292 ft
Aspect ratio:-	3.4
Root chord:-	0.5 ft
Tip chord:-	0.25 ft
Section:- $4\frac{1}{2}$% circular arc.	
Height of tailplane pivot above nacelle datum lines:-	0.682 ft
Distance of pivot aft of moment reference point:-	2.418 ft

Nacelles:

Distance of nacelle centre-lines outboard of fuselage centre-line:-	0.625 ft

Airbrakes:

Forward brakes:	
Gross area:-	3.03 $in.^2$
Open area:-	0.89 $in.^2$

TABLE 1 (CONTD.)

Airbrakes (Contd.) :-	
Aft brakes:	
gross area:-	3.05 in.^{2}
open area:-	0.79 in.^{2}
Roughness bands:	
Wings: band width:-	5% of chord
position of forward edge:-	$2\frac{1}{2}$% of chord
Aileron horns:- band width:-	0.25 in.
position of forward edge:-	0.25 in. aft of leading edge
Fuselage: band width:-	0.5 in.
position of forward edge:-	1.0 in. aft of nose
Fin: band width:-	0.5 in.
position of forward edge:-	at leading edge
Tailplane: band width:-	0.5 in.
position of forward edge:-	0.25 in. aft of leading edge
Nacelle cowls: band width:-	0.5 in.
position of forward edge:-	0.25 in. aft of lips
Nacelle centre bodies: band width	0.5 in.
position of forward edge:-	0.25 in. aft of apex

TABLE 2

List of configurations tested

	Configuration		Test range (see Table 3)
1	Clean aircraft;	tailplane -4°	A
2	Clean aircraft;	tailplane -10°	A
3	Clean aircraft;	tailplane -14°	B
4	Clean aircraft;	tailplane off	A
5	Clean aircraft;	tailplane and fin off	A
6	Ailerons -10° ;	tailplane -4°	C
7	Ailerons -20° ;	tailplane -4°	C
8	Ailerons -20° ;	tailplane and fin off	C
9	Rudder -2.5° ;	tailplane -4°	C
10	Rudder -5.0° ;	tailplane -4°	C
11	Airbrakes open;	tailplane -4°	C
12	Airbrakes open;	tailplane -10°	C

TABLE 3

Model attitude ranges

Incidence (degrees)	Sideslip (degrees)		
	Range A	Range B	Range C
-4	0, ±2	0, ±2	0, ±2
-2	0, ±2	0, ±2	0
0	0, ±1, ±2, +4, +6	0, ±1, ±2, +4, +6	0, ±1, ±2, +4, +6
2	0, ±2	0, ±2	0
4	0, ±1, ±2, +4, +6	0, ±1, ±2, +4, +6	0, ±1, ±2, +4, +6
6	0, ±2	0, ±2	0
8	0, ±1, ±2, +4, +6	0, ±1, ±2, +4, +6	0, ±1, ±2, +4, +6
10	0, ±2	0, ±2	0
12	0, ±2	0, ±2	0, ±2
14	0	0	0
16	-	0, ±2	
18	-	0	
20	-	0, ±2	

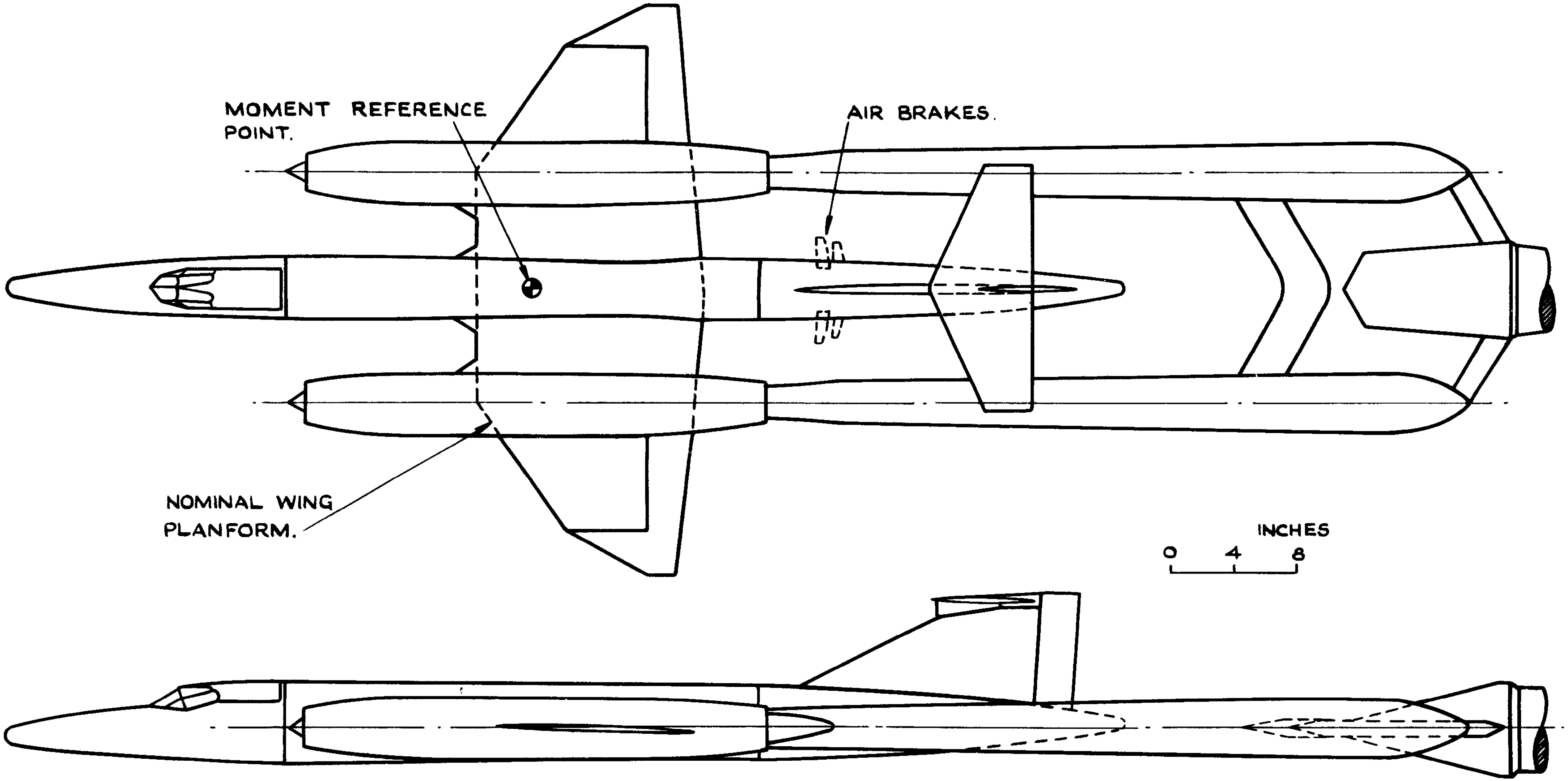

FIG. 1. GENERAL ARRANGEMENT OF MODEL AND SUPPORT SYSTEM

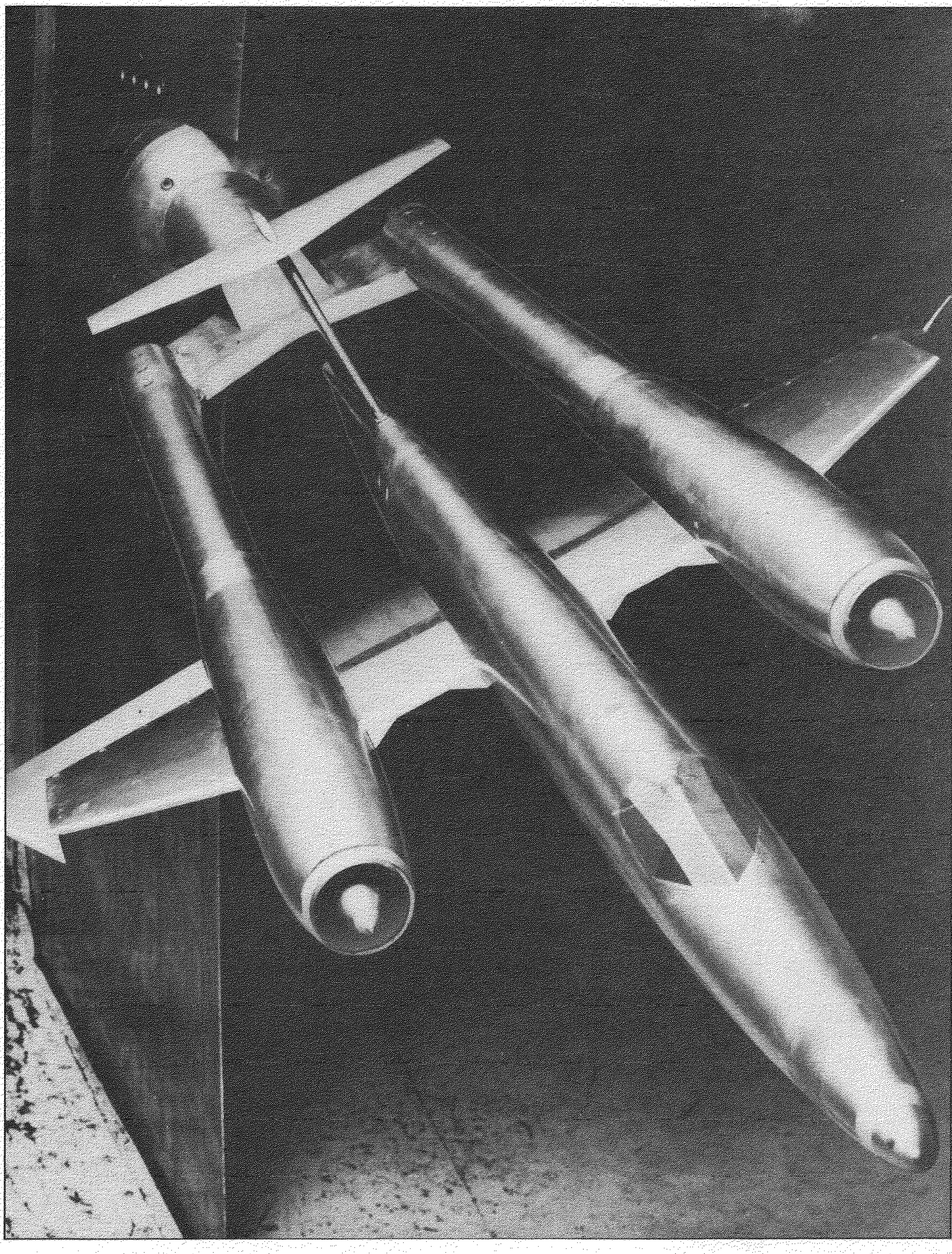

FIG.2. MODEL IN THE WIND TUNNEL

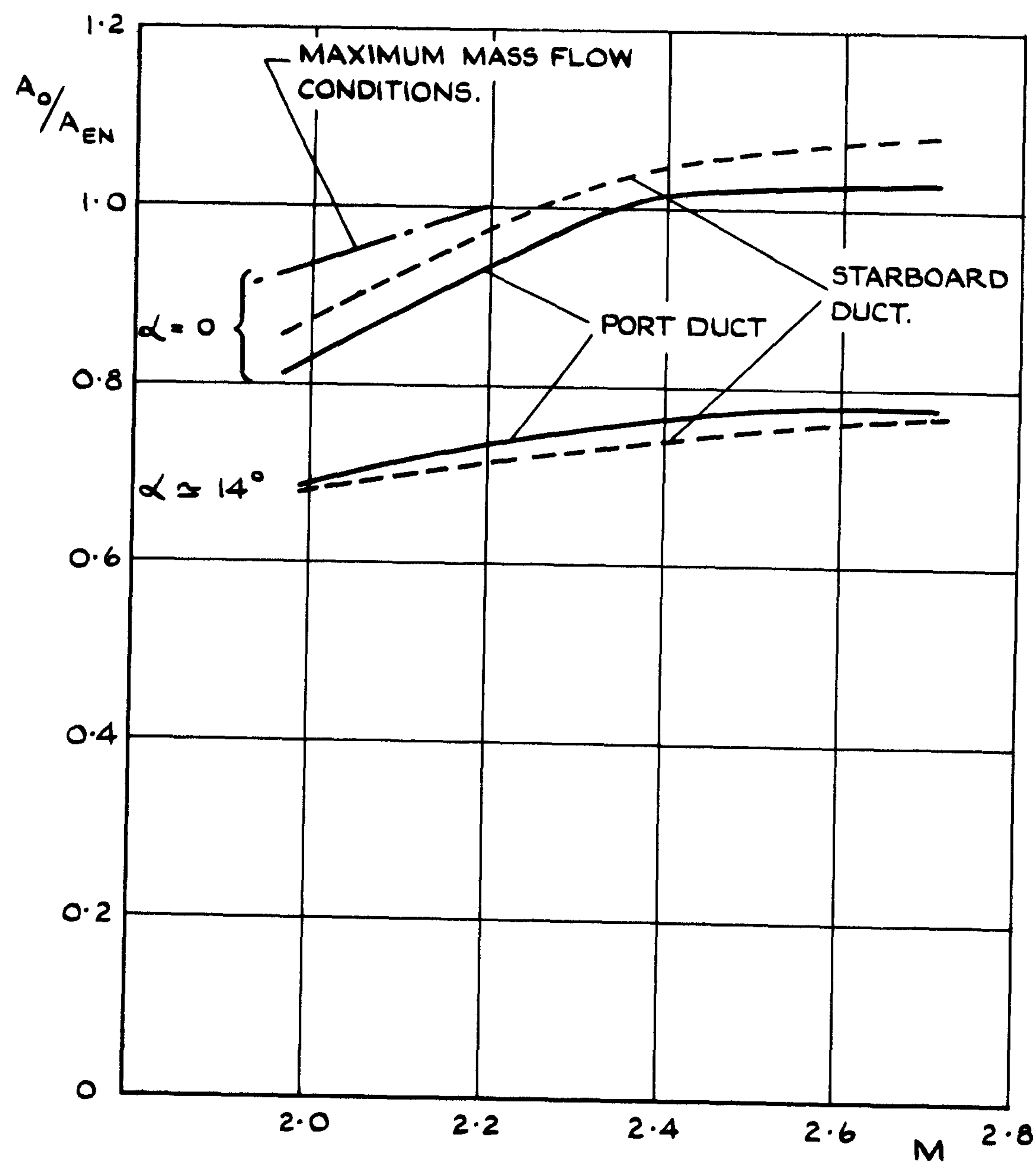

FIG. 3. DUCT MASS FLOW

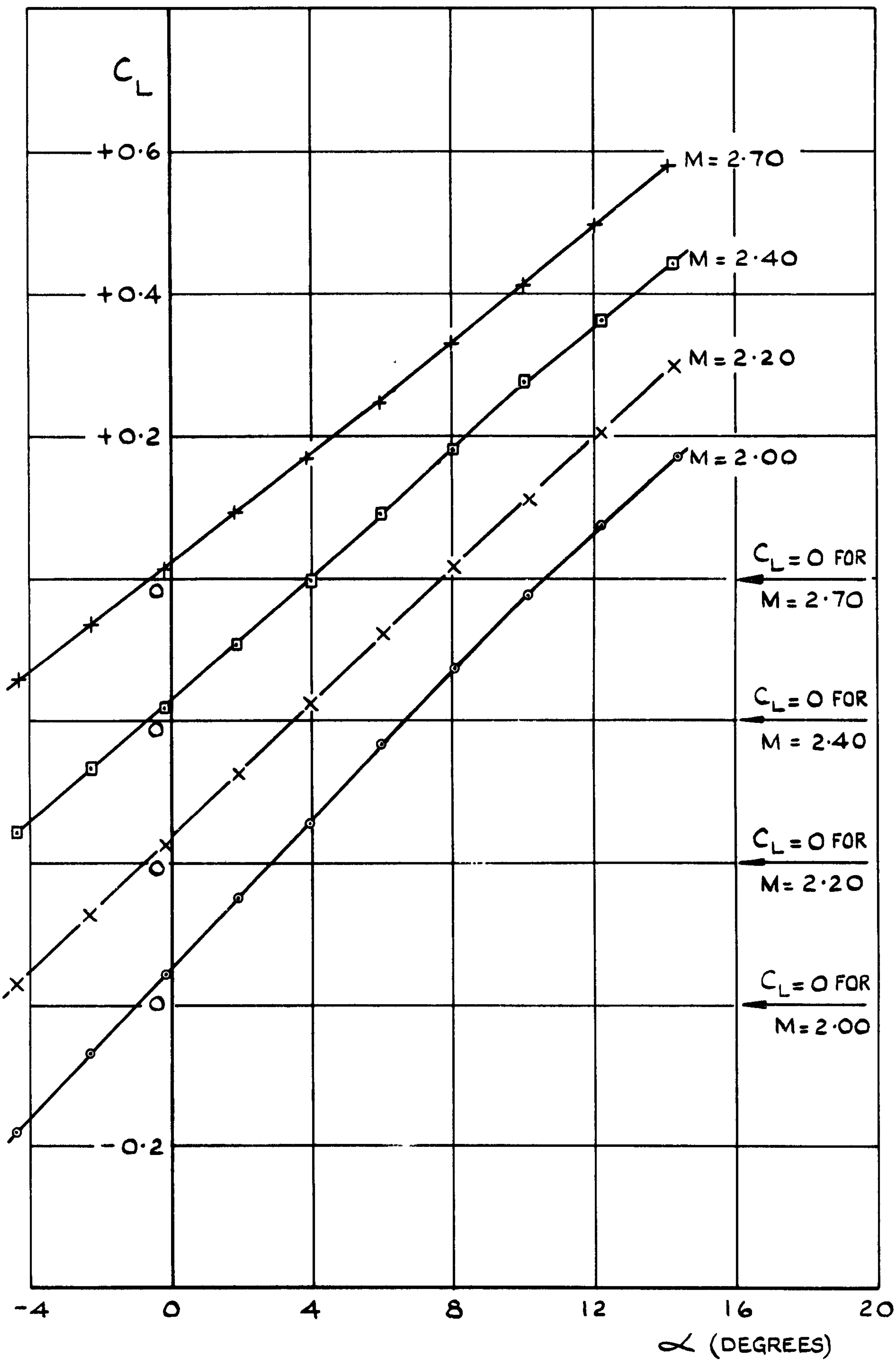

FIG. 4 VARIATION OF C_L WITH α AT CONSTANT MACH NUMBER : $\eta = -4^\circ$

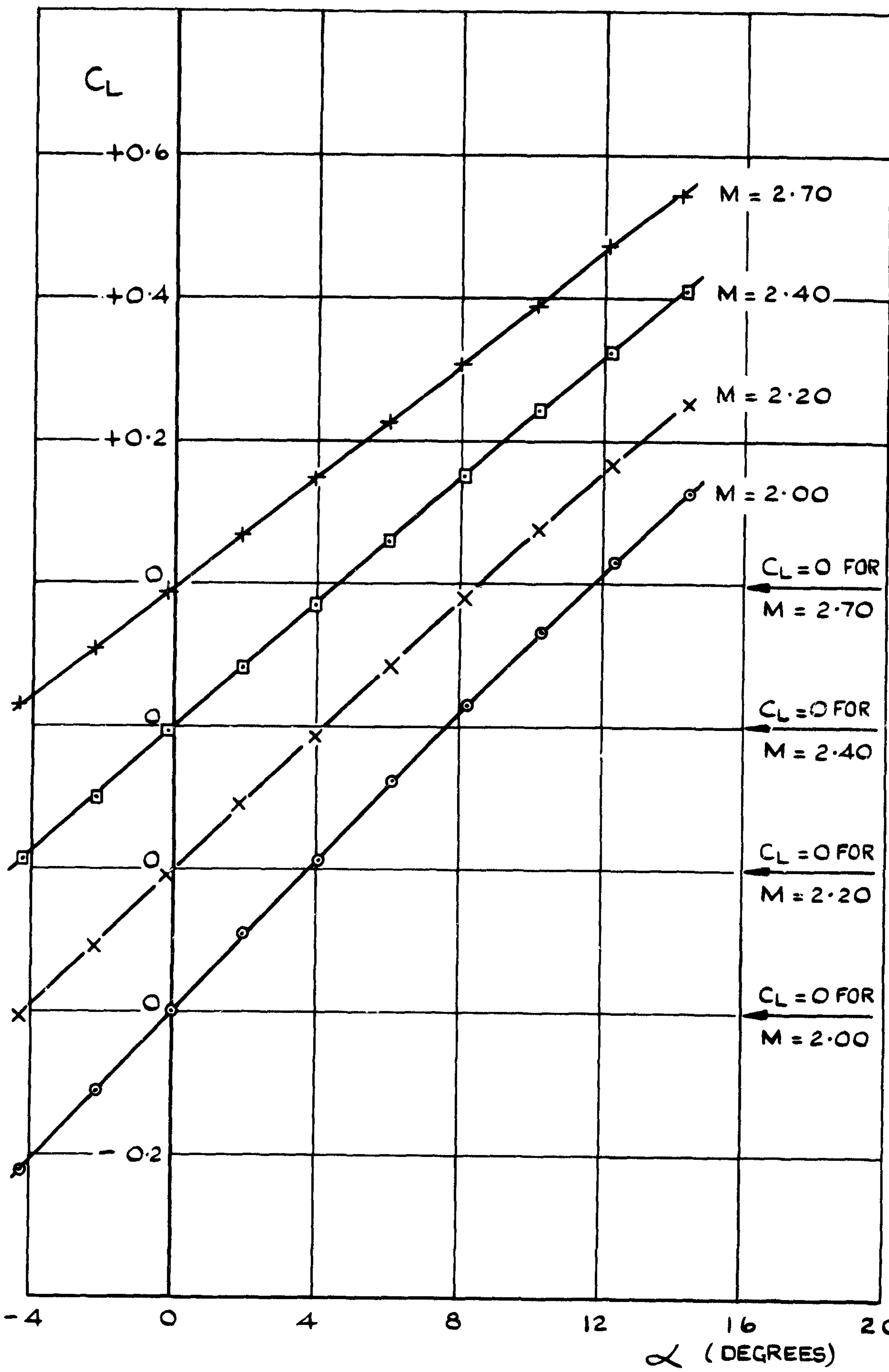

FIG. 5. VARIATION OF C_L WITH α AT CONSTANT MACH NUMBER : $\eta = -10^{\circ}$

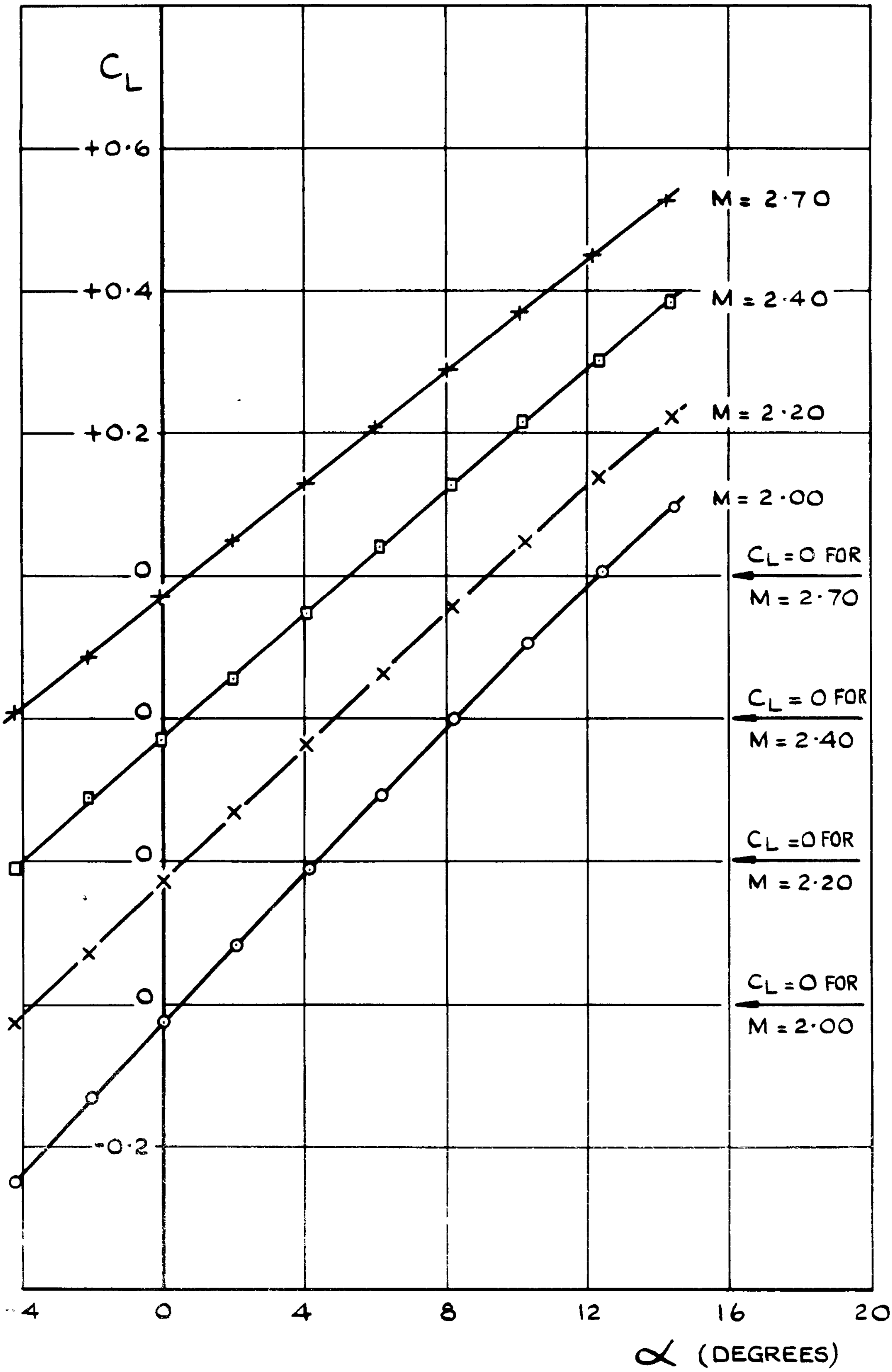

FIG. 6. VARIATION OF C_L WITH α AT CONSTANT MACH NUMBER : $\eta = -14°$

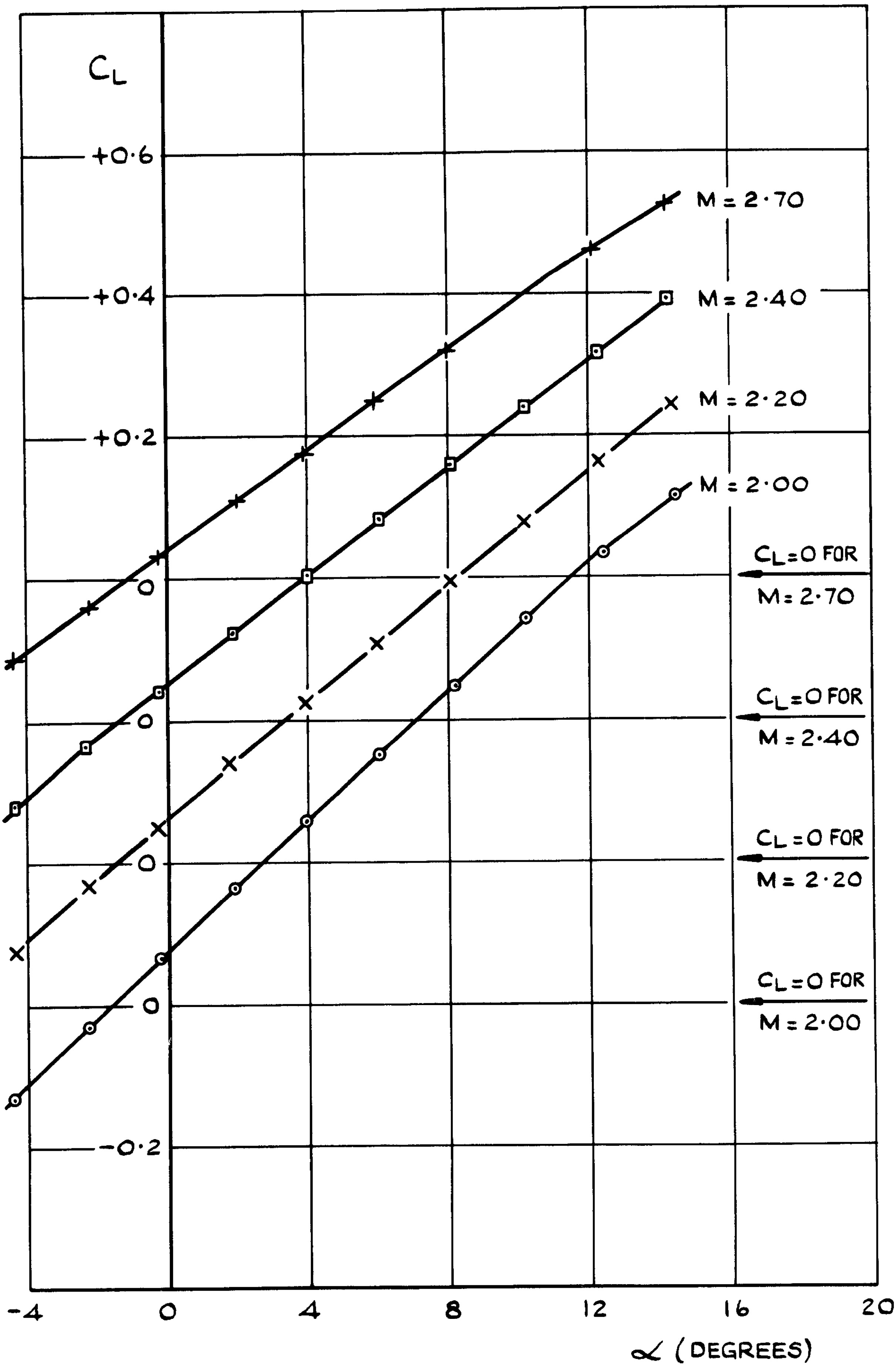

FIG. 7. VARIATION OF C_L WITH α AT CONSTANT MACH NUMBER: TAILPLANE AND FIN OFF

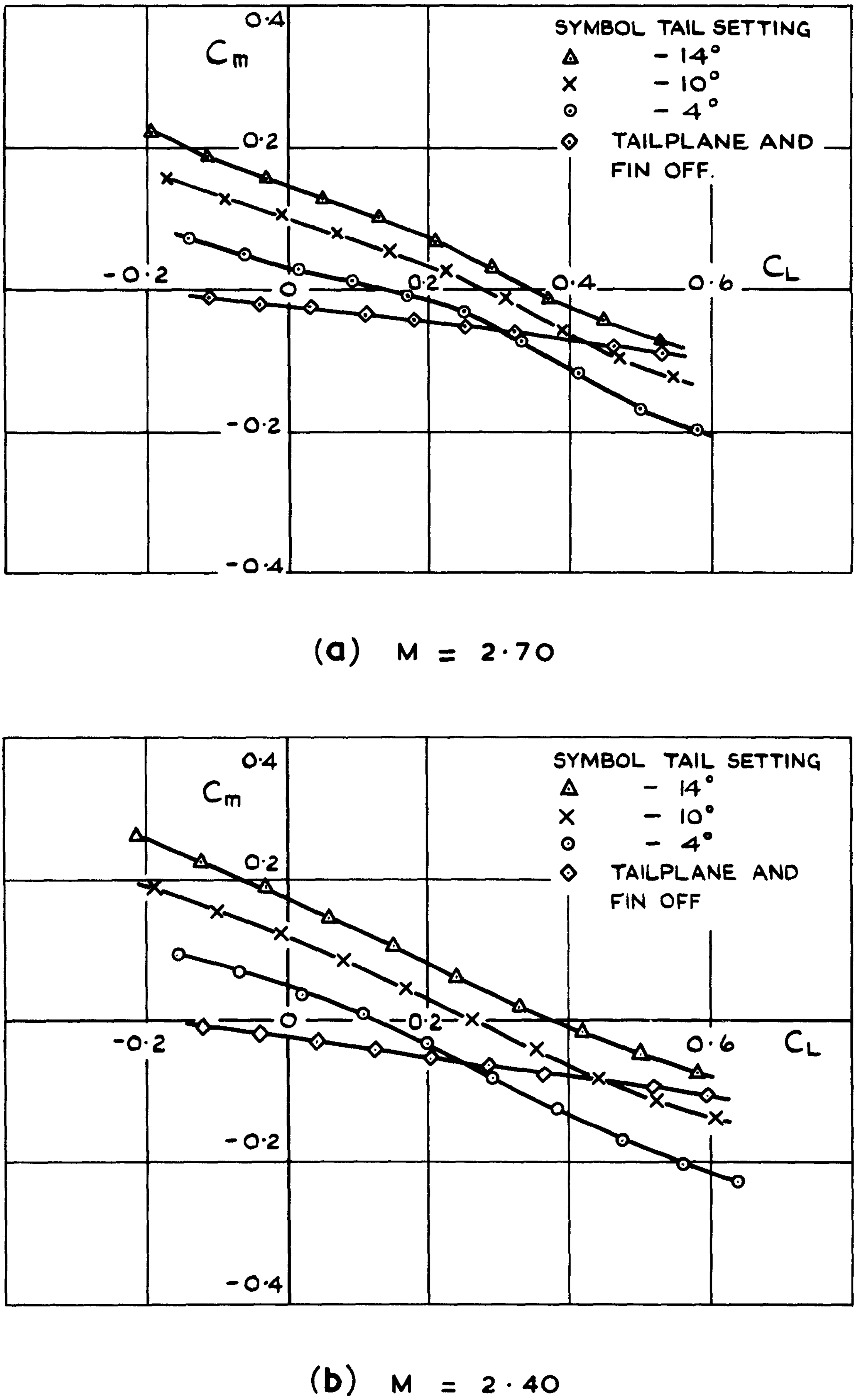

FIG. 8. VARIATION OF Cm WITH CL AT CONSTANT MACH NUMBER

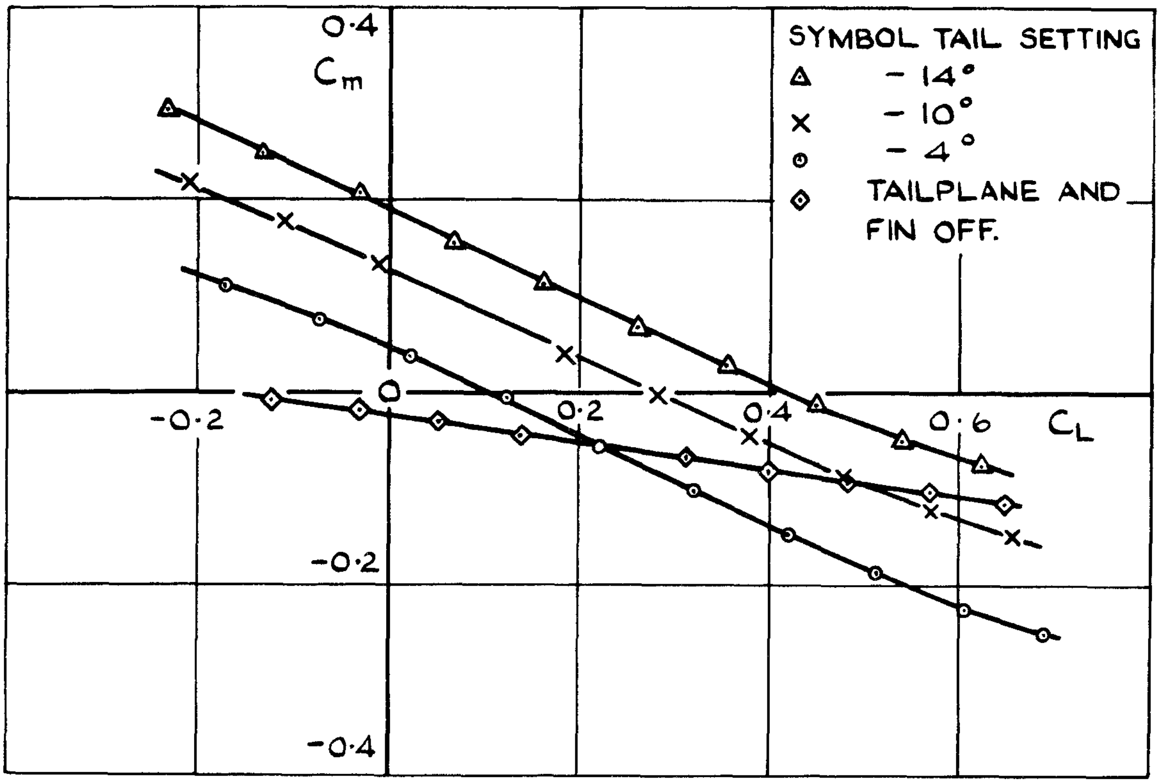

(c) M = 2·20

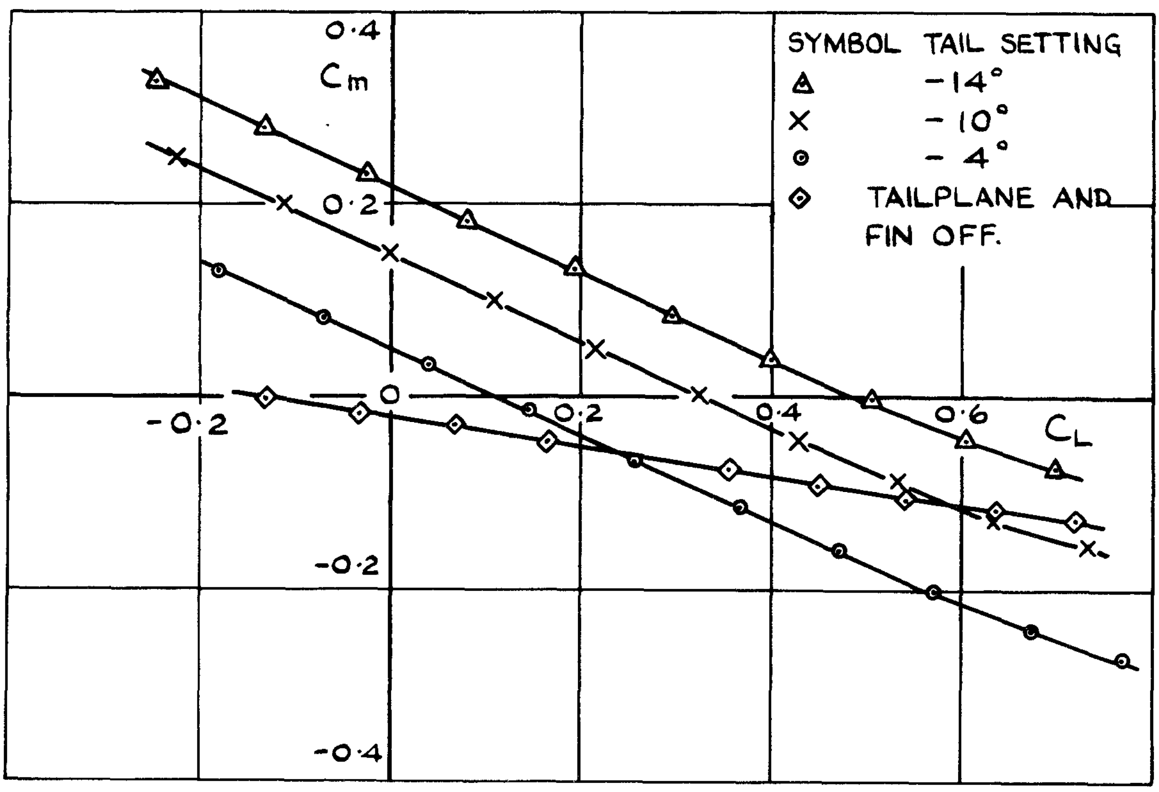

(d) M = 2·00

FIG. 8. (CONCLUDED)

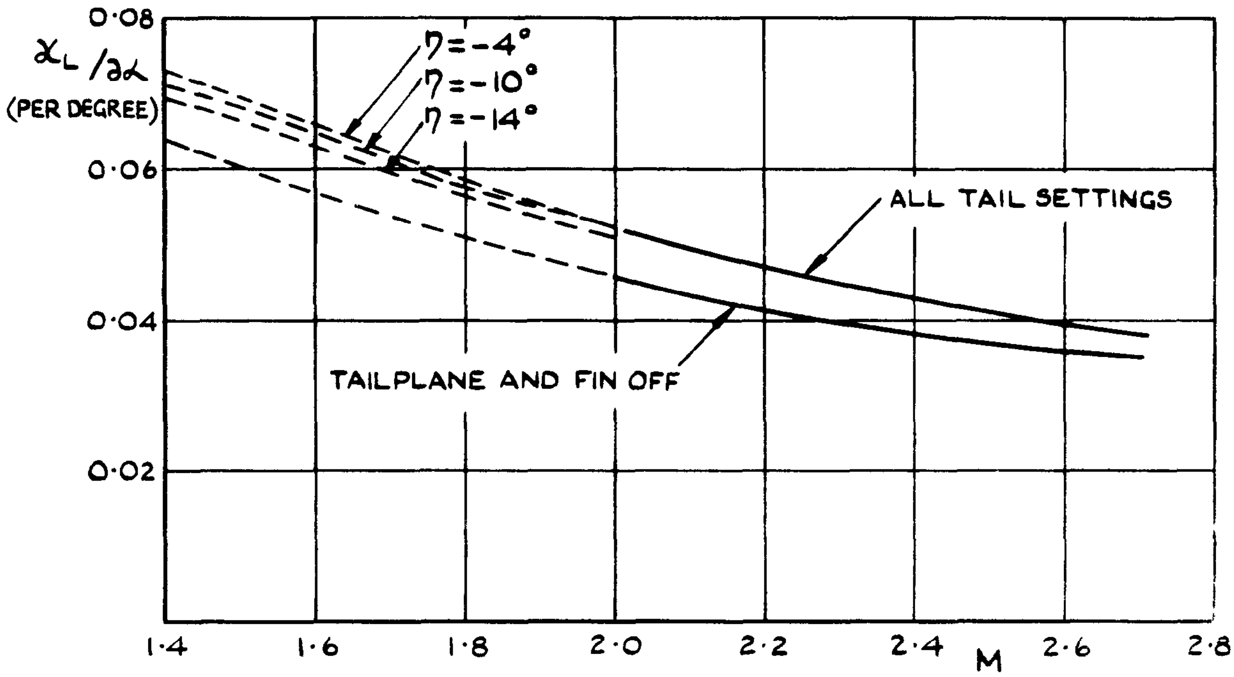

FIG. 9. LIFT-CURVE SLOPES AT ZERO INCIDENCE.

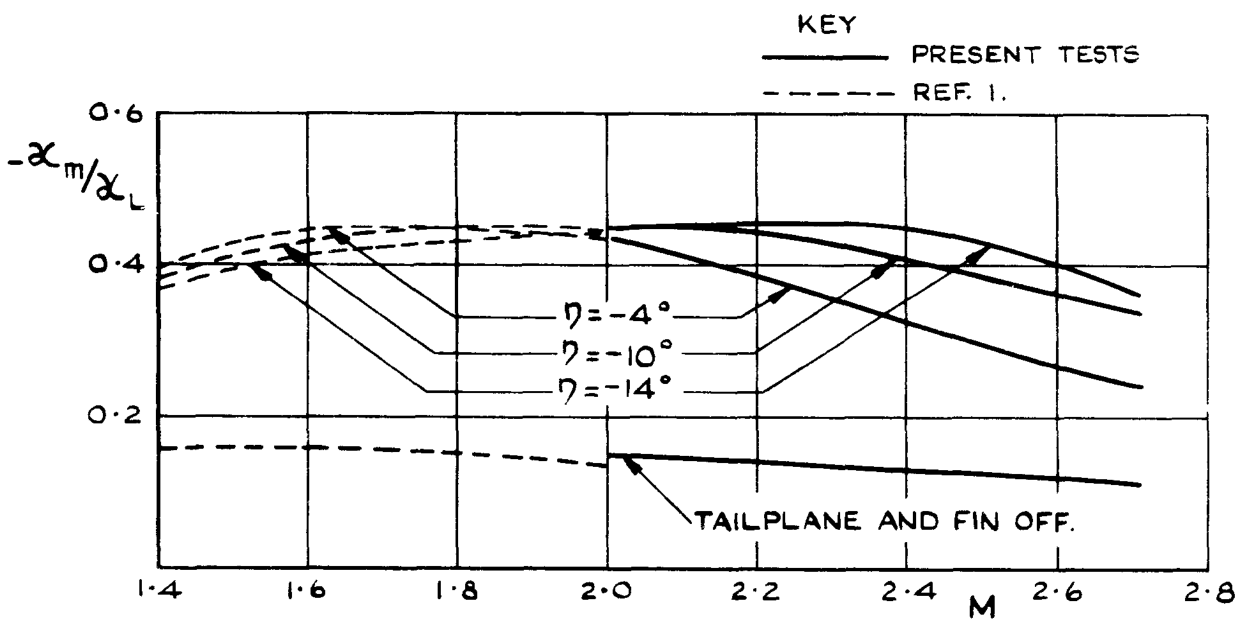

FIG. 10. LONGITUDINAL STABILITY SLOPES AT ZERO LIFT.

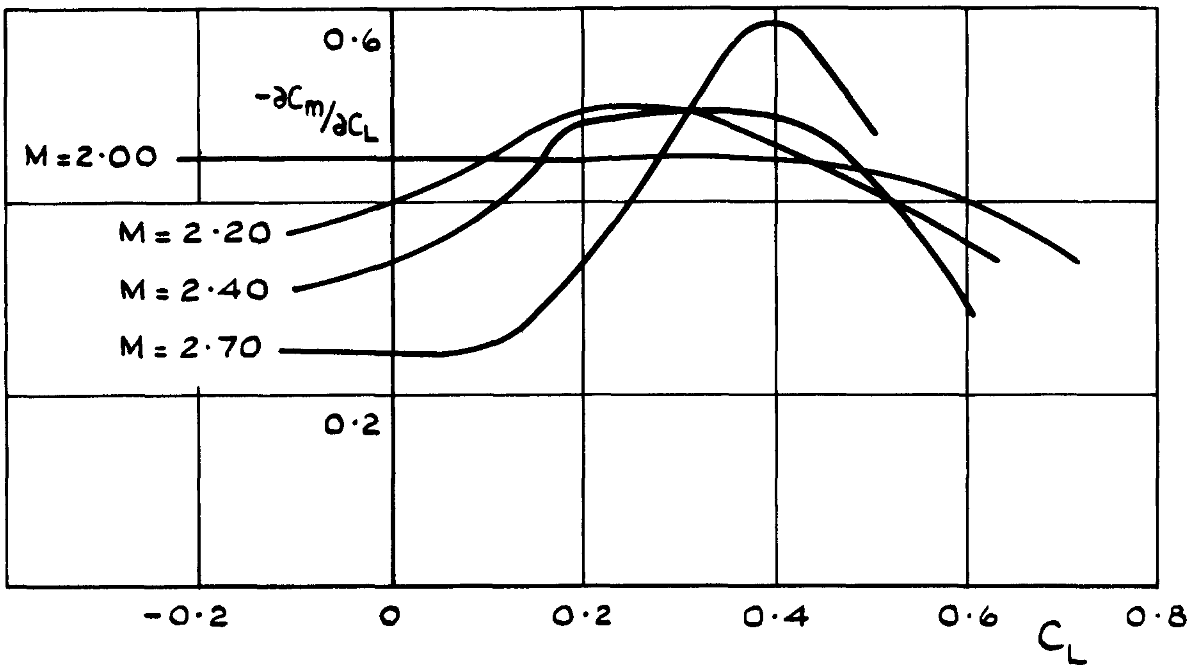

(a) TAILPLANE −4°

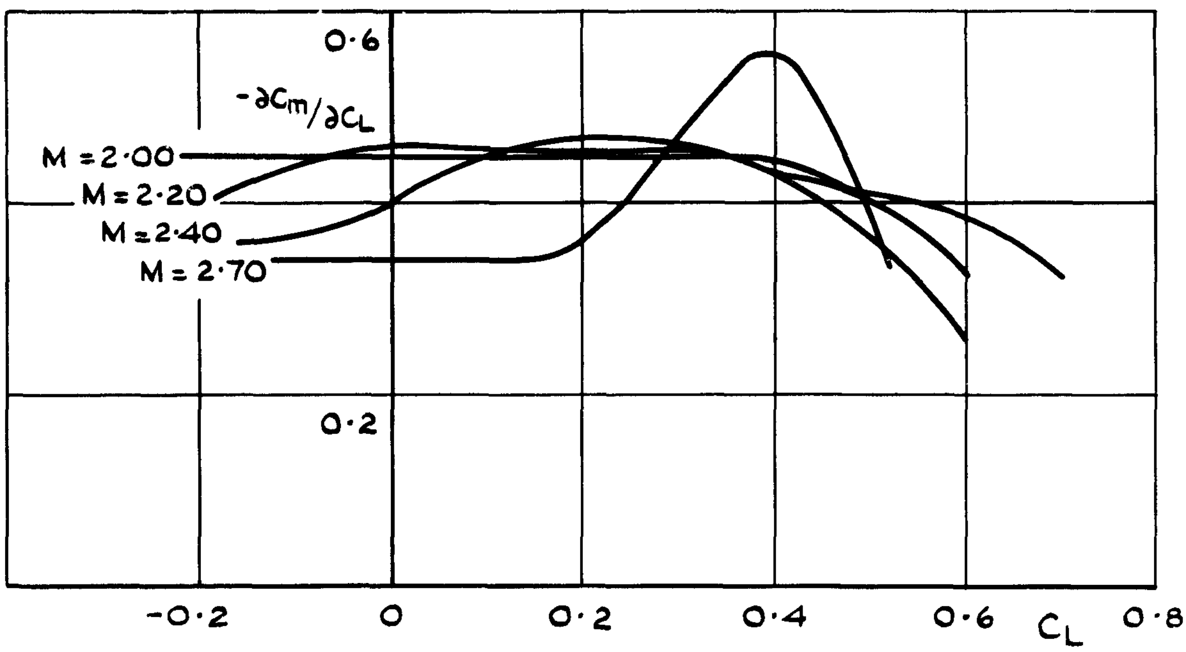

(b) TAILPLANE −10°

FIG. 11. VARIATION OF $-\partial C_m / \partial C_L$ WITH C_L

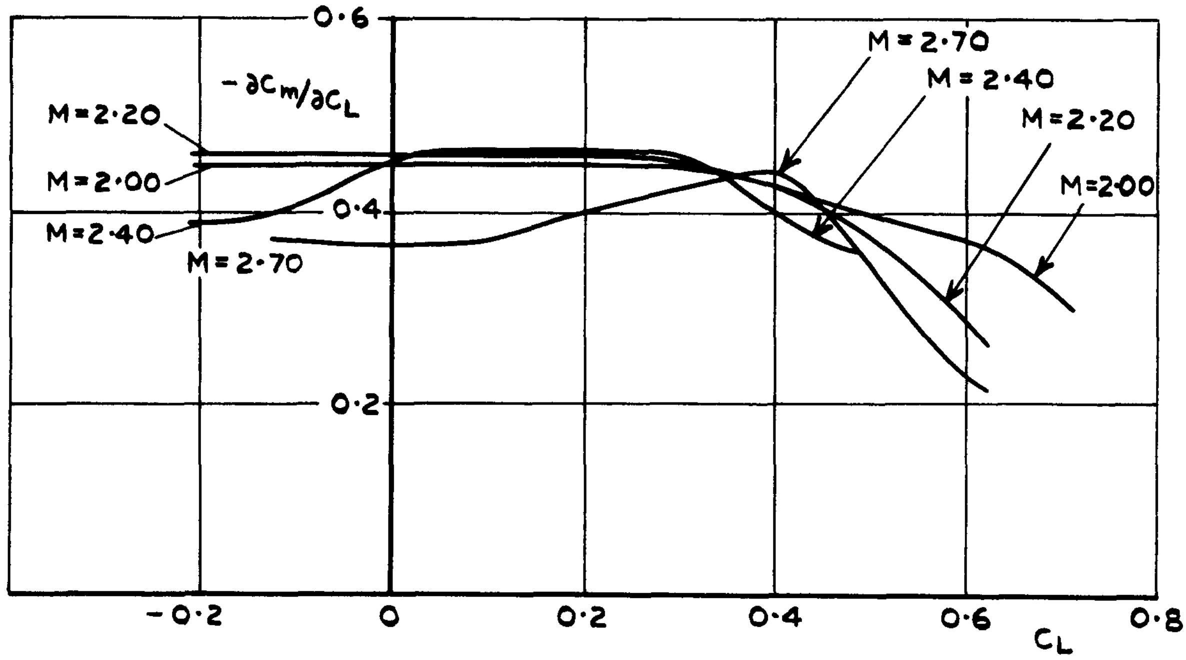

(c) TAILPLANE − 14°

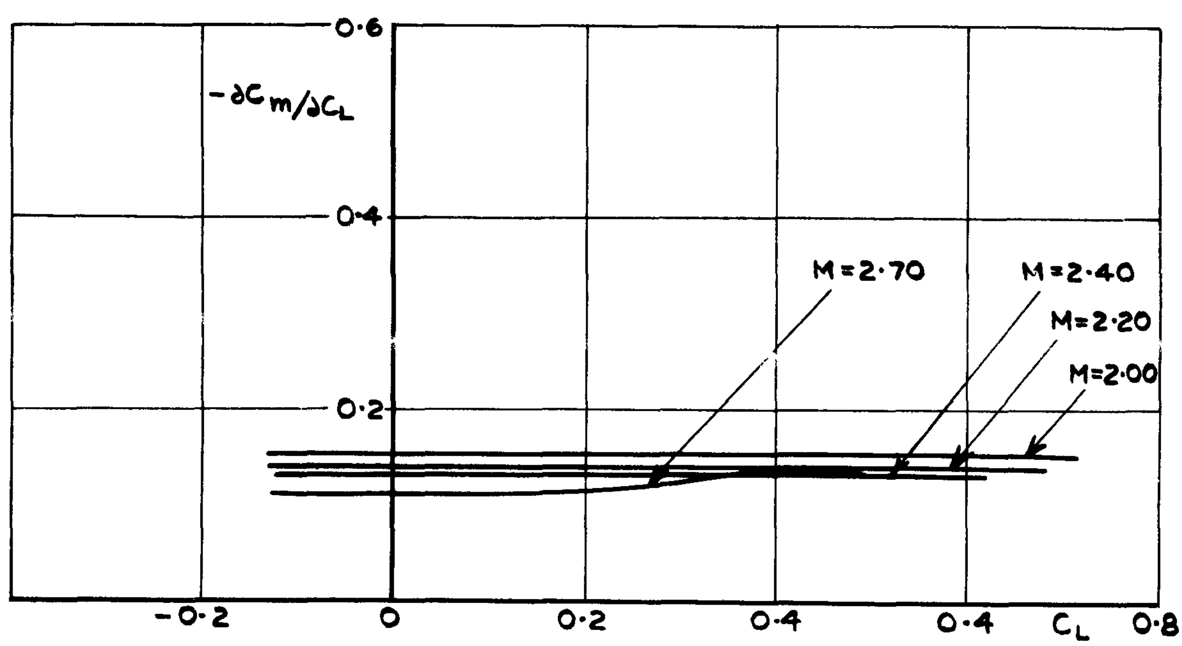

(d) TAILPLANE AND FIN OFF.

FIG. 11. (CONC.)

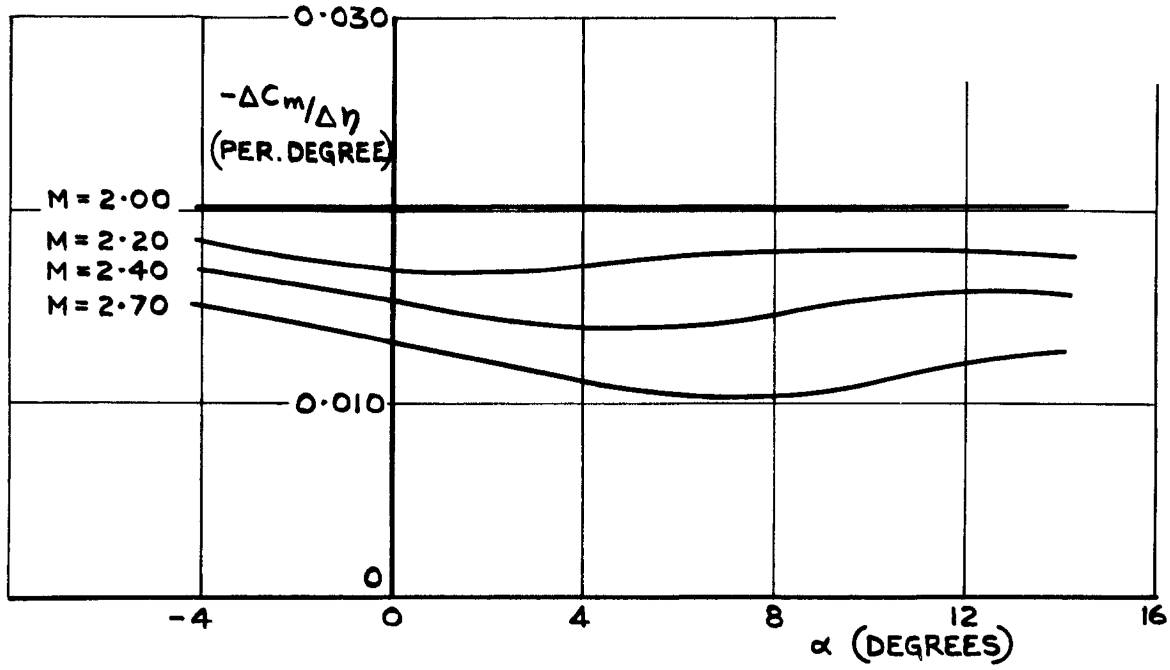

FIG. 12. VARIATION OF MEAN TAILPLANE POWER WITH MODEL INCIDENCE.

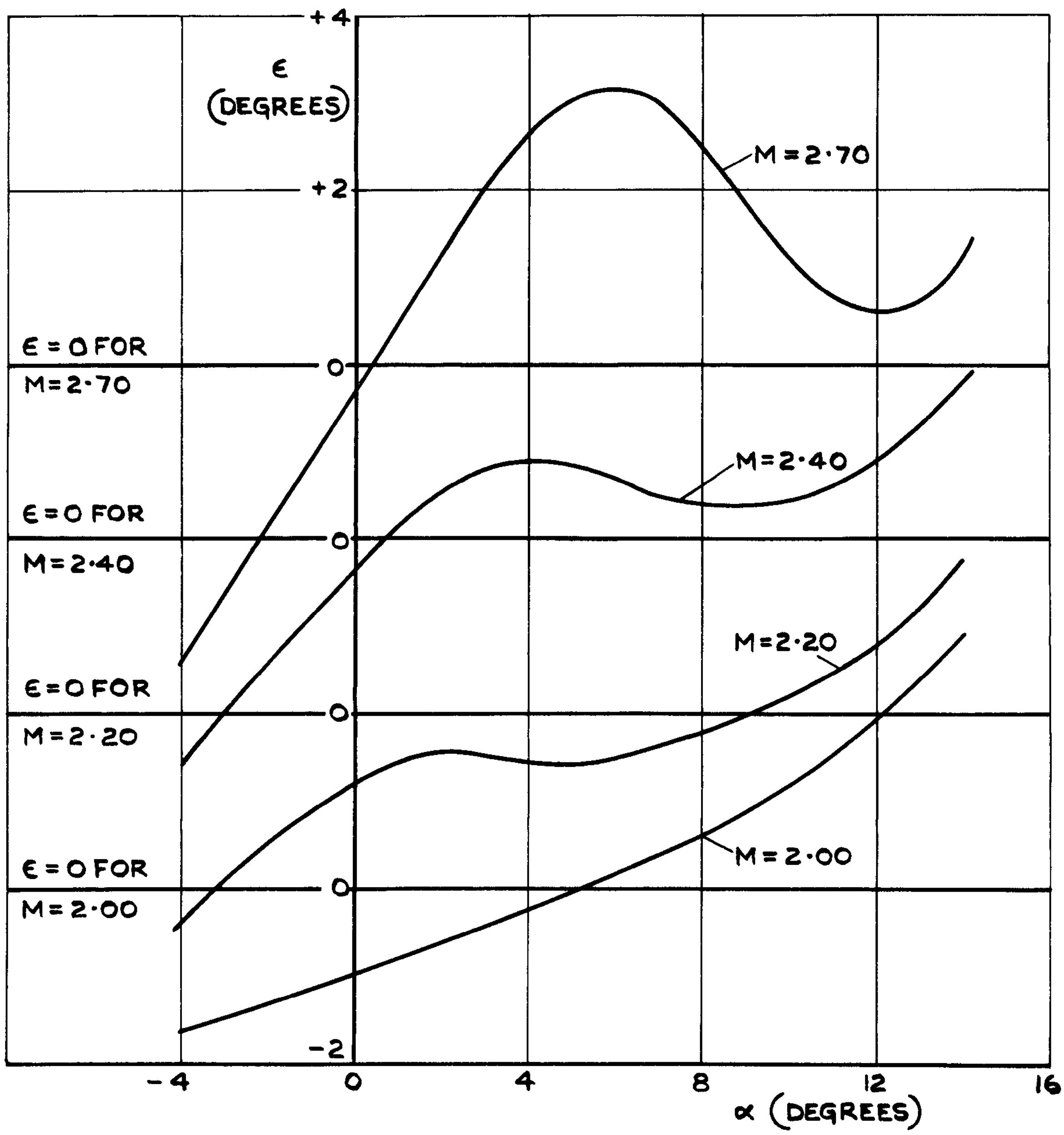

FIG. 13. VARIATION OF MEAN DOWNWASH AT POSITION OF TAILPLANE WITH MODEL INCIDENCE.

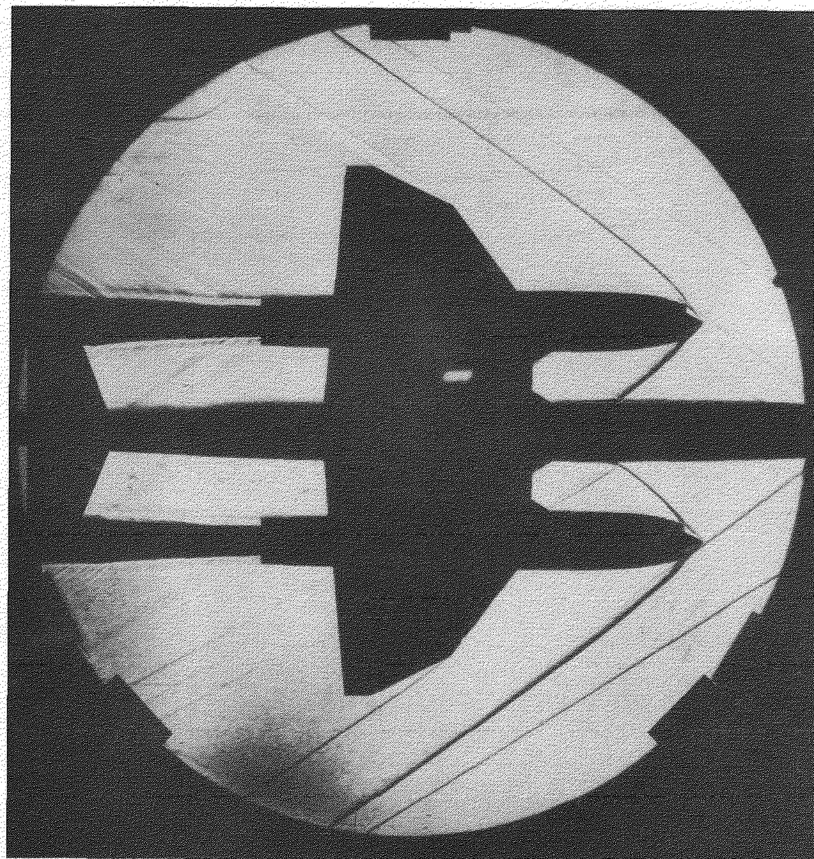

a. PLAN VIEW

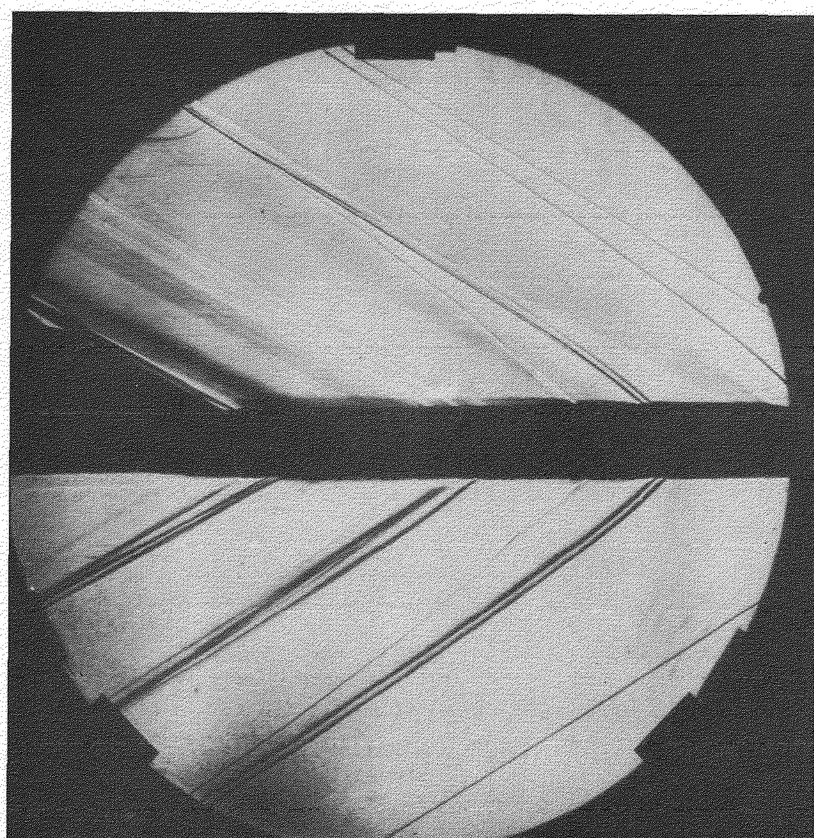

b. SIDE VIEW

FIG. 14. SCHLIEREN PHOTOGRAPHS OF CLEAN MODEL

$\alpha = \beta = 0^{\circ} \quad \eta = -4^{\circ}$

$M = 2.00$

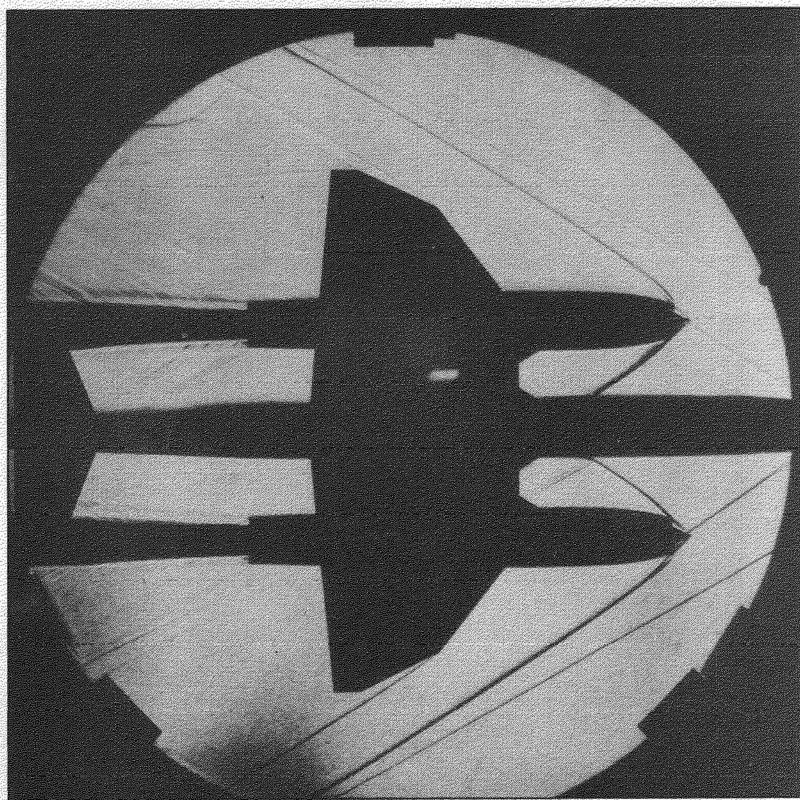

a. PLAN VIEW

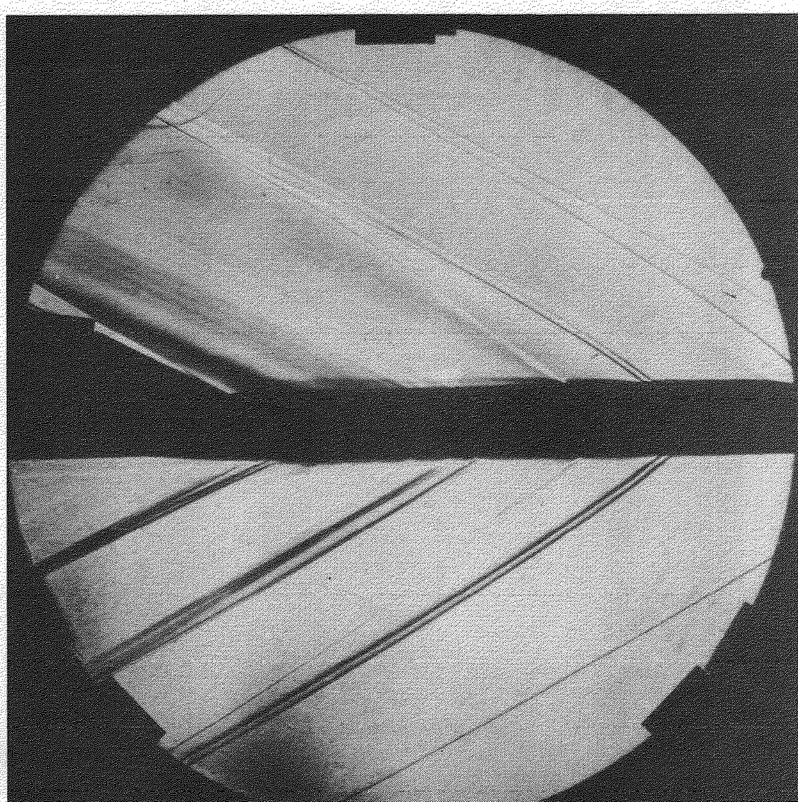

b. SIDE VIEW

FIG.15. SCHLIEREN PHOTOGRAPHS OF CLEAN MODEL

$\alpha = \beta = 0^\circ \quad \eta = -4^\circ$

$M = 2.20$

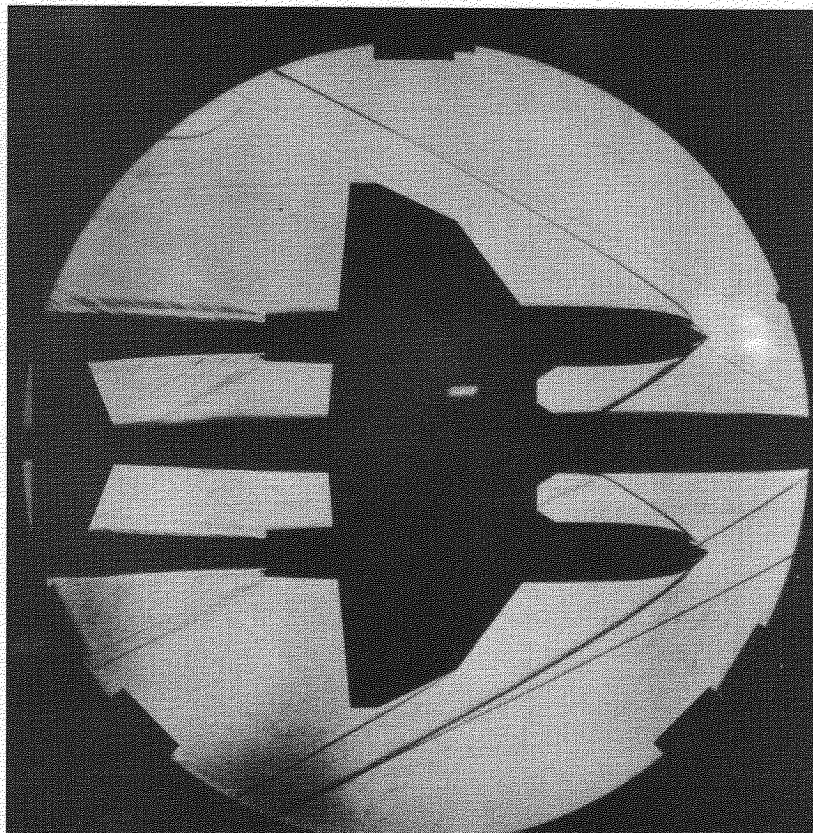

a. PLAN VIEW

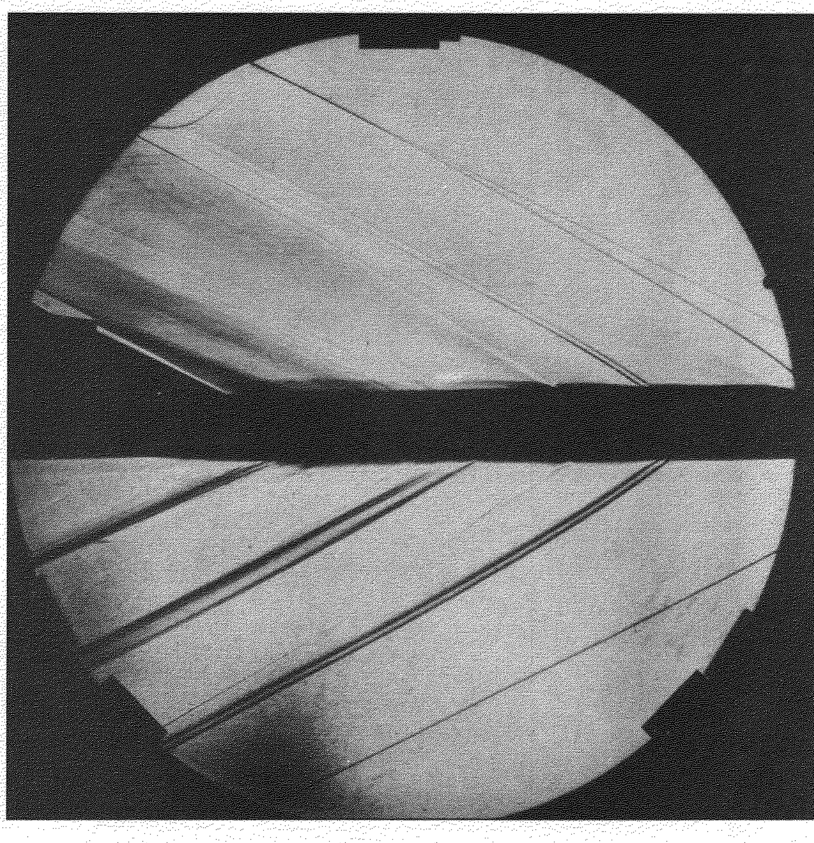

b. SIDE VIEW

FIG.16. SCHLIEREN PHOTOGRAPHS OF CLEAN MODEL

$\alpha = \beta = 0^{\circ}$ $\eta = -4^{\circ}$

$M = 2.40$

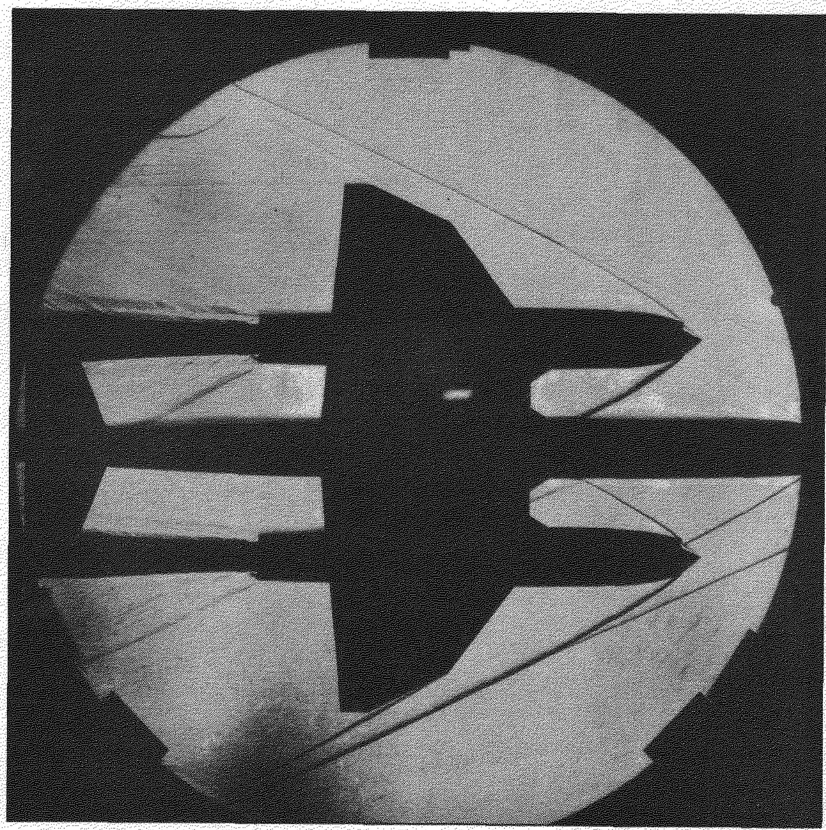

a. PLAN VIEW

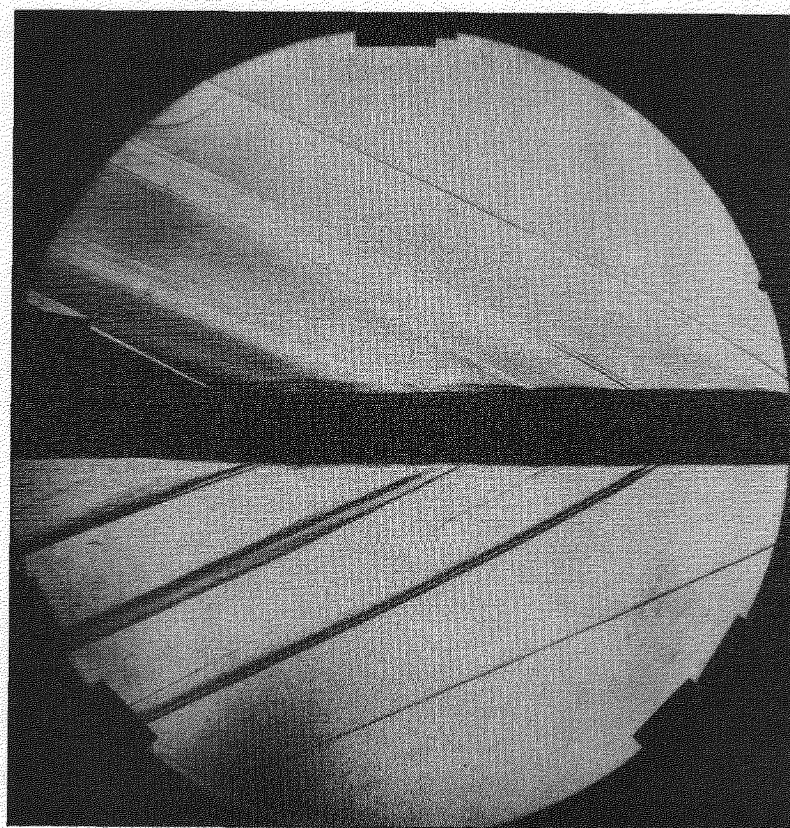

b. SIDE VIEW

FIG.17. SCHLIEREN PHOTOGRAPHS OF CLEAN MODEL

$\alpha = \beta = 0^{\circ} \quad \eta = -4^{\circ}$

$M = 2.70$

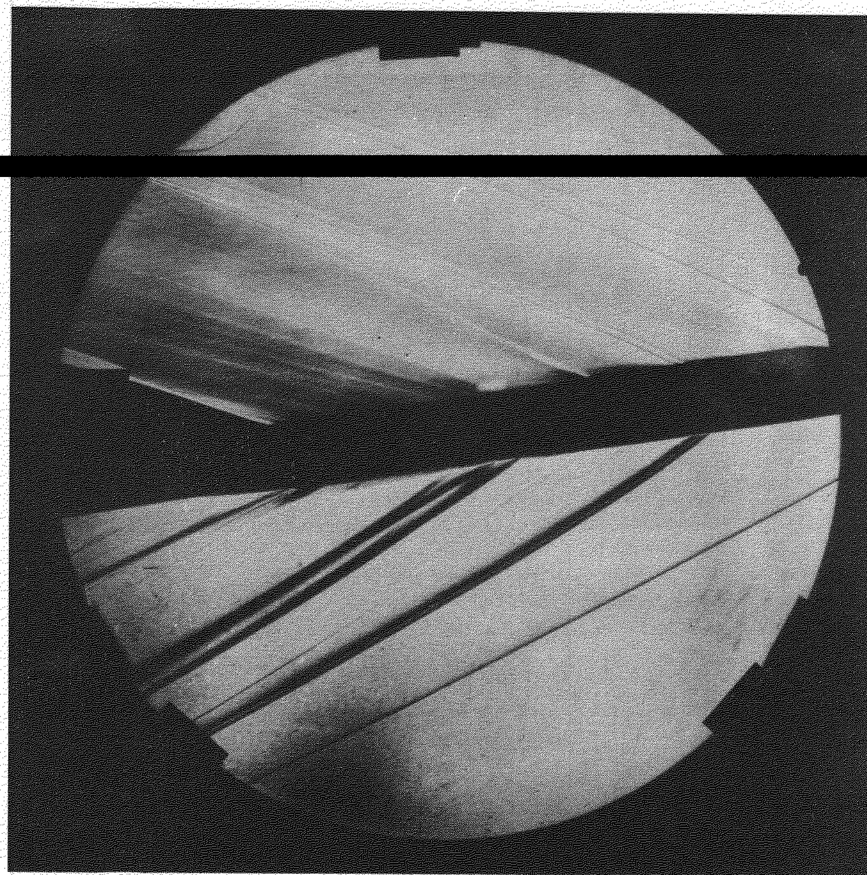

A. $\alpha = 4^{\circ}$

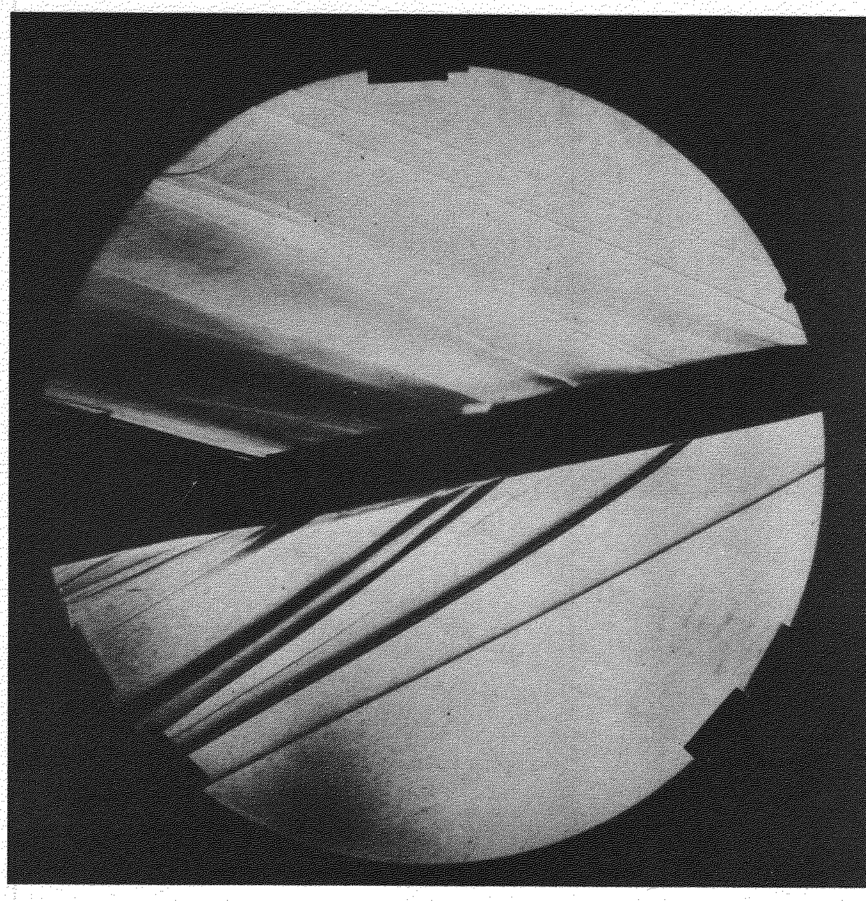

B. $\alpha = 8^{\circ}$

FIG.18. SCHLIEREN PHOTOGRAPHS OF CLEAN MODEL

$M = 2.70 \quad \eta = -4^{\circ}$

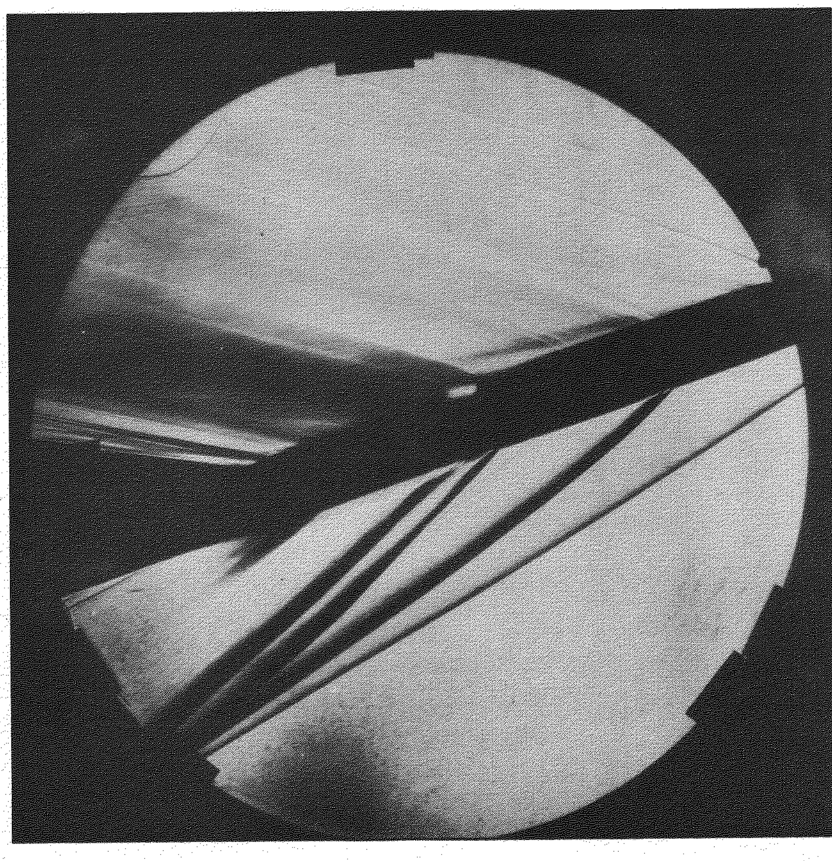

C. $\alpha = 12^{\circ}$

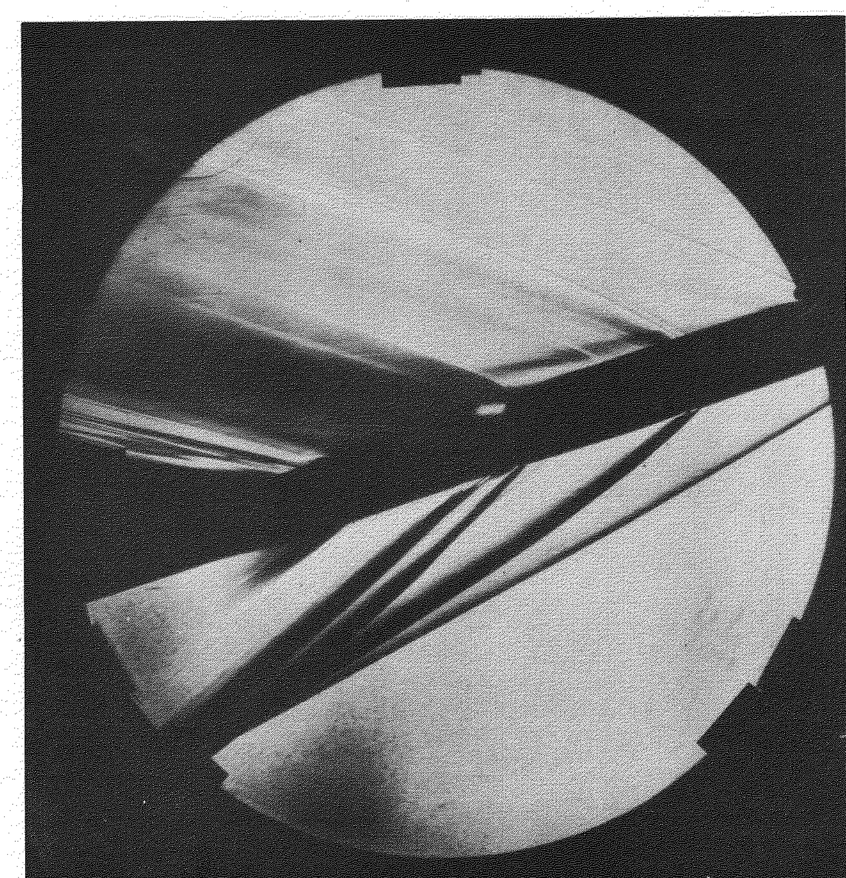

D. $\alpha = 14^{\circ}$

FIG.18. SCHLIEREN PHOTOGRAPHS OF CLEAN MODEL (concluded)

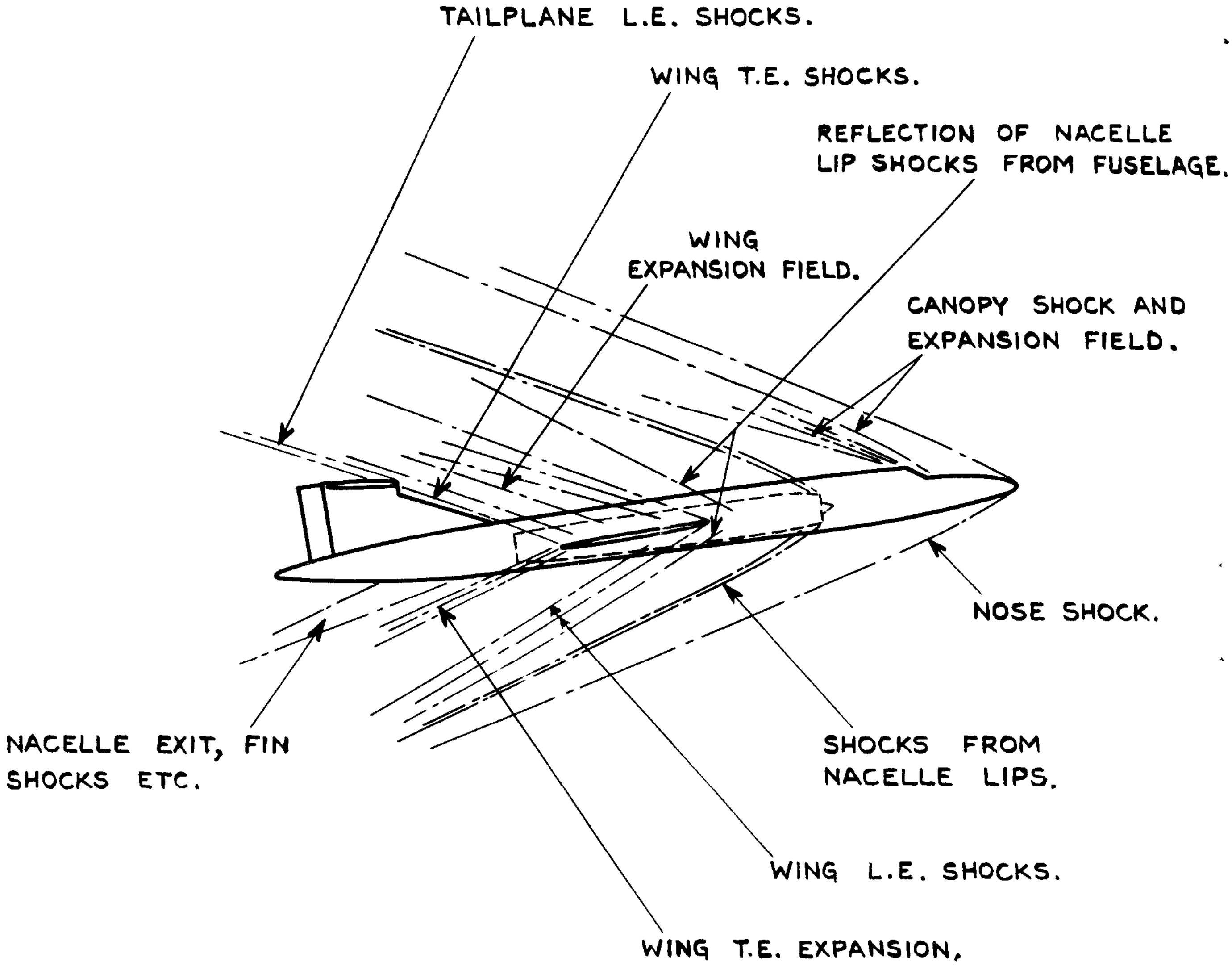

FIG. 19. EXPLANATION OF SCHLIEREN PHOTOGRAPH OF MODEL AT M=2·70 AND α=8°.

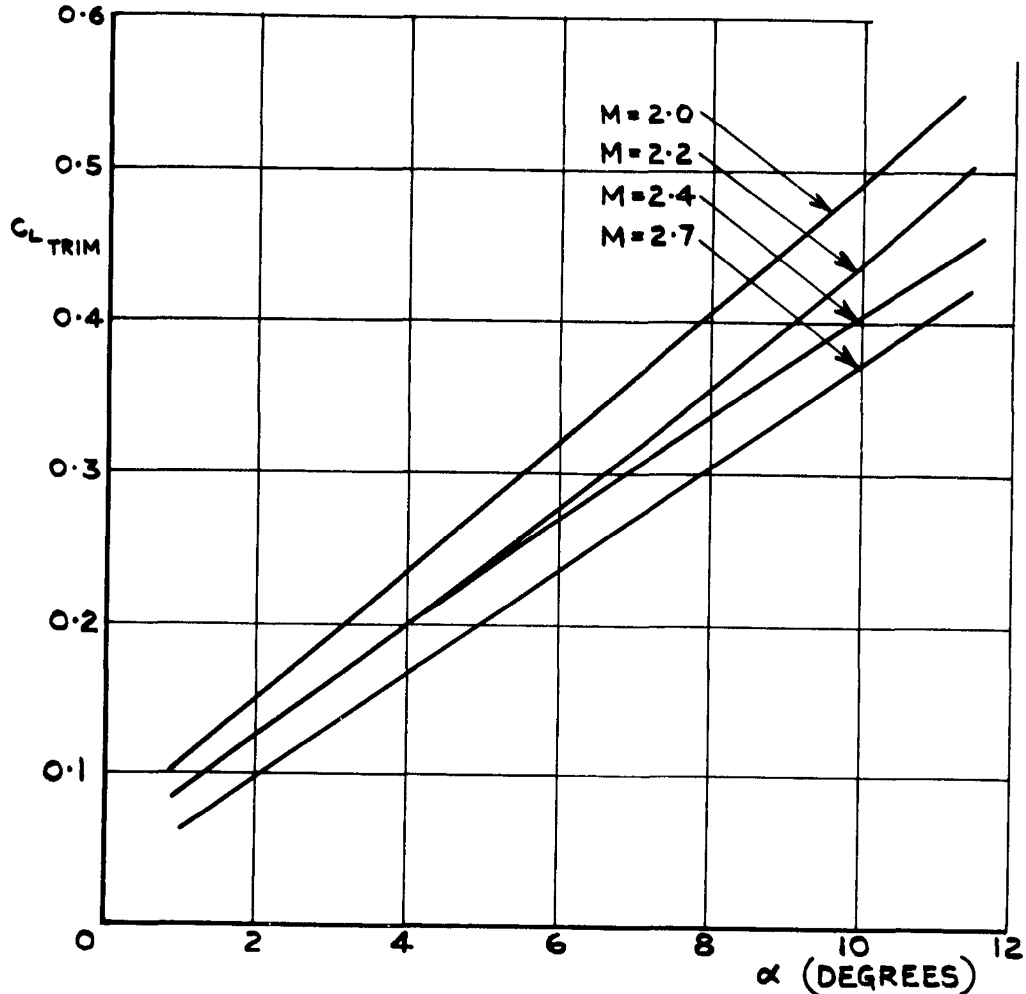

FIG. 20. TRIMMED LIFT COEFFICIENTS.

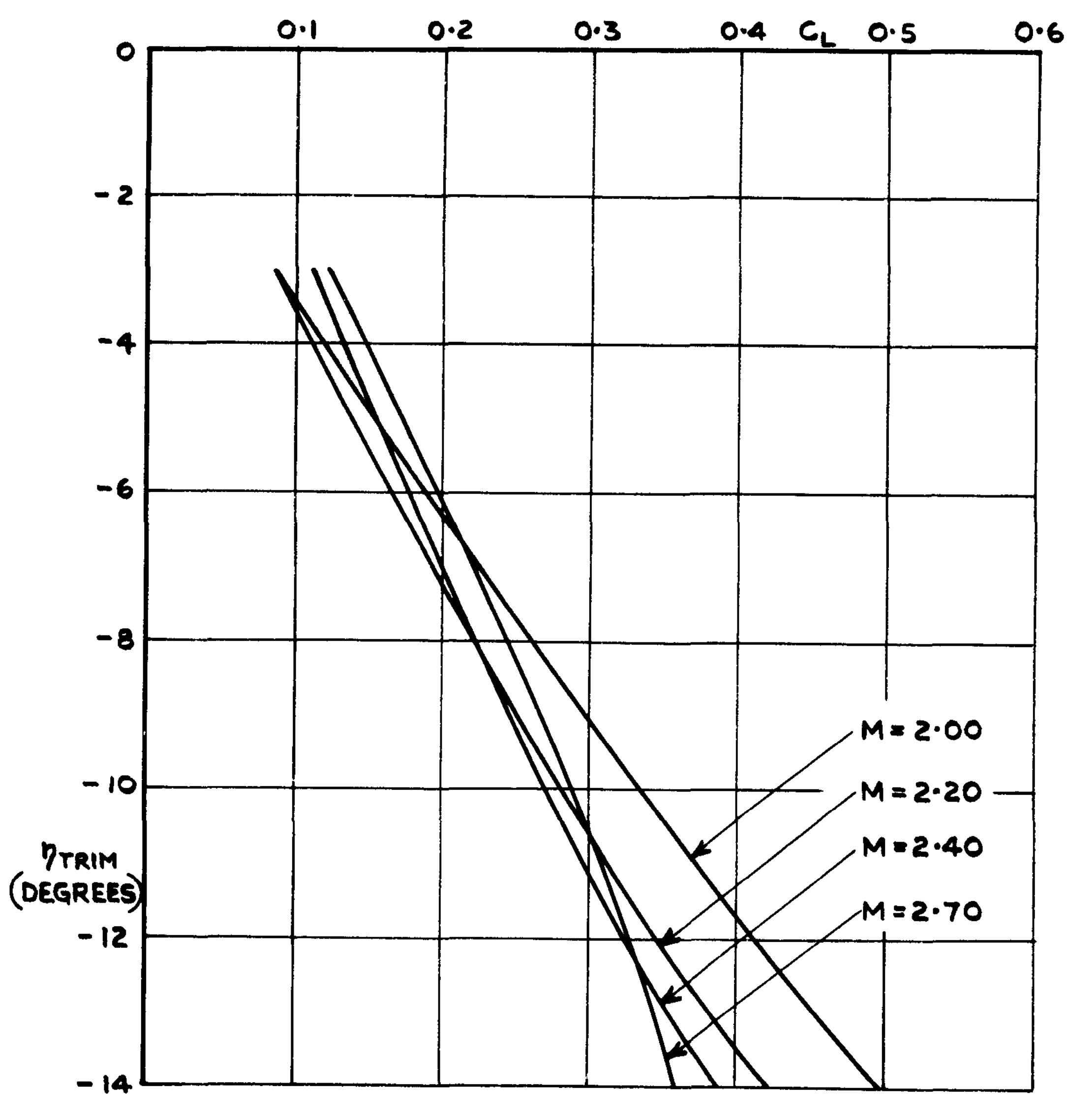

FIG. 21. TAILPLANE ANGLE TO TRIM.

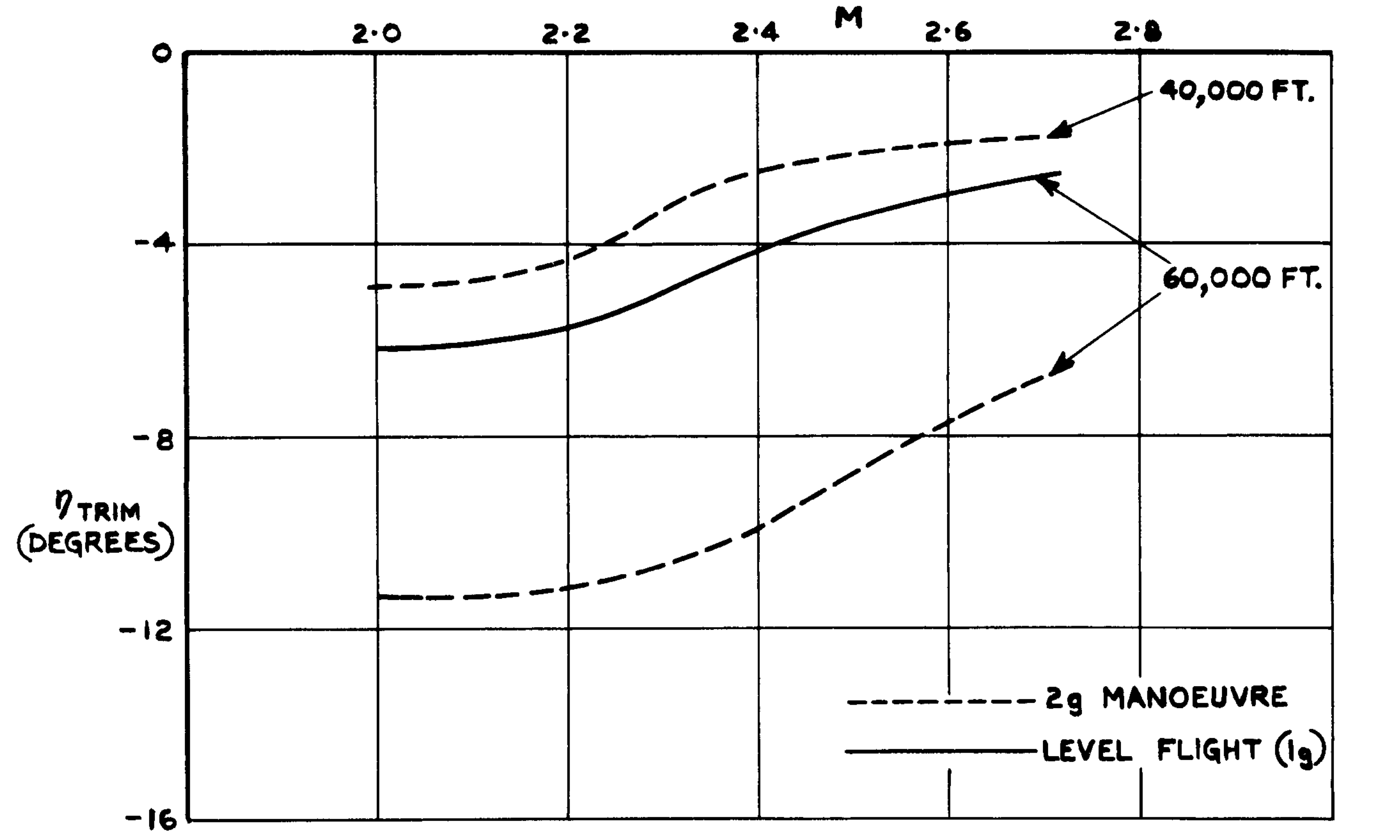

FIG. 22. TAILPLANE ANGLE TO TRIM FOR THE FULL-SCALE AIRCRAFT.

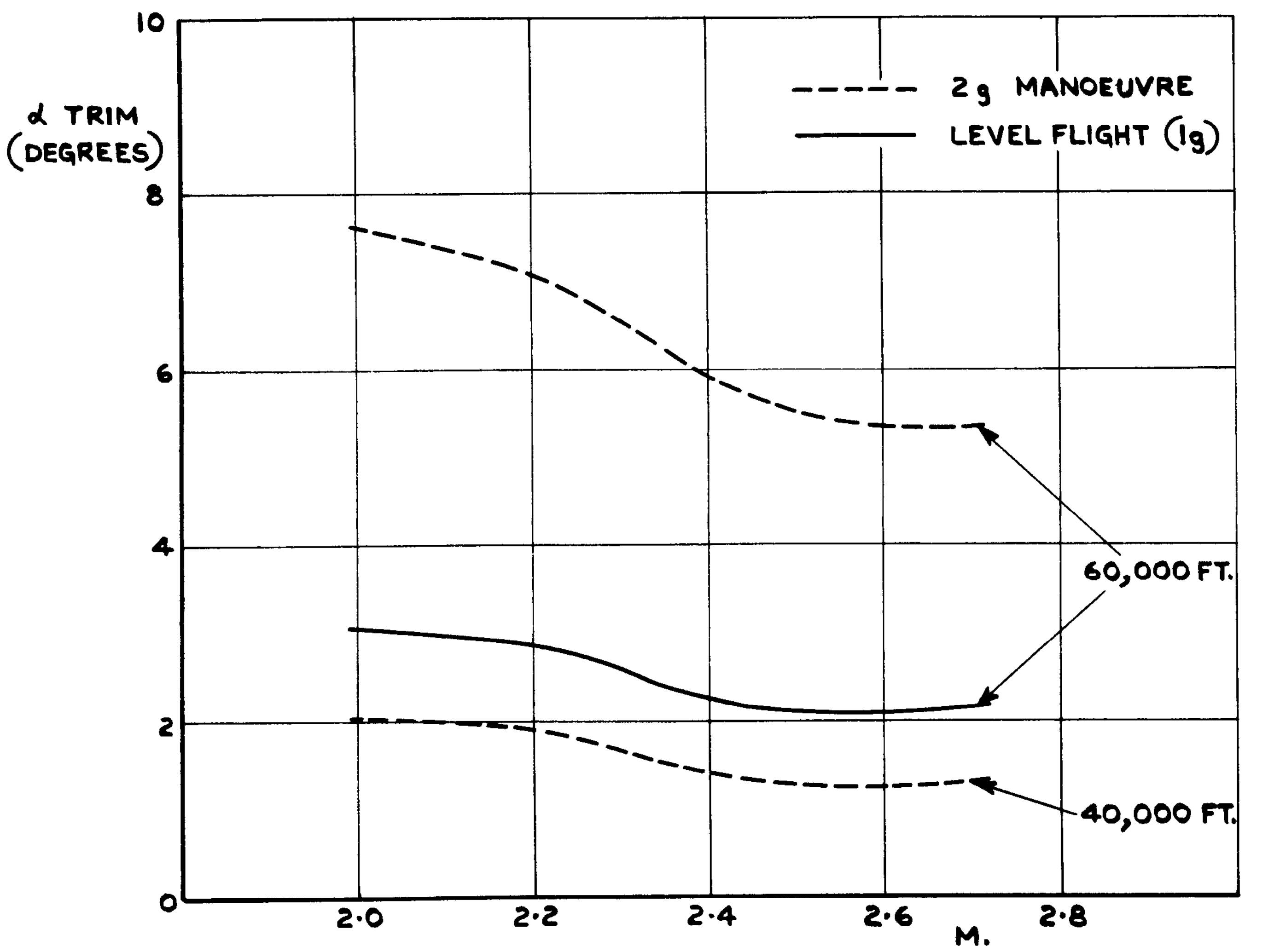

FIG. 23. INCIDENCE TO TRIM FOR THE FULL-SCALE AIRCRAFT.

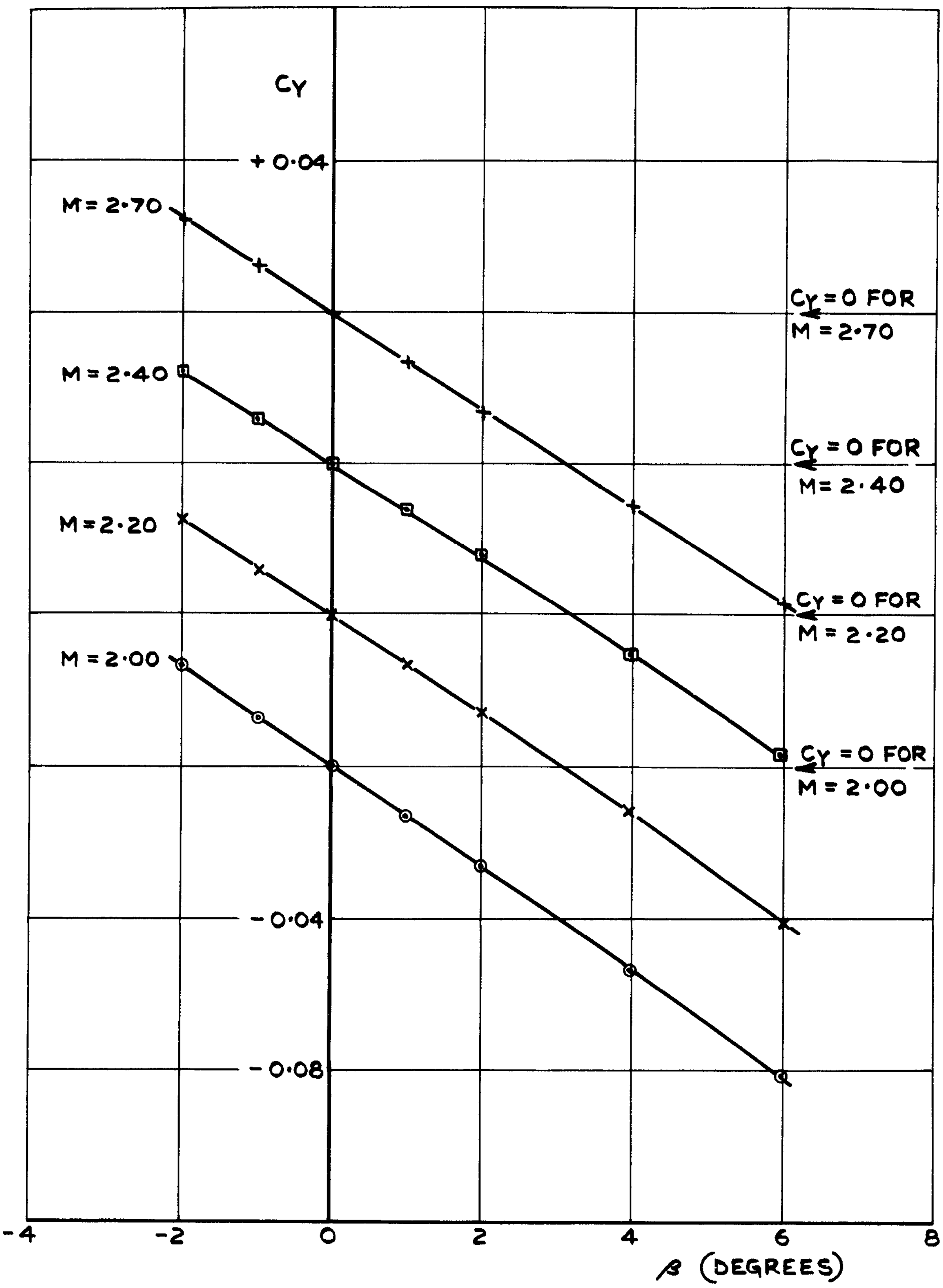

FIG. 24. VARIATION OF C_Y WITH β AT CONSTANT MACH NUMBER: $\eta = -4^\circ$; $\alpha = +4^\circ$.

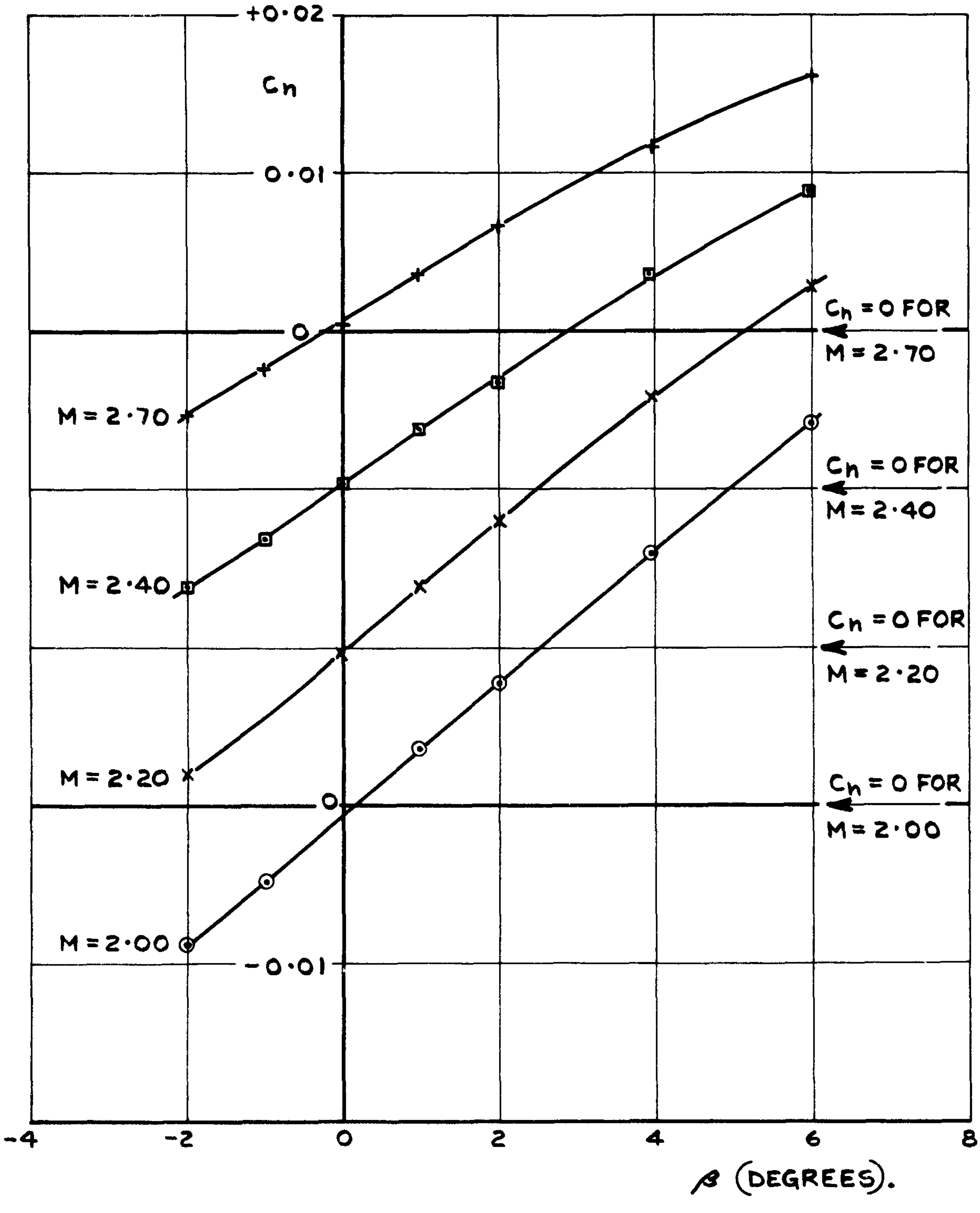

FIG. 25. VARIATION OF C_n WITH β AT CONSTANT MACH NUMBER: $\eta = -4°$; $\alpha = +4°$.

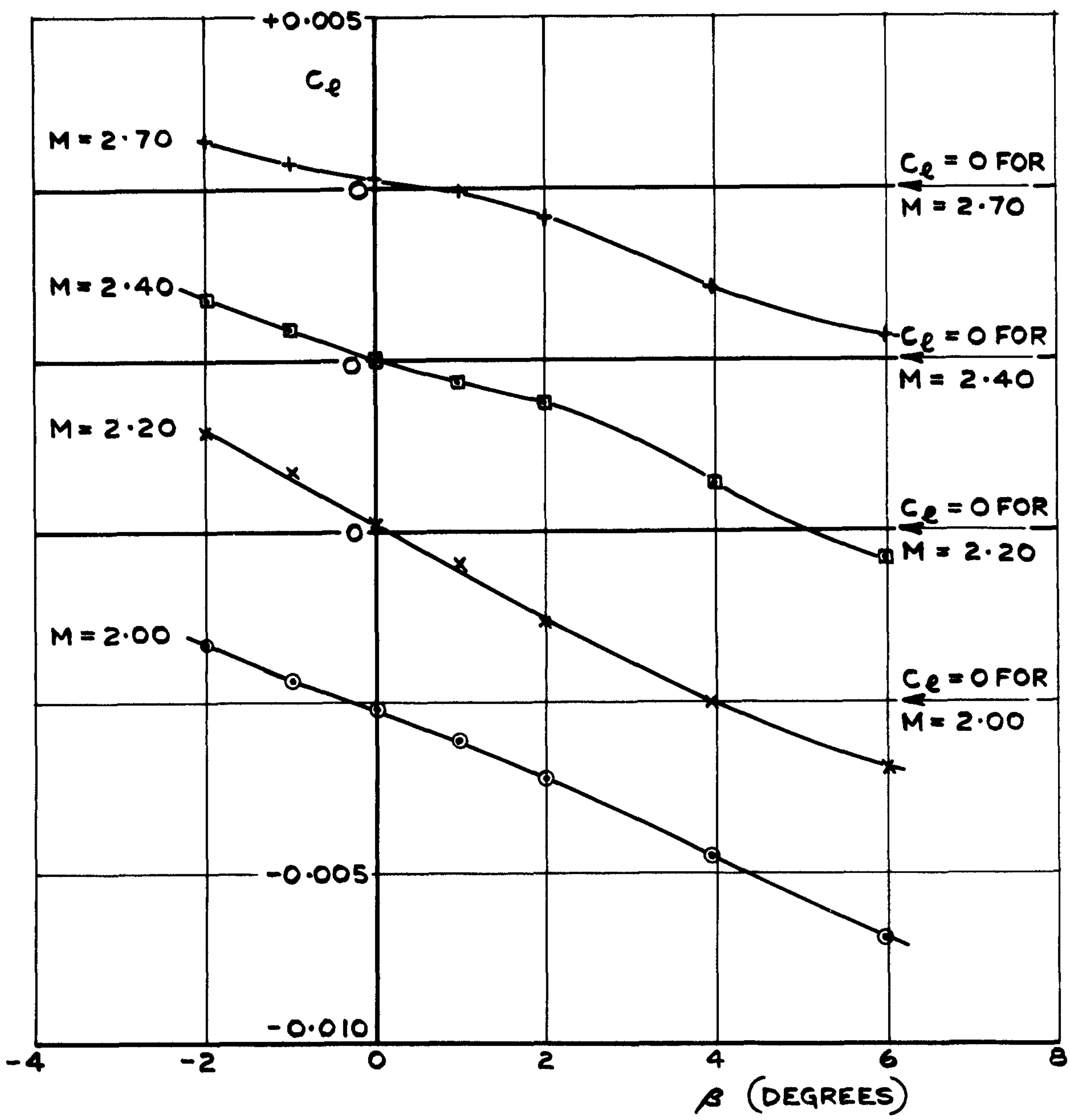

FIG. 26. VARIATION OF C_ℓ WITH β AT CONSTANT MACH NUMBER: $\eta = -4^\circ$; $\alpha = +4^\circ$.

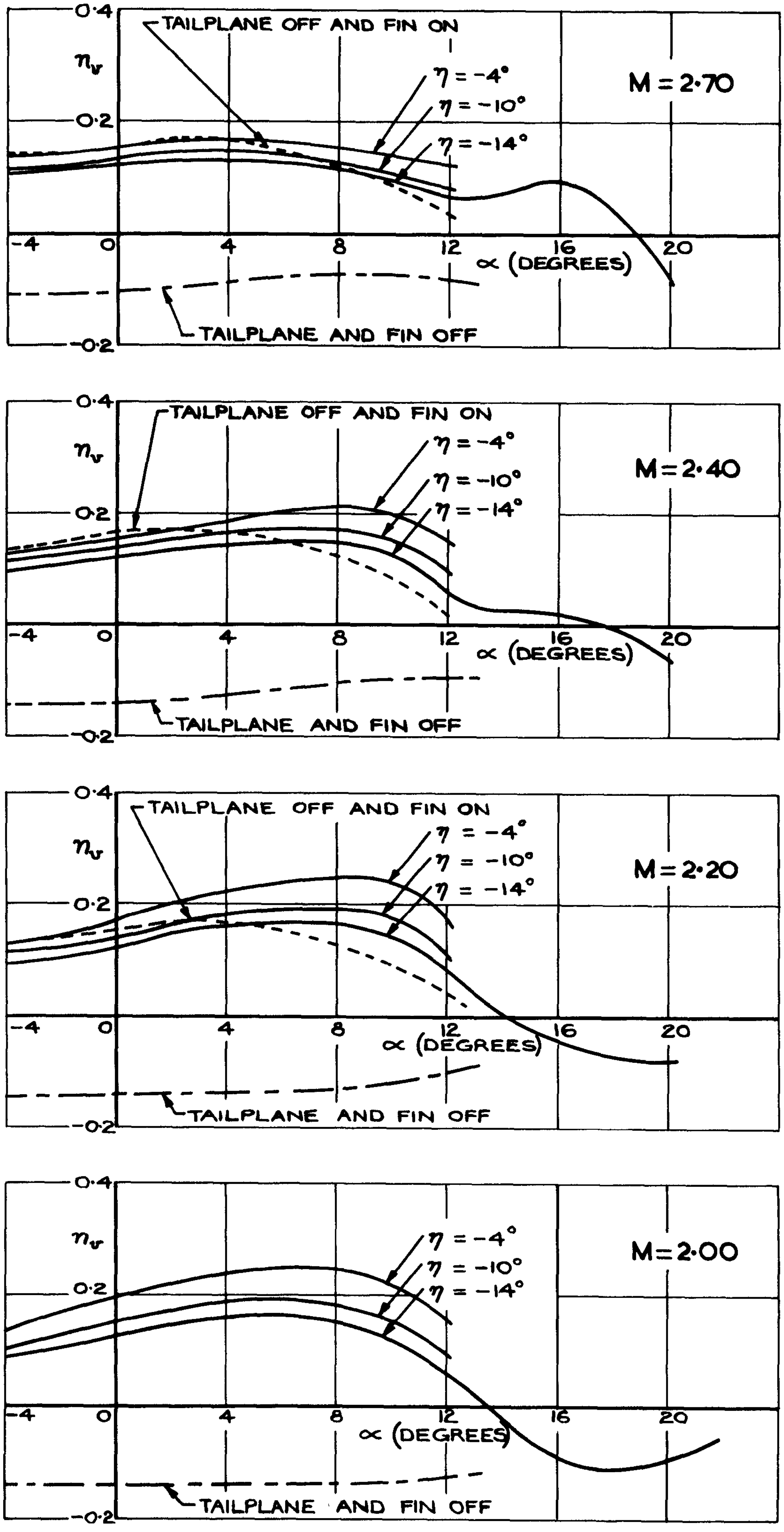

FIG. 27 VARIATION OF n_v WITH INCIDENCE

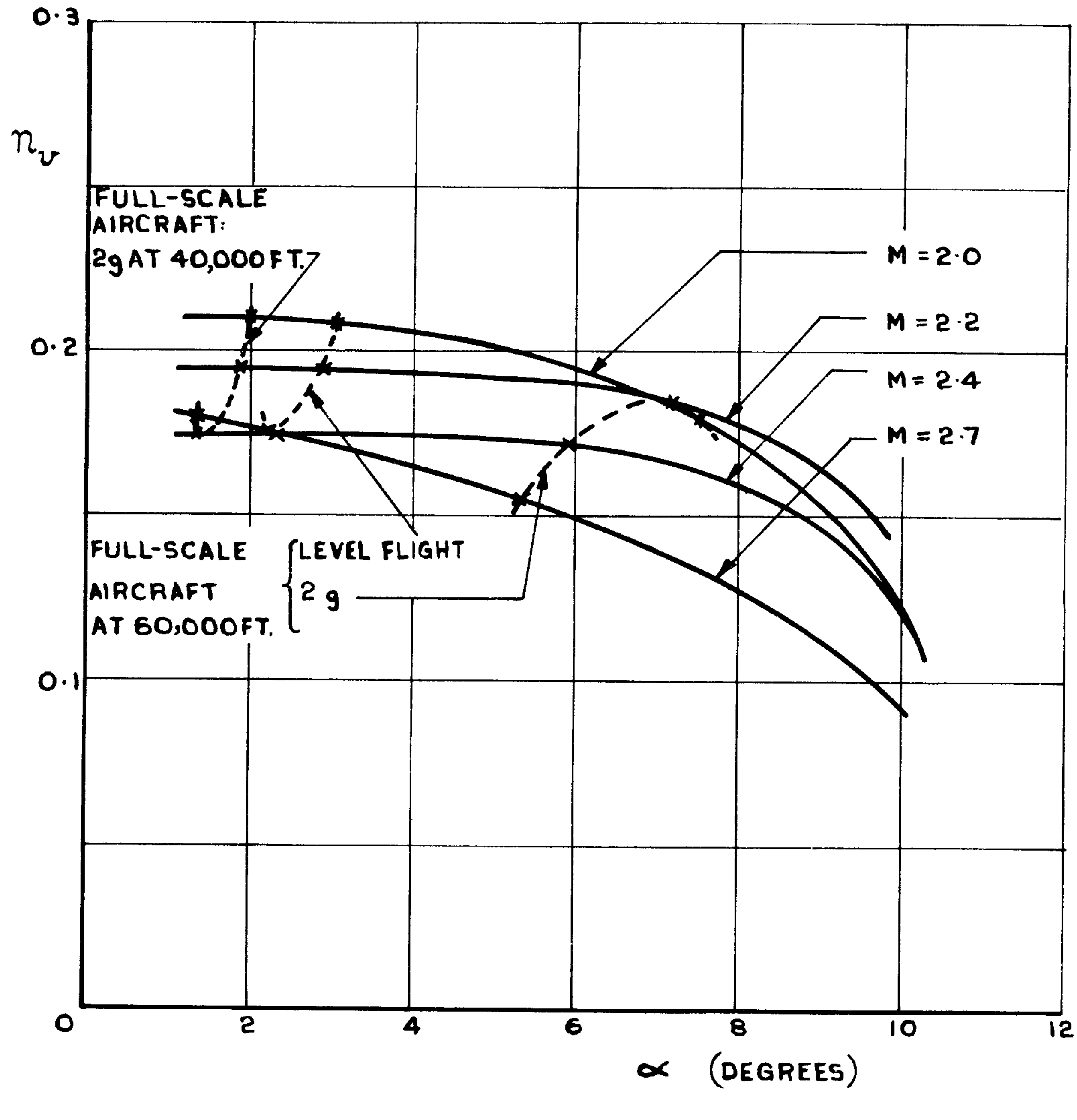

FIG. 28. VARIATION OF n_v WITH INCIDENCE FOR TRIMMED CONFIGURATION.

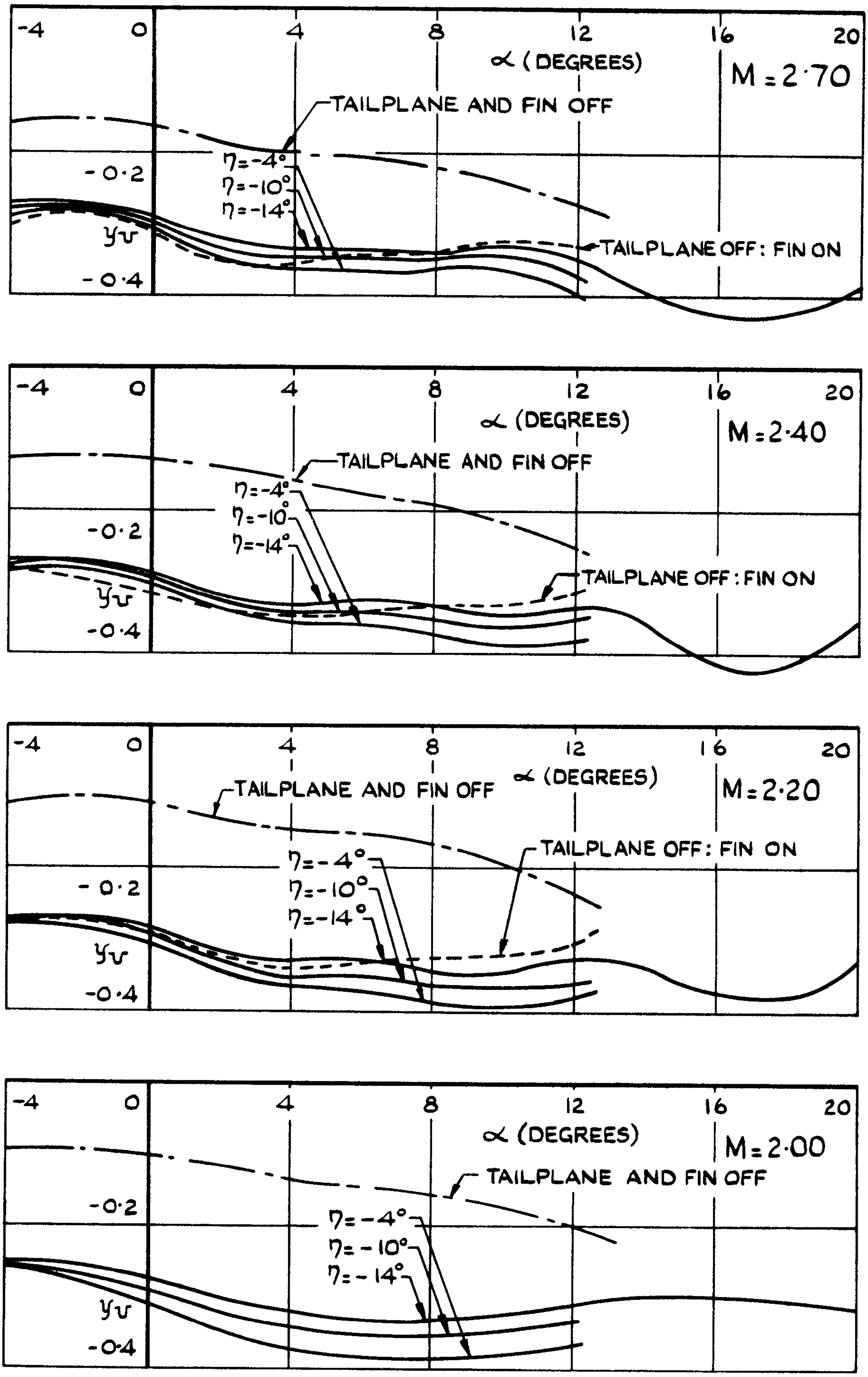

FIG. 29. VARIATION OF y_v WITH INCIDENCE.

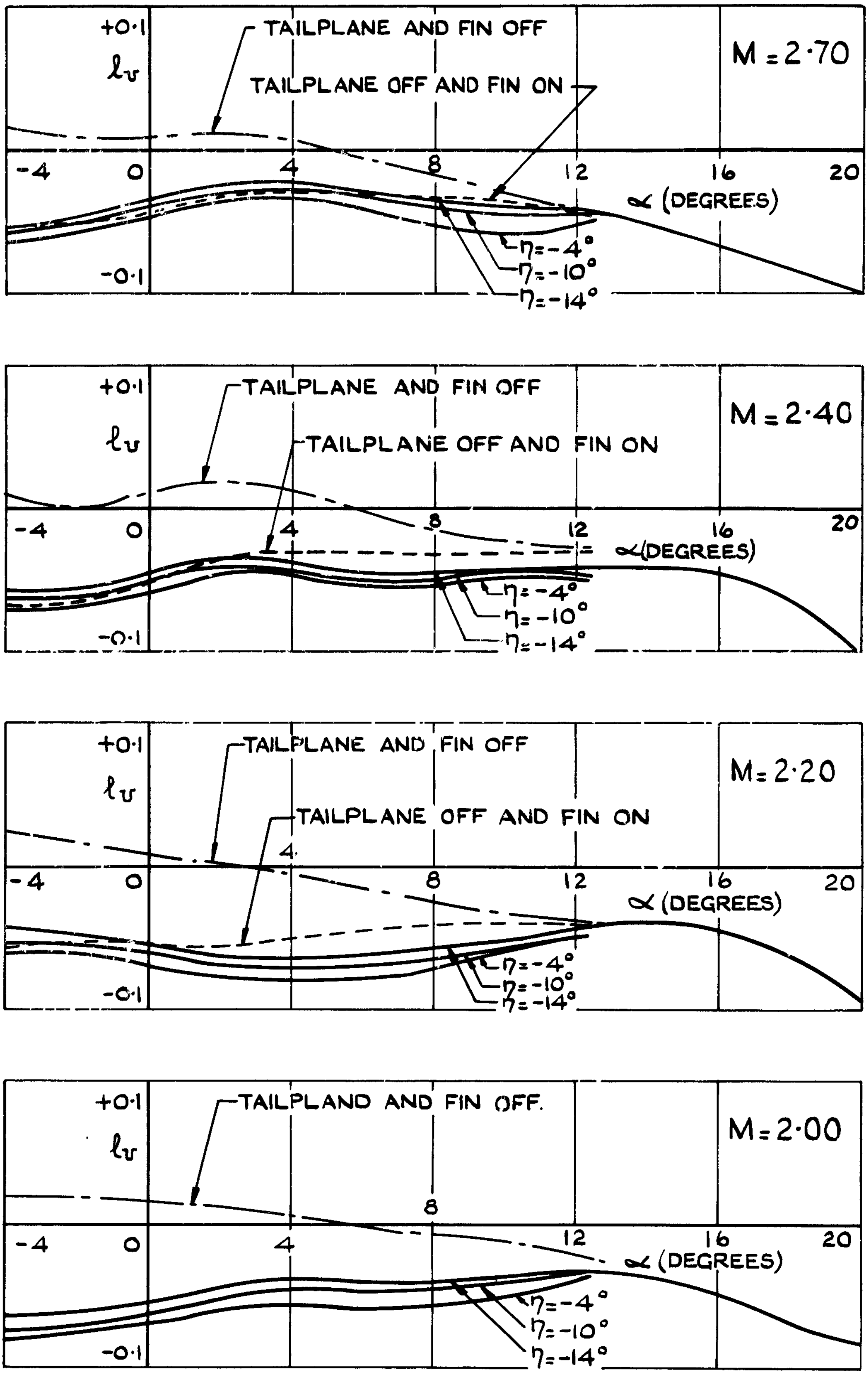

FIG. 30. VARIATION OF l_v WITH INCIDENCE

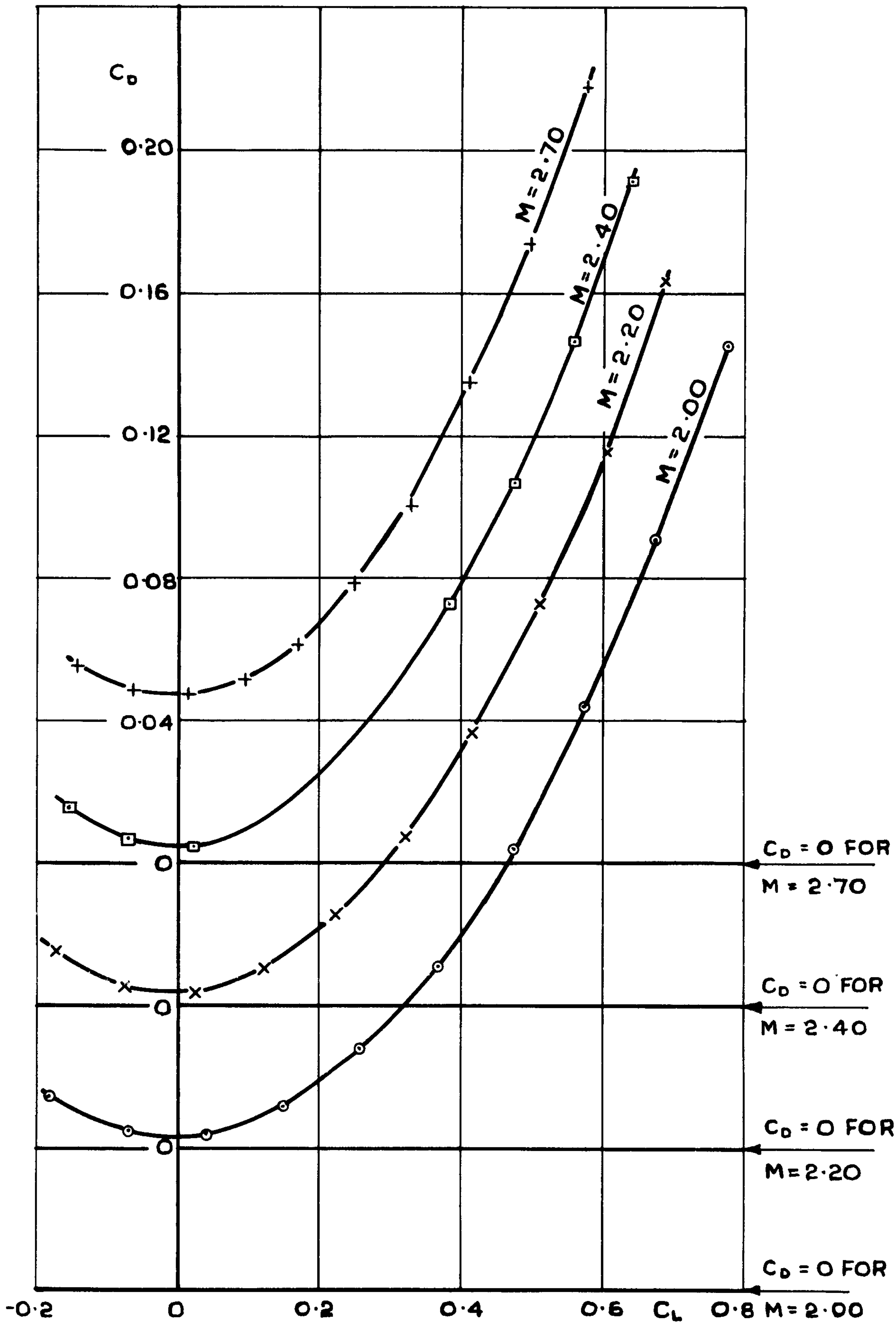

FIG. 31. VARIATION OF C_D WITH C_L AT CONSTANT MACH NUMBER : $\eta = -4^{\circ}$

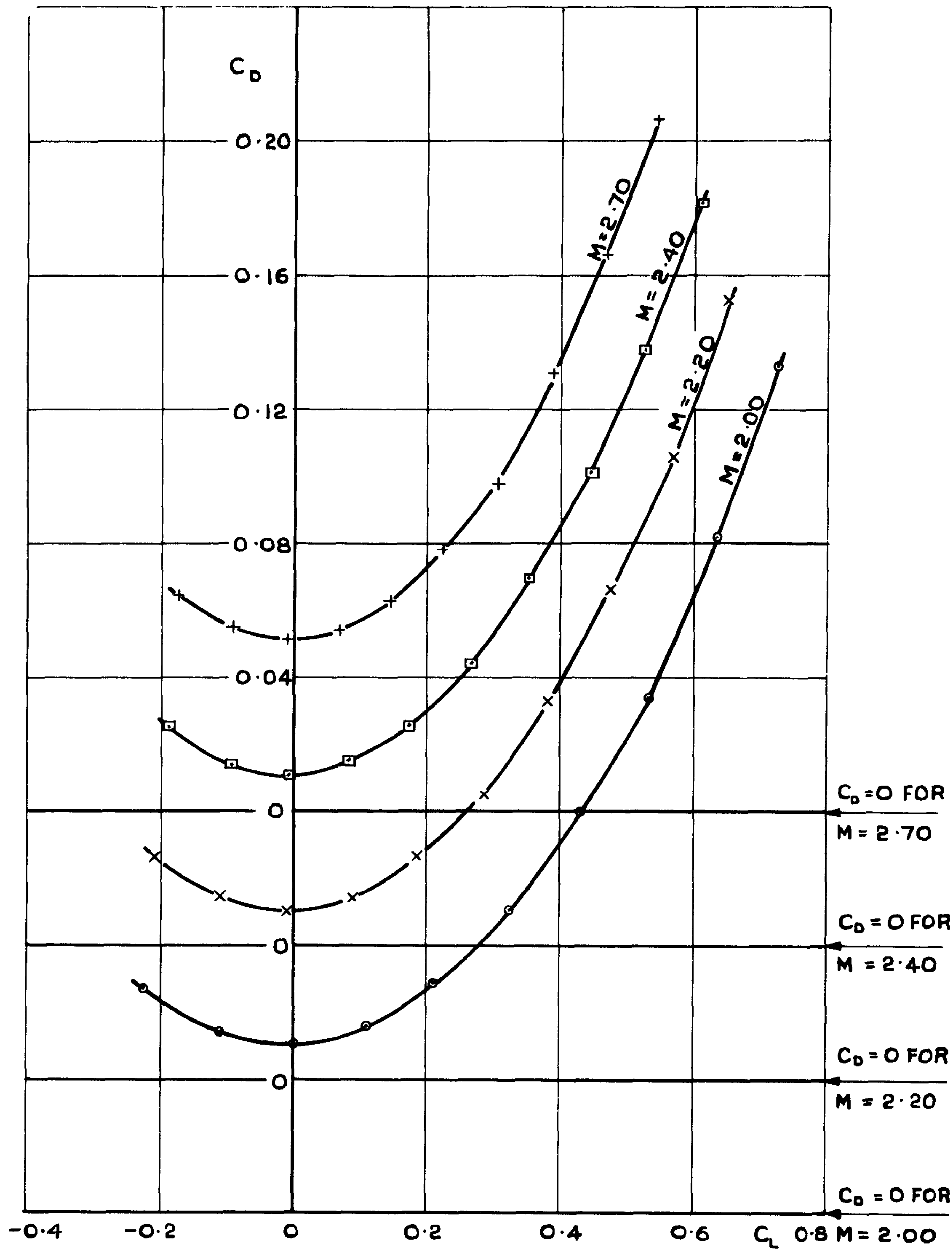

FIG. 32. VARIATION OF C_D WITH C_L AT CONSTANT MACH NUMBER : $\eta = -10^\circ$.

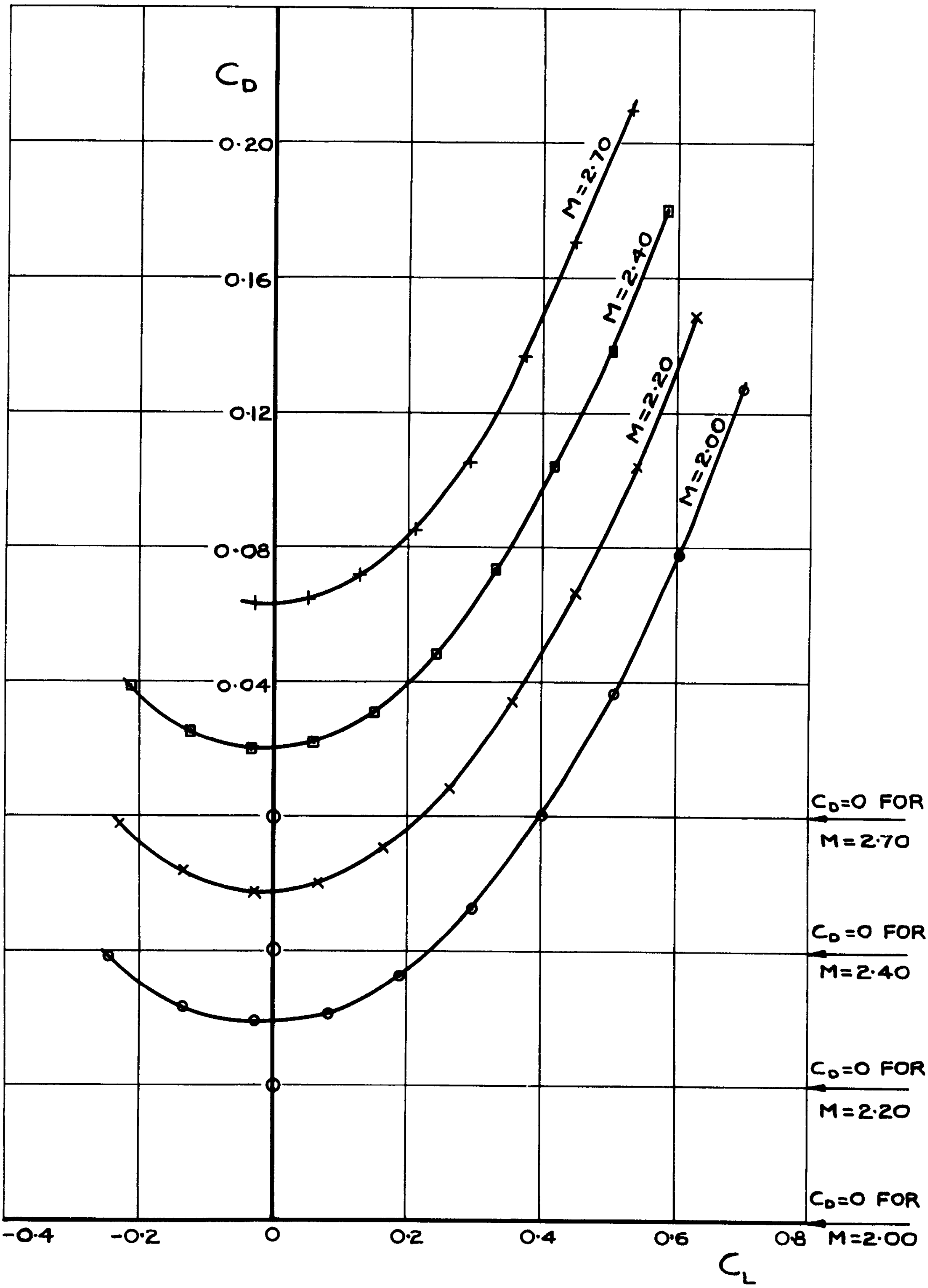

FIG. 33 VARIATION OF C_D WITH C_L AT CONSTANT MACH NUMBER: $\eta = -14^{\circ}$

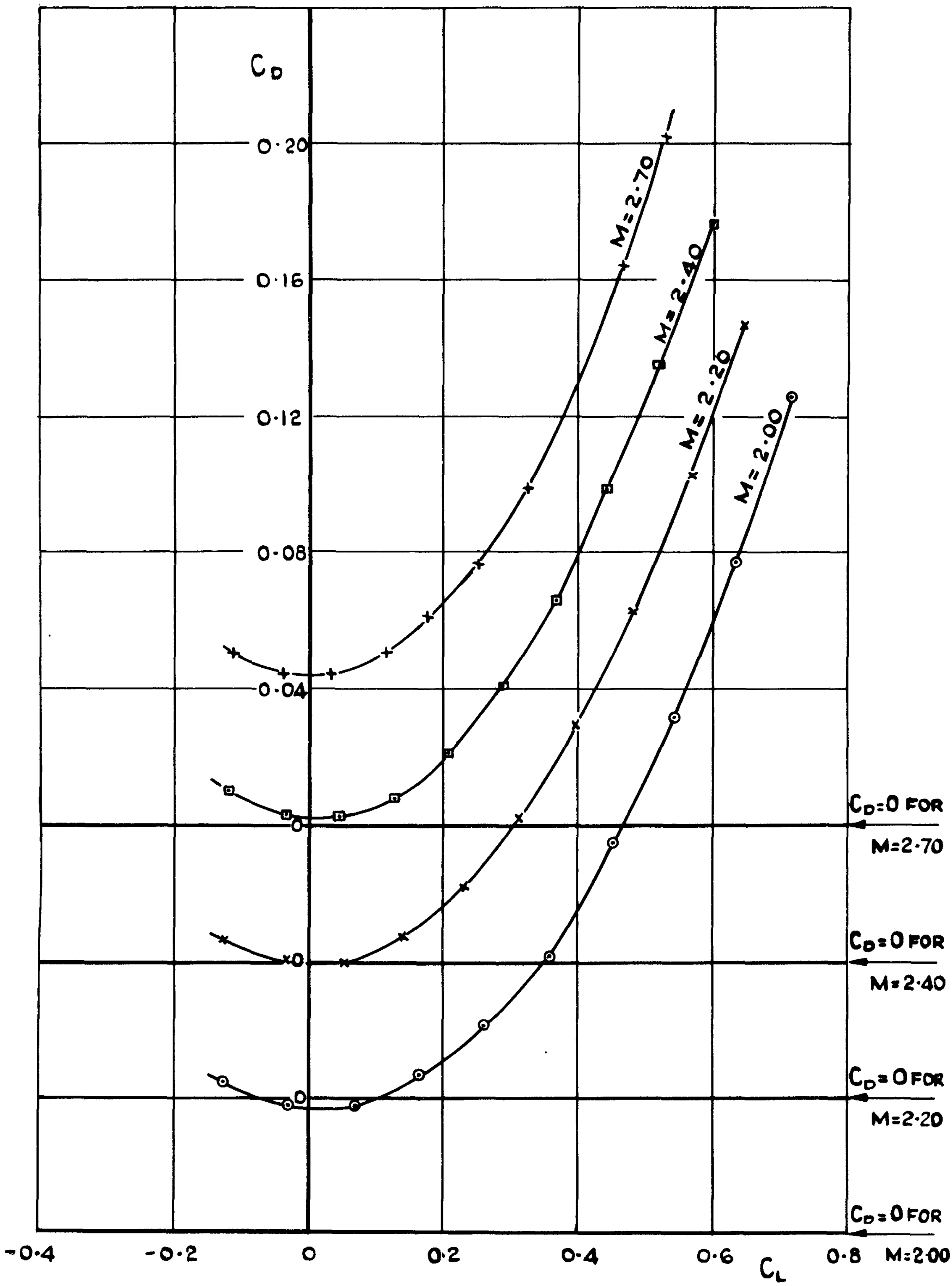

FIG.34. VARIATION OF C_D WITH C_L AT CONSTANT MACH NUMBER: TAILPLANE AND FIN OFF.

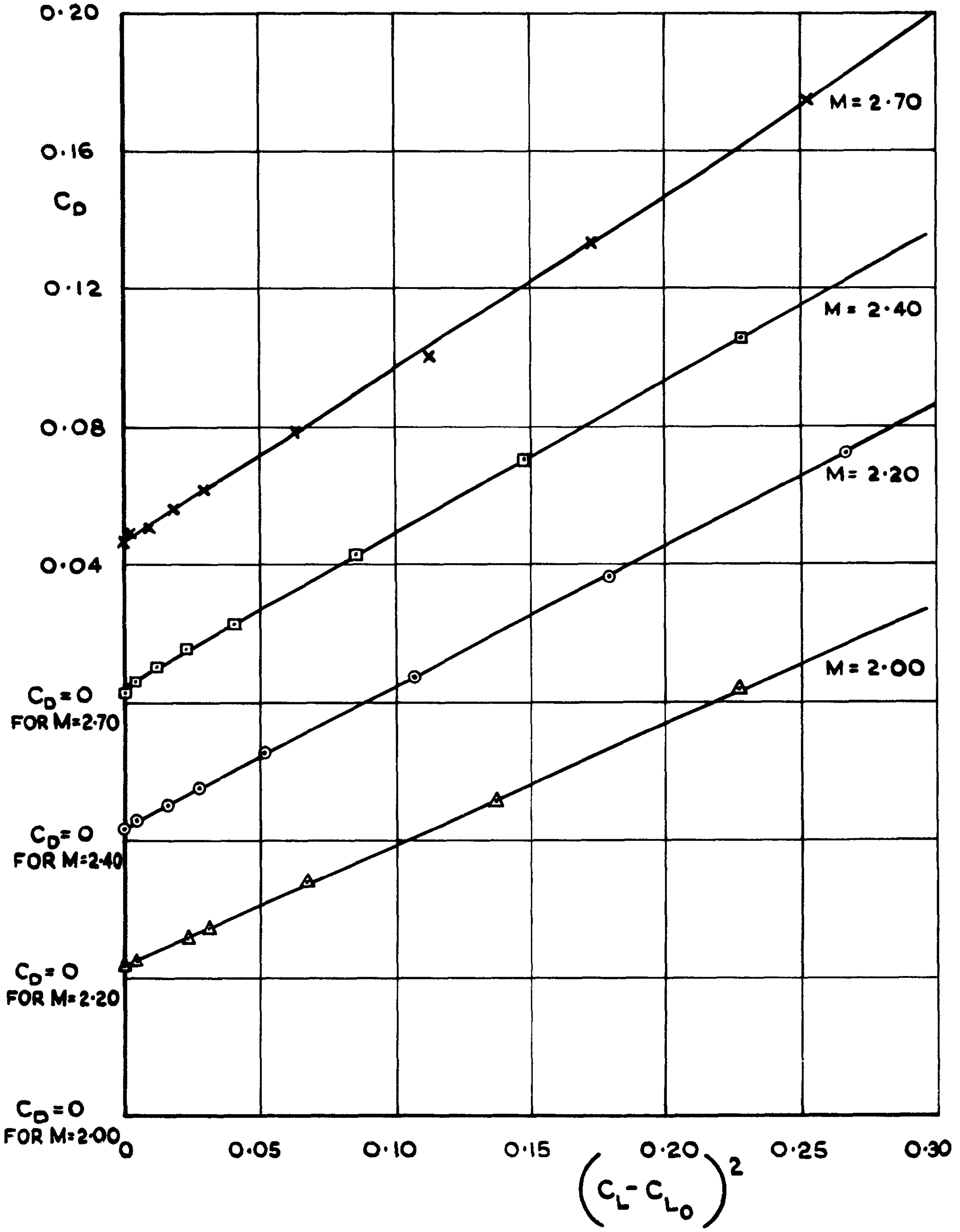

FIG.35. VARIATION OF C_D WITH $(C_L - C_{L_0})^2$: $\eta = -4^\circ$.

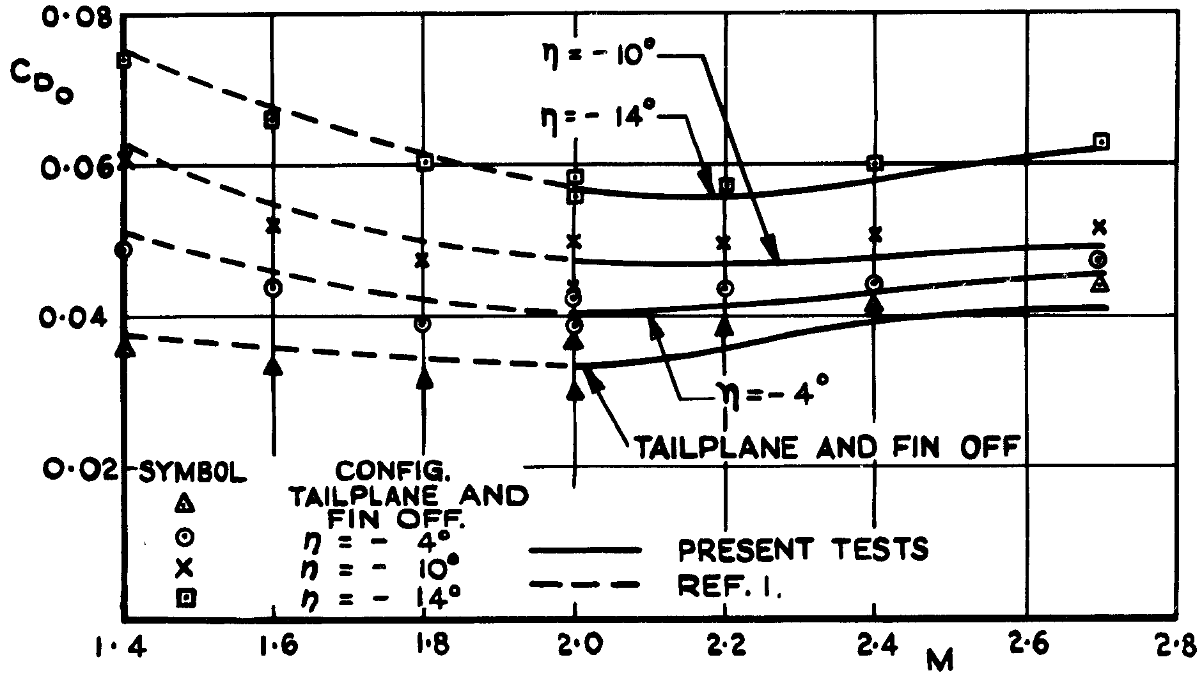

FIG.36. VARIATION OF MINIMUM DRAG COEFFICIENT WITH MACH NUMBER.

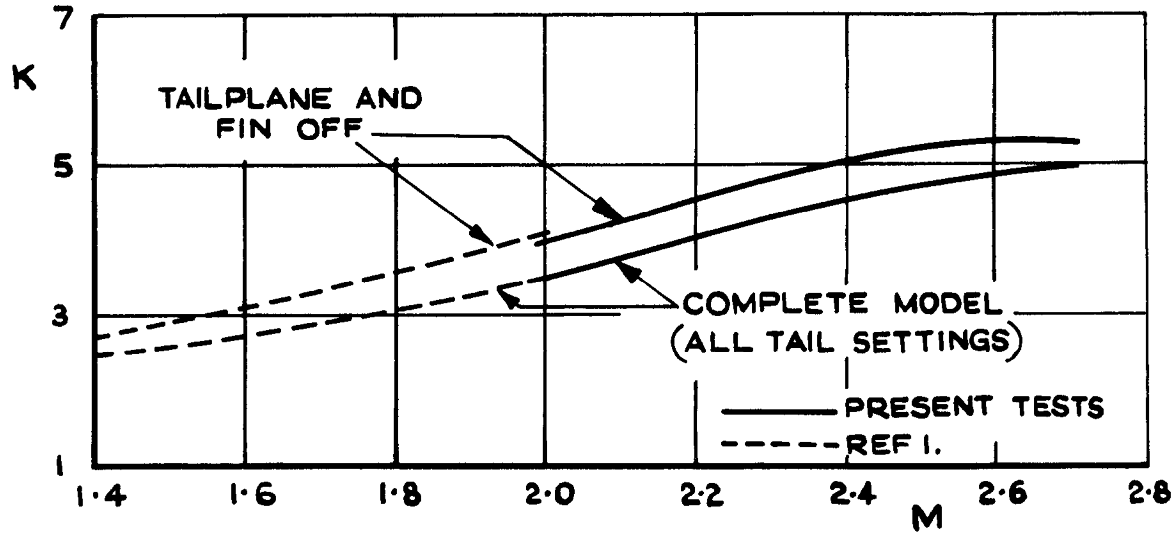

FIG. 37. VARIATION OF INDUCED DRAG FACTOR WITH MACH NUMBER.

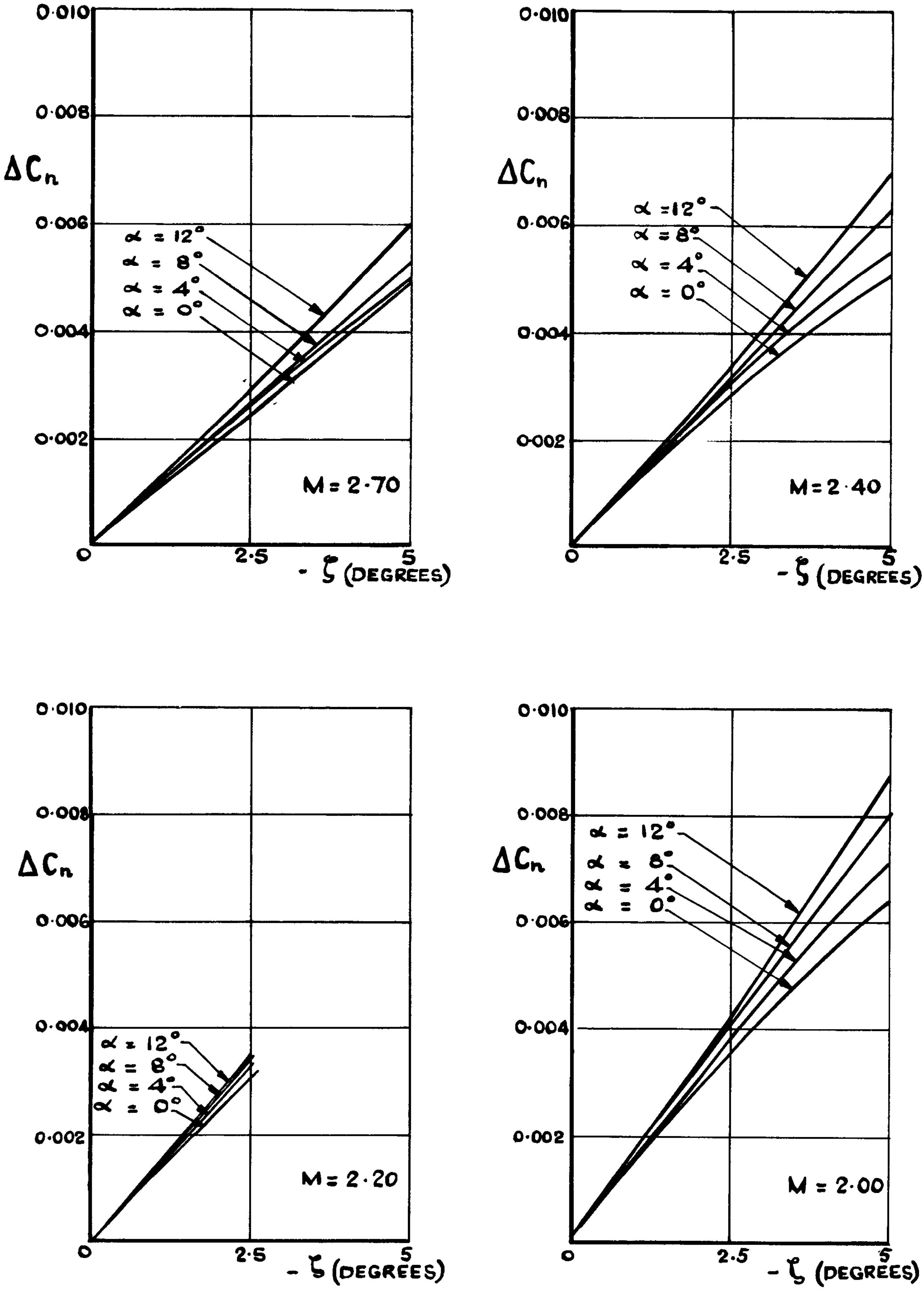

FIG 38. VARIATION OF YAWING MOMENT DUE TO RUDDER WITH RUDDER SETTING

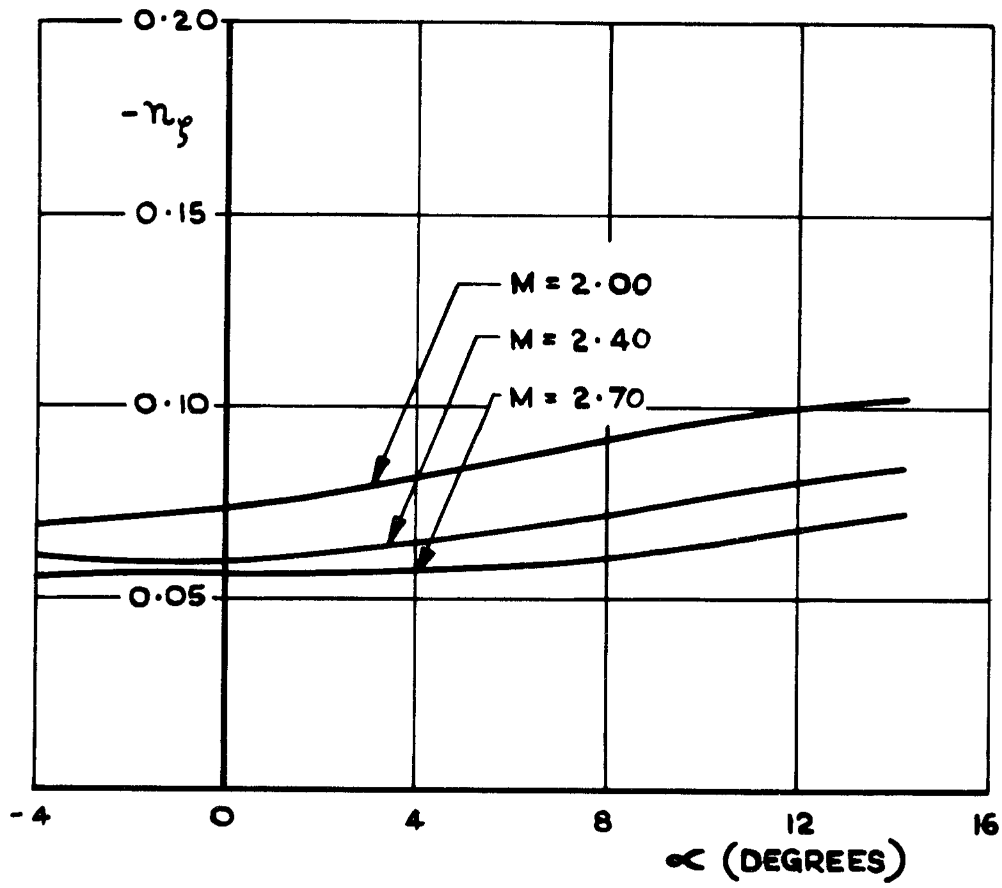

FIG. 39. VARIATION OF MEAN YAWING MOMENT DUE TO RUDDER WITH INCIDENCE.

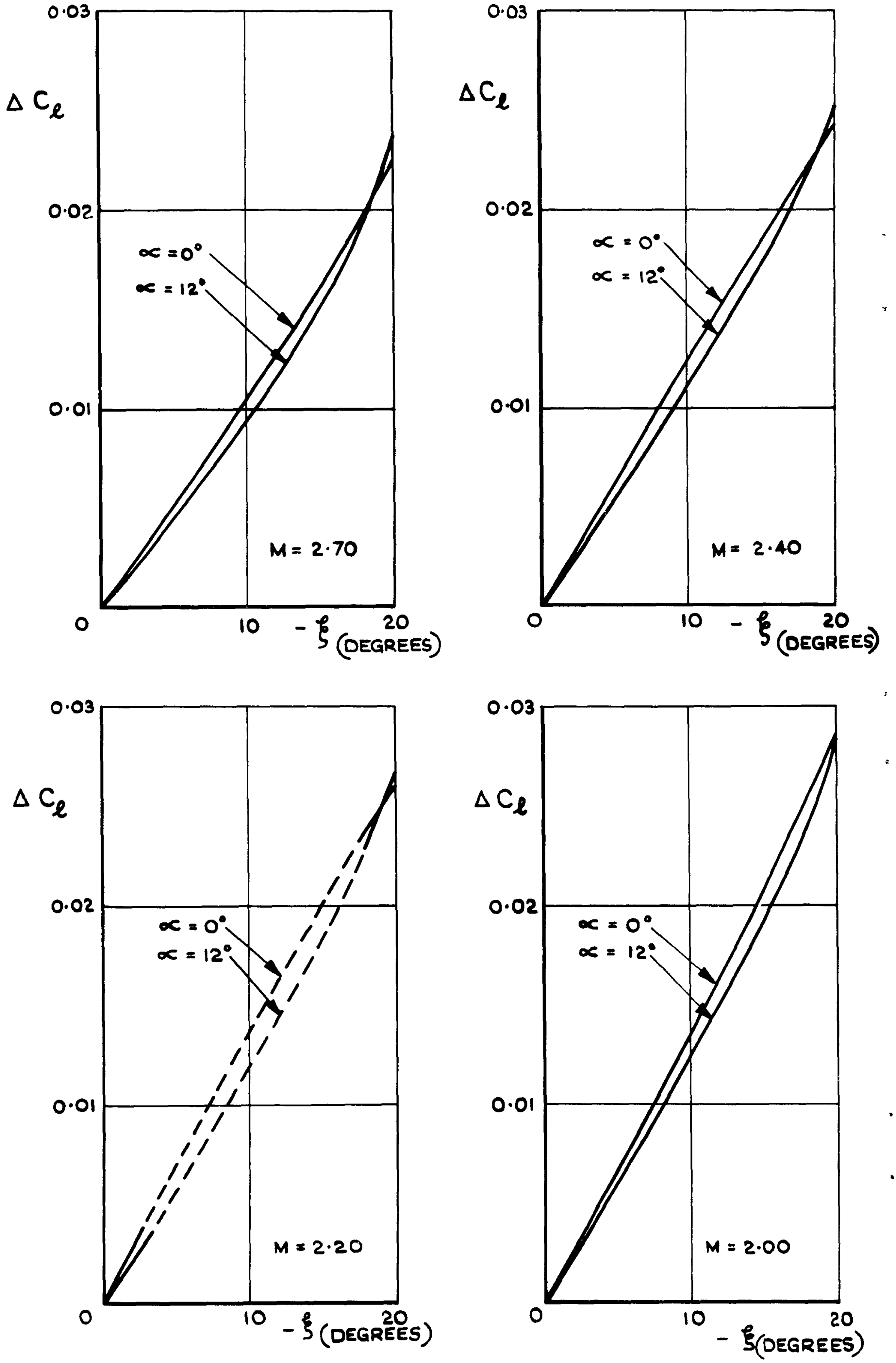

FIG. 40. VARIATION OF ROLLING MOMENT DUE TO AILERONS WITH AILERON SETTING.

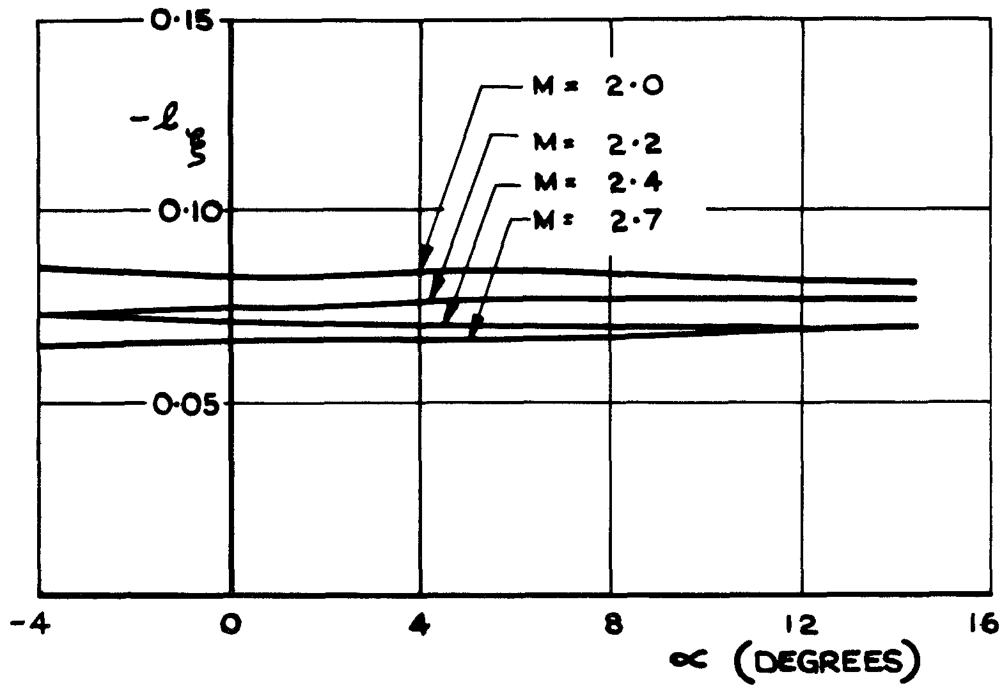

FIG. 41. VARIATION OF MEAN ROLLING MOMENT DUE TO AILERONS WITH INCIDENCE.

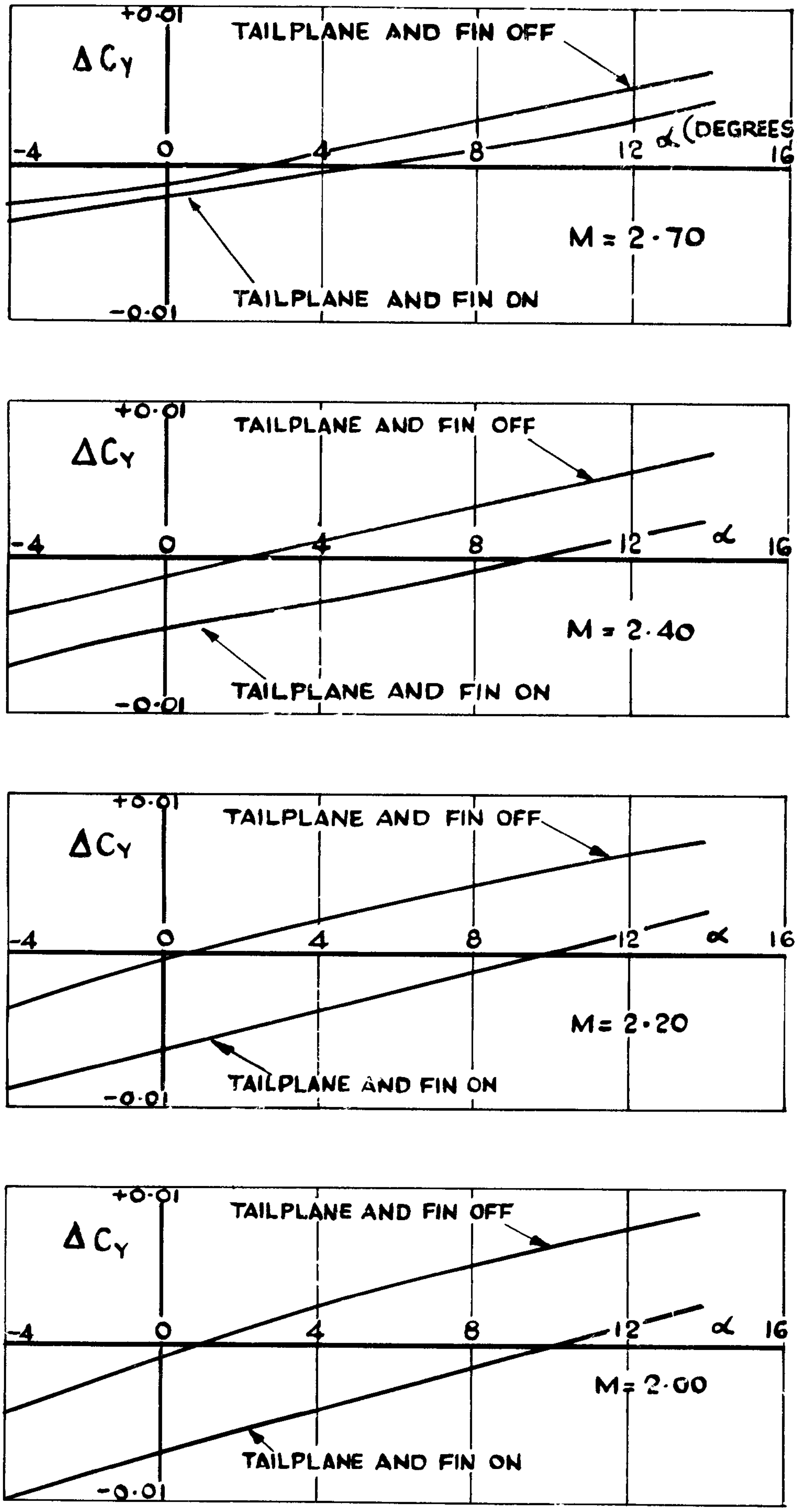

FIG 42. SIDE FORCE AT ZERO SIDESLIP DUE TO -20° AILERON SETTING

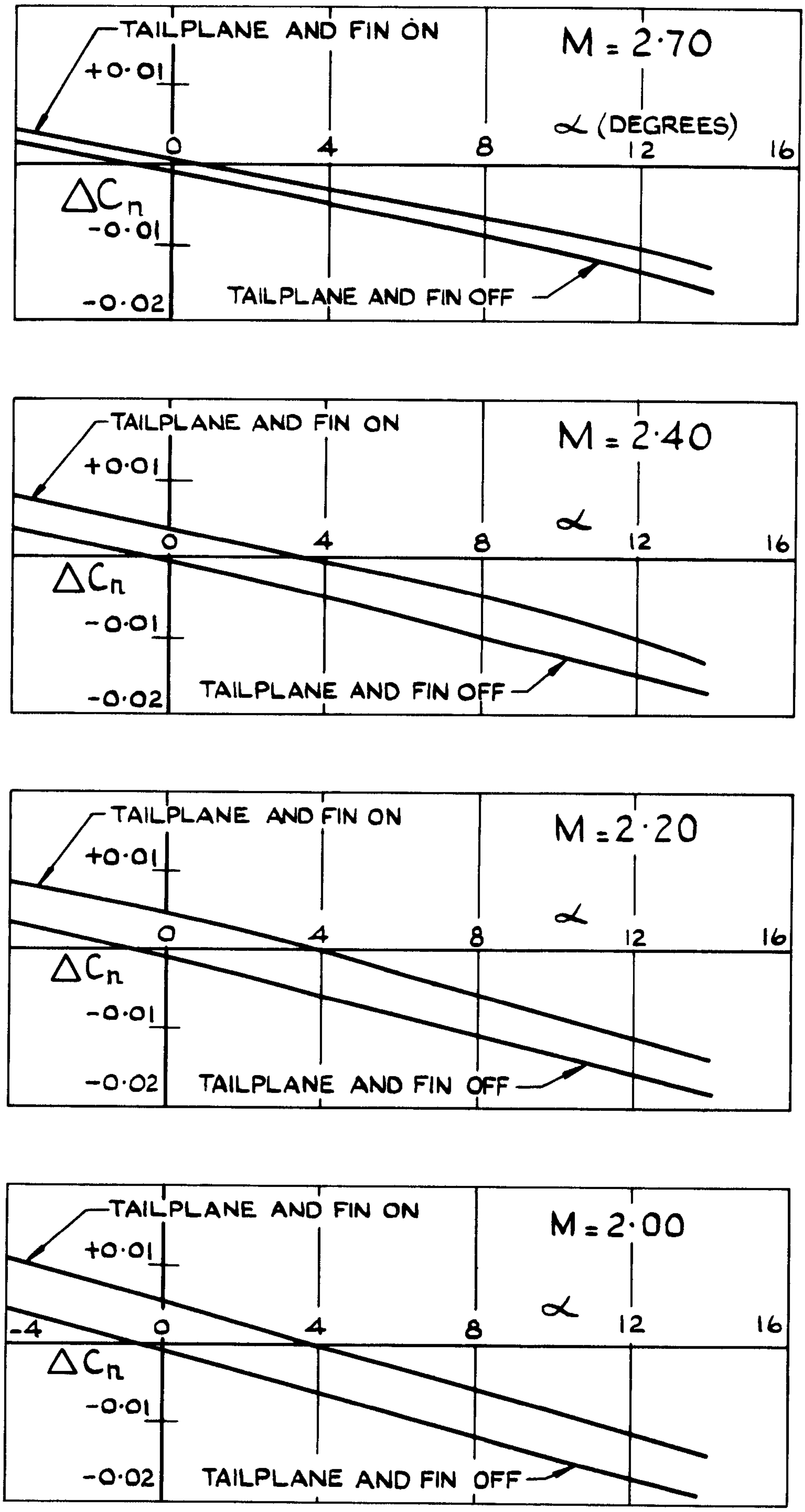

FIG. 43. YAWING MOMENT AT ZERO SIDESLIP DUE TO -20° AILERON SETTING

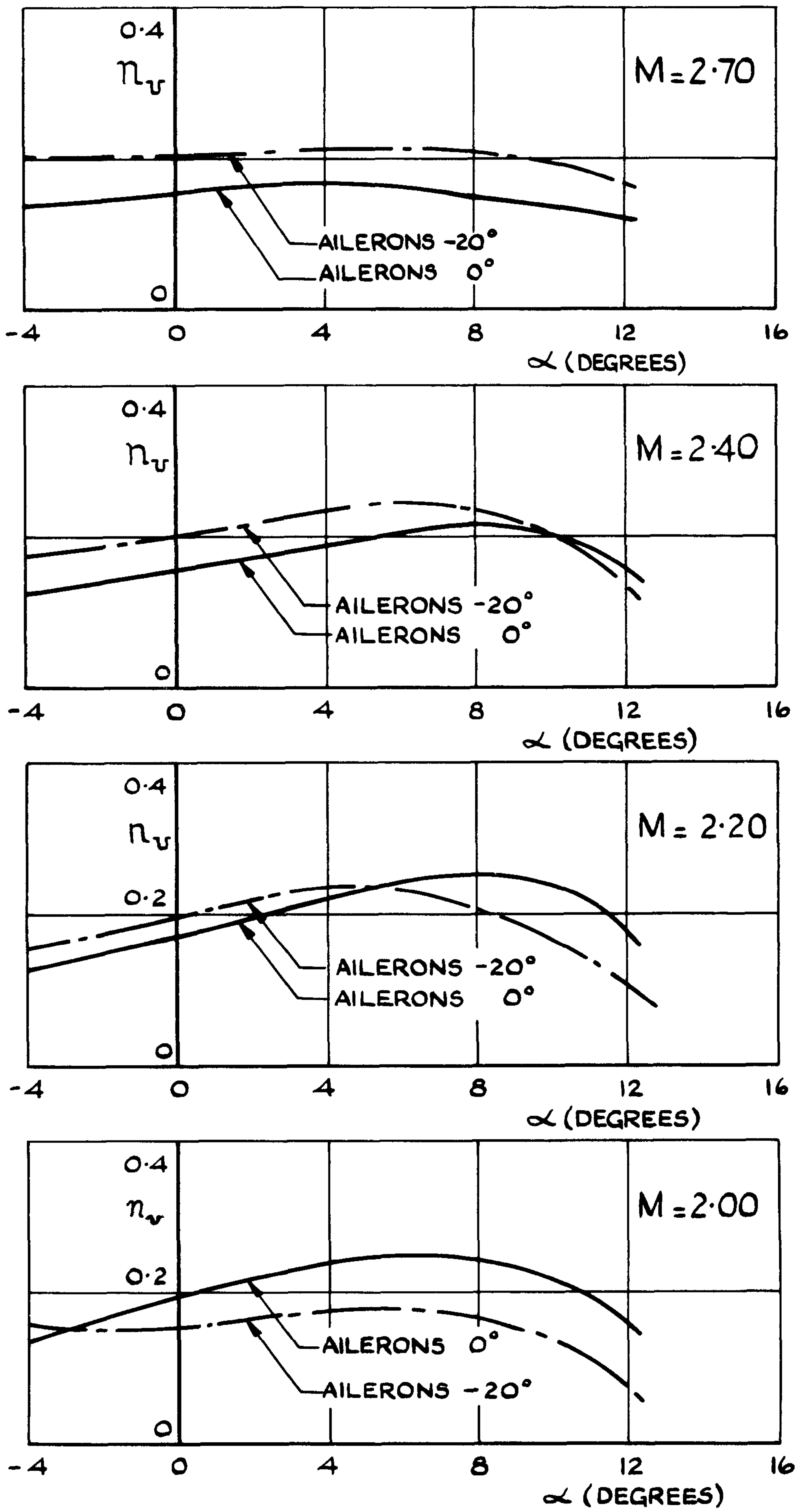

FIG. 44. EFFECT OF -20° AILERON SETTING ON VARIATION OF n_v WITH α

$\eta = -4^\circ$

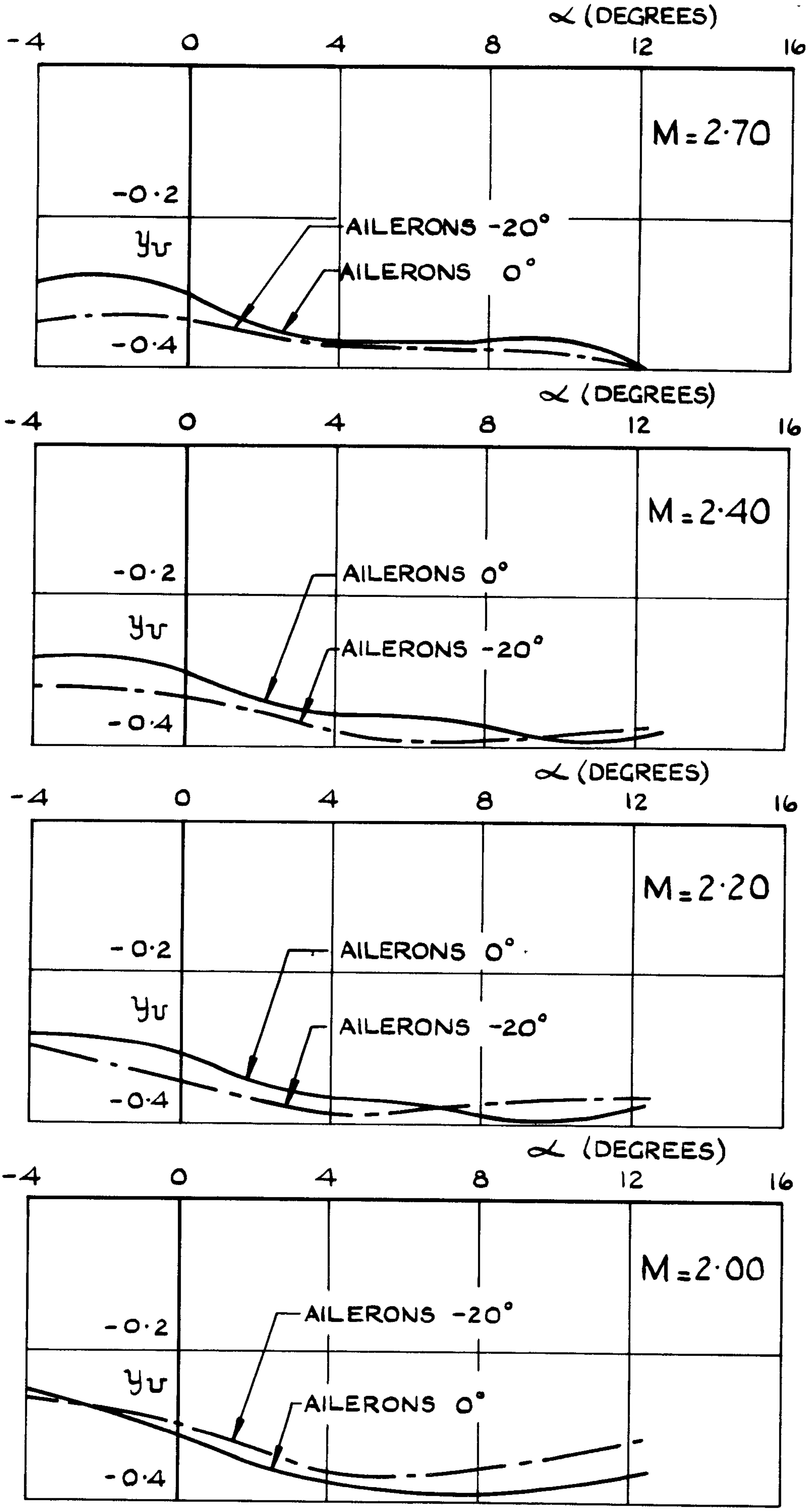

FIG. 45. EFFECT OF $-20°$ AILERON SETTING ON VARIATION OF y_v WITH α

$\eta = -4°$

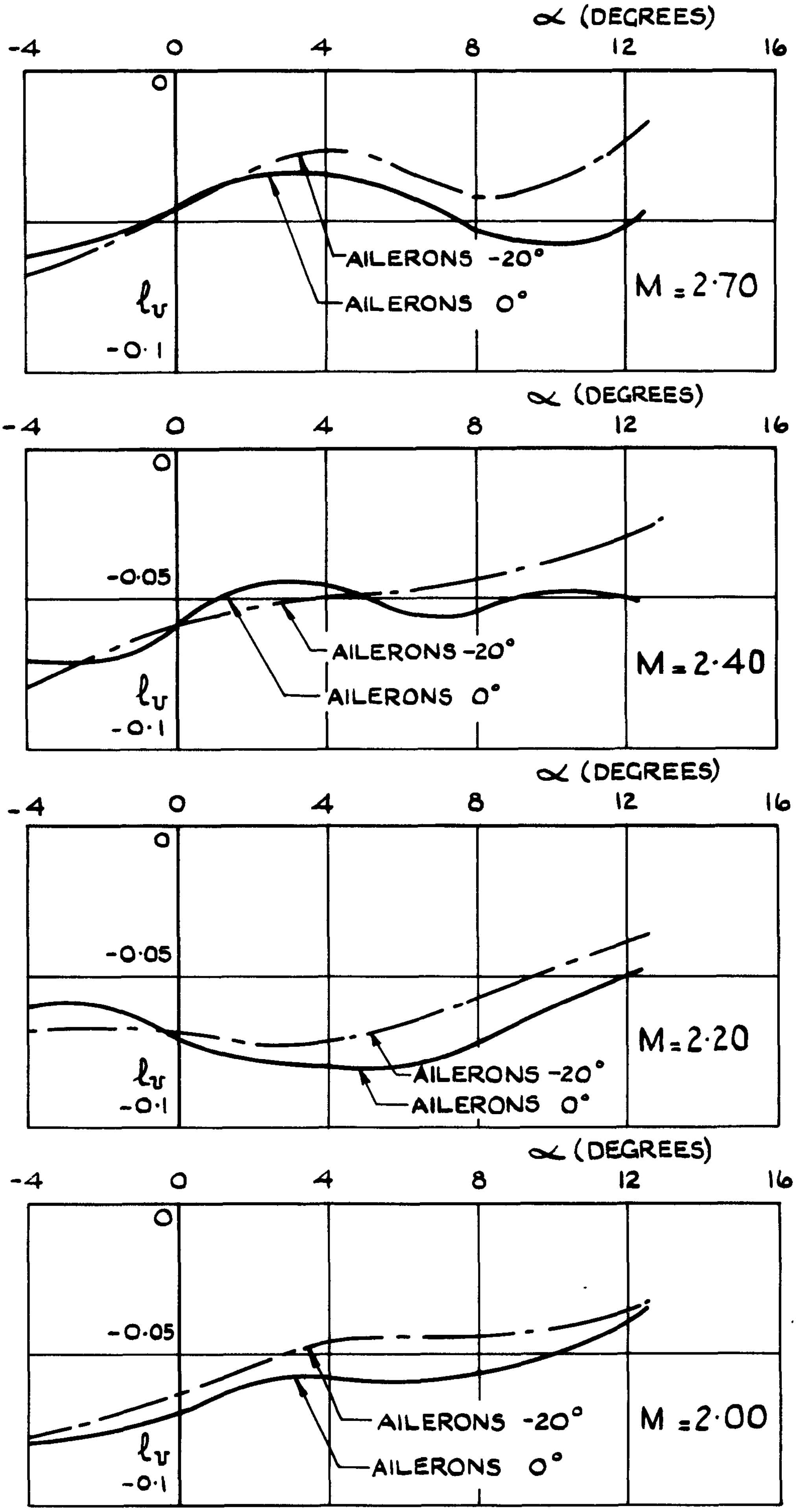

FIG. 46. EFFECT OF -20° AILERON SETTING ON VARIATION OF l_v WITH $\alpha°$

$\eta = -4°$

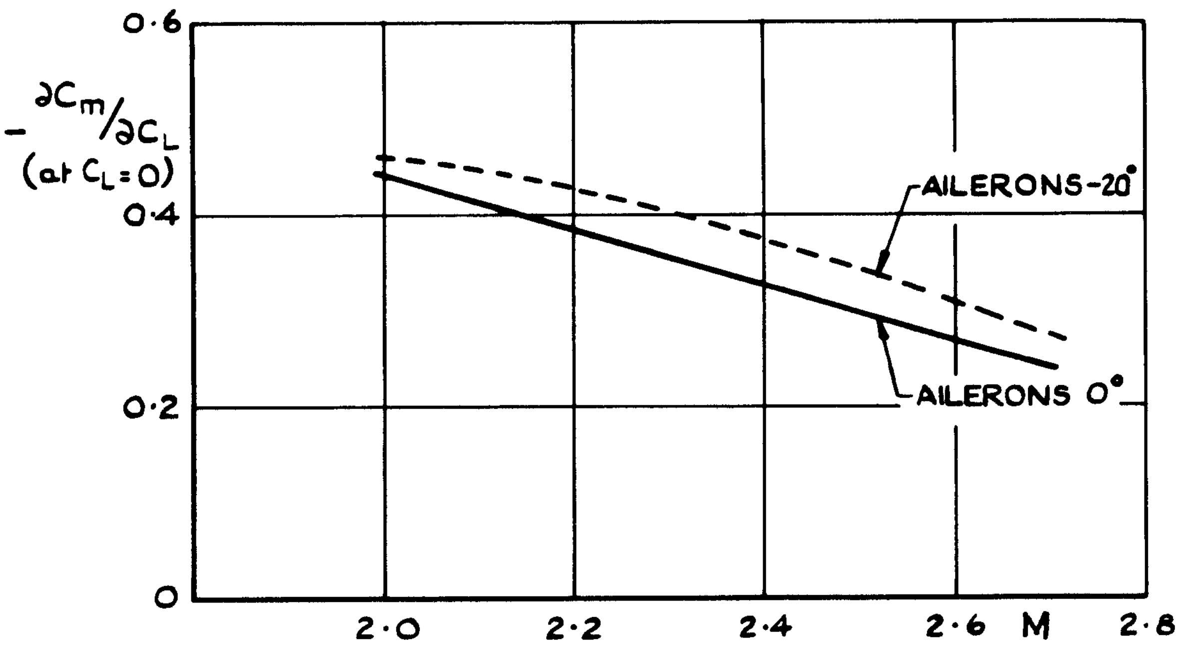

FIG. 47. EFFECT OF -20° AILERON SETTING ON LONGITUDINAL STABILITY : $\eta = -4°$

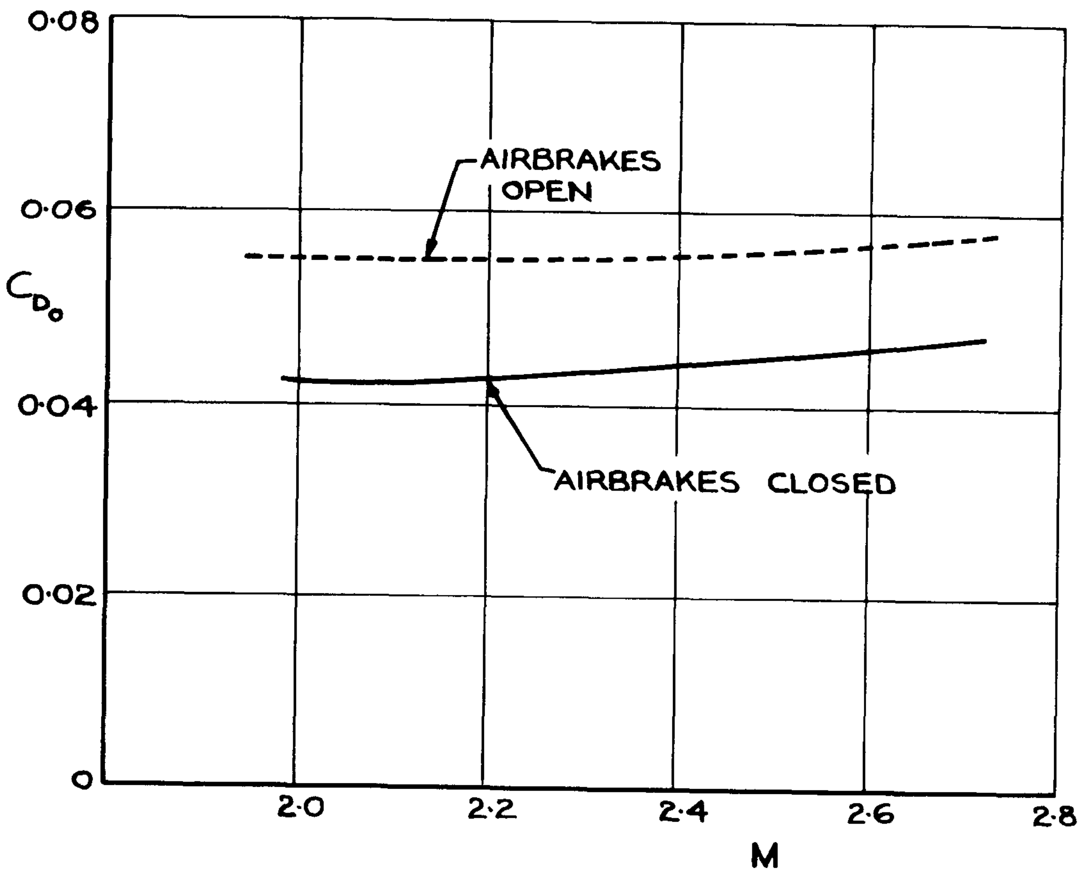

FIG. 48 EFFECT OF AIRBRAKES ON MINIMUM DRAG COEFFICIENT: $\eta = -4°$

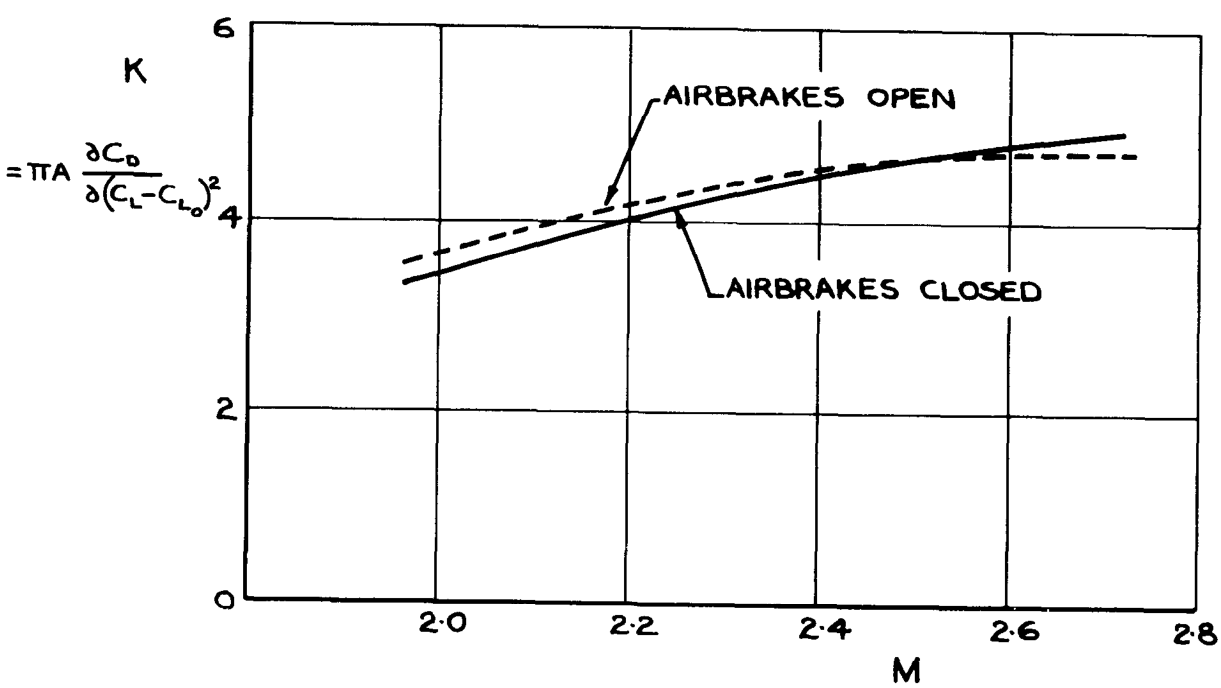

FIG. 49 EFFECT OF AIRBRAKES ON INDUCED DRAG FACTOR: $\eta = -4°$

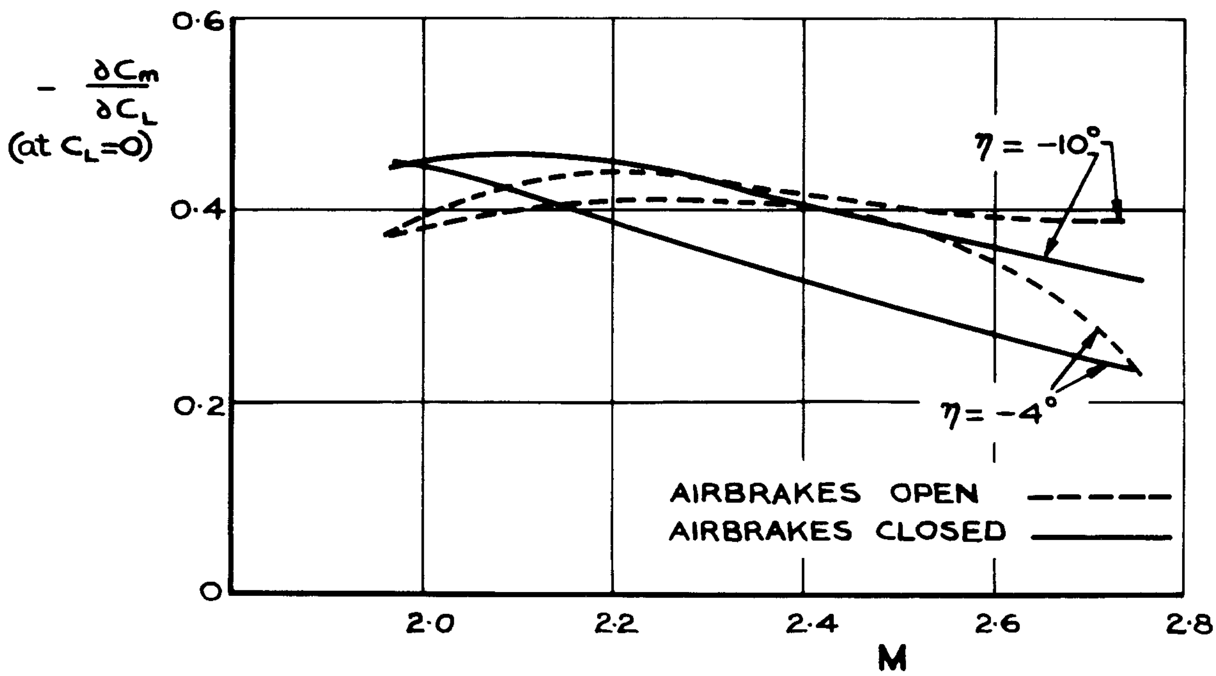

FIG. 50 EFFECT OF AIRBRAKES ON LONGITUDINAL STABILITY

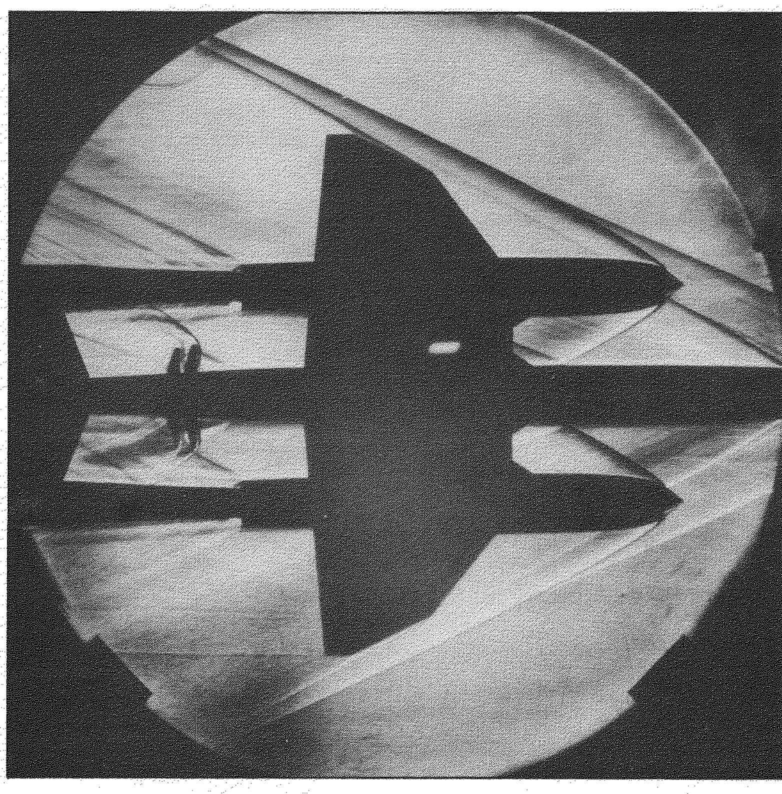

A. M = 2.70

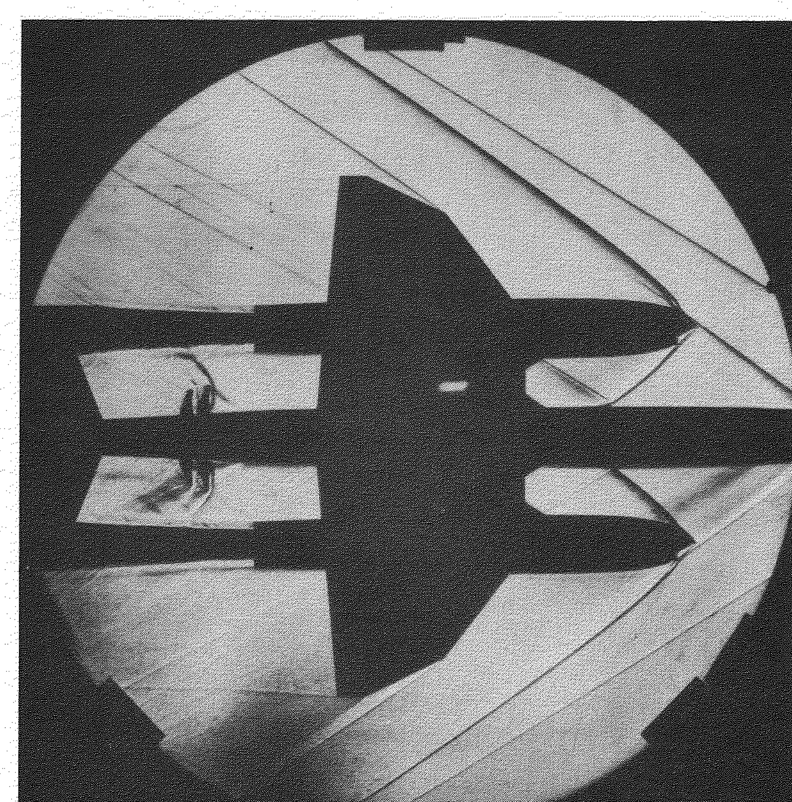

B. M = 2.00

FIG.51. SCHLIEREN PHOTOGRAPHS OF MODEL WITH AIRBRAKES OPEN

$\alpha = \beta = 0$

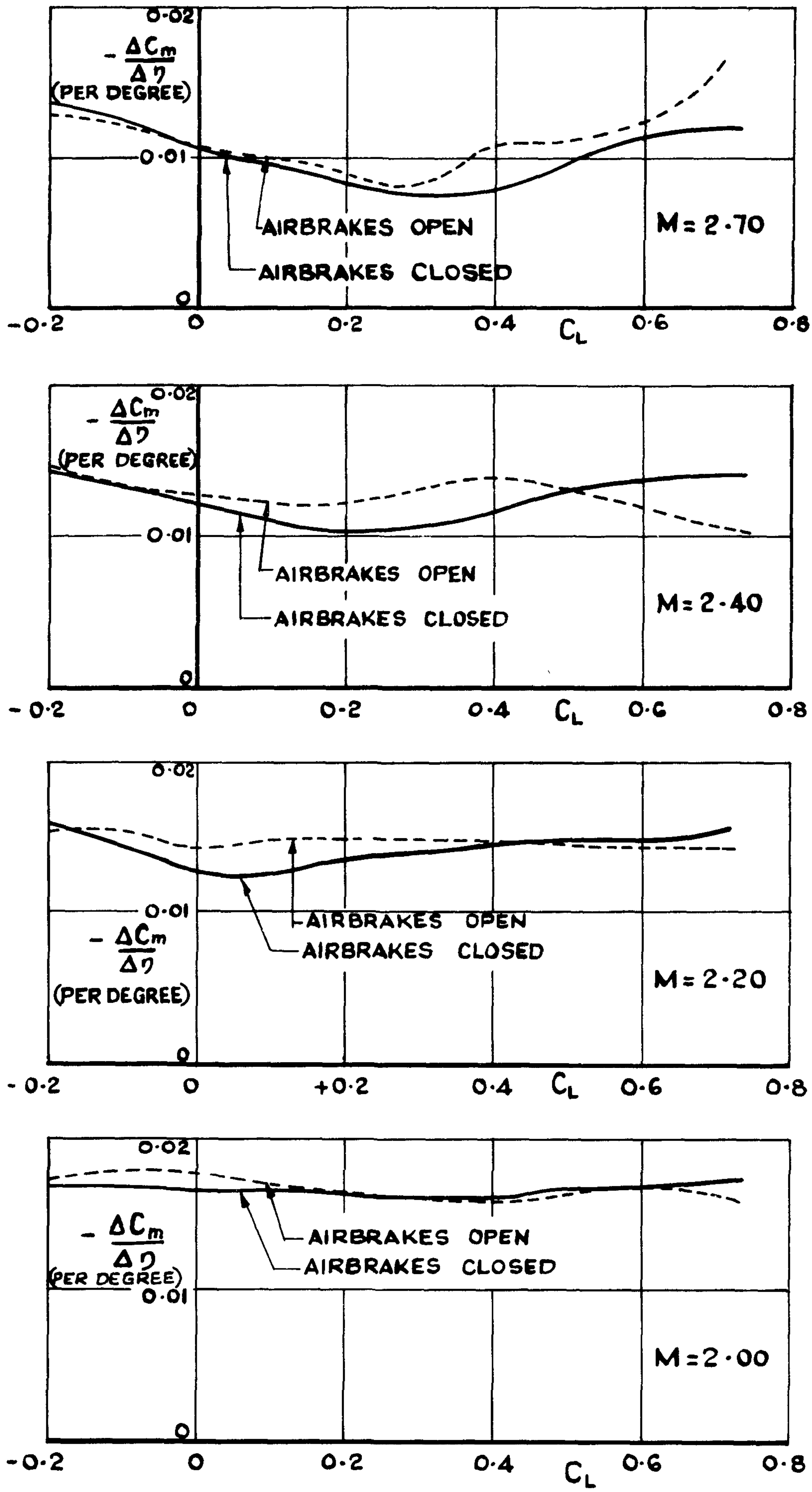

FIG 52. EFFECT OF AIRBRAKES ON TAILPLANE POWER

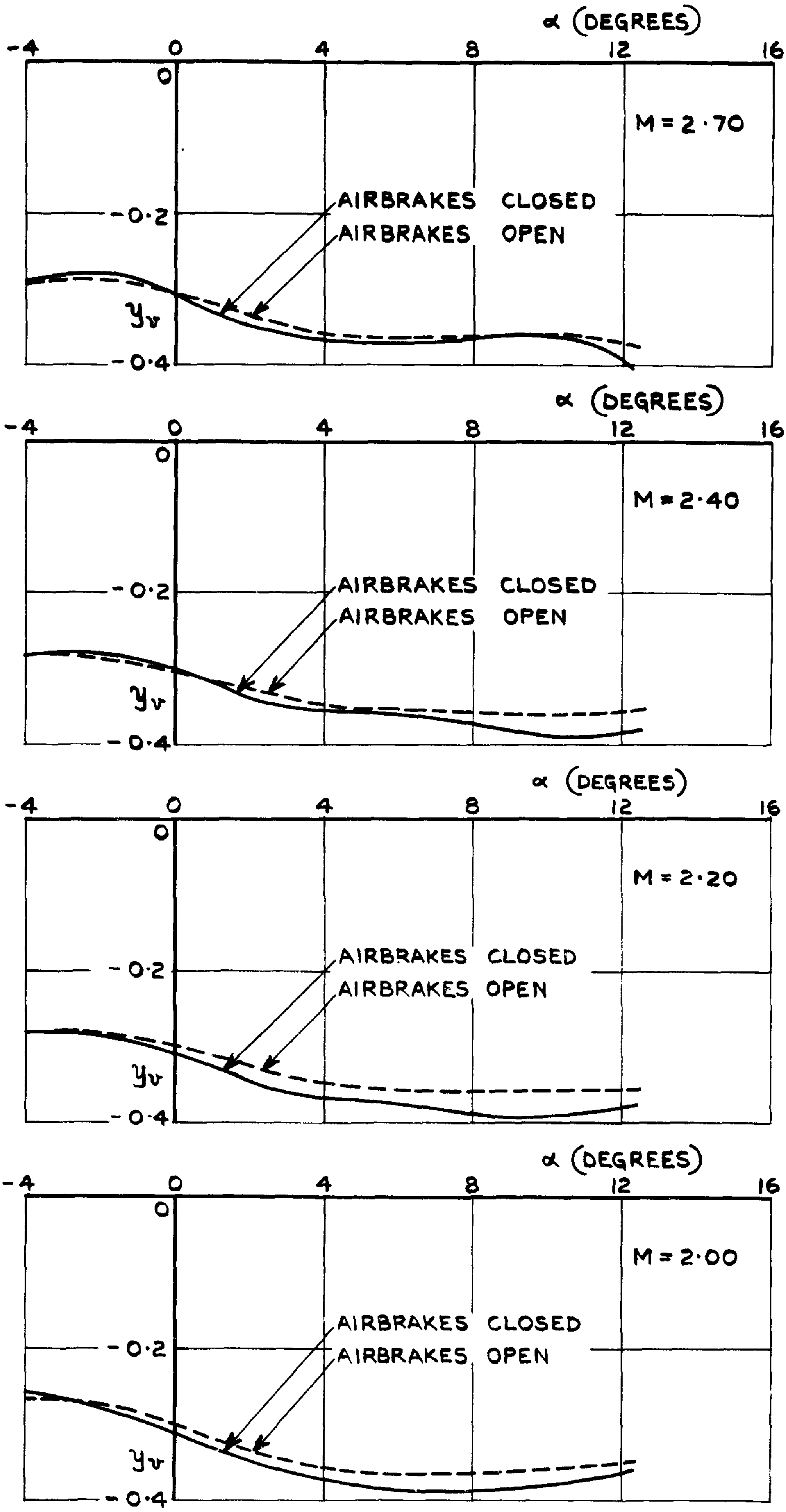

FIG. 53. EFFECT OF AIRBRAKES ON VARIATION OF y_v WITH α; $\eta = -4°$

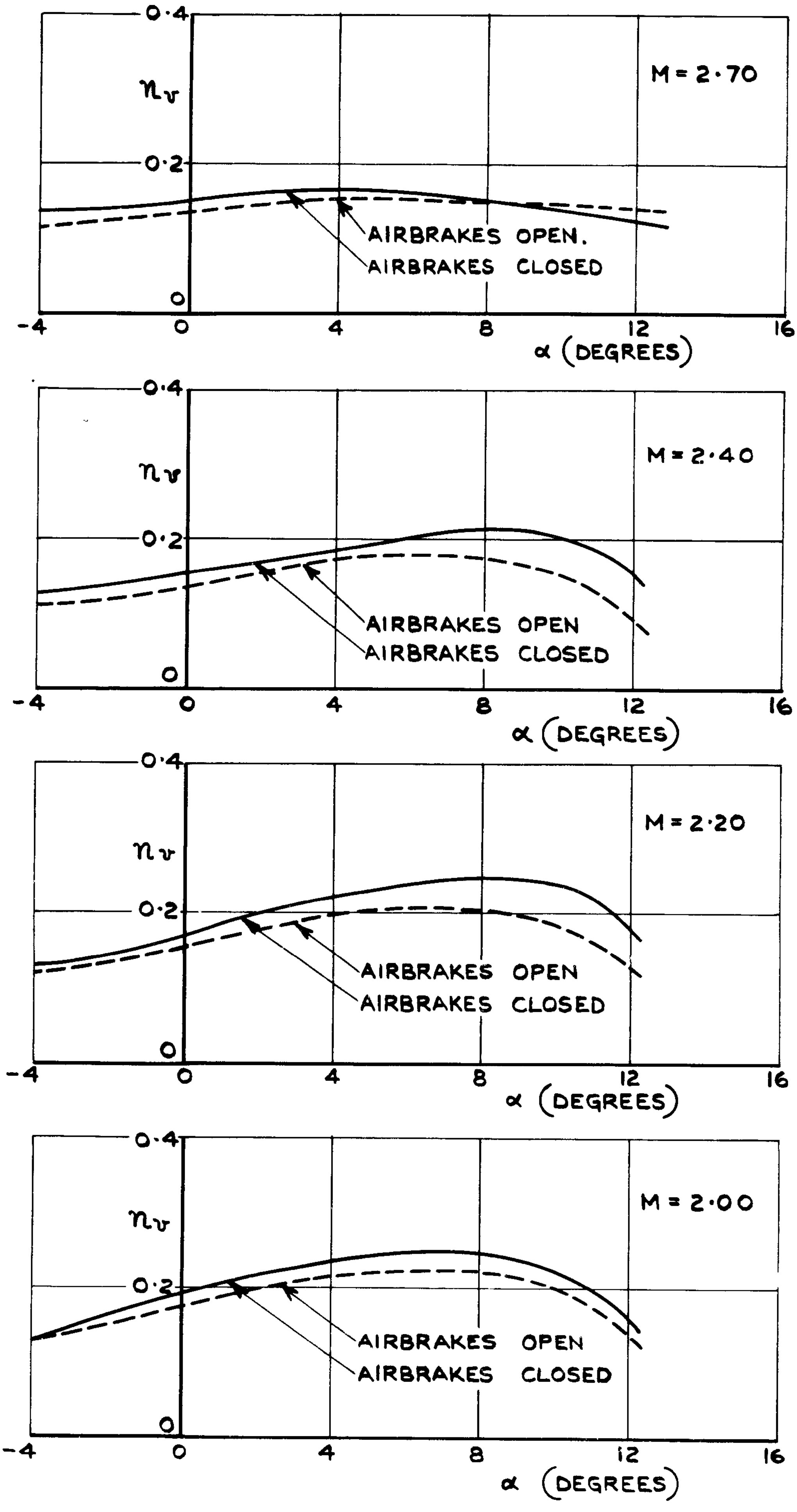

FIG. 54. EFFECT OF AIRBRAKES ON VARIATION OF n_v WITH $\alpha; \eta = -4°$.

Printed in England for Her Majesty's Stationery Office by the Royal Aircraft Establishment, Farnborough. W.T.61.K4.

A.R.C. C.P.No.818
September, 1961

A.I. (42) Bristol 188:
533.652.2:
533.6.011.5:
533.6.013.1:
533.6.013.4

SUPERSONIC WIND TUNNEL TESTS ON A 1/12TH SCALE MODEL OF THE BRISTOL TYPE 188 RESEARCH AIRCRAFT PART TWO: M = 2.0 to 2.7. Cook, T. A.

Six component force measurements have been made on a 1/12th scale model of the Bristol Type 188 in the 8 ft x 8 ft wind tunnel at R.A.E. Bedford, at Mach numbers of 2.00, 2.20, 2.40, and 2.70. The results of these measurements are presented graphically, with an analysis of the effects of tailplane movement, aileron and rudder controls, and airbrakes on longitudinal and lateral stability, and drag.

A.R.C. C.P.No.818
September, 1961

A.I. (42) Bristol 188:
533.652.2:
533.6.011.5:
533.6.013.1:
533.6.013.4

SUPERSONIC WIND TUNNEL TESTS ON A 1/12TH SCALE MODEL OF THE BRISTOL TYPE 188 RESEARCH AIRCRAFT PART TWO: M = 2.0 to 2.7 Cook, T. A.

Six component force measurements have been made on a 1/12th scale model of the Bristol Type 188 in the 8 ft x 8 ft wind tunnel at R.A.E. Bedford, at Mach numbers of 2.00, 2.20, 2.40 and 2.70. The results of these measurements are presented graphically, with an analysis of the effects of tailplane movement, aileron and rudder controls, and airbrakes on longitudinal and lateral stability, and drag.

A.R.C. C.P.No.818
September, 1961

A.I. (42) Bristol 188:
533.652.2:
533.6.011.5:
533.6.013.1:
533.6.013.4

SUPERSONIC WIND TUNNEL TESTS ON A 1/12TH SCALE MODEL OF THE BRISTOL TYPE 188 RESEARCH AIRCRAFT PART TWO: M = 2.0 to 2.7. Cook, T. A.

Six component force measurements have been made on a 1/12th scale model of the Bristol Type 188 in the 8 ft x 8 ft wind tunnel at R.A.E. Bedford, at Mach numbers of 2.00, 2.20, 2.40 and 2.70. The results of these measurements are presented graphically, with an analysis of the effects of tailplane movement, aileron and rudder controls, and airbrakes on longitudinal and lateral stability, and drag.

C.P. No. 818

Published by
HER MAJESTY'S STATIONERY OFFICE

To be purchased from
York House, Kingsway, London w.c.2
423 Oxford Street, London w.1
13A Castle Street, Edinburgh 2
109 St. Mary Street, Cardiff
39 King Street, Manchester 2
50 Fairfax Street, Bristol 1
35 Smallbrook, Ringway, Birmingham 5
80 Chichester Street, Belfast 1
or through any bookseller

C.P. No. 818

S.O. CODE No. 23-9016-18